

Time-lapse seismic within reservoir engineering

time-lapse seismic

reservoir engineering

time-lapse seismic

reservoir engineering

time-lapse seismic

reservoir engineering

time-lapse seismic

reservoir engineering



Tanja Oldenziel

Time-lapse seismic within reservoir engineering

Time-lapse seismic within reservoir engineering

PROEFSCHRIFT

ter verkrijging van de graad van doctor
aan de Technische Universiteit Delft,
op gezag van de Rector Magnificus prof. dr. ir. J.T. Fokkema,
voorzitter van het College voor Promoties,
in het openbaar te verdedigen op dinsdag 6 mei 2003 om 16.00 uur

door

Tanja Oldenziel

mijnbouwkundig ingenieur

geboren te Heerhugowaard

Dit proefschrift is goedgekeurd door de promotoren:

Prof. dr. ir. J.T. Fokkema
Prof. ir. C.P.J.W. van Kruijsdijk

Samenstelling promotiecommissie:

Rector Magnificus,	voorzitter
Prof. ir. C.P.J.W. van Kruijsdijk,	Technische Universiteit Delft, promotor
Prof. dr. ir. J.T. Fokkema,	Technische Universiteit Delft, promotor
Prof. dr. S.M. Luthi,	Technische Universiteit Delft
Prof. A. Gisolf,	Technische Universiteit Delft
Prof. dr. J.R. Fanchi,	Colorado School of Mines
Dr. ir. P.F.M. de Groot,	dGB, Enschede
Mr. P. Meldahl,	Statoil, Stavanger

Printed by:
Drukkerij Augustijn, Enschede

ISBN 90-9016829-X

Copyright © 2003 by T. Oldenziel

The research in this thesis has been financially supported by dGB and STW.

All right reserved. No parts of this publication may be reproduced, stored in a retrieval system or transmitted, in any form or by any means, electronic, mechanical, photocopying, recording, or otherwise, without the prior written permission of the author.

To Cor

Table of Contents

INTRODUCTION	1
1.1. Technical advances	2
1.2. Hydrocarbon shortage	3
1.3. Outline of this thesis	4
TIME-LAPSE SEISMIC	7
2.1. Current status	9
2.2. Challenges	10
2.2.1. <i>Link seismic to fluid-flow</i>	<i>11</i>
2.2.2. <i>Include seismic in reservoir engineering</i>	<i>14</i>
RESERVOIR MANAGEMENT	17
3.1. Integration	19
3.2. Upscaling	21
3.3. Reservoir simulator	22
3.4. History matching	24
3.4.1. <i>Parameterisation</i>	<i>26</i>

3.5.	Automated optimisation	28
3.5.1.	<i>Objective function</i>	28
3.5.2.	<i>Optimisation algorithm</i>	30
3.5.3.	<i>Stopping criteria</i>	32
3.6.	Production forecasting	32
3.6.1.	<i>Uncertainty quantification</i>	33
ROCK PHYSICS		35
4.1.	Reservoir parameters	37
4.1.1.	<i>Voigt and Reuss models</i>	38
4.1.2.	<i>Hashin-Shtrikman bounds</i>	39
4.2.	Wave propagation theories	40
4.2.1.	<i>Gassmann equations</i>	40
4.2.2.	<i>Biot's low frequency theory</i>	42
4.3.	Representative laboratory observations	45
4.3.1.	<i>Clay content, porosity, and lithology</i>	45
4.3.2.	<i>Pressure, temperature and saturation</i>	47
4.3.3.	<i>Anisotropy</i>	50
4.3.4.	<i>Attenuation and dispersion</i>	50
4.3.5.	<i>The reliability of core data</i>	52
4.4.	Application	52
SEISMIC MEASUREMENTS		55
5.1.	A structural image	57
5.2.	Inversion to rock properties	61
5.3.	Parameter sensitivity analysis	65
5.3.1.	<i>Water displacement in gas reservoir</i>	65
5.4.	Time-lapse seismic	69
5.4.1.	<i>Repeatability</i>	70
5.4.2.	<i>Seismic reservoir quantification</i>	71
5.4.3.	<i>Vicious circle</i>	74
DIRECTLY LINKING SEISMIC TO FLUID FLOW		77
6.1.	Procedure	79
6.1.1.	<i>Wavelet independency</i>	79
6.1.2.	<i>Frequency domain</i>	81
6.2.	Synthetic reservoir	83

6.2.1.	<i>Amplitude versus saturation</i>	86
6.3.	Results	90
6.3.1.	<i>Average frequency</i>	90
6.3.2.	<i>Resolution</i>	94
6.3.3.	<i>Geological robustness</i>	95
6.3.4.	<i>Repeatability</i>	97
6.3.5.	<i>Extraction time-gate</i>	98
6.4.	Discussion	100

INTEGRATING TIME-LAPSE SEISMIC WITH RESERVOIR ENGINEERING **101**

7.1.	Permeability inversion	103
7.1.1.	<i>Calculation of water cut profiles</i>	103
7.1.2.	<i>The underlying permeability field</i>	106
7.1.3.	<i>Results</i>	107
7.2.	Automated history matching	109
7.2.1.	<i>Objective function</i>	111
7.2.2.	<i>Optimisation</i>	112
7.3.	Geological parameterisation	112
7.3.1.	<i>Synthetic reservoir</i>	114
7.3.2.	<i>Results</i>	116
7.4.	Production forecast uncertainty	120
7.4.1.	<i>Scenario Test Method</i>	121
7.4.2.	<i>Synthetic reservoir</i>	123
7.4.3.	<i>Results</i>	124
7.5.	Seismic data	128
7.5.1.	<i>Noise level</i>	129
7.6.	Considerations	131

STATFJORD CASE STUDY **133**

8.1.	Geology	135
8.1.1.	<i>Stratigraphy</i>	135
8.1.2.	<i>Tectonic evolution</i>	136
8.1.3.	<i>Gravity collapse structures</i>	136
8.2.	Reservoir	138
8.2.1.	<i>Time-lapse seismic</i>	139
8.2.2.	<i>Reservoir model</i>	140
8.3.	Modified Gassmann model	140

8.3.1.	<i>Time-equivalent logs</i>	142
8.4.	Visual inspection of time-lapse seismic	143
8.4.1.	<i>Multi-attribute match</i>	144
8.4.2.	<i>Pattern recognition</i>	146
8.4.3.	<i>Non-repeatable noise</i>	149
8.5.	Saturation inversion	149
8.5.1.	<i>A non-linear approach</i>	149
8.5.2.	<i>A linear approach</i>	155
8.5.3.	<i>Discussion</i>	156
8.6.	Alternative to rock physical modelling	159
8.6.1.	<i>Procedure</i>	161
8.6.2.	<i>Results</i>	162
CONCLUSIONS AND FUTURE WORK		167
9.1.	Conclusions	167
9.2.	Recommendations	169
REFERENCES		171
LIST OF SYMBOLS		185
SUMMARY		189
SAMENVATTING		193
ACKNOWLEDGEMENTS		199
CURRICULUM VITAE		201

Chapter 1

Introduction

The first well in the world has not been drilled to find oil as is often thought, but salt! Salt has been harvested from natural brine pools as early as 6000 BC. It was in 252 BC that Li Bing made the very simple discovery that the natural brine did not originate in the pools but seeped up from underground. He ordered the first well to be drilled (Kurlansky, 2002). These first wells had wide mouths. As the Chinese learned how to drill, the shafts got narrower and the wells deeper. Sometimes the people who dug the wells would inexplicably become weak, get sick, and die. Occasionally, an explosion would kill an entire crew or flames spit out from the bore holes, today attributed to natural gas. The salt workers and their communities believed that an evil spirit from some underworld was rising up through the holes they were digging. Some wells became infamous as sites where the evil spirit emerged. By 100 AD, the well workers understood that the disturbances were caused by an invisible substance. They lit the holes and started placing pots nearby to cook with. Soon they learned to insulate bamboo tubes with mud and brine, and pipe the invisible force to boiling houses. These boiling houses were open sheds where pots of brine cooked until the water evaporated and left salt crystals. By 200 AD, the boiling houses had iron pots heated by gas flames. This is the first known use of natural gas in the world (Kurlansky, 2002).

In 1859, the most important oil well was drilled in northwestern Pennsylvania. It was one of the first successful oil wells drilled for the sole purpose of finding oil. The well is known as the Drake Well, after "Colonel" Edwin Drake, the man responsible for the well. It started an international search for petroleum, and in many ways changed our way of life (Yergin, 1992). McKain (2002) claims the first well was actually drilled as early as the 1820s in West Virginia. Oil drilled from these wells was used as a light source and an industrial lubricant. In fact, McKain claims, the Drake well even used "Pure West Virginia Lubricating Oil" to lubricate its drilling machinery.

For hundreds of years, people had known about oil seeps in western Pennsylvania. As far back as 1410 BC, Native Americans had been harvesting the oil for medicinal purposes by digging small pits around active seeps. European settlers had for years been using the petroleum as a source of lamp fuel and machinery lubrication. Today, the same principle of drilling after hydrocarbon seeps is still used although with more sophisticated tools (Aminzadeh *et al.*, 2002).

1.1. Technical advances

Since the Drake well in 1859, drilling, exploration and production technology has advanced considerably, especially after the introduction of among others rotary drilling, seismic, and computers. Today, drilling is performed with very sophisticated tools, although it is still based on the same technology. Colonel Drake would even now recognise a drilling rig. The modern rig can be considered a computer with a drill attached. It may not be hard to imagine near future instruments, programmed with data and loaded with sensors that could find their way to oil.

The exploration game changed from a "gambling" business into a "high-tech" industry. Nowadays exploration prospects are evaluated using detailed analysis of seismic and well log measurements. The advance of computing technology allows more information to be extracted from increasingly larger data volumes (Rauch, 2001). Geology, the discipline to analyse the subsurface, is the key to developing new prospects, understanding the hydrocarbon system, and for predicting occurrences in commercial quantities. The hammer and magnifying-glass have long been replaced by sophisticated software tools to describe the earth and model geological processes. As technology improved, the number of

dry holes decreased and this trend is continuing to date. For example, the introduction of 3D seismic allowed better imaging of the subsurface.

Production and associated reservoir management has witnessed a similar improvement over the years. In the old days, one preferred to produce as quickly as possible to make a fast return. In the USA, fast production also meant that your neighbour could deplete less from the same reservoir. These days, reservoirs are managed from an economic, political, environmental, and technical perspective. Reservoir management is aided by sophisticated reservoir models which allow analysing the observed behaviour and more importantly, to forecast future production.

1.2. Hydrocarbon shortage

One recurring question is “When do we run out of fossil fuels”? Over the centuries this question has been asked frequently, although related to different fuels. In the Middle Ages, the Dutch thought that the amount of peat would not last for another century. It was decided to impose a tax on peat. At the end of the 18th century, England almost became tree-less, especially after the invention of the steam engine. As a reaction, coal mining experienced a huge increase in activity. At the beginning of the 20th century, coal was replaced by oil. The coal reserves were not exhausted, oil was just cheaper, cleaner, and easier to use. A few decades later, natural gas was introduced as a fuel. Over the years, it has been predicted that oil and gas reserves would not last very long considering the consumption of hydrocarbons. For example, the Club of Rome predicted in 1972 that the reserves would not last more than 20 years. However, the known reserves have only grown since then! History tells us that, each time, before running out of a particular fossil fuel, a new fuel type replaces the old one. The same may happen for oil and gas. Something cheaper and cleaner will come along, and the oil age may end with large amounts of oil left in the ground. Most probably, we will rely on more than one fuel type in the future, fossil fuels as well as renewable energy (Sprangers, 2002).

Intuitively, the hydrocarbon reserves should decrease due to continued increasing consumption. There are several reasons why the known reserves increase rather than decrease. With the help of advanced technology deeper targets can be reached, new frontiers deep offshore can be explored, and from existing fields more hydrocarbons can be produced. Due to the complexity of

the reservoirs, the current average recovery is about 35%. With advanced technology, it should be possible to increase recovery, perhaps to an average of 70% in the future. Moreover, the industry is drilling fewer dry holes. Success rates have risen, even as difficulty increased due to improvements in seismic imaging, which gave geologists a much clearer image of the subsurface. For example, seismic advances have played a large role in giant discoveries as described by Pettingill (2001). Meanwhile, techniques such as directional drilling increased the yield per new well. Thus, due to technical advances the known hydrocarbon reserves increased and will continue to increase for the next few decades, although the earth's supply is limited.

Advances in technology are continuously occurring at several fronts, e.g. the introduction of time-lapse seismic. Time-lapse seismic refers to repeating seismic acquisition over time. It captures the dynamic behaviour of the reservoir and aids reservoir management, allowing to increase recovery. Reservoir management also benefits from advances in e.g. stochastic modelling and uncertainty quantification of the model's production forecast. The implementation of the above mentioned and other new developments requires further improvements as well as new advances in associated disciplines.

1.3. Outline of this thesis

In this thesis, the use of time-lapse seismic data within reservoir engineering is described. The main challenge when linking time-lapse seismic measurements to dynamic reservoir models is expressed as “How to optimally benefit from time-lapse seismic”. The challenge is divided in two main categories as described in Chapter 2. The first is to link the seismic measurement directly to fluid-flow properties. The second is to integrate the time-lapse seismic data into reservoir engineering.

A variety of disciplines is involved. As communication between the different disciplines is important, integration is a key element. Chapter 3 to 5 are introductory chapters to the various disciplines. Chapter 3 describes the discipline of reservoir engineering. Chapter 4 introduces rock physics; explaining the link between reservoir and seismic properties. Seismic measurements, and time-lapse seismic in particular, are explained in Chapter 5. In Chapter 6, the time-lapse seismic measurement is directly linked to the saturation changes in a reservoir. Different ways of integrating time-lapse

seismic with reservoir management are described in Chapter 7. The synthetic model employed in both chapters is modelled after the Statfjord field. In Chapter 8, the Statfjord field is described in detail as well as some specific time-lapse seismic applications. Conclusions and further work are described in the last chapter.

Chapter 2

Time-lapse seismic

Repeatedly acquired seismic is referred to as time-lapse seismic. It is a fairly new technology allowing dynamic characterisation of a reservoir in a true volumetric sense. The basic idea is that a production-induced change in the reservoir causes a change in the seismic signal over time. Often time-lapse 3D seismic is incorrectly referred to as 4D seismic, the fourth dimension being time. Using the same logic, time-lapse 2D seismic would confusingly be referred to as 3D seismic! The essence of time-lapse is looking at differences in order to capture the variation of a system over time. By investigating the difference between multiple seismic surveys, valuable information about changes in the reservoir state can be captured. The reservoir state is characterised by pore (fluid) pressure, temperature, and saturation or pore fluid fill. Currently, the main driver for time-lapse 3D seismic is its capability to indirectly measure the saturation. Knowing the reservoir's saturation distribution and its fluid flow behaviour, adds significant value and reduces risk in reservoir management. Time-lapse seismic contributes significantly to improved well placement and production strategies (Koster *et al.*, 2000).

The arrival of time-lapse seismic data has forced different disciplines to intensify their working relationship in order to optimally benefit from the dynamic information content of the data. These disciplines comprise, but are

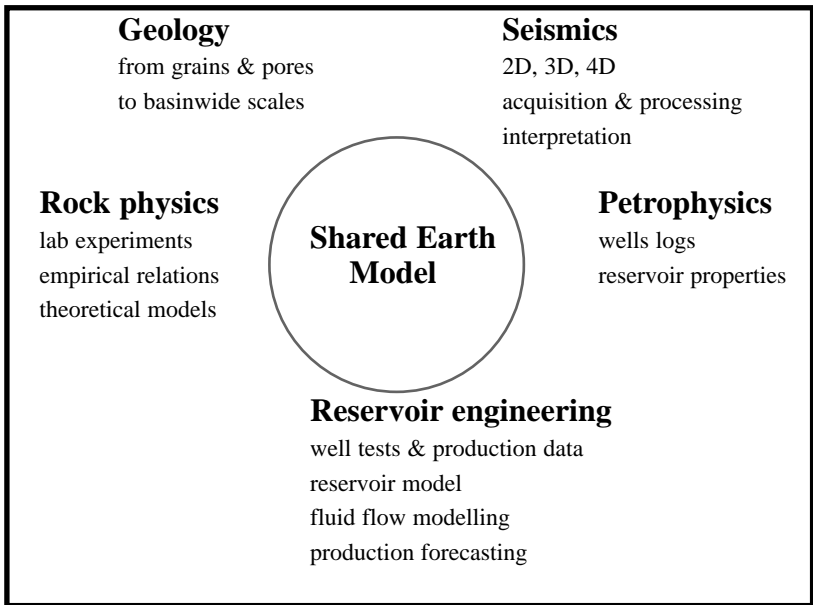


Figure 2.1 Schematic overview of different disciplines and data. In the shared earth model, the different pieces of data are incorporated.

not limited to, geology, petrophysics, rock physics, reservoir engineering, and seismic acquisition and processing (Figure 2.1). To allow communication and integration between disciplines, modifications have to be made within each discipline. Existing theories, algorithms, and models have to be revised or improved to suit time-lapse seismic interpretation. Some are appropriate for 3D data handling, but might not provide the answers for time-lapse seismic. For example, processing of 3D seismic is adapted to include cross-equalisation in order to allow comparison of different time-lapse seismic data sets (Ross *et al.*, 1996). Within rock physics the focus has to be on the combined effect of the changes in the reservoir rather than the effect of a pressure or a saturation change (Wang, 1997). To integrate the huge amount of data and information generated by time-lapse seismic, reservoir engineering practices have to be adapted (Arenas *et al.*, 2001).

2.1. Current status

The technique to infer dynamic reservoir information from time-lapse seismic is still in its infancy. A variety of approaches exists, most of which are case-specific. The methods are result-driven in order to gain quick valuable information regarding the reservoir state e.g. remaining or by-passed oil. There has not been enough time yet to validate all of the methods and justify their use for time-lapse interpretation. Due to the complexity of the problem and diversity of objectives, a single method is probably never developed.

The main purpose of 3D seismic has been to (structurally) image the subsurface. Acquisition and processing techniques have been developed accordingly. With time-lapse 3D seismic, the difference between surveys provides the information regarding the change in the reservoir. Their differences are related to reservoir changes only when the seismic measurements are repeatable. To achieve repeatability, acquisition and processing artefacts have to be eliminated by reproducing the acquisition set-up and re-processing of the seismic surveys, followed by cross-equalisation. The seismic measurement samples the subsurface in three dimensions using acoustic or elastic waves. By using an acquisition set-up similar to the previous seismic survey(s) the reservoir is similarly sampled. Even if vintages are identical, repeatability is a problem, due to variations in acquisition noise or because the environment has changed over time, e.g. when new production facilities were installed. Seismic (re-)processing thus plays a key-role in equalising the responses over the static parts. Cross-equalisation accounts for spatial differences including re-binning, amplitude differences, timing differences, source wavelet differences, etc. (Ross *et al.*, 1996). Besides repeatability, the time-lapse seismic signal has to be detectable above the seismic noise level. The next step is to interpret the time-lapse seismic signal in terms of changes in saturation, pressure, and/or temperature.

Depending on the rock and the reservoir, pressure, saturation, and temperature have different effects on the time-lapse signal. Rock physics plays an important role in describing and explaining how the (time-lapse) seismic signal is physically related to the rock properties and reservoir state. Due to the complexity of the rock, it is extremely difficult to quantitatively model or interpret the time-lapse signal. At the moment, the objective of time-lapse seismic interpretation is mainly to calibrate reservoir models and to extract saturation information. The effects of pressure and temperature on the time-

lapse seismic signal are often neglected. A variety of methods exists to obtain an estimate of the saturation or its change over time, e.g. as shown by Oldenziel *et al.* (2000) and Kvamme *et al.* (2000) on the Statfjord field. Each method involves multiple assumptions. In some methods, logs are modelled to represent the reservoir at the time of seismic acquisition. For that purpose the rock physical and reservoir model are assumed to provide the correct information. For all methods, a one-to-one relation is assumed between the seismic data and the saturation. In general, assumptions introduce bias that may lead to erroneous interpretations, bad reservoir management decisions, and economic miscalculations.

Reservoir management is a complex task that heavily depends on the reservoir simulation model. A reservoir simulation model allows analysing behaviour of the reservoir, but more importantly forecasting future behaviour. Constraining the model to all available information raises confidence in its forecasting capabilities. Time-lapse seismic information has recently been introduced as an additional constraint. Currently, it is mainly used to visually calibrate the reservoir model (Shyeh *et al.*, 1999). A 2D comparison is made on e.g. a saturation map inverted from the time-lapse seismic and a saturation map from the reservoir model. When both maps resemble each other, the reservoir model is considered constrained to the time-lapse seismic data. One can imagine far more sophisticated methods allowing integration of all information offered by time-lapse seismic (Arenas *et al.*, 2001). By integration, the benefit of time-lapse seismic is increased and the 3D character of its information respected. Besides saturation, time-lapse seismic offers additional information, currently often ignored, e.g. geological and pressure information (van Ditzhuijzen *et al.*, 2001).

2.2. Challenges

In general terms, the main challenge in linking time-lapse seismic measurements to dynamic reservoir models can be expressed as “How to benefit optimally from time-lapse seismic”. Achieving this, undoubtedly results in a wider acceptance of time-lapse seismic as a standard technique. The challenge is divided into two main categories (Figure 2.2). The first is to link the seismic measurement directly to fluid-flow properties. The second is to fully integrate the time-lapse seismic data with reservoir engineering.

2.2.1. Link of seismic to fluid-flow

Using 3D seismic, structural and static information about the reservoir is obtained, e.g. lateral extension, thickness, faults, porosity, etc. 3D seismic does not provide dynamic information. Time-lapse seismic, i.e. seismic acquired at different times, measures the changes in the reservoir state. Only recently, time-lapse seismic has been introduced, because repeatability could previously not be achieved. Repeatability indicates whether measurement differences are caused by changes in the system rather than by the measurement itself. To achieve repeatability for seismic measurements, the acquisition and processing artefacts have to be small compared to the seismic changes induced by the changes in the reservoir.

Acquisition and processing of time-lapse seismic is a challenge. For almost all fields, the initial or base 3D survey has been acquired without time-lapse seismic in mind. The technique used to shoot the base survey is outdated compared to the currently available technology, which is used for the repeat

Challenges

Link of time-lapse seismic to reservoir properties	Integrate time-lapse seismic with reservoir engineering
<ul style="list-style-type: none"> 1) Repeatability <ul style="list-style-type: none"> - acquisition - re-processing - cross-equalisation 2) Interpretation <ul style="list-style-type: none"> - rock physics - quantitative applicability - inversion 3) Lack of calibration data <ul style="list-style-type: none"> - validation of different methods 4) Decoupling of properties (e.g. pressure and saturation) 5) Definition of time-lapse attribute 	<ul style="list-style-type: none"> 1) Integration <ul style="list-style-type: none"> - huge amount of data - incommensurable data 2) Quicken integration loop to increase benefit of data 3) Parameterisation 4) Non-uniqueness 5) Automated history matching <ul style="list-style-type: none"> - misfit function - optimisation algorithm - stopping criteria

Figure 2.2 Overview of the main challenges in time-lapse seismic.

survey(s). Even when both base and repeat surveys are shot for time-lapse purpose with identical techniques, the question still needs to be addressed whether to work with the surveys separately or utilise their difference. Reprocessing is required for the latter to ensure the surveys can be compared to each other. Their difference should reflect a change in the measured medium, i.e. the reservoir. Processing and acquisition artefacts, positioning and timing errors, differences in amplitude and energy content, etc. have to be taken care of (Harris and Henry, 1998, Vauthin *et al.*, 1999). Reprocessing both surveys using the same procedure is sub-optimal with regard to imaging each survey. Ideally, two different versions of a survey should exist, one re-processed for time-lapse purposes, the other optimally processed for imaging the reservoir. When subtracting time-lapse surveys, only their differences are interpreted rather than information of the two surveys. For example, the same difference of 100m/s in velocity can have a different meaning when occurring for 3200m/s or 4000m/s.

Special reprocessing to preserve a certain time-lapse seismic character, which could be lost during regular 3D processing, might provide an answer. At the moment, these 4D attributes are not well defined. They have to be defined such that they can be linked directly to fluid flow properties. Only with such attributes is it possible to test whether a one-to-one relation exists between seismic and fluid flow characteristics.

The main deliverable and one of the main challenges of time-lapse seismic is to interpret the seismic in terms of reservoir or fluid flow properties. The end users, e.g. reservoir engineers, are not used to handling the seismic signal directly. The time-lapse seismic signal is induced by one or more changes in the reservoir state. Each of these production-induced changes can have a different effect on the seismic signal (Batzle *et al.*, 1998). Decoupling of these effects is crucial and quantification of the reservoir changes a major challenge. The properties with the greatest impact on seismic are pore fluid-fill and effective pressure. Temperature is of interest when large temperature differences are observed e.g. for steam injection or near (cold) water injectors (Ecker *et al.*, 1999). Other reservoir properties may fluctuate over time, e.g. porosity, but in general these effects are small on time-lapse seismic. Obviously there are always exceptions such as the change in porosity and rock structure in less consolidated reservoirs (Minkoff *et al.*, 1999).

Obstacles have to be overcome when interpreting the time-lapse seismic signal in terms of the above described reservoir properties. Rock physics and petrophysics try to overcome one, i.e. explaining the actual relation between

both sets of properties, but are not always successful (Wang, 2000a). Rock physics is mainly based on models describing laboratory experiments or empirical relations. It does not describe the complex physics in case a rock is excited by a seismic wave. Each rock is different in texture on the smallest scale, which determines the actual behaviour for the rock as a whole. The pore fluids contribute on top of this. To simplify matters and because the seismic measurements are on a larger scale than microscopic level, the rock is often described as an effective medium within the realm of rock physics.

Rock physical models describe how reservoir parameters relate to elastic properties. The elastic properties comprise density and the elastic moduli; shear and bulk modulus. For example, a change in effective pressure affects the bulk and shear modulus, whereas a change in pore fluid-fill affects the bulk modulus and density. The elastic properties of a rock determine its P-wave velocity and S-wave velocity, both of which can be measured in the field. The P-wave velocity is determined by all three elastic properties. The S-wave velocity is determined from density and shear modulus. As a result, the S-wave velocity is insensitive to the fluid except for a small contribution of the density. In case both pressure and saturation change due to production, their effects in the seismic signal can only be decoupled if both elastic moduli and density are known. It is common in seismic acquisition to measure only the P-wave. This does not allow determining the three elastic properties uniquely. By performing Amplitude versus Offset (AVO) analysis it is possible to perform a unique P-wave inversion under the assumption that one elastic property is constant (Gray *et al.*, 1999). AVO behaviour contains indirect information on the S-wave, as conversion from P-to-S wave, occurring at angles different than 0, varies with offset. It does not always allow gaining proper S-wave information. In general it is better to record the actual S-wave. For marine S-wave acquisition, geophones have to be placed at the ocean bottom, because the S-wave does not travel through fluids.

The ultimate objective is to link the time-lapse seismic directly to fluid flow. At the moment, no evidence is available that such a direct relation exists. Nevertheless, the relation is often assumed in order to allow gaining information on the reservoir state from time-lapse seismic, thereby introducing a bias. Its impact is often neglected when analysing the information gained from time-lapse seismic, e.g. an up-to-date saturation distribution of the reservoir and information on remaining oil.

2.2.2. Include seismic in reservoir engineering

The objective of reservoir management is to produce each reservoir optimally according to economic, political, technical, and environmental constraints. Reservoir management is a complex task heavily depending on the reservoir model. This reservoir model allows analysing behaviour of the reservoir, but more importantly to forecast future production behaviour. Building the reservoir model is initiated when the first data on the reservoir becomes available and continues as long as additional data is gained during production. The reservoir model is continuously updated to match the observed behaviour. At the least, the reservoir model has to correspond to the historical behaviour of the actual reservoir, before one may trust production forecasts and handle accordingly. Other factors also influence the reliability of the forecast, e.g. the choice of fluid flow simulation algorithm, initial model, and parameterisation (Floris *et al.*, 2001).

Until recently, the reservoir behaviour has only been monitored at the wells via production rates and well tests. Since the introduction of time-lapse seismic, the reservoir state or its change over time can be indirectly measured. Thus, time-lapse seismic may serve as an additional constraint for the reservoir model. Assuming that time-lapse seismic signals can be interpreted in terms of reservoir properties, two challenges remain. To benefit from all the information, including its 3D character, large amounts of data have to be incorporated. Furthermore, the time-lapse seismic information has to be integrated with production and other available data. A complicating factor is that the information provided by time-lapse seismic is indirect and incommensurable with respect to other data.

A reservoir model has to be constrained to the observed static and dynamic data. Static data comprise core data, logs, geological data, etc. Dynamic or historical data comprise production, well test, and time-lapse seismic data. The reservoir model is often constrained directly to the static data. Constraining the reservoir model to the historical data is performed indirectly. This inversion process is referred to as history matching. During history matching the objective is to obtain a better match between modelled and observed data by iteratively perturbing model parameters. The quality of the fit between reservoir model and actual reservoir is determined visually or described with an objective function, most often a sum-of-squares function. History matching is most often performed manually and can be labour-intensive. Abundant experience is available on how to obtain a better fit for the production and well test data. With

regard to time-lapse seismic data, a trial-and-error approach is used as experience is lacking.

In theory, all reservoir model parameters can be perturbed during history matching, which would result in an unmanageable large parameter space. In practice, the parameter space is decreased by sampling, i.e. by choosing only a few parameters for history matching. This process is referred to as parameterisation and is usually based on reservoir engineering judgement. The parameter set can be quite limited and biased, affecting the type and quality of reservoir model that is obtained. With time-lapse seismic, different history matching parameters might be introduced and chosen in a more sophisticated manner.

During history matching, the structural and geological input to the reservoir model is kept fixed. Given time-lapse seismic, this procedure might be altered. Time-lapse seismic provides a second image of the same subsurface, most often an enhanced image as seismic acquisition and processing techniques have improved over time. The new information either confirms or causes to revise the original geological model. Moreover, the dynamic content of time-lapse seismic provides additional information on structural, geological, and sedimentological characteristics. One can think of the sealing capacity of faults (Oldenziel *et al.*, 2002) and a preferred fluid flow direction dictated by a sedimentation direction or geological bodies (van Soest, 2001). To incorporate the above-mentioned information, a wider range of history matching parameters is required spanning structural and geological properties besides the standard reservoir properties.

The actual integration of the different data sources at hand occurs at two places within reservoir simulation; first when developing the initial reservoir model, and secondly during history matching. For the latter, the integration takes place in the objective function, or misfit function, between the actual reservoir and the model. Different forms of the objective function can be chosen, but in each the integration is performed likewise. The objective function can consist of different sub-functions, e.g. a production term, a seismic term and a geological term. Every data type in any of the terms is corrected for its variance as well as for the number of data points. This ensures that all data is handled equally. Moreover, each term can be weighted allowing confidence information to be incorporated, e.g. one may put more emphasis on production than on seismic data. The geological term is usually in the form of a penalty function; when the updated model drifts too far from the assumed geology, the misfit function is increased rather than decreased (Bissell *et al.*, 1997).

The history matching procedure is non-unique, i.e. more than one set of model parameters corresponds to the observed data. Nevertheless, often a single deterministic model is constructed as the representation of the actual reservoir. In practice, constructing multiple models is impeded, because history matching is labour intensive and computer power might be limited. A semi-automated procedure speeds up the history matching process. It allows for construction of multiple reservoir models. By analysing multiple models, the non-uniqueness of the history matching procedure can be taken into account. Within the automated procedure, integration of the huge amounts of time-lapse seismic data is also facilitated. Currently, it may take up to a year before time-lapse seismic information is actually integrated with reservoir engineering. The benefit and information content of time-lapse seismic information is much higher when it could be made available in a shorter time span.

Chapter 3

Reservoir management

The challenge of reservoir management is to produce each reservoir optimally according to economic, political, technical, and environmental constraints. Reservoir management is therefore a complex task, which depends heavily on the reservoir simulation model. A reservoir simulation model allows analysing behaviour of the reservoir, but more importantly to forecast future behaviour. Building the reservoir model starts when the first reservoir data becomes available and continues during production as additional data is acquired. The model is continuously updated to fit the observed behaviour. Only when the model fits the historical behaviour of the actual reservoir, one may trust production forecasts and manage the reservoir accordingly.

Before start of production, only static data is available comprising geology of the area, knowledge from surrounding fields, seismic data, and well data from exploration wells. Based on the static data, a detailed geological model is constructed for the reservoir at hand. The seismic data is used to delineate the subsurface structure including the reservoir. In exploration and appraisal wells, logs and core samples are acquired. Log data and laboratory tests on cores reveal detailed information about the reservoir lithologies and properties. Integration of all different sorts of data is an important part in construction of the geological model.

The geological model is too small-scaled to allow fluid-flow simulation; it needs to be upscaled (Section 3.2). Often, the upscaled version, or initial reservoir model, does not directly fit the observed historical behaviour of the reservoir, since fluid flow characteristics are not necessarily incorporated in the geological model. The reservoir simulation model comprises these fluid flow characteristics. To fit the observed behaviour or dynamic data, the reservoir simulation model parameters are perturbed. This process is referred to as history matching. The reservoir simulation model is defined by a large set of parameters, some of which are specified for each grid block, others apply to the entire model. Perturbing all parameters involved is not feasible from a computational perspective. Moreover, the amount of data is insufficient to justify resolving all parameters. In other words, the problem is under-determined; more than one combination of parameters fits the observed data. The parameter space has to be reduced by defining only a few parameters to be perturbed. This process, referred to as parameterisation, can be performed using different approaches and is based on experience or uncertainty and sensitivity analysis of the parameters. Parameterisation affects the type and quality of the solution that is obtained by history matching.

History matching is an optimisation process, which is performed manually or in an automated fashion (Section 3.4 and 3.5). For the latter, an optimisation algorithm is used to find the parameter set that best fits the observed data. Depending on the type of problem, different optimisers can be used. All try to minimise the misfit between the modelled and observed data to find the best fitting parameter set. A stopping criterion is used to define when the history matching process can be terminated. The objective of stopping criteria is to ensure that the proper parameter combination(s) is (are) found given the data available.

The main purpose of a reservoir model is to predict future behaviour of the reservoir and to analyse the effect of reservoir management decisions. The forecasts are based on the reservoir model that best fits the observed static and dynamic data. An important issue is the quantification of the uncertainty of the production forecast (Section 3.6). The uncertainty is related to the measurement error and information content of the data, parameterisation, upscaling, type of reservoir simulation model, and history matching process.

3.1. Integration

Within reservoir management, integration is considered a crucial element. It plays a vital role when constructing the fine-scaled geological model as well as when history matching the upscaled reservoir model. A variety of data types differing in accuracy, resolution, and conditioning volume have to be integrated (Figure 3.1). Before start of production, information is obtained about the static characteristics of the reservoir. The static data comprises seismic data, well data, core data, geology of the area, knowledge from surrounding fields, etc. The acquired seismic provides regional information on geology and the structure of the reservoir. Using 2D seismic, one has to be aware that apparent dips of layers and faults are measured rather than the true dip and azimuth. Exploration wells are drilled to assess the hydrocarbon potential and measure reservoir properties. Often core samples are taken in the borehole. Both well logs and core samples yield detailed information (1D) on the reservoir properties, e.g. porosity, net-over-gross, thickness, permeability, tortuosity, wettability, etc. The interpolation between the wells of this information is tackled using geological, geo-statistical or physical principles. The hydrocarbon potential of the reservoir is estimated based on the (interpolated) well information and the lateral extent of the reservoir derived from seismic. If the results are promising, appraisal wells are drilled to further assess the quality, distribution, and extent of the reservoir.

As soon as production commences, dynamic data is acquired. Production and time-lapse seismic data are examples of dynamic data. Both provide information about the dynamic characteristics of the reservoir. The former comprises well tests, production logging tests, and production history. Well tests or pressure transient tests are carried out to assess the fluid flow performance of the well. The pressure behaviour in a well is observed during a few hours or days of production. Valuable information is deduced on permeability, wellbore skin and flow barriers, e.g. sealing faults and reservoir boundaries. The wellbore skin quantifies how production is impeded by the well bore damage due to drilling activities. The accuracy and resolution of well tests are reasonably good. The conditioning volume depends on the duration of the well test. If the well tests are favourable, the reservoir is produced. Over the life of a field, the production is monitored by measuring e.g. cumulative oil production, or Gas Oil Ratio (GOR). The production history yields indirect information on the reservoir. As time increases, the measurement volume increases.

In addition to production data, time-lapse seismic data is classified as dynamic data. Time-lapse, or 4D, seismic refers to repeatedly acquired 3D seismic. The basic idea is that a change in the reservoir state due to production induces a change in the seismic signal over time. The actual interpretation of the time-lapse seismic is often rather complex, see Chapter 5 for a detailed explanation. Information that in principle can be inferred from time-lapse seismic comprises change in saturation, pressure anomalies, etc. Similar to 3D seismic, its conditioning volume is large but resolution and accuracy are low.

When integrating the different types of data, special care has to be taken to respect their specific characteristics. Every piece of data contains valuable information and deserves to be incorporated when constructing a geological model. Consistency between the data has to be checked and guaranteed. Integration is considered a multi-disciplinary discipline. Best practice is to construct a shared earth model incorporating all available data.

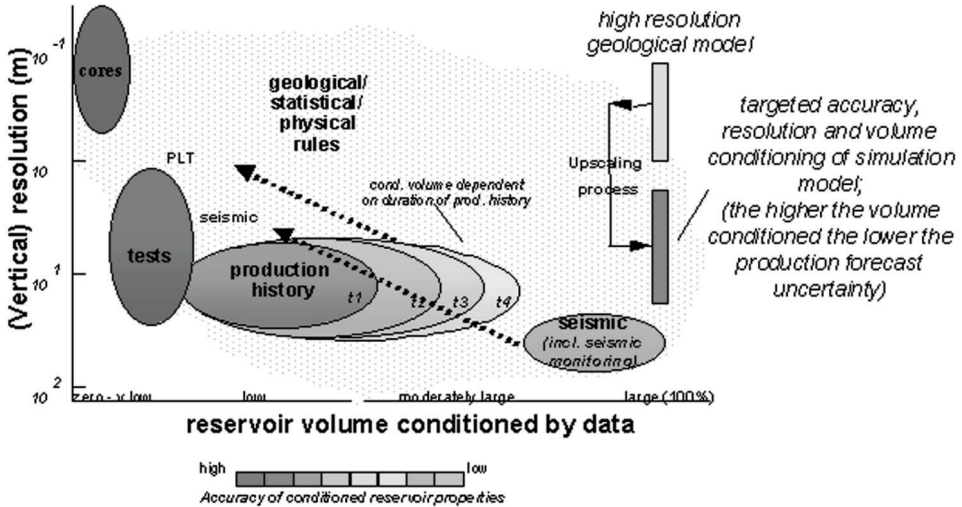


Figure 3.1 Diagram illustrating different data types according to resolution, accuracy, and measurement volume after Bos and van Kruijsdijk (1995).

3.2. Upscaling

The data describing the reservoir differs in resolution and measurement volume. When building a model, either geological or reservoir, a choice has to be made at which scale the model is to be constructed. An option is to construct a model at the finest scale, i.e. core scale. It is simple to incorporate all the fine scale data in this model. Coarse scale data is incorporated by constraining averages of the fine scale grid blocks to the coarser scale data. For fluid flow simulation it is not feasible to use such a fine-scaled model. It would require large memory and long processing time. In addition, history matching would be a daunting challenge if not impossible. For simulation purposes, a coarse scale model has to be constructed (Figure 3.2).

The construction of the coarse scale model involves re-gridding or up-gridding. The lateral distribution of the grid blocks has to be designed, as well as their thickness. When designing the coarse grid, structural features such as faults and

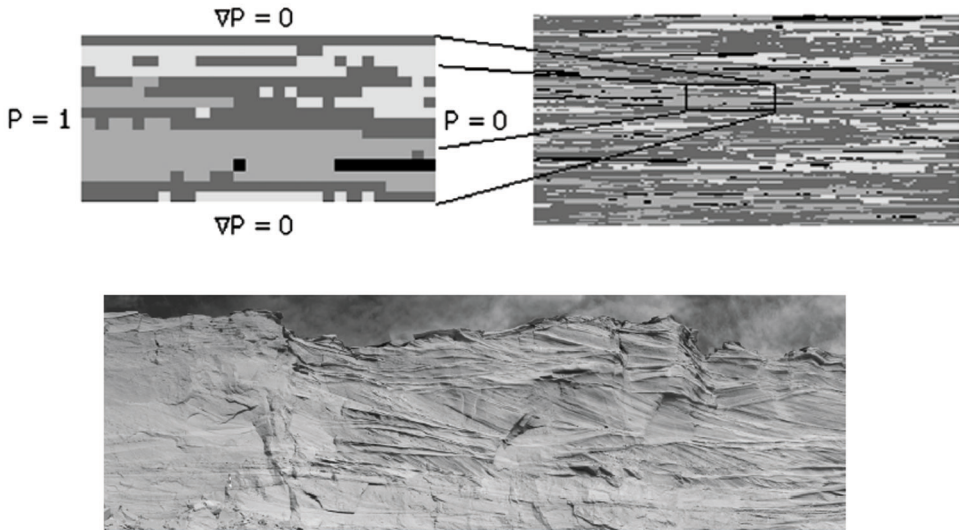


Figure 3.2 Schematic illustration (top) of flow-based upscaling for single-phase flow to obtain the effective permeability of the coarse cell (from Christie, 2001). The fine scale model itself is an upscaled representation of the geology (bottom), an aeolian outcrop (courtesy C.Y. Hern & Genetic Units Project, Heriot-Watt University).

horizons are honoured as well as the coarse characteristics of the geological model. To that effect, choices are made about the co-ordinate system, orientation, block geometry, local grid refinement, etc.

The grid blocks are generally in the order of few tens to hundreds of meters in the x and y direction. The thickness of the grid blocks is often much smaller, 10 to 20m. The coarse fluid flow model has to honour the behaviour at the pore-scale. Upscaling allows working with larger grid blocks, while the model still reflects the behaviour of the fine-scale model. By upscaling, the fine-scale data, such as obtained from core plugs and logs, is incorporated. For most properties assigned to the fine scale grid blocks, arithmetic, geometric or harmonic averages are used to calculate the effective property of the coarse grid block. For example, porosity is easily calculated from a collection of fine-scale blocks. However, for certain properties upscaling is complex, e.g. permeability, relative permeability, and capillary pressure vs. saturation curves. For these type of properties, one cannot simply average to obtain the effective properties of the coarse grid block.

A variety of different upscaling techniques exists. Christie (2001) gives an excellent overview that includes the latest developments. Using single-phase upscaling techniques, an effective permeability is obtained to reproduce the fine scale behaviour (Renard and de Marisly, 1997). The available techniques comprise among others, arithmetic and harmonic means, power law averaging, and flow-based methods. Using two-phase upscaling techniques, an upscaled relative permeability or pseudo-relative permeability curve is obtained. Two-phase upscaling techniques comprise steady-state (Pickup *et al.*, 2000) and dynamic methods (Barker and Dupouy, 1999, King *et al.*, 1993). The techniques have been shown to be successful for a range of problems. However, there are still many unresolved issues (Christie, 2001): the choice of correct boundary conditions, grouping of upscaled relative permeabilities, robustness, and process independence.

3.3. Reservoir simulator

Four basic oil recovery mechanisms can be identified: fluid expansion, displacement, gravity drainage, and capillary imbibition. When pressure declines, fluid expands inducing flow through the porous rock to the production wells. Displacement occurs due to injected gas or water. A natural water drive

from a nearby aquifer can also stimulate oil production. Due to the density difference, oil recovery is aided from below by an advancing bottom-water drive and/or from above by a declining gas-oil contact. Imbibition can be an important mechanism in lateral water floods in heterogeneous sands with large vertical permeability variation.

An oil and/or gas field is only produced once, whereas a reservoir model allows production being simulated many times at a low cost and in a short period of time. Observation of the model performance under different producing conditions helps selecting the optimal production scenario for the field. An appropriate reservoir simulator is selected depending on the objectives and the field, i.e. type of reservoir and production mechanism. Each simulator is a set of equations describing the physical processes occurring in the field. In general, the reservoir is subdivided into grid blocks for simulation purposes. For each grid block the simulator calculates the volumetric material balance for each phase. A detailed description of the simulators is not given, but can be found in Odeh (1969). Odeh gives an excellent description of the conceptual simplicity of a simulation model. A variety of simulators are available ranging from black oil to compositional simulators and from streamline simulators to finite element methods. The black oil simulator is most commonly used and accounts for the basic mechanisms in simulation. This isothermal model applies to reservoirs containing immiscible water, oil, and gas phases with simple pressure-dependent solubility of the gas component in the oil phase.

The simulation model equations express conservation of mass of each reservoir fluid component for each grid block. Within each grid block, reservoir properties and fluid properties are assumed constant. Fluid properties for each grid block vary with time due to production. The phase flow rates between each grid block and its adjacent blocks are represented by Darcy's law modified by the relative permeability concept

$$u = -\kappa \frac{k_{r,a}}{\eta} \Delta P \quad , \quad 3.1$$

where u is fluid flow velocity, κ is total permeability, $k_{r,a}$ is relative permeability for phase a , η is viscosity, and P is pressure.

Inputs to the reservoir model are geometry, grid size specifications, properties per grid block (permeability, porosity, elevation, etc.), relative permeability and capillary pressure vs. saturation curves, fluid properties (formation volume factors, viscosities, etc.), well locations, perforated intervals, production indices, and production/injection rate schedule or pressure. The output consists

of spatial distribution of saturation, fluid pressure, and composition, and at the wells the production behaviour. Figure 3.3 illustrates this schematically.

3.4. History matching

The initial reservoir model is constructed from the geological model. The reservoir model is an upscaled version of the geological model, as the latter is too fine-scaled to allow feasible fluid flow simulation. The fluid flow behaviour of the initial reservoir model does not directly fit the observed dynamic data, since the geological model does not necessarily take fluid flow characteristics into account. The reservoir model has to be constrained to the observed historical data either manually or in an automated fashion. The observed historical data comprises well tests, production data measured at the wells, and time-lapse seismic data.

Fluid flow is simulated for the reservoir model and a comparison is made between the simulated production behaviour and the observed behaviour. When the misfit is smaller than a chosen criterion, the reservoir model is said to be history matched. Otherwise, reservoir parameters are perturbed until agreement between modelled and observed behaviour is reached. This inversion process, often referred to as history matching, involves several important steps (Figure

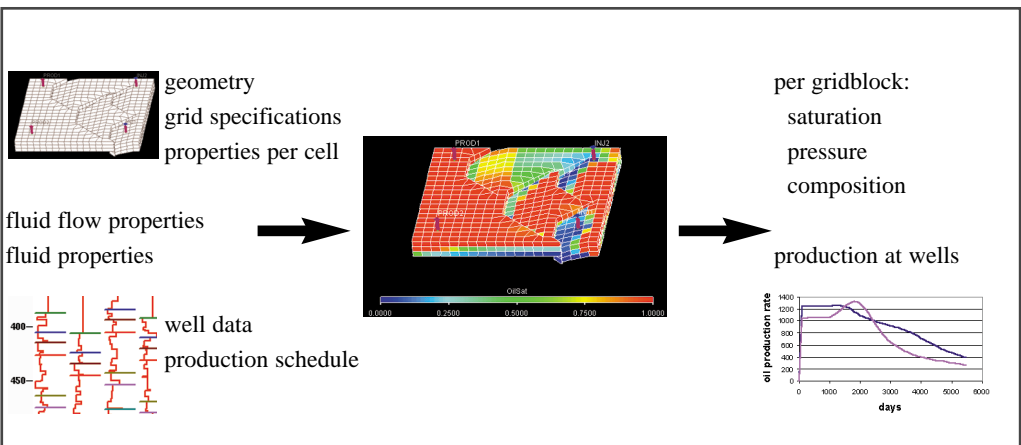


Figure 3.3 Schematic illustration of input and output of reservoir model.

3.4). First, the inversion parameters are chosen. Second, the misfit function is defined quantifying the disagreement between modelled response and actual measurements. This function allows ranking of the different realisations during the inversion and guides the inversion. Given the inversion parameters, the question remains how to perturb the parameters. This is based on the reservoir engineer's experience or determined by an optimisation algorithm. Last but not least, a criterion is chosen to define when agreement between observed and modelled data is reached. When this stopping criterion is reached, the iterative history matching loop is terminated.

History matching is often performed manually by the reservoir engineer. In most cases, only production and well test data are available to constrain the reservoir model. For decades, models have been matched to production data and abundant experience is available. Using this experience and rules-of-thumb, the reservoir model is perturbed to fit the observed data. Typical inversion parameters are layer thickness, porosity, permeability, capillary pressure-saturation curves and relative permeability curves. Varying thickness and porosity affects the total amount of hydrocarbon volume in the reservoir. Perturbing (relative) permeability and capillary pressure characteristics directly influences fluid flow.

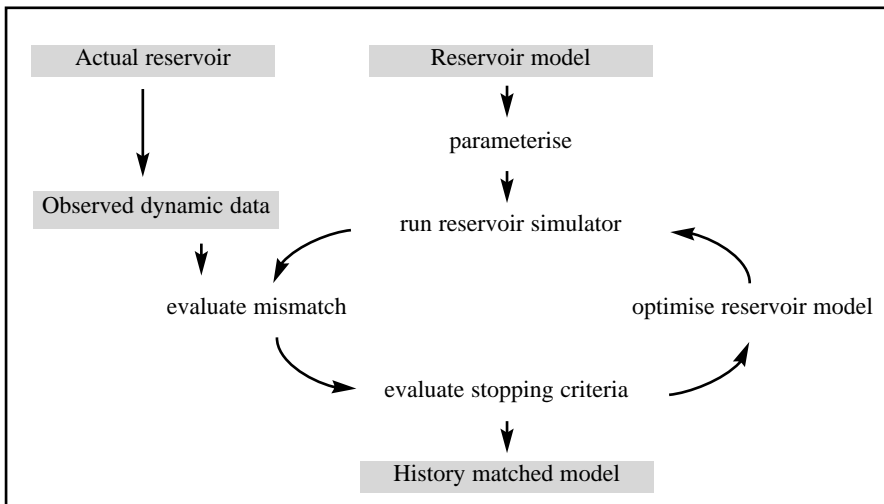


Figure 3.4 Schematic overview of history matching loop.

With the introduction of time-lapse seismic as additional constraint, history matching enters a different league. A huge amount of data has to be incorporated, whereby the 3D character has to be respected to optimally benefit from the data. Using time-lapse seismic derived information requires a different attitude towards history matching. There is no experience as to which parameters are selected as history matching parameters in order to obtain a fit to both observed production and time-lapse seismic data.

3.4.1. Parameterisation

Parameterisation is a crucial step in the history matching procedure. The number of parameters that can be estimated or inverted using history matching is limited. The reservoir simulation model is defined by a large set of parameters, some of which are specified for each grid block, others apply to the entire model. Perturbing all parameters is not feasible from a computational perspective. Moreover, the amount of observed data is insufficient to justify resolving all parameters. In other words, the problem is under-determined, since more than one combination of parameters fits the observed data. The parameter space has to be reduced by defining only a few parameters to be perturbed. The selection of these inversion parameters has to be limited to those parameters that have a first order impact on the reservoir performance. The selection of these parameters is often based on the reservoir engineer's experience. A formal way of selecting does not exist and bias is usually introduced. Parameters with a high degree of uncertainty should be selected. For example, the porosity near a well should not be selected, as it is already known within a few tenths of a percentage. Moreover, the reservoir performance should be sensitive to the inversion parameters. A sensitivity and uncertainty analysis is often a prerequisite if the inversion parameters are selected in an automated manner. Non-uniqueness also has to be taken into account when selecting the parameters. There are always several unrelated scenarios all of which lead to a solution of the problem. Improper selection of the inversion or history matching parameters thus impacts the obtained solution.

One has to keep in mind that the purpose of the reservoir model is to forecast future production. It makes sense to include parameters to which the forecast is sensitive or believed to be sensitive. However, the history match may be insensitive to these parameters. It requires a thorough integration of the geological and reservoir engineering disciplines.

The observed production behaviour may be insensitive to certain parameters. As a result, the uncertainty of these parameters cannot be reduced by history matching to production data. Consider, for example, a region where little flow has occurred. One can take any permeability value in this region and still obtain a good history match. To solve this problem, one can gather other data or wait until flow occurs in this region. In some cases, it might be a combination of parameters expressing insensitivity, referred to as correlated parameters. A modification in one parameter is compensated for by a modification of the other parameter. A remedy is to group them together or gather more data.

Two approaches for parameterisation are widely used, voxel modelling and object modelling. Using the former approach, the history matching parameters may have a different value in each voxel, i.e. grid block. In a typical reservoir model it is not feasible to determine the values in every grid block. Fewer grid blocks in critical locations are generally selected for perturbation. An example of this approach is the pilot point method as described by Bissell *et al.* (1997) and Ramarao *et al.* (1995). Object modelling provides an alternative to voxel modelling. The properties (permeability etc.) of each grid block are a function of a set of parameters, which describe an object. Objects may include geological objects such as channels, faults, fractures, and sand bodies. Using object modelling large-scale geological information in the history matched model is preserved. For example, with only a few parameters the shape and properties of a channel can be described (Bissell, 1994). The *gradzone* method is an example of object modelling, where grid blocks are grouped to reduce the number of parameters. To each group either one constant value is assigned for each property or a multiplier is assigned per property, e.g. a pore volume multiplier. In the latter case, the grid blocks in one gradzone can have different pore volume values but their values relative to each other remain constant as the multiplier is perturbed.

Quite often, the structural properties of the model remains fixed during history matching. For several reasons, one might choose a different approach. The geological model is based on limited data, while more and higher quality data is acquired over the years yielding additional information about the structure. Time-lapse seismic indirectly measures information regarding structural properties, such as location of (unknown) faults and their sealing capacity (Lumley *et al.*, 1999).

3.5. Automated optimisation

The history to automated history matching has been full of failed attempts, since it is difficult to develop a robust procedure. Nevertheless, it will become standard technology in the near future for several reasons. Computers are getting faster and data storage is becoming cheaper. With an automated procedure it is feasible to construct multiple models and analyse the associated uncertainty rather than work with one deterministic model. Constraining the different models to the observed data is labour intensive unless (semi)-automated procedures are introduced. In the future, more time-lapse seismic surveys will be acquired. To optimally benefit from the information, time-lapse seismic has to be truly integrated and its 3D character respected. To handle and constrain the model(s) to the large amount of seismic data, computer power is required.

Reservoir engineering knowledge has to be transferred to rules, which are to be used in the automated procedure. These rules have to co-exist with mathematical algorithms. A mathematical solution to the history matching problem can be a non-physical model, which is significantly different from the input model. Key challenges are how to define the misfit function between modelled and observed data, how to parameterise the model, how to optimise the inversion parameters, and when to stop the iteration procedure.

3.5.1. Objective function

A misfit function is defined to quantify the mismatch between the modelled and observed production behaviour. The misfit or objective function allows the ranking of different model realisations. Moreover, in automated history matching the misfit function is used by the optimisation algorithm to determine how to perturb the inversion parameters. During subsequent iterations, the objective is to minimise the misfit function. The objective function can also be used as a stopping criterion. When its value becomes less than a predefined (small) number, the reservoir model is considered to be history matched.

Several types of objective functions exist, but the most commonly used is the sum-of-squares objective function. It calculates the sum of the squares of the differences between modelled and observed data. A residual, res , is defined to be the difference between the modelled and observed value of an observable

quantity, such as bottom-hole pressure (bhp), water cut or gas-oil-ratio

$$res_{bhp} = bhp(\text{measured}) - bhp(\text{calculated}).$$

The objective function includes the residual for a variety of variables. These variables are chosen by the reservoir engineer and comprise production and/or time-lapse seismic data (Huang *et al.*, 1997). Production data is available for all wells and measured frequently. Time-lapse seismic is areally densely distributed and often only available at a limited number of time steps. With the objective function a comparison is made between two history matches in a quantitative way by means of a single number. For example, for matching bottom-hole pressure and water cut simultaneously, the objective function is

$$X^2 = w_1 \sum_j \sum_i \frac{res_{bhp}^2(i, j)}{\sigma_{bhp}^2} + w_2 \sum_j \sum_i \frac{res_{wcut}^2(i, j)}{\sigma_{wcut}^2}, \quad 3.2$$

where j is an index running over the number of wells, i is the index over the measurements for each well, w_1 and w_2 are weighting factors, and the different σ 's denote a normalisation factor expressing the data accuracy or information content for a given observable variable.

The objective function is not limited to quantifying differences between dynamic data. It can also be extended to include terms for quantifying differences in several other types of data such as: (1) a priori geological knowledge (Bissell *et al.*, 1997, Wences *et al.*, 1998) and (2) the shape, or trend, of a data set (Monico, 1998). The inclusion of geological knowledge and data-trends in the objective function is a way of constraining the models produced by history matching. They provide a way of achieving algorithmic uniqueness by providing plausibility criteria (Xue and Datta-Gupta, 1997). Plausibility criteria are defined in different ways such as: smoothness of the solution, lower and upper bounds, or distance from prior appropriate estimates of the solution. Without such plausibility criteria, the solution of the inverse problem could fit the data very well, but might be physically meaningless. Therefore, the predictive power of the model could be inferior to that of a less well-calibrated model that is closer to physical reality.

To each of the components in the objective function, X^2 , an arbitrary weighting factor can be assigned expressing the relative confidence. In addition, if it is known that the conditioning data depend on each another, covariance matrices can be included to describe the interdependence between the data sets.

Assuming that the conditioning data sets are independent of one another, the objective function can be expressed as

$$X^2 = w_1 X_{well}^2 + w_2 X_{seis}^2 + w_3 X_{geol}^2 + w_4 X_{shape}^2, \quad 3.3$$

where, X_{well}^2 quantifies the misfit between the modelled and observed well data, X_{seis}^2 quantifies the misfit between the modelled and observed seismic data, X_{geol}^2 quantifies the difference between the expected value (mean) of a given history matching parameter and the value in the model, and X_{shape}^2 quantifies the difference in the shape between the modelled and observed data set. The more information is added to the objective function, the better the history match that is obtained. Every piece of additional conditioning data reduces the non-uniqueness inherently associated with the inverse problem of history matching.

3.5.2. Optimisation algorithm

In the automated history matching procedure, an optimisation algorithm is employed to find the optimal solution. The optimal solution is a combination of parameters, or set thereof, that best fit the observed dynamic data, i.e. exhibit the smallest misfit. The optimisation algorithm tries to find this minimum in the misfit or objective function. Optimisation algorithms can be divided into two groups according to the type of objective function and amount of noise they can handle. Global optimisers are capable of handling multi-modal functions and are better able to handle noise on the objective function. They generally succeed reaching the global minimum. However, they require a large number of function calls. Especially within reservoir engineering this is considered a drawback, because a single simulation easily takes a few hours. Efficient sampling of the parameter space may provide a solution. Local optimisers such as a gradient optimiser are not very well suited to handle noisy objective functions and tend to get stuck in a local optimum. A gradient optimiser is capable of handling a certain amount of noise as long as large steps can be taken to calculate the gradient. Near the solution the increments to calculate the gradients have to be small and the algorithm is affected by the noise.

The type of optimiser to be used is problem specific. Not only is the type of objective function an issue, also the amount of parameters and run time of the simulation model affect the choice. A method used by many scientists due to its simplicity is the steepest descent technique (Fletcher, 1987). It is known for its robustness, but its performance deteriorates as the solution is approached. More

advanced methods require that the objective of misfit function is twice differentiable. The Gauss-Newton method is widely applied and uses an approximation of the second order derivative (Fletcher, 1987). In the final phase the inversion is highly efficient. For highly non-linear problems or if the initial guess is far from the solution, the algorithm may become unstable. The Levenberg-Marquardt method (Levenberg, 1944, Marquardt, 1963) introduces a regularisation term to overcome this problem. It can be regarded as a hybrid between the steepest descent method (away from the solution) and Gauss-Newton (when the solution is approached). The difficulty is to update the Marquardt parameter, which is often based on empirical criteria. The Fletcher-Powell method (Powell, 1971) is also a hybrid between steepest descent and Gauss-Newton, but an improvement over the Levenberg-Marquardt algorithm.

All methods discussed above are local optimisers. Global optimisers are able to find the global optimum, but in general require a large number of function calls. Only when the number of iterations can be kept low, are these methods regarded as an alternative to local optimisers. The parameter space has to be sampled efficiently. Global optimisation algorithms comprise simulated annealing and genetic algorithms. Genetic algorithms solve complex problems by emulating principles of biological evolution: the survival of the fittest (Goldberg, 1989). A genetic algorithm comprises an initial population of individuals, each member represented by a binary string within computer memory. These strings represent chromosomes and contain the genes describing individual members of the population. A quality of fitness (objective function) is determined for each individual chromosome. The quality of fitness is used to determine the probability that an individual is permitted to reproduce. Breeding occurs by exchanging substrings of genes between parents creating a new population. Over many generations, the population steadily increases in overall fitness. Many variations of this algorithm have been applied with different strategies for selection, crossover, and mutation.

Simulated annealing is a generalisation of a Monte Carlo method for examining the equations of state and frozen states of n-body systems (Metropolis *et al.*, 1953). The concept is based on how liquids freeze or metals recrystallise in the process of annealing. In this process a disordered melt, initially at high temperature, is slowly cooled such that the system is approximately in thermodynamic equilibrium at any time. As cooling proceeds, the system becomes more ordered and finally approaches a “frozen” ground state. The process can be thought of as an adiabatic approach to the lowest energy state. If the initial temperature of the system is too low or cooling is proceeded too quickly, the system may become quenched, forming defects or freezing out in metastable states. This corresponds to being trapped in a local minimum energy state.

3.5.3. Stopping criteria

When does a model fit the observed data, or, in other words, when is it possible to stop the automated history matching process? The definition of an appropriate stopping criterion is complex and problem specific. One can choose to stop optimisation when the modelled data is within a certain range of the observed data, e.g. within 1% of the bottom hole pressure or within 1000 barrels of total production after a year of production. If this criterion is set too loose, the model might not be optimally history matched. Alternatively, the objective function can be used as a threshold. Below a certain value, or when the misfit function is not improved over x consecutive runs, models are said to be history matched. However, this does not guarantee that the observed data is matched closely, or that any models satisfy this criterion. Sometimes, it seems unavoidable to optimise “too far” before being able to define an appropriate stopping criteria.

The objective of stopping criteria is to ensure that the proper model(s) is (are) found given the data available. The parameter space has to be sampled sufficiently to ensure the proper model is found (van Soest, 2001). Definition of the stopping criteria is related to the amount, quality, and type of constraining data available, and type of optimiser used. Especially for global optimisers it is important that the parameter space is properly sampled and the number of iterations is not too limited.

3.6. Production forecasting

A reservoir simulation model allows analysing the observed behaviour of the reservoir, but more importantly to forecast future behaviour. Using the reservoir model, future production behaviour can be predicted allowing economic evaluation of the field. For example, revenues are estimated on the amount of produced oil and/or gas and costs are estimated based on the amount of produced water and/or unwanted gas. The reservoir model can answer also other questions, e.g. the moment of water breakthrough in a particular well, or the reservoir response to an infill well. Sensitivity analysis after the best drilling locations or optimal production scenario can be performed. The reservoir is managed according to the simulated behaviour of the reservoir model in different scenarios.

During the life of a field, the reservoir model is continuously updated to fit the observed behaviour. The reservoir model at least has to fit the observed data, before its forecast can be trusted. However, a good history match does not necessarily yield a reliable or accurate production forecast. Due to the non-uniqueness of the inversion, more than one realisation of the reservoir model fits the observed data. Not all of these correctly represent the reservoir and its future behaviour. Therefore, it is important to quantify the uncertainty associated with the production forecast.

3.6.1. Uncertainty quantification

One of the major challenges within reservoir management is to quantify the production forecast uncertainty. The uncertainty is related to several factors: amount and quality of conditioning data, fluid flow simulation algorithm, upscaling, parameterisation, mismatch function, etc. Traditionally, reservoir management is based on the production forecast from a single history matched reservoir model. Risk is assessed by analysing the sensitivity of the forecast from some extra simulation runs. In this manner, not all aspects are taken into account. Due to the non-uniqueness of the inversion, more than one realisation fits the observed data. Each realisation of the reservoir model yields a different production forecast. Some realisations are more probable than others. The different realisation and their probability have to be taken into account if the uncertainty of the production forecast is to be quantified. In theory, the entire parameter space needs to be sampled to properly quantify the uncertainty. However, this is not feasible due to the cost associated with the required number of simulations. Often, only the area around the optimum is searched yielding an average value rather than the true variance. A compromise must be found between the systematic exploration of the uncertainty domain and the search for the model optimally matching the data but only producing a single forecast, which is not necessarily correct.

Barker *et al.* (2001) and Floris *et al.* (2001) give an overview of the different approaches to quantify the production forecast uncertainty. A comparison is made between the methods as applied to a representative synthetic reservoir (Bos, 2000). The uncertainty can be quantified by locally characterising the objective function around the optimum solution. Local linearisation and the Scenario Test Method (Roggero, 1997) are examples of this approach. Another approach is to start from multiple initial reservoir models. If the objective function is multi-modal, different conditioned models are expected, yielding

different forecasts. Both methods can also be combined, i.e. locally characterise the objective function around each of these optima. Information is neglected when locally characterising around the optimum/optima. The uncertainty range can be underestimated and bias may be introduced. The full uncertainty can only be quantified by sampling the complete objective function. The Markov-Chain Monte-Carlo technique (Hegstad and Omre, 1997) allows a statistically correct sampling. The method requires a large number of samples, even though many adaptations are made to reduce this number. Oliver *et al.* (1996) merged the advantages of the above approaches. Their method aims to sample from the complete distribution, but using an optimisation technique to reduce the number of reservoir simulations needed. For Gaussian models, a correct sampling can be proven. For multi-phase problems, there is no proof that the approach correctly samples the posterior distribution.

For several methods, the estimated uncertainty ranges do not include the actual values of the synthetic reservoir. This confirms the general experience that the uncertainty is often underestimated. The choice of reservoir simulation model and initial model may introduce a significant bias in the estimated uncertainty range. As a result, a comparison between the different approaches is difficult to make.

Chapter 4

Rock physics

Seismic methods have a proven track record in the exploration for hydrocarbon resources. Their application in reservoir management are numerous and include porosity mapping, fracture detection, stress determination, anomalous pore pressure detection, monitoring gascap movement, thermal fronts, water influx, and CO₂ flooding. However, many researchers believe that the benefit of seismic methods within reservoir characterisation and engineering is not fully explored yet. Unquestionably, in the future (time-lapse) seismic methods will play a bigger role in helping to solve increasingly demanding and complex production and recovery problems. It is crucial to understand more fully what the seismic waves can reveal about the reservoir, and how to extract the desired information.

The seismic signal is a continuous time function through the subsurface. At the surface, the signal is recorded at a fixed sampling rate. The seismic signal is also spatially sampled, since the recording occurs by geophones at different locations. Typical values for the sampling rate are 1, 2, or 4ms, while the spacing between geophones is usually 25m. The seismic signal can be described in the time domain as well as in the frequency domain by sinusoidal components obtained from the Fourier transform. The seismic measurement is based on the fact that the various earth layers exhibit different elastic properties;

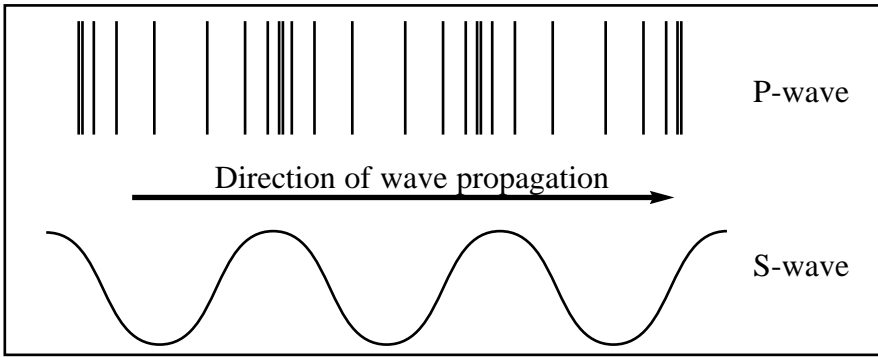


Figure 4.1 Illustration of a P-wave and S-wave in an arbitrary plane.

density, shear modulus, and bulk modulus. The seismic signal, excited by an external source, is reflected and refracted at elastic interfaces between layers. Therefore, the seismic measurement comprises information about the elastic contrasts in the subsurface. The amount of energy reflected and refracted is related to the contrast in impedance across the boundary (Section 5.1). The impedance is the product of density and velocity. In general, the higher the impedance contrast, the better the layer boundary is resolved.

Two types of waves can be measured in the field. The compressional or P-wave has its particle motion parallel to the direction of its propagation (Figure 4.1). The shear or S-wave exhibits particle motion perpendicular to the wave propagation. A vertical and a horizontal S-wave are specified according to the direction of the elongation. The propagation velocity of both P-wave and S-wave are depending on the elastic moduli and density of the material (Section 4.2). For a porous rock, it is complicated to define the elastic properties due to its complex geometrical structure. Its pores are either “empty” (dry) or saturated with water or hydrocarbons. Even if the elastic properties of the constituents are known with enough accuracy, the question remains how to represent the mixture by effective properties.

Numerous experiments have been performed to study the effect of rock properties and in-situ conditions on the effective elastic moduli and density (Wang and Nur, 1989)(Section 4.3). From these experiments empirical relations have been derived. Theoretical models have been developed to model the observed behaviour under different conditions (Wang and Nur, 1992). Ideally, a rock physical model takes into account all aspects related to the rock matrix, the

pore-fill, the in-situ conditions, and physical phenomena of wave propagation. However, it is impossible to consider all aspects of the problem in one model given the extraordinary complexities of most rocks. Every theoretical model therefore has its simplifying assumptions that result in a workable model.

4.1. Reservoir parameters

Porosity, saturation, mineralogical composition, temperature, permeability, and effective stress are important reservoir parameters. Some of these are required when estimating a saturated rock's density and elastic moduli, i.e. bulk and shear modulus. The bulk modulus represents the resistance of the medium to a change in stress state. For a fluid-filled rock, the bulk modulus is divided into the modulus of the fluid, K_f , the modulus of the rock forming mineral, K_m , and the moduli of the total rock, K_d and K_{sat} . The quantity K_d is the dry rock bulk modulus and K_{sat} is the modulus for the saturated rock. The resistance of the rock to shear stress is expressed by the shear modulus. A distinction is made between the dry rock shear modulus, μ_d , and the shear modulus of the saturated rock, μ_{sat} . Gas and most liquids do not support shear stress, but viscous oils do. A rock saturated with non-viscous liquids has the same shear modulus as the dry rock, i.e. μ_{sat} equals μ_d .

In general, to estimate the elastic properties one needs to specify

1. volume fractions of the various phases
2. elastic moduli and density of the various phases
3. geometric details of how the phases are arranged to each other

The various phases refer to the minerals making up the rock, the pores, as well as the fluids filling the pores. The volume fraction of pores in the porous medium is represented by the porosity ϕ . The water saturation, S_w , quantifies the volume fraction of water. Depending on the reservoir, the hydrocarbon phase fraction is denoted by the hydrocarbon saturation, S_{hc} , oil saturation, S_o , or gas saturation, S_g .

The bulk density of a saturated rock, ρ , is defined as

$$\rho = (1 - \phi)\rho_s + \phi\rho_f, \quad 4.1$$

with

$$\rho_f = S_w \rho_w + (1 - S_w) \rho_{hc}, \quad 4.2$$

containing ρ_s , the density of the solid, ρ_f , the density of the fluid, ρ_w , the water density, and ρ_{hc} , the hydrocarbon density.

Several models exist that relate the reservoir parameters to the rock's elastic moduli. These models are often grouped after their type or function. Here, only the bounding models are described, while a complete description of all models is found in Wang and Nur (1992). When the geometric details are omitted, only the lower and upper bounds of the elastic moduli can be predicted. The Voigt-Reuss and Haskin-Shtrikman models are theoretical models that determine these upper and lower bounds for the elastic moduli. At any given volume fraction of the constituents, the moduli fall between those bounds but the precise values depend on the geometric details. The models are mostly used to predict the fluid bulk modulus K_f , the matrix shear modulus μ_m , and the matrix bulk modulus K_m . In general, the bounding models are not accurate enough to calculate the dry bulk modulus K_d and dry shear modulus μ_d , because both are complex moduli and depend on porosity, clay content, and effective stress. There are several empirical equations relating these reservoir parameters with K_d and μ_d (Wang and Nur, 1989).

4.1.1. Voigt and Reuss models

The simplest bounds are the Voigt upper bound (Voigt, 1928) and the Reuss lower bound (Reuss, 1929). Voigt's model assumes that the strain for all of the constituents is the same and is referred to as the *isostrain* model:

$$K_V = \sum_{i=1}^n Vol_i K_i, \quad 4.3a$$

and
$$\mu_V = \sum_{i=1}^n Vol_i \mu_i, \quad 4.3b$$

with Vol_i the volume fraction of the constituents. K_i is the bulk modulus of the i -th component and μ_i is the shear modulus of the i -th component, with n standing for the number of phases.

Reuss's model assumes that stress is uniform throughout the aggregate, hence the name *isostress* model:

$$\frac{1}{K_R} = \sum_{i=1}^n \frac{Vol_i}{K_i}, \quad 4.4a$$

and
$$\frac{1}{\mu_R} = \sum_{i=1}^n \frac{Vol_i}{\mu_i}. \quad 4.4b$$

The mathematical average of the lower and upper bound is referred to as the Voigt-Reuss-Hill model. This approach has no physical meaning, because the geometrical details are not considered. It is given by

$$K_{VRH} = 0.5(K_V + K_R).$$

4.1.2. Hashin-Shtrikman bounds

The best bounds, defined as giving the narrowest possible range without specifying geometrical details, are the Hashin-Shtrikman bounds (1963).

$$K_{HS\pm} = K_1 + \frac{Vol_2}{(K_2 - K_1)^{-1} + Vol_1(K_1 + \frac{4}{3}\mu_1)^{-1}}, \quad 4.5a$$

and
$$\mu_{HS\pm} = \mu_1 + \frac{Vol_2}{(\mu_2 - \mu_1)^{-1} + \frac{2Vol_1(K_1 + 2\mu_1)}{5\mu_1(K_1 + \frac{4}{3}\mu_1)}}, \quad 4.5b$$

where K_1 and K_2 are the bulk moduli of the individual phases or minerals and μ_1 and μ_2 are the shear moduli of the individual phases. The volume fractions are given by Vol_1 and Vol_2 . The upper bound is given by + while the lower bound is represented by -. Upper and lower bounds are computed by interchanging phase 1 and 2. A detailed explanation of the physical background is found in Wang and Nur (1992).

4.2. Wave propagation theories

A variety of models theoretically describe the relation between elastic moduli and seismic velocities (Wang and Nur, 1992). The Gassmann equations and Biot theory are used most often, and are both straight-forward in their use. Moreover, the required parameters can be measured or calculated using theoretical or empirical models.

4.2.1. Gassmann equations

The equations derived by Gassmann (1951) calculate the bulk modulus of a fluid-saturated porous medium, K_{sat} , using the known bulk moduli of the solid matrix (mineral modulus), K_m , the frame, K_d , and the fluid, K_f . In the equations, the water saturation, the effective stress, and the temperature are indirectly present. These reservoir parameters influence the elastic moduli present in the Gassmann equations. The Gassmann model also relates the shear modulus of the saturated rock, μ_{sat} , with the shear modulus of the dry rock, μ_d . The Gassmann equations underlie the following assumptions:

1. The shear modulus of the rock is not affected by the fluid saturation. The assumption is valid when the pores are filled with a frictionless fluid.
2. The rock is macroscopically homogeneous and isotropic.
3. All the pores are interconnected and communicating. This implies that porosity and permeability are usually high and there are no isolated pores.
4. The solid-fluid system under study is closed (undrained).
5. *The relative motion between the fluid and solid is negligibly small compared to the motion of the saturated rock itself when the rock is excited by a wave.* This is the most important assumption by Gassmann. For this to be true the wave frequency has to be low. At low frequencies the induced pore pressures, due to a passing seismic wave, can be equilibrated throughout the pore space. At higher frequencies relative motion between the solid and the fluid exists, causing the wave to be dispersive.
6. The pore fluid does not interact with the solid in a way that would change the shear rigidity of the frame, there are no chemical or physical interactions between the rock and the fluid.

For a rock, the solid matrix consists of the rock-forming minerals, whereas the frame refers to the rock sample with empty pores (dry rock). The pore fluid can be oil, gas, water or a mixture of these. The equations become (Mavko *et al.*, 1998),

$$K_p = \frac{(1 - \frac{K_d}{K_m})^2}{\frac{\phi}{K_f} + \frac{1-\phi}{K_m} - \frac{K_d}{K_m^2}}, \quad 4.6$$

where $K_{sat} = K_d + K_p, \quad 4.7a$

and $\mu_{sat} = \mu_d + \mu_p, \quad 4.7a$

with K_{sat} bulk modulus and μ_{sat} shear modulus of the fluid-filled rock and K_p bulk modulus and μ_p shear modulus of the pore. Gassmann assumes that the shear moduli of the fluids are zero and thus have no influence on the saturated rock.

The P-wave phase velocity becomes

$$V_p = \sqrt{\frac{K_d + K_p + \frac{4}{3}\mu}{\rho}}. \quad 4.8$$

The S-wave phase velocity is given by

$$V_s = \sqrt{\frac{\mu}{\rho}}. \quad 4.9$$

The density ρ is the density of the saturated rock calculated according to Equation 4.1.

The four parameters in the Gassmann equations, K_f , K_m , K_d , and ϕ , are related to the reservoir parameters. The saturation influences K_f and ρ . The effective stress has its influence on K_m , μ , and ϕ .

Differences have been observed between velocities measured in an experiment or in the field and the Gassmann predicted velocities (Wang, 2000a). This can have several causes

1. The presence of microfractures in a rock lowers the velocity, especially V_p in dry rocks. As the effective pressure increases, the cracks are closed and velocities are closer to those predicted by

- the Gassmann equations.
2. Uncertainties in the input parameters. Especially in K_m and μ_m where the effective medium theories are used to predict the effective modulus.
 3. Nonconformance of real rocks to Gassmann's assumptions. Water and oil are not really frictionless, especially oils, and some pore fluids interact with the rock matrix in a way that changes the moduli of the rock.
 4. The presence of another solid phase, especially of clay, requires a modification of the Gassmann equations.

4.2.2. Biot's low frequency theory

Another important wave propagation theory has been developed by Biot (1956). Biot developed a theory for the propagation of waves in porous elastic solids containing compressible fluids. The theory covers the whole frequency range, whereas the Gassmann equations are only valid at zero or low frequency. A distinction is made between the low frequency and the high frequency range. This distinction is based on the type of flow occurring in the solid when a wave passes. When the fluid flow satisfies Poiseuille type flow, the low frequency theory is valid. When other high frequency flow mechanisms come into play the high frequency theory is to be used. The Biot theory is derived from the wave equation, which in itself is based on Hooke's Law and Newton's second law (Biot, 1956). The solution of the wave equation used for the Biot theory shows two compressional waves in a fluid-saturated rock, the fast P-wave and the slow P-wave. The latter attenuates exponentially as the wave travels and has the nature of a diffusion process. When the P-wave is referred to, the fast P-wave is intended. The Biot theory is not given in detail, but can be found in Wang and Nur (1992).

The basic assumptions underlying the Biot theory are:

1. Shear modulus of the rock is not affected by the fluid saturation, because the shear modulus of the fluid in the solid is zero.
2. The rock is macroscopically homogeneous and isotropic.
3. All the pores are interconnected and communicating and have fairly uniform size distribution. This implies that usually porosity and permeability are high and there are no isolated pores.
4. The wavelength is appreciably larger than the largest dimension of the rock's grains.

5. Thermal effects due to dissipation of energy during the wave propagation are neglected.
6. Pore fluid does not interact chemically with the rock matrix.
7. Rocks are without micro-fractures or cracks.
8. The solid-fluid system under study is closed (undrained).
9. *The relative motion between the fluid and the rock exists and follows Darcy's (Poiseuille type flow) law for fluid flow through porous medium.*

The major difference between the Gassmann equations and Biot theory is that the latter allows relative motion between the fluid and the solid and takes into account viscoelastic effects. This relative motion leads to dispersion and attenuation. When the wave frequency approaches zero, the Biot theory reduces to the Gassmann equations. At the high-frequency limit, the relative motion between the solid and the fluid is at a maximum, the coupling between the rock and the pore fluid is at a minimum. Fluid movement relative to the solid, when a seismic wave passes, causes energy dissipation in terms of velocity dispersion and attenuation. The velocity dispersion is the dispersal of the velocity with frequency. In a dispersive wave the different frequencies travel with different speeds. Attenuation is an inelastic process which dissipates seismic energy by conversion to heat, thus decreasing the amplitude and modifying the frequency and phase content of a propagation wavelet. Dispersion and attenuation are intertwined and occur simultaneously.

The assumption of Poiseuille flow, which defines the low frequency range of the Biot theory, is only valid below a certain frequency f_t , which depends on the kinematic viscosity, ν , of the fluid and the size of the pores (Biot, 1956), according

$$f_t = \frac{\pi\nu}{4d^2}, \quad 4.10$$

with d being the diameter of the pores. The kinematic viscosity, ν , is related to the density of the fluid, ρ_f , and the viscosity, η , by the equation

$$\nu = \frac{\eta}{\rho_f}. \quad 4.11$$

The Biot theory also defines a characteristic frequency (Wang and Nur, 1989),

$$f_c = \frac{\eta\phi}{2\pi k\rho_f}, \quad 4.12$$

with ϕ the porosity, k the permeability and ρ_f the fluid density. The

characteristic frequency may be considered as a frequency scale of the material. It is large in poorly permeable rocks and in rocks saturated with highly viscous fluids.

The P-wave and S-wave velocity dispersion with respect to their reference velocity is generally expressed by,

$$\frac{V_X(f)}{V_X^{ref}} \tag{4.13}$$

The reference velocity V_X^{ref} corresponds to no relative motion between the solid and the fluid, i.e. Gassmann velocity. The above is applicable to both P-wave and S-wave velocity. The velocities depend on frequency. Figure 4.2 is taken from the article of Biot (1956). It shows the P-wave and S-wave velocity dispersion for several elastic cases when the frequency increases. These

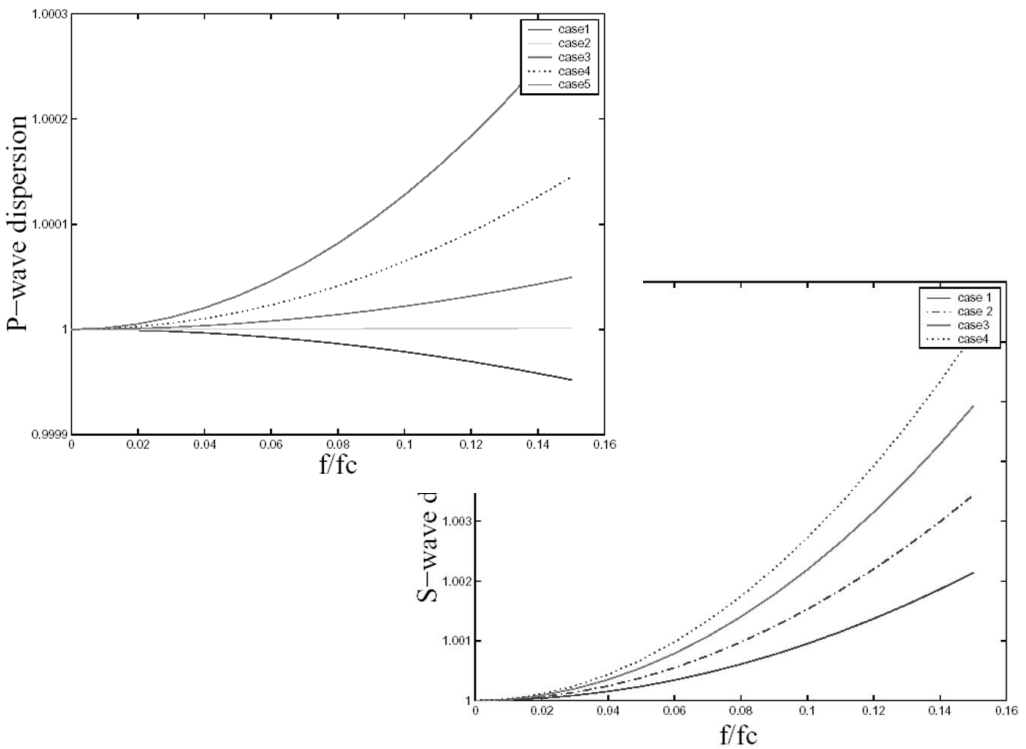


Figure 4.2 P-wave dispersion (left) and S-wave dispersion (right) for different elastic cases 1 to 5 after Biot (1956).

different cases stand for different water saturations and different elastic parameters. The general principle deduced from the plot is that in the low frequency range, $f / fc < 0.15$, both P-wave and S-wave velocity dispersion is lower than 1% for all the cases.

In current seismic practice a frequency to a maximum of 250 Hz is used. The fraction, f / fc , then becomes very small, ranging from 0.005 for a water saturated sandstone with 30% porosity to 0.000005 for a rock filled with oil. In that range the P-wave and S-wave velocity dispersion and the attenuation can be neglected. When working with seismic frequencies, it is justified to use Biot's low frequency theory. Doing so, the energy losses caused by attenuation and dispersion are neglected corresponding to no relative motion between the fluid and the solid. In its lower frequency limit the Biot theory reduces to the Gassmann equations (Wang and Nur, 1992).

4.3. Representative laboratory observations

In this section a variety of experiments is described to illustrate the effect of reservoir parameters and in-situ conditions on the seismic wave. Both static and dynamic reservoir parameters are discussed. Dynamic parameters are those that change over time due to production in the reservoir. Anisotropy is discussed briefly. Attenuation and dispersion is discussed in more detail. Attenuation is an important issue when comparing high frequency laboratory experiments to low frequent seismic data.

4.3.1. Clay content, porosity, and lithology

P-wave and S-wave velocity generally decrease with increasing porosity and clay content as shown by Han *et al.* (1986) in a comprehensive study. In Figure 4.3 this behaviour is shown for different water-saturated rocks. Compressional velocity and shear velocity were measured as a function of pressure in sandstones with varying clay content and porosity. The clay content and the porosity (Tosaya and Nur, 1982) affect the shear modulus more than the bulk modulus for shaly sandstones. Clays are effective in decoupling the contacts between the grains and thus in reducing the shear modulus. Any model used to fit the P-wave and S-wave velocity data in shaly sandstones must therefore include a clay-content term.

The ratio between P-wave and S-wave velocity, V_P/V_S , can be used as a lithology indicator, as Pickett (1963) showed with different V_P/V_S ratio values for limestones, dolomites, and clean sandstones (Figure 4.4). In order to use the velocity ratio as a lithology indicator, it is necessary to know whether the rocks contain gas. The V_P/V_S ratio of gas saturated rocks often increases markedly with increasing effective pressure and decreases slightly with increasing

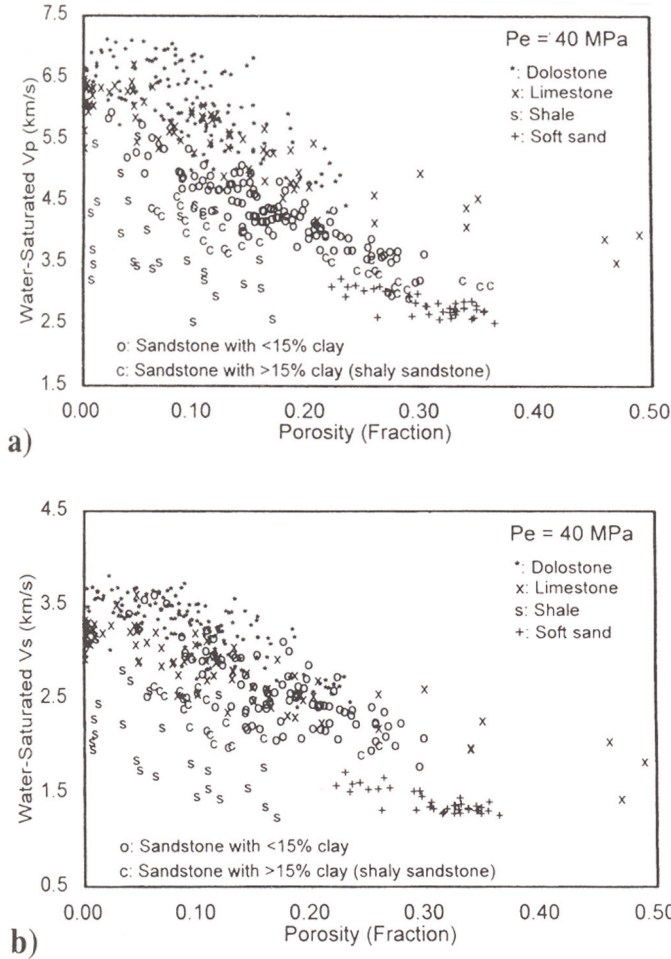


Figure 4.3 Compressional and shear velocities versus porosity in water-saturated sedimentary rocks after Wang (2000b). Large scatter exists in the data. The figures show that it is impossible to obtain accurate porosity values from either V_P or V_S without knowing the lithology or vice versa.

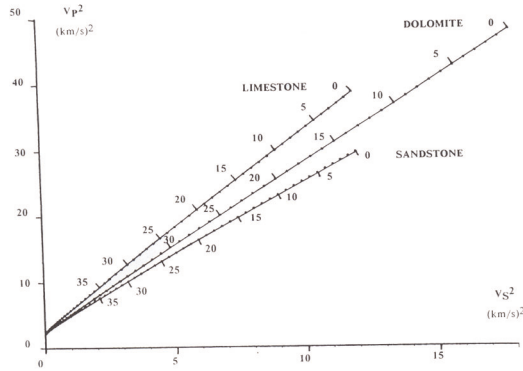


Figure 4.4 The relationship between V_p or V_s differs per lithology for water-saturated sandstone, dolomite, and limestone after Krief *et al.*(1990).

temperature (Wang, 1988). Castagna *et al.* (1985) report on dry and water-saturated clastic rocks that P-wave velocity is approximately linearly related to S-wave velocity (mudrock line). In dry sandstones, the V_p/V_s ratio is nearly constant. In wet sandstone and mudstones, the V_p/V_s ratio decreases with increasing P-wave velocity.

4.3.2. Pressure, temperature and saturation

Assuming constant porosity, the main factors controlling the P-wave and S-wave velocity in a porous rock are confining pressure, pore pressure, and the level of saturation (Nur and Simmons, 1969b). Both P-wave and S-wave velocity increase as effective pressure, i.e. the difference between confining and pore pressure, increases (Domenico, 1977). For a completely water-saturated sample the pressure dependence of the P-wave velocity is smaller than for a dry or gas-saturated sample (Figure 4.5). The P-wave and S-wave velocity in dry rock increase markedly with overburden pressure. The effect of pore pressure counteracts that of the overburden or confining pressure. High pore pressure mechanically opposes the closure of cracks and grain contacts, thus leading to low effective moduli and velocities.

The effect of temperature on velocities in dry and gas-saturated rocks is usually small (1-7% at 100 degrees) and often considered of second order. The decrease as temperature increases is caused by the softening of the rock matrix due to thermal expansion and the slight porosity increase due to differential thermal

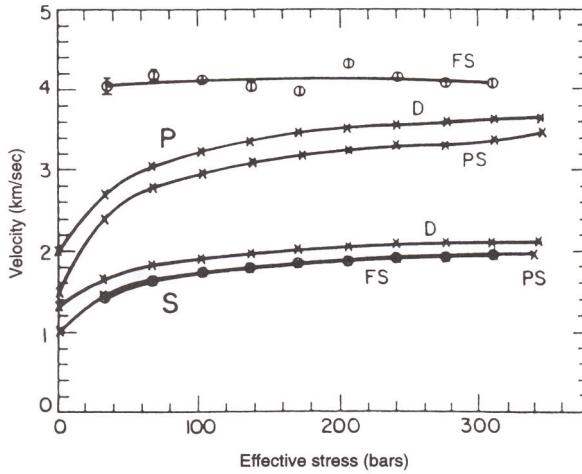


Figure 4.5 Illustration of the effect of water saturation and effective stress on wave velocities in Massillon sandstone after Winkler and Nur (1982). D is dry, PS is partially saturated (90%), and FS is fully saturated.

expansion of the mineral constituents (Kern, 1982). Bell and Shirley (1980) show that the P-wave velocity dependence on temperature in unpressurised sediments is dominated by the temperature dependence of P-wave velocity in the pore fluid. The S-wave velocity is fairly independent of temperature. When the rocks are saturated with heavy hydrocarbons, P-wave velocity decreases considerably (10-35%) as shown by Wang and Nur (1988).

From dry sand to about 10% water saturation, the P-wave velocity in unconsolidated sand decreases due to the overall density increase of the rock (Elliott and Wiley, 1975). In the 10 to 90% water saturation interval, P-wave velocity is more or less constant, implying that the modulus increase due to increasing water saturation is cancelled by the increase in density. As water saturation further increases to 100%, P-wave velocity increases sharply due to the large increase of the bulk modulus (Figure 4.6). This behaviour resembles that of high porosity sands (Gregory, 1976b). The fact that the P-wave velocity is quite insensitive to saturation except when it becomes close to 100%, indicates that velocity measurements cannot yield information on the degree of partial saturation in reservoir rocks. Actually, at low frequencies the increase in P-wave velocity is sharp and occurs when saturation rises from about 90% to 100%. In contrast, the increase of P-wave velocity is gradual with saturation

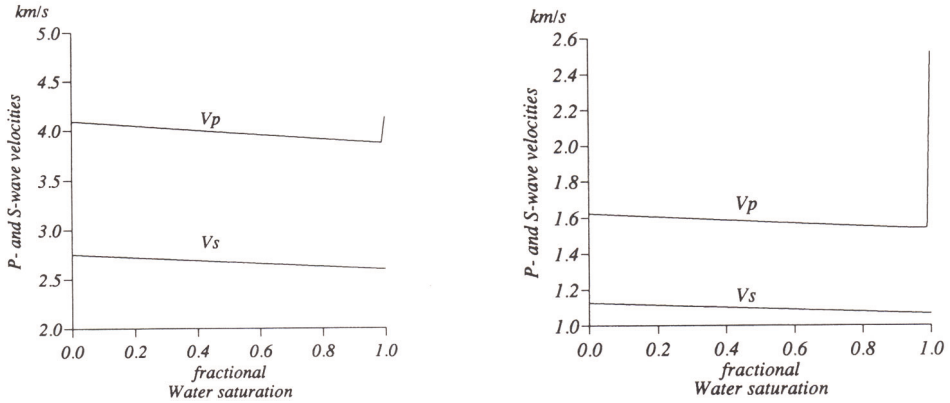


Figure 4.6 Illustration of the effect of water saturation on P-wave and S-wave velocities. The other fluid is a gas. The sample is a clean sandstone (left) and a shaly sandstone with 30% clay content (right). In both cases, the porosity is 22%, after Xu and White (1996).

from 50% to 100% at higher frequencies. The effect of complete liquid saturation on P-wave velocity is larger for low porosity rocks than high porosity rocks.

Domenico (1977) showed that S-wave velocity decreases consistently as water saturation increases due to the density increase of the sample. Murphy *et al.* (1984) report something similar, but distinguish the decrease of S-wave velocity in two zones. At low water saturation (30%) the decline is most pronounced and results from adsorption of water molecules on the granular frame. Above 30% the decline is primarily due to the fact of increasing effective fluid density and agrees with Domenico (1977). The shear modulus is barely changed by variation in fluid compressibility, because the viscosity of the pore fluid is low, so that the stiffness in shear remains the same when the pore fluid is changed from air to brine.

Studies have shown that acoustic wave velocities in fluid-saturated rocks are related to pore fluid-type (King, 1965, Wang *et al.*, 1988a). Besides the effect of the bulk modulus of the pore fluid, the viscosity and chemical effect of the fluid on the surface of the rock grains can also play a role on the velocity in the rock-fluid aggregate (Murphy *et al.*, 1984, Wang *et al.*, 1988b).

4.3.3. Anisotropy

Velocity anisotropy is generally caused by the preferential alignment of grains and cracks (lithological or intrinsic anisotropy) or the application of directional stress (stress-induced anisotropy). In geophysics, the most common types of anisotropy that have been studied extensively are transverse isotropy and azimuthal anisotropy. Nur and Simmons (1969a) report on stress-induced anisotropy, and show that the P-wave and S-wave velocity change with stress and direction of stress. The P-wave velocity travels fastest in the direction of applied stress and shear waves travel with generally different velocities in any direction. Such velocity variations with stress and stress direction are caused by the closure of cracks. White *et al.* (1983) show that the velocities vary with angle of propagation of the waves. At higher confining pressure, cracks are closed and anisotropy decreases (Lo *et al.*, 1986). Rai and Hanson (1987) show that velocity anisotropy in shale samples is essentially independent of both uniaxial and hydrostatic stresses, suggesting that anisotropy is caused mainly by the preferential alignment of the clay particles.

4.3.4. Attenuation and dispersion

It has long been recognised that the wave propagation velocities are a function of frequency. This velocity dispersion is common in fluid-saturated rocks. Wave velocities increase with increasing frequency of the waves due to inertial drag of the pore fluid or pore pressure gradients caused by the compliance heterogeneity of the pores. Of special concern is the magnitude of velocity dispersion in fluid saturated rocks between seismic and laboratory ultrasonic frequencies. In the field it is very difficult to obtain high frequency wave data, whereas in the laboratory the longest wavelength is limited to twice the sample length. In order to use laboratory obtained velocity data (50kHz-MHz) for seismic (10-250Hz) and log interpretation (to 100kHz) it is necessary to know the magnitude of dispersion for both P-wave and S-wave velocity. Murphy (1984) shows that P-wave velocity at 200kHz is about 15% higher than at 2kHz, and the S-wave velocity about 10% higher.

Many physical mechanisms have been proposed and modelled to explain velocity dispersion and attenuation in rocks. Experimental observations indicate several mechanisms for attenuation in rocks. Most important are solid friction losses (Walsh, 1966, Johnston *et al.*, 1979), squirt flow losses (Mavko and Nur, 1979, Murphy *et al.*, 1984, Jones, 1986, O'Connell & Budiansky, 1977,

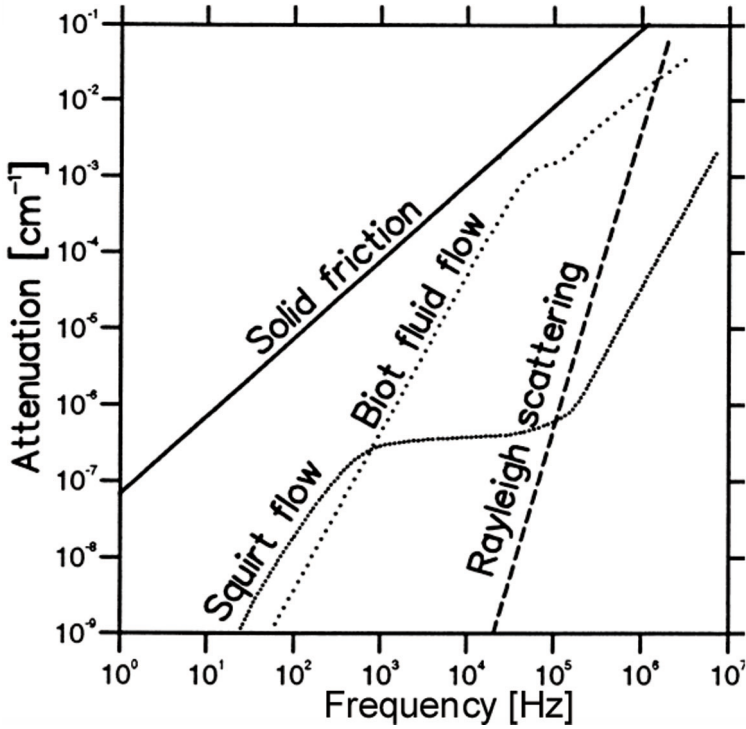


Figure 4.7 Schematic illustration of various contributions to acoustic attenuation in a sandstone after Johnston et al. (1979).

Winkler, 1986), Biot fluid flow losses, and Rayleigh scattering. The solid friction losses occur as the sound waves induce displacements between grains or in cracks resulting in friction. The absorption contribution increases proportional to frequency. A saturating fluid lubricates the grain contacts and leads to increased attenuation. Squirt flow losses are important in (partly) saturated rocks. Fluid flows between open pores and narrow cracks and channels. Biot losses arise due to fluid flow relative to the solid grains and are related to porosity and effective pressure. The Rayleigh scattering occurs due to the impedance contrast between solid and the pore fluid. The effect is stronger in dry than in saturated rocks, and decreases with increasing pressure. See Figure 4.7 for attenuation versus frequency.

Han (1986) shows that the Biot dispersion, which is relatively small (1%), increases with increasing porosity and decreases with increasing clay content. The apparent or squirt flow dispersion, usually 3-8%, decreases with increasing porosity and increasing with clay content. Wang (1988) concludes that pore

fluid viscosity, permeability, and pore geometry are the major factors affecting velocity dispersion. His research includes pressure, temperature, and porosity as well. Rocks saturated with low viscosity fluids have low apparent dispersion and vice versa, which is also consistent with the squirt or local flow mechanism.

4.3.5. The reliability of core data

According to Nes *et al.* (2000), there is potential for improving the reliability of standard core test for seismic monitoring studies. A primary concern is to quantify and correct for core damage effects, which significantly enhances the stress dependency of wave velocities. Careful laboratory procedures and modelling efforts may reduce such effects. However, no simple procedure is currently available to eliminate this problem. The use of simplified laboratory test procedures, in particular application of an inappropriate effective stress principle, may lead to erroneous interpretations. The effect of core damage is often neglected, and the importance of using proper stress conditions during experiments is not recognised. Nes *et al.* (2000) convincingly illustrate pitfalls in the common use of so-called effective stress principle.

4.4. Application

Rock physical models serve two purposes within the time-lapse seismic domain. They are utilised to model the effect of a change in the reservoir on the seismic signal. This knowledge is used in the sensitivity analysis to assess the potential of time-lapse seismic before it is actually acquired. After time-lapse seismic is acquired, rock physical models are used to interpret the observed time-lapse seismic signal. Depending on the reservoir and the expected changes a suitable rock physical model is chosen.

The objective of any rock physical model is to describe the physical behaviour of the rock when excited by a seismic wave. Due to the complexity of the rock and the impact of the pore fluid, it is impossible to take all aspects into account. For this reason, rock physical models might under- or overpredict the observed time-lapse seismic changes. Qualitatively, rock physical models are expected to properly describe the seismic changes.

In the reservoir, changes in saturation, pore pressure, and temperature might occur due to hydrocarbon production. Each affects the time-lapse seismic signal differently depending on the rock and reservoir conditions. The separate effects on the time-lapse signal may be of opposite or similar character. The combined effect can thus be misleading and, respectively, show a weakened or amplified time-lapse response. Decoupling of the combined signal is crucial for the interpretation in terms of the separate reservoir changes. The Biot-Gassmann model accounts for saturation changes indirectly via a change in the fluid moduli. A pore pressure change affects the dry rock modulus. None of the rock physical models explicitly accounts for a change in the pore pressure or effective stress for a saturated rock. Often, pore pressure and saturation changes occur simultaneously. Decoupling of their effects when interpreting time-lapse seismic data is currently not possible using any rock physical model.

Another consideration when using rock physical models is attenuation and dispersion. With different frequencies, the saturated rock might exhibit different elastic properties. Generally, a low and a high frequency range are distinguished between which the rock-fluid interaction behaves differently. Depending on the rock and the fluid mobility, core, log, and seismic measurements are assigned to one or the other frequency range (Batzle *et al.*, 1999). Often, rock physical models are calibrated to core measurements or log data. If the seismic measurement covers a different frequency range than the core and log data, dispersion and attenuation have to be taken into account.

Chapter 5

Seismic measurements

For the purpose of hydrocarbon exploration and subsequent reservoir characterisation, the subsurface must be imaged. Various geophysical measurements are routinely acquired, processed, and interpreted for this purpose. Over the last two decades, 3D reflection seismic data has emerged as the most cost-effective tool in the production of hydrocarbons. High cost drilling and development decisions are based to a large extent on interpretations from seismic data, which image the deeper subsurface (2-4km) over larger areas, typically several tens or hundreds of square km. The seismic method gathers elastic wave information from the subsurface. Seismic waves are excited by an external source and are reflected and refracted at elastic interfaces between layers. Therefore, the seismic measurement comprises information about the elastic contrasts in the subsurface. On land, explosives or vibroseis trucks are used to create the desired signal. Geophones placed at the earth surface record the returning signal. Offshore, airguns generate the signal and hydrophones towed behind a ship or geophones placed at the ocean bottom record the signal.

In early years, seismic data was acquired in 2D lines thus illuminating a cross-section through the subsurface. Since a few decades, seismic data is also acquired in 3D mode. Basically, in a 3D seismic data set adjacent 2D lines are

acquired so close to each other that the same sampling rate is obtained in inline and crossline directions. 3D seismic gives a much better insight into the actual subsurface structure and provides information about reservoir rock and fluid properties. The development of 3D seismic has benefited considerably from the fast growth in computer processing capability. In the last decade time-lapse 3D seismic, often referred to as 4D seismic, has been introduced. It is only recently that repeatability of the time-lapse measurements is sufficient to allow interpretation of the time-lapse signal. For some fields, the recovery is expected to increase from 25-30% using 2D seismic, to 30-40% when using 3D seismic and ultimately to 65-75% due to the information obtained from time-lapse seismic¹. In the future, time-lapse seismic is expected to become a standard interpretation tool and the number of monitor surveys is expected to increase significantly (Figure 5.1).

In general, additional costs are associated with acquiring new data and gaining new knowledge. Compared to 2D seismic, 3D seismic is roughly 3 times more expensive². Not only is 3D seismic acquisition more expensive, also processing

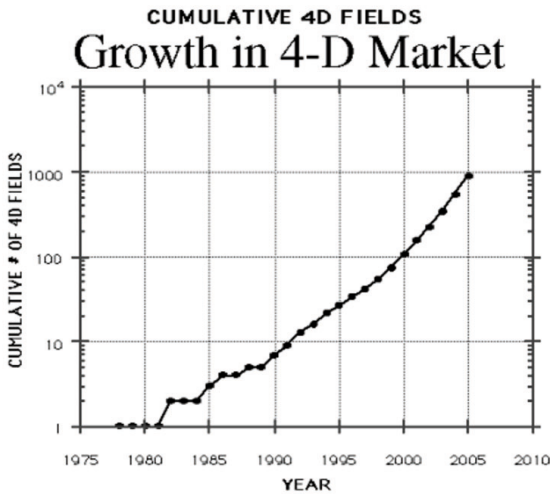


Figure 5.1 Exponential growth of 4D as foreseen by Lamont Doherty Earth Observatory, Columbia University

of 3D seismic is more labour-intensive, thus more expensive. Compared to 3D seismic, time-lapse 3D seismic is generally 2 times² as expensive mostly due to extra processing that is required to guarantee repeatability, but also due to tighter acquisition constraints. In some special cases, multi-component (time-lapse) seismic is acquired. Multi-component seismic allows measuring both P-waves and S-waves. Besides the expensive equipment, processing is very time-consuming due to the decomposition of the different wave fields (Schalkwijk *et al.*, 1999). Compared to 3D

¹ BP/Shell Foinaven estimate, Petroleum Engineer International, January 1996

² Personal communication with Erik Håvarstein, Statoil

seismic, multi-component seismic is 5 to 10 times² as expensive. Multi-component seismic is used when the S-wave is expected to provide information, which cannot be obtained using conventionally acquired P-wave data, for example, to facilitate decoupling of the pressure and saturation effect on time-lapse seismic. The P-wave is sensitive to both changes, while the S-wave is only sensitive to the pressure changes. With each type of seismic data, the benefit has to balance the associated cost.

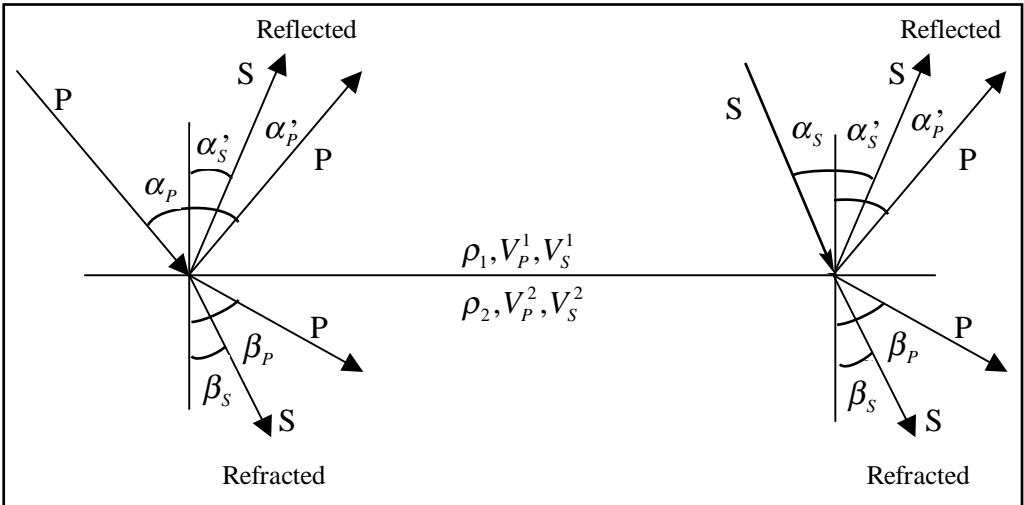


Figure 5.2 Plane waves at an elastic boundary when a P-wave hits the boundary (left) and when a S-wave hits the boundary (right).

5.1. A structural image

3D seismic provides structural information about the subsurface including the reservoir. The dip and azimuth (orientation) of different layers, their thickness, faults, etc. can be mapped using the 3D seismic image. The seismic measurement is based on the fact that the various earth layers exhibit different elastic properties; density, shear modulus, and bulk modulus. At the interface between layers of different elastic character, an incident compressional plane wave is refracted and reflected into a P-wave and S-wave (Figure 5.2). The same applies to an incident shear plane wave. The angle of refraction β_x is calculated using Snellius law (Aki & Richards, 1980). Snellius law states that

1. The angle of reflection is equal to the angle of incidence

$$\alpha_p = \alpha_p', \quad 5.1$$

$$\alpha_s = \alpha_s',$$

with α_p the incidence angle for the compressional plane wave, and α_s the incidence angle for the shear plane wave. The ' denotes the reflection angle.

2. The ray parameter p is constant crossing the interface

$$\frac{\sin(\alpha_p)}{V_p^1} = \frac{\sin(\beta_p)}{V_p^2} = \frac{\sin(\alpha_s)}{V_s^1} = \frac{\sin(\beta_s)}{V_s^2} = p, \quad 5.2$$

with p the ray parameter, V_x the P-wave or S-wave propagation velocity, β_x the refraction angles of the different waves and the 1 and 2 denoting the layers.

For each incident wave, two reflection and two transmission coefficients are distinguished, yielding eight in total. They respectively express the amount of energy being reflected or refracted. The reflection and transmission coefficients are dependent on the angle of incidence α_x . The four reflection coefficients are given by (Aki & Richards, 1980)

$$RC_{PP} = \left[\left(b \frac{\cos(\alpha_p)}{V_p^1} - c \frac{\cos(\beta_p)}{V_p^2} \right) F - \left(a + d \frac{\cos(\alpha_p)}{V_p^1} \frac{\cos(\beta_s)}{V_s^2} \right) H p^2 \right] / D, \quad 5.3$$

$$RC_{PS} = -2 \frac{\cos(\alpha_p)}{V_p^1} \left(ab + cd \frac{\cos(\beta_p)}{V_p^2} \frac{\cos(\beta_s)}{V_s^2} \right) p V_p^1 / (V_s^1 D), \quad 5.4$$

$$RC_{SS} = - \left[\left(b \frac{\cos(\alpha_s)}{V_s^1} - c \frac{\cos(\beta_s)}{V_s^2} \right) E - \left(a + d \frac{\cos(\beta_p)}{V_p^2} \frac{\cos(\alpha_s)}{V_s^1} \right) G p^2 \right] / D, \quad 5.5$$

$$RC_{SP} = -2 \frac{\cos(\alpha_s)}{V_s^1} \left(ab + cd \frac{\cos(\beta_p)}{V_p^2} \frac{\cos(\beta_s)}{V_s^2} \right) p V_s^1 / (V_p^1 D), \quad 5.6$$

with

$$a = \rho_2(1 - 2(V_s^2 p)^2) - \rho_1(1 - 2(V_s^1 p)^2),$$

$$b = \rho_2(1 - 2(V_s^2 p)^2) + 2\rho_1(V_s^1 p)^2,$$

$$c = \rho_1(1 - 2(V_s^1 p)^2) + 2\rho_2(V_s^2 p)^2,$$

$$d = 2\rho_2(V_s^2)^2 - 2\rho_1(V_s^1)^2,$$

$$E = b \frac{\cos(\alpha_p)}{V_p^1} + c \frac{\cos(\beta_p)}{V_p^2},$$

$$F = b \frac{\cos(\alpha_s)}{V_s^1} + c \frac{\cos(\beta_s)}{V_s^2},$$

$$G = a - d \frac{\cos(\alpha_p)}{V_p^1} \frac{\cos(\beta_s)}{V_s^2},$$

$$H = a - d \frac{\cos(\beta_p)}{V_p^2} \frac{\cos(\alpha_s)}{V_s^1},$$

and

$$D = EF + GHp^2.$$

For normal incidence the above-defined reflection coefficients reduce to

$$RC_{PP} = \frac{\rho_2 V_p^2 - \rho_1 V_p^1}{\rho_2 V_p^2 + \rho_1 V_p^1}, \quad 5.7$$

and

$$RC_{SS} = \frac{\rho_2 V_s^2 - \rho_1 V_s^1}{\rho_2 V_s^2 + \rho_1 V_s^1}. \quad 5.8$$

In general, the product of density and velocity is referred to as the impedance. For normal incidence, the impedance is referred to as acoustic impedance, otherwise elastic impedance is used.

The elastic moduli, bulk and shear modulus, as well as the density determine the P-wave velocity. The S-wave velocity is defined by the shear modulus and density as given in Chapter 4

$$V_p = \sqrt{\frac{K_d + K_p + \frac{4}{3}\mu}{\rho}},$$

and

$$V_s = \sqrt{\frac{\mu}{\rho}},$$

where ρ is bulk density, K_d is the dry bulk modulus, K_p is the pore bulk modulus and μ is the shear modulus. Based on only the P-wave velocity data, it is not possible to gain unique information about the two elastic moduli and the density. Both P-wave and S-wave velocity are required to uniquely invert to the elastic properties.

In most common seismic surveys only P-wave data are acquired. For the purpose of delineating the subsurface and for reservoir characterisation purposes, P-wave data usually suffices. For example, a reservoir might lack an acoustic impedance contrast and be invisible on P-wave data. When this reservoir exhibits a shear impedance contrast, S-wave data allows imaging the reservoir (MacLeod *et al.*, 1999). Within reservoir characterisation, the inversion to lithology or fluid-fill might be impeded by the lack of S-wave data. The S-wave is insensitive to the fluid, except for a small contribution of the density. Fluids cannot sustain shear forces, thus in a porous fluid-filled medium the S-wave travels mainly through the rock matrix shedding a different light on the rocks. A solution has been found by performing Amplitude versus Offset (AVO) analysis (Castagna & Backus, 1993). The reflection at the interface into a P-wave and S-wave is angle dependent. By analysing the P-wave behaviour for different incidence angle (or offset), indirect information is gained on the S-wave.

To gain proper S-wave information, it is in general better to record the full wave field referred to as multi-component seismic. The different components often comprise a hydrophone, a vertical geophone, and two horizontal geophones oriented perpendicular to each other. The latter record the converted S-wave, while the P-wave is recorded by geophones and hydrophones. Offshore, multi-component seismic requires ocean bottom acquisition rather than streamer data, because the S-waves do not travel through water. Several challenges have to be faced when measuring Ocean Bottom Cable data (OBC) (Caldwell, 1999 and Gaiser, 1999). In processing the multi-component data, the full wave field has to be decomposed (Zhu *et al.*, 1999).

Compared to P-wave data, the acquisition and processing of multi-component seismic is far more expensive, roughly 5 to 10 times. The extra cost associated with multi-component seismic has to be justified and balance the additional information. For time-lapse seismic interpretation, the S-wave information from multi-component seismic might be valuable enough to justify the additional costs. Time-lapse P-wave velocity is sensitive to a change in pore pressure and saturation. Based on P-wave data, the effects of saturation and pore pressure cannot be decoupled. By using S-wave data, decoupling is possible, as the S-wave mainly propagates through the rock matrix and is insensitive to pore fluid changes. Multi-component data also allows studying anisotropy and its time-lapse changes. The anisotropy is related to the stress distribution (Sayers, 2002) and perhaps even to permeability (Rasolofodaon and Zinszner, 2002).

5.2. Inversion to rock properties

For each seismic measurement, a seismic signal is created using explosives or vibroseis on land or airguns when working offshore. The initial seismic signal exhibits a certain character expressed by the source wavelet. The seismic signal ultimately returns to the surface where it is recorded by geophones and/or hydrophones. The seismic signal is continuously altered in the subsurface as it propagates through layers of different elastic properties. Within each layer, the propagation velocity is determined by the layer's properties. The seismic signal T is a combination of the wavelet W and the earth response E

$$T = f(W, E), \quad 5.9$$

where the earth response is expressed as the reflection coefficient versus depth. Figure 5.3 illustrates how a seismic trace is obtained by convolving the reflection coefficient (RC) series with a wavelet. The source wavelet W changes during the seismic measurement, as the wave travels through the subsurface. The seismic measurement operates within a frequency bandwidth, in general up to frequencies of 100Hz. Figure 5.3 illustrates the bandlimited character as the high and low frequencies are lacking.

As described in the previous section, one of the purposes of seismic data is to obtain a structural image of the subsurface. Moreover, seismic data is used to obtain information about the rock properties, e.g. lithology and porosity,

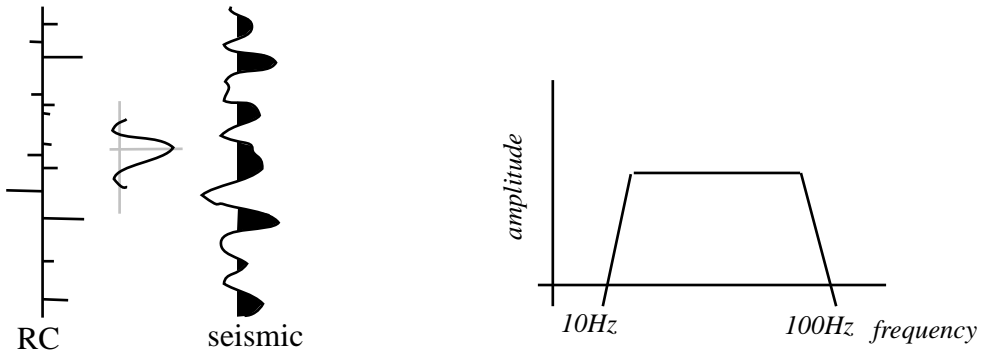


Figure 5.3 By convolving the reflection coefficient response with a wavelet, the seismic trace is obtained (left). The seismic measurement has a limited frequency content (right).

referred to as seismic reservoir characterisation. The seismic data is a contrast measurement and only indirectly measures the rock properties. As a result, the seismic has to be inverted to allow interpretation in terms of rock properties. In the industry, a variety of inversion methods exists (Weimer and Davis, 1996). For two reasons, most inversion methods use an intermediate step, in which the seismic is inverted to acoustic or elastic impedance. First of all, in the industry it is quite common to generate an impedance volume, because it has value of its own. Second, impedance is related to a variety of rock properties: lithology, porosity, pore-fill, etc. Both in the inversion to impedance and to other rock properties, calibration to well log data is a pre-requisite. The well log data

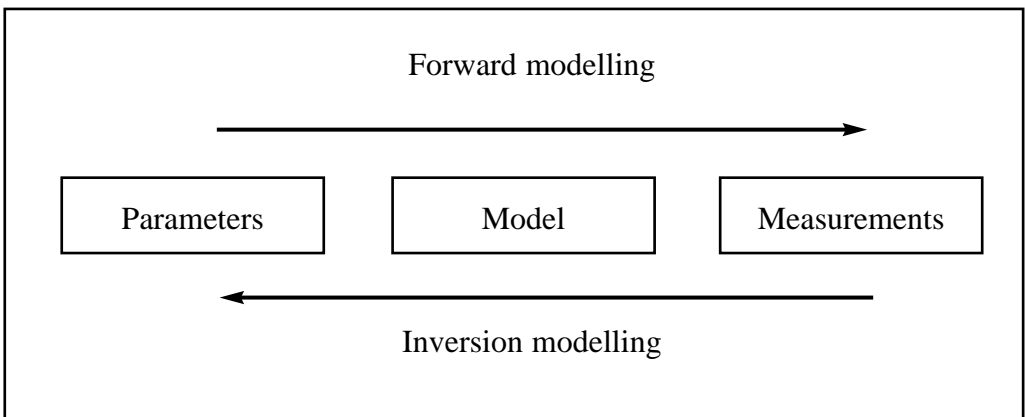


Figure 5.4 Schematic view of inversion and forward modelling.

provide the rock properties at the well location. The inverted reservoir properties serve as input to a geological and reservoir simulation model.

Inversion is referred to as the opposite of forward modelling. Figure 5.4 illustrates both principles. Given the parameters, its response is estimated by forward modelling. For example, given the elastic properties of the subsurface layers, the corresponding synthetic seismic response is modelled. Conversely, given the measurement, the parameters are estimated using inversion. One has to bear in mind that the inversion and forward modelling are not necessarily directly related to each other. The inversion is in general non-unique: multiple parameter sets fit the measurement. As a result, one does not necessarily obtain the appropriate or actual parameter set by inversion. This explains why a variety of different inversion approaches exists.

In the oil industry it is very common to generate an impedance volume once 3D seismic has been acquired. The main benefit is that the impedance is an intrinsic rock property related to lithology, porosity, pore fill, etc., whereas seismic reflectivity is a contrast property. The impedance volume facilitates further inversion to these rock properties. A second benefit is that in the impedance inversion process non-seismic information can be incorporated. The non-seismic data carries low and high frequency information, which is lacking in the band-limited seismic data. By incorporating this information, the inverted impedance volume exhibits a complete frequency range. On the other hand, one should realise that bias is introduced by using the additional information.. The high frequencies are important for resolution. The higher the frequency, the

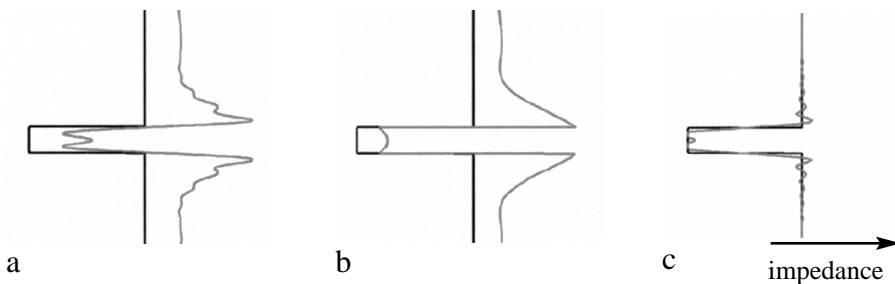


Figure 5.5 A simple impedance layer model (black) is filtered to three different frequency ranges (grey) (a) 10-80Hz, (b) 1-500Hz, and (c) 0-80Hz. The inclusion of the high frequencies (b) allows interpretation of the location of the layer boundaries more accurately, but it is the inclusion of the very low frequencies (c) that allows obtaining absolute values for use in the quantitative interpretation of the rock properties. This example is from Latimer et al., 2000.

higher the resolution, and the better the layer boundaries are defined (Figure 5.5b compared to 5.5a). The low frequencies are critical for an accurate inversion result. Figure 5.5c illustrates that the absolute value is only obtained when low frequencies are incorporated. Low frequency information can be derived from log data, velocity models, and/or a regional gradient. High-frequency information can be inferred from well data using geostatistical analysis.

The inversion from seismic to impedance, either acoustic or elastic, is not straight-forward. The inversion is non-unique. There are multiple solutions to arrive at an appropriate reflection series. A variety of methods exists, which differ mainly in how the non-seismic information is included. Latimer *et al.* (2000) give an overview of the different methods. The seismic signal is a combination of the source wavelet and the earth response or reflection series (Figure 5.3). Both are not exactly known. When inverting for the earth response it is important to utilise the correct source wavelet matching the phase and frequency of the seismic data. An error in estimating the wavelet directly yields an error in the inversion to e.g. impedance. A too high frequency causes the result to be smeared. Wavelets with an incorrect phase or amplitude spectrum can result in erroneous time shifts that can contain extra side lobes, which create false geological events and result in mis-ties with the logs.

Inversion to rock properties can be performed using a variety of methods, either directly or via impedance inversion. For all methods, the calibration to well data is a pre-requisite (Figure 5.6). The well data provide the rock properties

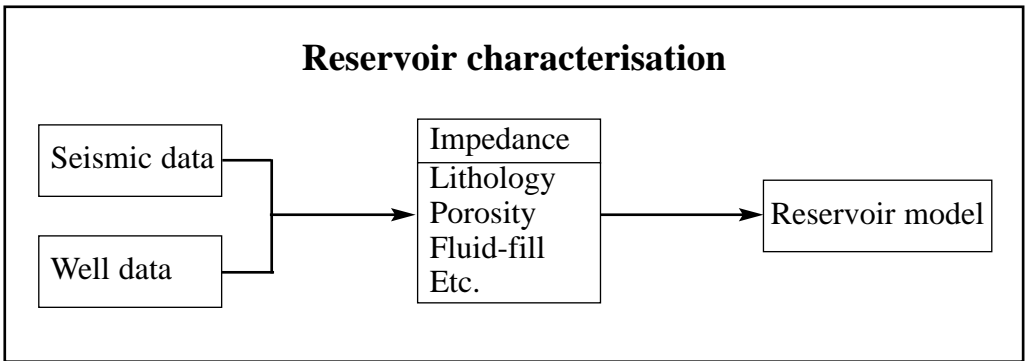


Figure 5.6 Typical 3D inversion scheme from seismic to reservoir properties, either direct or via impedance. The well data is crucial to the inversion. The reservoir properties are used as input to the reservoir model.

corresponding to the seismic signal at the well location. Three types of inversion methods can be distinguished: a physical, a statistical, and a hybrid approach combining the first two. In the first approach, physical models and relations are employed to interpret the seismic data. In the statistical approach, a statistical relation is derived from the data for interpretation. For example, a neural network is employed to find a non-linear relation between the seismic signal and porosity (Oldenziel *et al.*, 2000).

5.3. Parameter sensitivity analysis

Usually, a feasibility study is performed before a decision is taken to acquire time-lapse seismic data. The purpose of a feasibility study is to analyse whether the seismic signal is sensitive to the expected changes in the reservoir. Lumley *et al.* (1997) prepared a risk analysis spreadsheet to quantify a reservoir's suitability for time-lapse seismic monitoring. Acquisition, processing, non-repeatable noise, type of reservoir, etc. are all to be taken into account. Of crucial importance is the translation of expected change in the reservoir properties to synthetic seismic. Below, an example is shown of fluid replacement for a three-layer shale-sand-shale model. This model can be regarded as a simple representation of a reservoir. A modified Gassmann equation (Furre and Brevik, 2000) is used to model the change in elastic properties, see Chapter 8 for more details. Table 5.1 shows the properties and model parameters for the different lithologies and pore fluids.

5.3.1. Water displacement in gas reservoir

The model represents a gas reservoir, where water is used to displace the gas. Table 5.2 shows the reservoir and seismic properties in case the reservoir is filled with 10% water. The P-wave velocity and density, thus impedance, of the sand layer is smaller than for the layer above it. As a result, reflection and transmission coefficients are negative for normal incidence. The same applies to the S-wave reflection coefficient.

	Sand	Shale		
Density (kg/m ³)	2650	2650		
Shear modulus (Pa)	41e+9 Pa	10e9 Pa		
Mineral modulus (Pa)	36e+9 Pa	30e+9 Pa		
Porosity	0.28	0.125		
γ	12.28	3.89		
δ	18.3	5.16		
	Water	Gas	Light Oil	
Density (kg/m ³)	2650	1161	804	
Fluid modulus (Pa)	2.71e+9	0.1417e+6	0.55e+9	

Table 5.1 Properties per lithology and fluid type. γ and δ are specific parameters used in a modified Gassmann model (Section 8.3).

Lithology	ϕ	Sw	ρ	μ_d	K_f	K_d	V_P	V_S
Shale	0.125	1	2444	6.1e6	2.7e6	2.0e7	3521	1577
Sand	0.25	0.1	2000	6.7e6	1.6e2	8.1e6	2966	1859
Shale	0.125	1	2444	6.1e6	2.7e6	2.0e7	3521	1577

Table 5.2 Reservoir and seismic properties.

Incident P-wave - Reflected P-wave

Figure 5.7a shows the reflection coefficient versus the incidence angle of an incident compressional plane wave reflected as a P-wave. The reflection coefficient varies non-linearly with water saturation. The largest change is observed when a few percent of gas is present compared to a fully water saturated sand. The relation between reflection coefficient and incidence angle varies only slightly from fully gas saturated to 90% water saturated. Figure 5.8 shows the P-wave velocity and impedance for different water saturations. Both are sensitive to changes in fluid density and fluid modulus. The effect of fluid density change is linear over the entire saturation range. The effect of fluid modulus change dominates in the region between a few percentage gas and fully water saturated. This explains the large jump for the reflection coefficients between fully water saturated and a few percentages of gas.

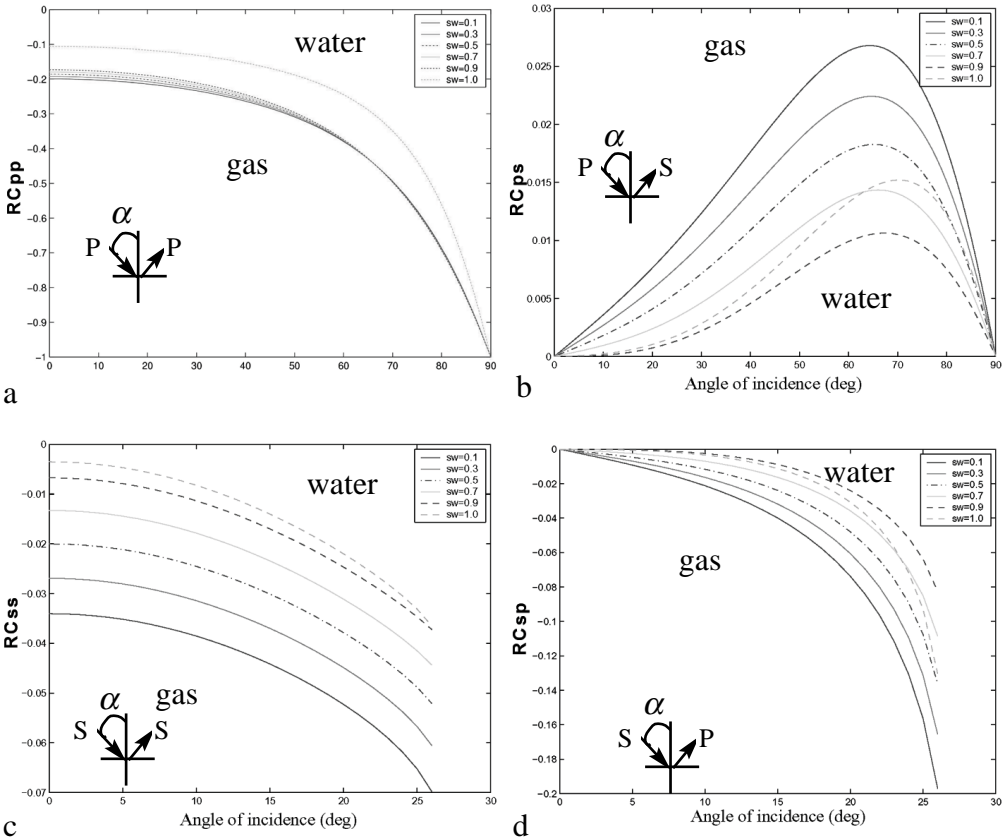


Figure 5.7 Reflection coefficients for incident P-wave (top) and S-wave (bottom) and reflected P-wave (a,d) and reflected S-wave (b,c) versus angle of incidence α for different water saturations.

Incident P-wave - Reflected S-wave

The behaviour for an incident P-wave reflected as S-wave is different than for a reflected P-wave (Figure 5.7b). The reflection coefficient is sensitive over the entire saturation interval. All curves, except the fully water saturated curve, display a maximum reflection coefficient at incidence angle of 65 degrees . The water curve is shifted towards a higher angle of incidence and reaches a higher reflection coefficient than the curves for 0.9 and 0.7 water saturation. Most probably, this behaviour is caused by the change from a few percentage of gas to a fully water saturated sand. In the region of 0 to 15 degrees incidence angle,

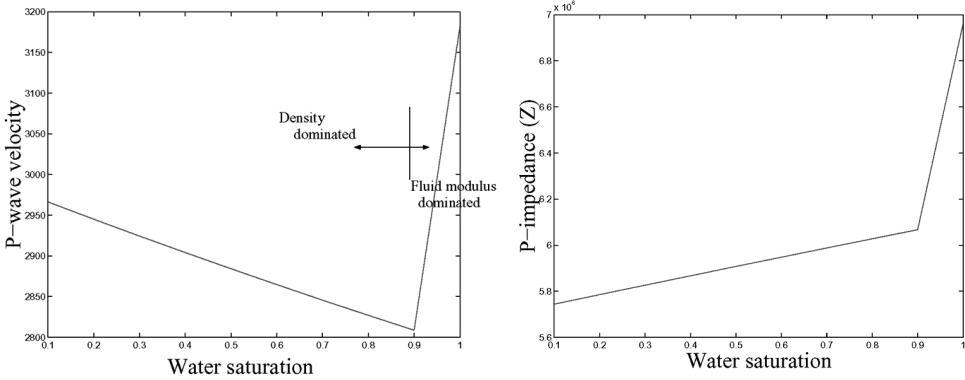


Figure 5.8 Compressional velocity (left) and impedance (right) with changing water saturation.

the reflection coefficient of the water-dominated sands is zero. On the other hand, the gas dominated sands display a non-zero reflection coefficient. Overall, the reflection coefficient for incident P-wave and reflected S-wave is sensitive to saturation over the entire saturation range. In comparison, the P-P section is indifferent to the gas saturation and only a distinction between water and gas saturated sand can be made. At an incidence angle of 60 degrees, a water saturation change from 0.3 to 0.5 yields a 22% decrease in the reflection coefficient.

Incident S-wave - Reflected S-wave

Figure 5.7c shows the reflection coefficient for different angles of incidence, up to 25 degrees. The reflection coefficient for incident S-wave reflected as S-wave is sensitive to saturation. With increasing water saturation, the reflection coefficient decreases uniformly. For each 0.2 step in saturation, the decrease for reflection coefficient is equal. Moreover, the reflection coefficient for a fully water saturated sand does not display anomalous behaviour. The shear wave is only dependent on the fluid density and not to the fluid modulus, which causes the large step between fully water saturated and a few percentages of gas for incident P-waves. An increase in water saturation from 0.3 to 0.5 causes a 32% decrease in the reflection coefficient.

Incident S-wave - Reflected P-wave

Similar to the S-S section, the reflection coefficient for the reflected P-wave caused by an incident S-wave decreases with increasing water saturation

(Figure 5.7d). In general, the reflection coefficient increases with increasing angle of incidence. The curve for the 100% water saturation displays behaviour different from the other curves. Similar to the P-S conversion, the water-dominated sands do not show on seismic sections between 0 and 10 degrees. At an intermediate angle of 15 degrees, a 22% decrease is observed for a water saturation increase from 0.3 to 0.5.

The results described above indicate the expected changes in seismic signal when gas is displaced by water. A similar analysis can be performed for different scenarios (Jooris, 2000). The sensitivity analysis only yields a qualitative measure, because other issues have to be taken into account to model the actual time-lapse signal. Based on the P-wave data it is not possible to quantify the change in gas saturation, except when gas is entirely displaced by water. The S-wave is sensitive to the gas saturation in the entire range from fully water to fully gas saturated sands. Therefore, to quantify the gas saturation, either P-wave AVO or multi-component seismic is required.

5.4. Time-lapse seismic

3D seismic acquired at different times is referred to as time-lapse seismic. It is used to obtain information regarding the changes in the reservoir state. The reservoir state is characterised by saturation, effective pressure, and temperature. Hydrocarbon production induces a change in one or more aspects of the reservoir state in turn affecting the elastic properties of the rock. The objective of time-lapse seismic is to measure this change in elastic properties and relate this to the change in reservoir state.

According to Waggoner (2001), the time-lapse seismic signal can be used for reservoir interpretation in any of following four methods applied to the following fields:

- | | | |
|--------------------------------|-----------------|-------------------------------|
| 1) visual inspection | Gannet C | (Koster <i>et al.</i> , 2000) |
| 2) quantitative interpretation | Statfjord | (Kvamme <i>et al.</i> , 2000) |
| 3) model screening | Draugen | (Koster <i>et al.</i> , 2000) |
| 4) seismic history matching | South Timbalier | (Hang <i>et al.</i> , 1997) |

Excellent examples of each are given in parenthesis. The first step in time-lapse seismic analysis is visual inspection of the seismic attributes (Section 8.4).

Qualitative or quantitative interpretation of the observed time-lapse anomalies is often the next step (Section 8.5). Correlation to well data and the reservoir model allows interpretation in terms of production-induced reservoir changes.

5.4.1. Repeatability

In general, repeatability between measurements has to be assumed in order to compare data. In time-lapse seismic interpretation, one has to assume that the seismic experiments are repeatable over time. The source wavelet and the acquisition parameters impact the resulting seismic image of the subsurface. Acquiring time-lapse seismic surveys with varying acquisition settings impedes comparison of the data. The observed time-lapse differences can be due to dynamic changes in the reservoir state but equally well due to the variations in acquisition settings. The observed differences can be attributed to the reservoir only if static parts of the subsurface have identical seismic responses on base and monitor survey(s). Ideally, seismic acquisition and (re-) processing for all surveys are identical, but in practice this condition is difficult to meet.

Whether onshore or offshore, acquisition for time-lapse purposes requires special attention. To ensure repeatability, the acquisition set-up of the base survey is re-produced when acquiring the monitor survey(s). One has to bear in mind that many base surveys are not acquired for time-lapse seismic purposes but are shot at a time that little information is available about the reservoir. Using the latest technology and knowledge about the reservoir, a repeat survey can be constructed such as to optimally image the reservoir. However, for time-lapse purposes repeatability is crucial. The strive for repeatability is often conflicting with the effort to obtain an optimal image of the reservoir.

Even when vintages are identical, repeatability remains a challenge. Variations in acquisition noise occur and the environment may have changed over time, e.g. through installation of a production platform. Weather and sea conditions, performance of crew and equipment, etc. are beyond human control. Ronen *et al.* (1999) quantify various effects of acquisition and processing by analysing repeat multi-component seabed data. Cooper *et al.* (1999) compare streamer versus OBC time-lapse seismic over the Foinaven field. For both, the acquisition set-up is re-produced. The time-lapse signals observed in both types of acquisition are qualitatively consistent.

Seismic (re-)processing plays a key-role in equalising the responses over the static parts, because the acquisition cannot be exactly repeated. Beasley *et al.*

(1997), Vauthrin *et al.* (1999), and Huang *et al.* (1999) have analysed whether legacy, of-the-shelf, base surveys can be compared to monitor surveys. All state that re-processing, preferably from pre-stack data, yields the best results. A side effect of re-processing is that the individual surveys are processed sub-optimally with respect to obtaining an image of the subsurface. Cross-equalisation between the time-lapse data sets is a crucial step in re-processing. The fact that the overburden does not change over time is used as a constraint. Both time-lapse data sets are corrected for spatial position and binning discrepancies, as well as differences in timing, wavelet phase, and amplitude. Ross *et al.* (1996) give an excellent overview of the importance of cross-equalisation and the impact of incorrect cross-equalisation.

5.4.2. Seismic reservoir quantification

Compared to 3D seismic inversion (Section 5.2), inversion of time-lapse seismic is more complicated. First repeatability has to be assumed before the time-lapse signal can be interpreted in terms of (a change in) reservoir properties. The inversion of the time-lapse seismic signal to the reservoir properties is performed either directly or by using inverted impedance (Figure 5.9). Calibration at control points, such as wells, is a pre-requisite. Both base and monitor survey(s) have to be calibrated using well logs. The relation between seismic and well log data is crucial. A requirement is that the well logs represent the reservoir state at the time of seismic acquisition. Such well logs

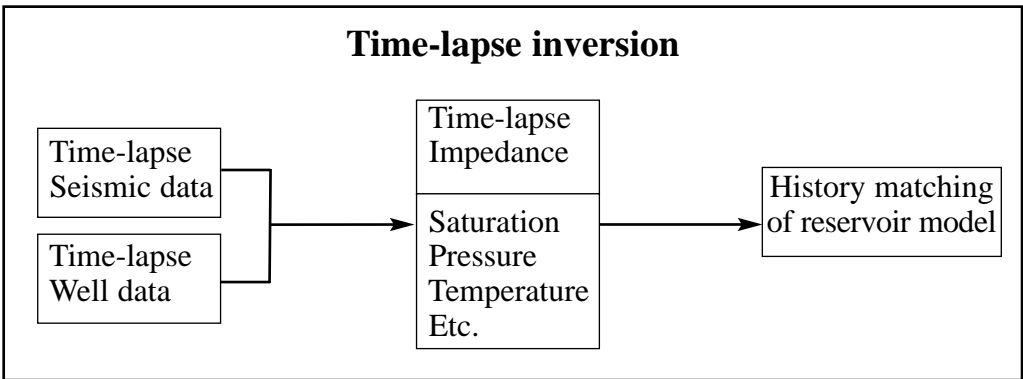


Figure 5.9 Typical time-lapse seismic inversion scheme to reservoir property saturation, where the inversion is either direct or via time-lapse impedance. The time-lapse well data is crucial to the inversion. The reservoir properties are used to constrain the reservoir model.

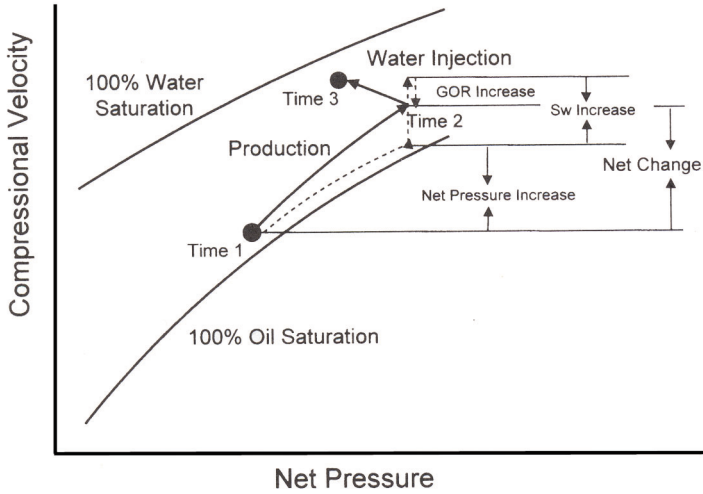


Figure 5.10 Combined effect of oil production and water injection on the compressional velocity. As the field is produced, formation pressure drops, thus overburden pressure increases, and water saturation increases. As water is injected, formation pressure increases, thus overburden pressure decreases, and water saturation increases, after Wang (1997)

are referred to as time-equivalent logs. Therefore, well logs should ideally be recorded concurrent with the time of seismic acquisition. Logs representing a different reservoir state introduce bias. This applies not only to the dynamic properties but also to inversion of static properties, e.g. porosity, because static and dynamic properties are coupled in their seismic imprint (Oldenziel *et al.*, 2000). Depending on the reservoir and the objectives, the time-lapse seismic data is inverted to saturation, pressure and/or temperature changes. These estimates of the change in the reservoir state are subsequently used to test and constrain the reservoir model as described in Chapter 3.

The inversion of time-lapse seismic is complicated, because often more than one reservoir property changes over time. For example, during production pore pressure decreases and water saturation increases. These changes influence the time-lapse seismic signal differently (Figure 5.10). Their effects can be of opposite character yielding a weaker signal. On the other hand, the combined effect can also yield a stronger time-lapse signal. To avoid erroneous interpretation, the time-lapse seismic effects of the different changes need to be decoupled.

Decoupling of the pressure and saturation induced effects can be done based on P-wave and S-wave information as shown by Tura and Lumley (1999) and Landro (1999). The former show that based on the P-wave and S-wave impedance the pressure and saturation changes are decoupled. For a synthetic model, they crossplot the S-wave and P-wave impedance in the time-lapse domain. Natural clusters can be defined, which correspond to saturation or pressure changes (Figure 5.11). In general the shear modulus is more sensitive to pressure than the bulk modulus. Pressure changes thus tend to cluster between the diagonal and the time-lapse S-wave impedance axis. A saturation change affects the bulk modulus and density, but not the shear modulus. Points corresponding to saturation changes cluster along the time-lapse P-wave impedance axis, as the S-wave impedance is only slightly affected by the minor density change. Combined pressure and saturation changes are found between the diagonal and the time-lapse P-wave impedance axis. Using this natural clustering, the time-lapse seismic signal can be translated to pressure and saturation changes.

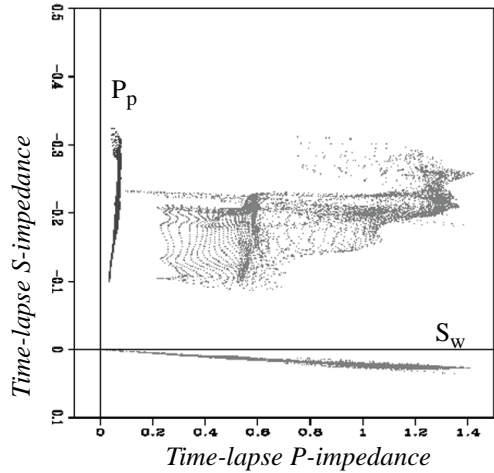


Figure 5.11 Pore pressure (P_p) changes cluster along the I_s axis, water saturation (S_w) changes along the I_p axis and combined changes along the diagonal, after Tura and Lumley (1999)

Points corresponding to saturation changes cluster along the time-lapse P-wave impedance axis, as the S-wave impedance is only slightly affected by the minor density change. Combined pressure and saturation changes are found between the diagonal and the time-lapse P-wave impedance axis. Using this natural clustering, the time-lapse seismic signal can be translated to pressure and saturation changes.

Landro (1999) derives explicit expressions for computation of pressure and saturation changes from P-wave AVO data. Typical relations between velocity and pressure and saturation are integrated in the approximate expression for P-wave reflectivity derived by Smith and Gidlow (1987). The procedure has been successfully tested on a North Sea data set. Some leakage from the pressure to the saturation attribute cube has been observed.

5.4.3. Vicious circle

As stated above, well logs are crucial for inversion of (time-lapse) seismic data. They provide the relation between reservoir properties and seismic signal. In most fields, well logs are not (re-)run for each time-lapse seismic acquisition. Often it is not possible to re-enter the wells for economical, logistical, and other reasons. Even if feasible, the logging tools have to measure reservoir properties beyond the production damaged zone into the virgin zone. Without time-equivalent logs, time-lapse seismic cannot properly be inverted. Neither can the rock physical model be calibrated. To overcome the lack of time-equivalent logs, the industry has adopted a workaround. Instead of being measured, the time-equivalent logs are modelled from the measured logs (Furre and Brevik, 2000). Using a rock physical model the measured logs are modified to represent the reservoir state (saturation and pressure) at the time of seismic acquisition. However, one has to be aware of the vital aspect that the reservoir state in the wells at the time of seismic acquisition is unknown! No well logs have been acquired to measure it. The closest is an estimate from the reservoir simulator. Using the information from the reservoir model, the time-equivalent logs are modelled. Based on these modelled logs, it is possible to interpret and invert the time-lapse seismic. However, without realising, a Catch-22³ situation has arisen (Figure 5.12).

“There was only one catch and that was Catch-22, which specified that the reservoir state at the wells was needed to interpret the time-lapse seismic. The reservoir state at the wells could have been measured, but in practice never was, so they used the reservoir model to estimate the reservoir state. To prove that the reservoir model was correct they decided to test against measurements of the reservoir state. These measurements were called time-lapse seismic and to interpret these they used the reservoir state at the well locations from the reservoir model.” (Oldenziel, 2002)

Provided production well logs are acquired concurrent with each seismic acquisition, the Catch-22 does not arise. The measured time-lapse logs are then used for inversion to impedance or reservoir properties, which serve as constraints to the reservoir simulation model. Sophisticated and exciting technologies are being developed to monitor the reservoir at the wells, e.g. permanent sensors in the wells using fibre optic cables (Hottman and Tuttle, 2001).

Regarding existing fields, the Catch-22 has to be dealt with. Relying on the reservoir model for the interpretation of time-lapse seismic will bias the end result and has to be justified. Most of all, one has to be aware of the assumptions and the consequences of the Catch-22. A solution to the Catch-22 would be to

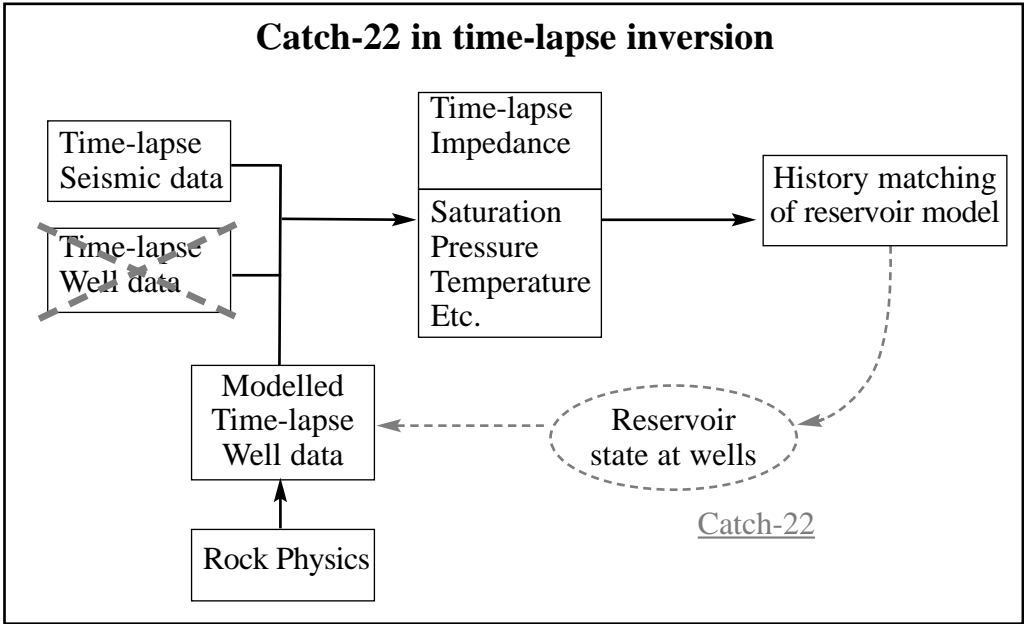


Figure 5.12 When time-lapse logs are lacking, the reservoir state representative for the seismic acquisition time is unknown and instead taken from the reservoir model. This gives rise to a Catch-22 situation: time-lapse seismic is used to check the reservoir, whereas the latter is required to interpret the time-lapse seismic.

³ From Joseph Heller's 'Catch 22'.

'There was only one catch and that was Catch-22, which specified that a concern for one's safety in the face of dangers that were real and immediate was the process of a rational mind. Orr was crazy and could be grounded. All he had to do was ask; and as soon as he did, he would no longer be crazy and would have to fly more missions. Orr would be crazy to fly more missions and sane if he didn't, but if he was sane he had to fly them. If he flew them he was crazy and didn't have to; but if he didn't want to he was sane and had to. Yossarian was moved very deeply by the absolute simplicity of this clause of Catch-22 and let out a respectful whistle.

"That's some catch, that Catch-22," he observed.

"It's the best there is," Doc Daneeka agreed.'

develop alternative methods, which do not require time-lapse well logs concurrent with each time-lapse survey. A (time-lapse) seismic attribute, which can be directly linked to the fluid flow properties would avoid using the time-lapse seismic well logs.

At the moment, it is possible to respect the Catch-22 by using an iteration loop comprising both the reservoir model and the time-lapse seismic interpretation. A changed interpretation of one leads to re-interpretation of the other. All relevant data could be included in the iteration loop. An integrated flow model (Pagano *et al.*, 2000) is one way to facilitate this iteration loop. It can be extended to incorporate other available data, e.g. geological, core, welltest data. Each piece of information is independently measured, while all are related to the reservoir. Special treatment is to be reserved for the rock physical model, which plays a key role in the integration of all information, because it defines how reservoir and seismic properties are related. Rock physics is not always considered a strong link and thus should not be treated as a static entity in the proposed iteration loop. It should be allowed to be flexible and to be updated in each iteration loop.

Chapter 6

Directly linking seismic to fluid flow

The main deliverable and one of the main challenges of time-lapse seismic is to interpret the seismic in terms of reservoir and fluid properties. The time-lapse seismic signal is influenced by one or more changes in the reservoir state. Each of these production-induced changes can have a different effect on the seismic signal (Batzle *et al.*, 1998). Decoupling of these effects is crucial and quantification in terms of reservoir changes poses a major challenge. In practice, the information carried by the time-lapse seismic is qualitatively or quantitatively translated to e.g. fluid fronts and saturation maps. Currently, either the amplitude or impedance is used, or their time-lapse difference. Most often, a 2D (grid) estimate of a global reservoir property is obtained at the top of the reservoir as an average over the entire reservoir.

A major drawback of current methods is that they rely on numerous assumptions, each of which impacts the final inversion result. For example, all methods assume a one-to-one relation between (time-lapse) seismic and saturation. The seismic measurement is affected by the elastic or acoustic contrasts in the subsurface. In its simplest form the seismic response is described as the convolution of the seismic source signal that generates the action and the earth response reflecting the subsequent layers in the earth (Section 5.2). Both source signal and earth response are not exactly known. To

estimate the earth response, assumptions have to be made about the wavelet, and vice versa. To interpret the seismic or earth response in terms of subsurface or reservoir properties, well measurements are required. The well data provide the rock properties corresponding to the seismic signal at the well location. Two obstacles have to be overcome. First, the well log and core data are measured at frequencies different from the seismic data. Especially for fluid-filled rocks, the dispersion effect can have a large impact (Section 4.3.4) and has to be considered before using the well log and core data for interpretation of seismic data. Secondly, bias is introduced when well and seismic data are not acquired at the same time. To allow interpretation of the seismic, the well and seismic data should correspond to the same reservoir state. If measured at different times, the well and seismic data do not necessarily represent the same state. Especially for time-lapse seismic, this can have a significant impact (Section 5.4.3). The next complicating factor is that rock physical models are not capable of describing all physical processes that occur in the rock (Chapter 4). For example, rock physical models are incomplete with respect to modelling a combined change of saturation and pressure. Often, rock physical models do not necessarily describe the rock's behaviour at the seismic scale. Therefore, it is hard to translate observed seismic behaviour in terms of rock or reservoir properties.

The exact relation between time-lapse seismic and reservoir state is rather complex. Interpretation of the time-lapse signal in terms of reservoir properties is far from straight-forward. When we observe a change over time in the seismic character, we know that the reservoir state has changed in the same time period due to production. This basic physical fact holds as long as repeatability of the seismic measurement can be assumed. In other words, the time-lapse changes are physically related to the changes in the reservoir when the acquisition and processing artefacts are small compared to the production-induced changes on the seismic. Using this physical fact, we propose an alternative method and directly link the observation to its cause. This method yields information about the material (rock and reservoir) parameters at the seismic scale. We formulate a 4D attribute without referring to rock physical modelling, requiring assumptions on the character of the seismic wavelet, or using well data.

6.1. Procedure

6.1.1. Wavelet independency

To allow interpretation of the seismic signal in terms of rock properties, the effect of the wavelet should be eliminated. Deconvolution of the seismic response removes the wavelet from the seismic measurement yielding the earth response (Section 5.2). The earth response has the form of a relative impedance or spike trace (reflection series). It contains information about the impedance contrasts in the earth, thus indirectly about the actual impedance in each layer. The wavelet required for deconvolution is never exactly known; it has to be derived or assumed affecting the result. When two traces exhibit the same wavelet, the wavelet can be removed in the frequency domain using an alternative manner. In the frequency domain, a trace T is regarded as the multiplication of the earth response E and the wavelet W

$$T = EW . \quad 6.1$$

The effect of the wavelet is eliminated by dividing two traces, T_1 and T_2 , exhibiting the same wavelet. In generic terms subscripts 1 and 2 denote different states. This yields a quotient of the earth responses of both traces

$$\frac{T_1}{T_2} = \frac{E_1 W}{E_2 W} = \frac{E_1}{E_2} . \quad 6.2$$

In the following, we use a normalisation to eliminate the wavelet instead of the quotient from Equation 6.2

$$\frac{T_1 - T_2}{T_1 + T_2} . \quad 6.3$$

We define this as the normalisation attribute, which is a wavelet independent measure of the seismic. Notice the resemblance to the reflection coefficient (Equation 5.7). The only requirement for the above is that the wavelet for both traces T_1 and T_2 are equal. For neighbouring traces, this is a reasonable assumption. The result is a quotient of the earth responses of the two neighbouring traces. It can be seen as a normalisation of the trace by its neighbour.

Applying the same normalisation for time-lapse seismic data sets, would allow studying the dynamic changes in the earth response over time in a wavelet independent manner. The purpose of the normalisation is to correct for changes in acquisition and processing between surveys. The change in the normalised attribute between the data sets captures the information about the change in dynamic reservoir properties

$$\frac{T_1 - T_2}{T_1 + T_2} \Big|_{time1} - \frac{T_1 - T_2}{T_1 + T_2} \Big|_{time2} . \quad 6.4$$

For time-lapse purposes, normalisation of a reservoir trace by its neighbouring trace is not practical. The reservoir trace and its neighbouring trace change over time due to production. This impedes the comparison between the base survey normalisation attribute with the monitor normalisation attribute. For time-lapse purposes, the normalisation should be consistent over time. A solution is found in using a trace, or piece thereof, from the overburden at the same position as the reservoir trace. The overburden remains constant over time. Moreover, the overburden trace exhibits the same wavelet as the reservoir trace. Differences between time-lapse surveys observed in the overburden trace are only induced by differences in seismic acquisition and/or processing between the time-lapse surveys. Therefore, the overburden trace is very well suited to serve as a normalisation trace. From the overburden, one can choose a variety of trace segments for the purpose of normalisation. To ensure consistency for normalisation of the time-lapse data sets, we recommend using a trace segment corresponding to a lateral consistent reflector not too far above the reservoir. In the normalisation procedure, unwanted signal is introduced when the phase of the overburden trace segment is different from the phase of the reservoir trace. When phase alignment is used, the overburden trace segment is not necessarily constant over time. As a solution, it is better to employ a phase independent measure.

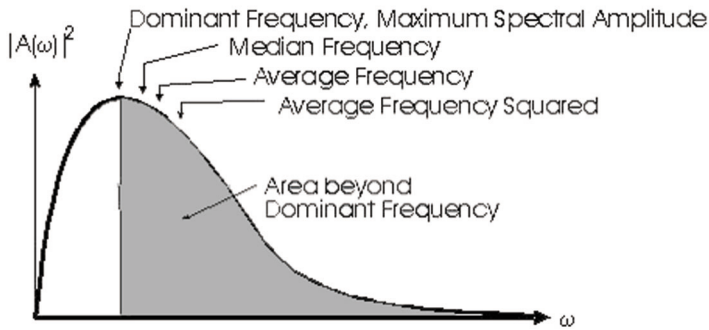


Figure 6.1 Illustration of frequency spectrum with some examples of time-frequency attribute.

6.1.2. Frequency domain

The amplitude-frequency spectrum is a phase independent measure of the seismic. Figure 6.1 illustrates the amplitude-frequency spectrum. An extensive range of time-frequency attributes can be defined to describe the spectrum. The spectrum may be sensitive to the time-gate used to calculate the spectrum. The principle of normalisation, as explained in the previous section, can also be employed in the frequency spectrum. By using the amplitude-frequency spectrum, phase mis-alignment problems are avoided. Furthermore, the amplitude-frequency spectrum is less sensitive to the exact trace segment taken for normalisation. Figure 6.2 illustrates the principle of normalisation in the amplitude-frequency spectrum for a time-lapse data set. The spectrum of the overburden is used to normalise the spectrum of the reservoir. The normalisation is applied over the entire spectrum rather than to one or more of the time-frequency attributes. A separate normalised spectrum is obtained for base and monitor survey. Subtraction of the base survey normalised spectrum from the monitor survey normalised spectrum yields the time-lapse normalised spectrum. The time-lapse normalised spectrum captures the time-lapse behaviour of the normalised amplitude-frequency spectrum. Thus, it captures the time-lapse behaviour of the seismic signal itself. The time-lapse change of the normalised spectrum is related to the production induced changes in the reservoir that occurred between base and monitor survey. For example, in Figure 6.2, the time-lapse signal is caused by a saturation increase from base to monitor survey.

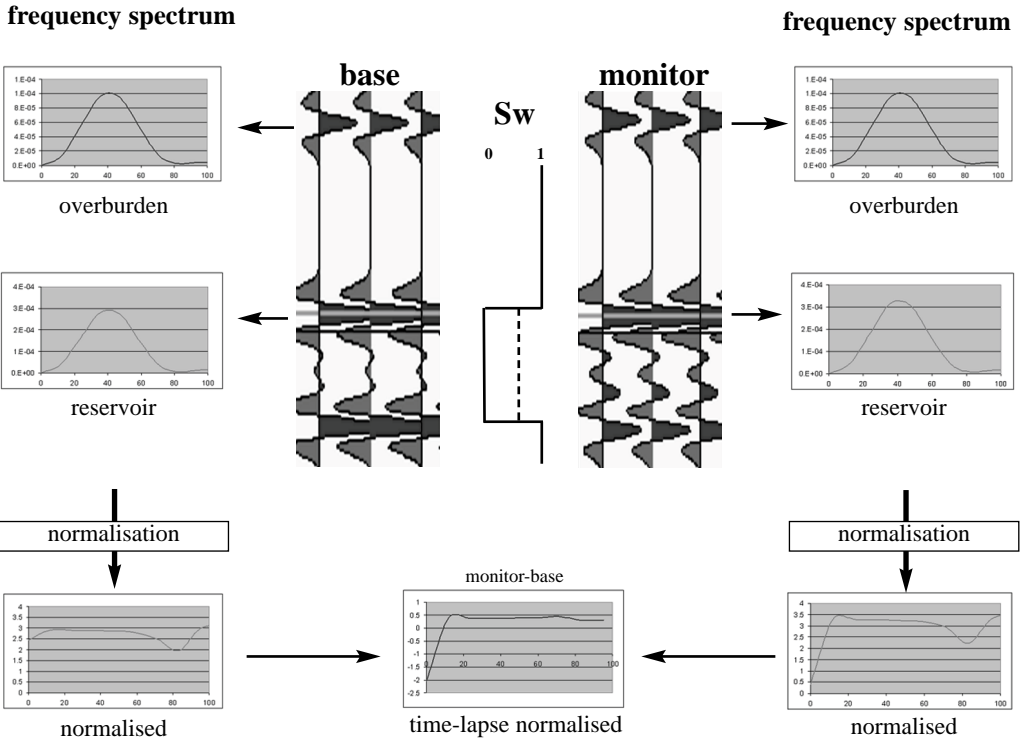


Figure 6.2 The amplitude-frequency spectrum is calculated for the overburden (top left and right) and the reservoir (middle left and right) for the base and monitor survey. Normalisation of the reservoir spectrum by the overburden spectrum yields the normalised spectrum (bottom left and right) for the base and monitor survey. Subtraction of the normalised spectra of the base survey from the monitor survey yields the time-lapse normalised spectrum, from which a series of attributes can be defined and extracted. The time-lapse change of the normalised spectrum is related to the saturation change from base (solid line) to monitor survey (dashed line).

6.2. Synthetic reservoir

The 3D synthetic reservoir used in this chapter is modelled after the Statfjord field (Chapter 8). The model is described in detail in Section 7.3.1. It consists of 1200 blocks divided over three layers of each 400 blocks. Each layer has 20 blocks in the x-direction and 20 blocks in the y-direction (Figure 6.3). A grid block is 50m long by 50m wide and 30m thick. The reservoir model is thus 90m thick and measures one km in the x-direction and y-direction. The reservoir grid is bounded by four faults, which serve as no-flow boundaries. The tectonic dip is ignored. Producing wells are in the west of the field (left side of Figure 6.3) and water injectors are in the east. As in the Statfjord Field, the open side of the listric slumps is also pointed in the downdip direction. The synthetic reservoir has four slumps of different size; each with a throw of 50 m. Figure 6.3 shows the oil saturation after 15 years of production. At this point, approximately 65% of initial oil in place has been produced. The residual oil saturation is taken as zero and 100% recovery is possible. The bottom layers have been largely produced and are now filled with water. Still a considerable amount of oil is left in the top layer. Water injected by injector 1 (lower right corner) does not flow

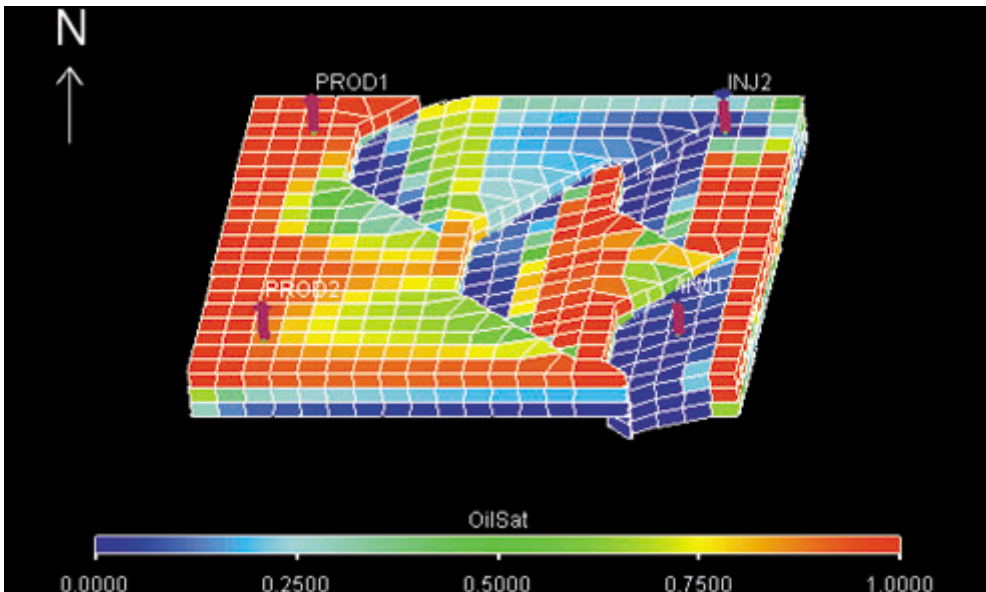


Figure 6.3 Oil saturation after 15 years of production in the synthetic reservoir.

in the upper layer due to the nearby slump. From the area around injector 2 (upper right corner) injected water flows preferentially in and around the slump but not toward injector 1. Oil is trapped in the middle of the reservoir model and below injector 2. The reservoir exhibits a laterally varying geology, modelled via a laterally varying density. The layers above and below the reservoir are modelled as a thick layer with laterally varying properties. Over time, these layers do not change.

Production and saturation data are generated using a reservoir simulator (Eclipse, 1999). Using the Gassmann equations (Gassmann, 1951), the density, P-wave velocity, and S-wave velocity are corrected for the change in saturation. The effect of a pressure change is neglected. Before generating the synthetic seismic, the model is downscaled by interpolation to 120x120x30 blocks. In the downscaled model, each grid block is 8.3m long and wide and 3m thick. Using the downscaled model, the synthetic seismic exhibits a less blocky (more continuous) character. Synthetic time-lapse P-wave seismic data are generated using the convolutional approach to obtain an ideal imaging result. A 30Hz Ricker wavelet is used (Figure 6.4a). Table 6.1 gives some reference values for the density and velocity for the reservoir and layers above and below. Figure 6.5

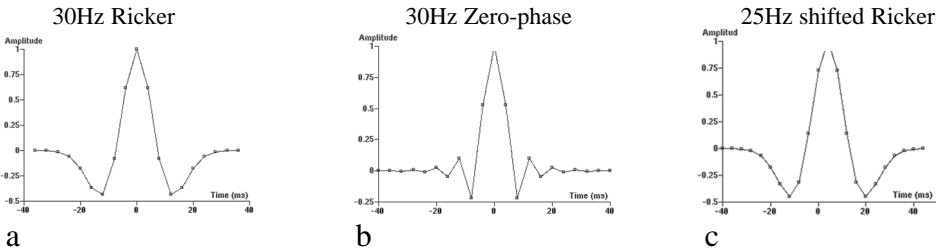


Figure 6.4 Different wavelets used to generate synthetic seismic.

	Density(kg/m ³)	P-wave (m/s)	AcImp(kg/m ² s)
Top Layer	2250	2100	4725000
Reservoir (Sw=1)	±2450	±2700	6615000
Reservoir (Sw=0)	±2325	±2350	5463750
Bottom Layer	2600	2700	7020000

Table 6.1 Characteristic values for the density, P-wave velocity, and acoustic impedance (AcImp) of the synthetic model.

Directly linking seismic to fluid flow

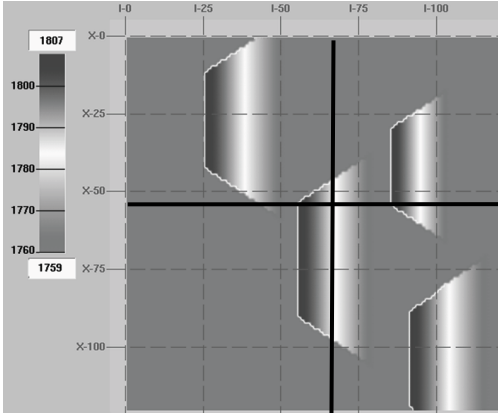


Figure 6.5 Top reservoir map illustrating the four slumps and their depth in two-way time [msec]. Black lines correspond to the inline 65 and crossline 55, which are shown in Figure 6.6.

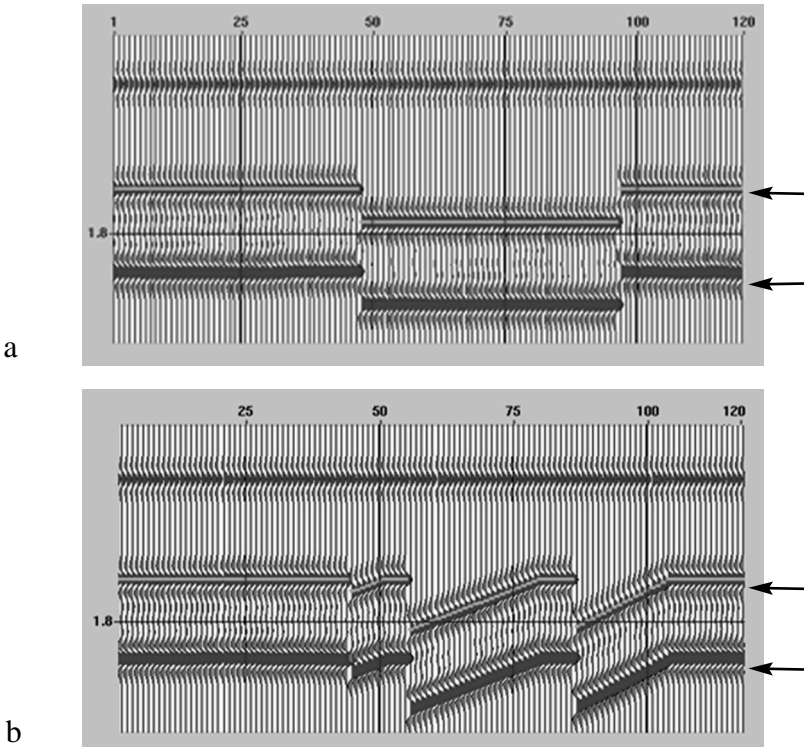


Figure 6.6 a) Inline 65 through the synthetic model taken from the base survey. b) Crossline 55 through the synthetic model taken from the base survey. The reflectors corresponding to the top and bottom of the reservoir are denoted by the arrows.

shows the top reservoir horizon. Figure 6.6 shows an inline and crossline through the base survey. Thirteen time-lapse surveys are generated within the first 15 years of production. The base survey is denoted by T00, the monitor surveys by T05, T10, etc. to T60. The notation Txx refer to reservoir simulation time steps, where each step xx corresponds to a period of 3 months.

6.2.1. Amplitude versus saturation

In conventional time-lapse seismic interpretation, the amplitude or the inverted impedance is used. The amplitude at top of the reservoir for the synthetic model is shown in Figure 6.7. A comparison is made between the base survey (T00) and monitor surveys T25 and T50. Monitor surveys T25 and T50 correspond to 6.25 years and 12.5 years of production, respectively. At T00, the reservoir is oil-filled. The variation in amplitude at the top reservoir is due to the geological

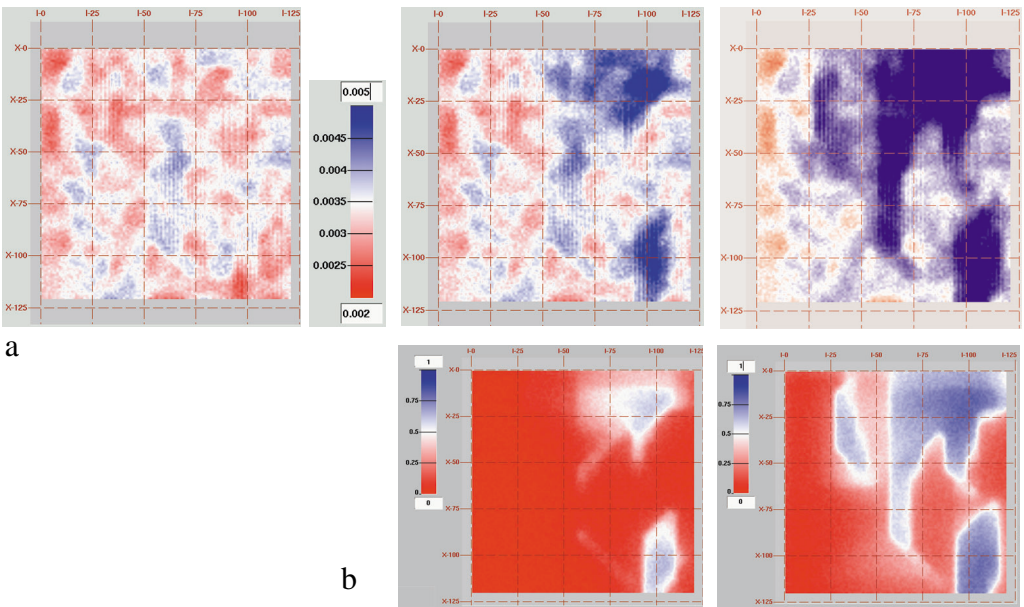


Figure 6.7 a)The amplitude at top of the reservoir for the base survey (left), monitor surveys at T25 (middle) and monitor survey T50 (right). T25 and T50 correspond to reservoir simulation time-steps at 6.25 years and 12.5 years of production, respectively. All three images are plotted using the same colour scale. b)The corresponding water saturation with water in blue and oil in red. The water saturation for the base survey is 0.

heterogeneity of the synthetic model. Water injection starts simultaneously with oil production at day 1. As water replaces oil the amplitude at the top reservoir increases. This can be explained as follows. The P-wave reflection coefficient for the interface between the layer above and the reservoir determines the strength of the reflected signal, i.e. the amplitude. The P-wave reflection coefficient is calculated from the impedance contrasts between two layers (Section 5.1). The acoustic impedance is the product of density and velocity

$$RC_{PP} = \frac{\rho_2 V_P^2 - \rho_1 V_P^1}{\rho_2 V_P^2 + \rho_1 V_P^1}, \quad 6.5$$

where ρ is the density and V_P the velocity of layer 2 (reservoir) and layer 1 (top layer). Based on the values in Table 6.1, the reflection coefficient or impedance contrast between the overburden and a water-filled reservoir is larger than for an oil-filled reservoir. As a result, the amplitude for the water-filled reservoir is larger than for an oil-filled reservoir. In Figure 6.7a, the images are plotted at the same colour scale. The increase in amplitude associated with the water injection is shown in blue. The injected water front originates from the injectors in the east. Figure 6.7b shows the corresponding water saturation of the monitor surveys.

Figure 6.8 shows the relation between the observed time-lapse signal and the saturation. The amplitude differences are calculated at different levels within the reservoir and plotted against the corresponding saturation changes. The different levels correspond to 4msec, 12msec, 36msec, 48msec, and 64msec below the top reservoir. The entire reservoir is roughly 72msec thick. The data is taken from crossline 55 through the base (T00) and monitor (T25, T50) surveys of the synthetic model. The relation between observed time-lapse amplitude difference and saturation difference is changing along the reservoir. For Figure 6.8, the three surveys are generated using exactly the same wavelet. In practice, 100% repeatability between the different seismic measurements is never achieved and each survey is acquired differently. For our synthetic model, we emulate the lack of repeatability by using different wavelets when generating the different synthetic seismic surveys. Figure 6.4 shows the 30Hz Ricker wavelet, that has been used so far, and two slightly different wavelets. For the data in Figure 6.9, the zero-phase 30Hz wavelet (Figure 6.4b) is used to generate seismic for monitor survey T25. The 25Hz wavelet (Figure 6.4c) is used to generate seismic for the T50 monitor survey. The same analysis as in Figure 6.8 is carried out for these seismic data sets. Figure 6.9 shows the relation between time-lapse amplitude and saturation difference. The relation

Amplitude difference versus saturation difference

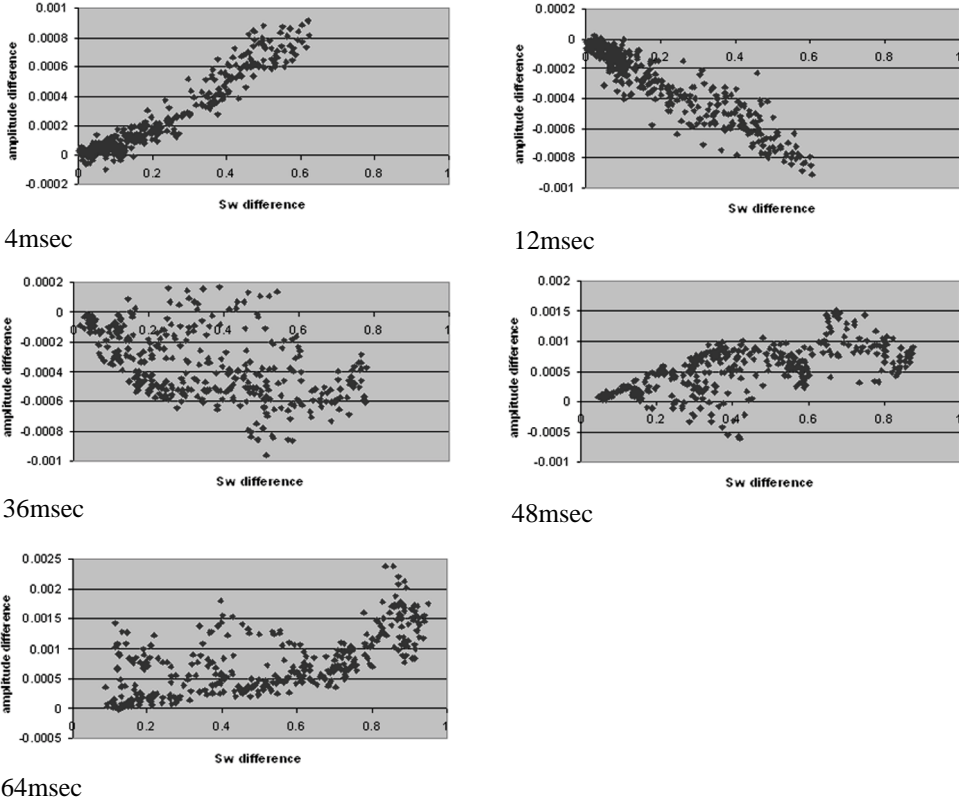
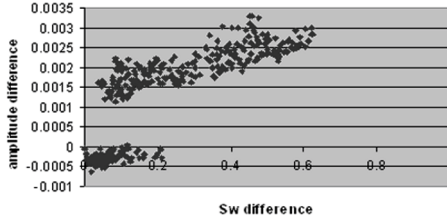


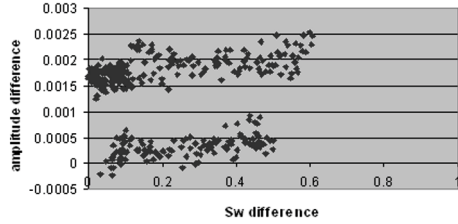
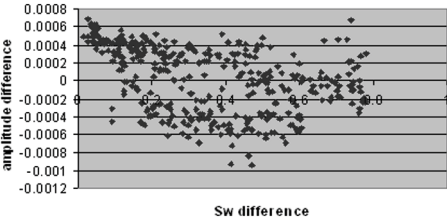
Figure 6.8 The time-lapse amplitude difference versus the time-lapse saturation difference for different levels within the reservoir. The plots correspond to 4msec, 12msec, 36msec, 48msec, and 64msec below the top reservoir. The data is taken from crossline 55. Time-lapse difference between the base survey (T00) and monitor surveys (T25, T50) is used. The surveys are generated using a 30Hz Ricker wavelet.

deteriorates compared to Figure 6.8. More importantly, for most levels in the reservoir, two relations are observed, which are the result of the difference in seismic acquisition. It shows the importance of correcting the data for the impact of a difference in acquisition between time-lapse surveys. For this reason, we suggest the normalisation of the seismic signal.

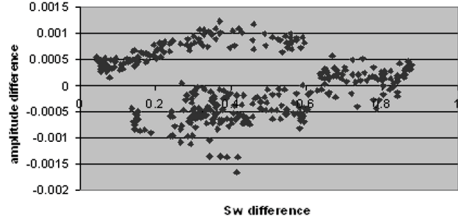
Amplitude difference versus saturation difference



4msec

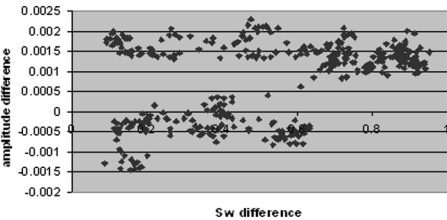


12msec



36msec

48msec



64msec

Figure 6.9 The time-lapse amplitude difference versus the time-lapse saturation difference for difference levels within the reservoir. The plots correspond to 4msec, 12msec, 36msec, 48msec, and 64msec below the top reservoir. The data is taken from crossline 55. Time-lapse difference between the base survey (T00) and monitor surveys (T25, T50) is used. Each survey is generated using a different wavelet.

6.3. Results

6.3.1. Average frequency

The advantage of normalisation as described in section 6.1 is that the effect of the wavelet is eliminated without requiring assumptions on the wavelet character. By subtracting the normalised amplitude-frequency spectra of time-lapse surveys, the time-lapse normalised spectrum is obtained. A variety of different attributes can be defined to characterise this spectrum. Some, but not all are related to the changes in the reservoir, e.g. the saturation change. Those that are related to the reservoir changes can be considered 4D attributes.

We first analyse, which attribute serves our purpose by using three different time-lapse surveys of our synthetic model. The three surveys (T00, T25, and T50) correspond to the base survey before production and two monitor surveys after 6.25 and 12.5 years of production, respectively. All three surveys are generated using a 30Hz Ricker wavelet (Figure 6.4a). We focus on the seismic trace at position inline 65 and crossline 55. The normalised amplitude frequency spectra for the three surveys at top of the reservoir are shown in Figure 6.10a. The spectrum for the reservoir and overburden are extracted in a time-gate of 24msec, i.e. [-12,12msec] around the top reservoir. The normalised spectra are shown for base survey (T00) and monitor surveys (T25 and T50). The corresponding water saturation for base and monitor surveys is 0.11, 0.24, and 0.66. With higher water saturation the normalised spectrum exhibits higher values at this particular location.

The time-lapse normalised spectrum is obtained by subtracting the normalised spectra of the different surveys. Figure 6.10b shows the time-lapse normalised spectra between surveys T00 - T25, T00 - T50, and T25 - T50. The time-lapse water saturation difference is 0.13 for base survey (T00) to the first monitor survey (T25), 0.42 for first (T25) to second monitor survey (T50) and 0.55 for base (T00) to second monitor survey (T50). The time-lapse behaviour of the normalised spectrum is related to the time-lapse saturation difference. With higher saturation difference, the time-lapse normalised spectrum displays higher values. Based on this and other results not discussed here, the average over the frequency range [10-60Hz] is chosen as an attribute to characterise the time-lapse normalised amplitude-frequency spectrum.

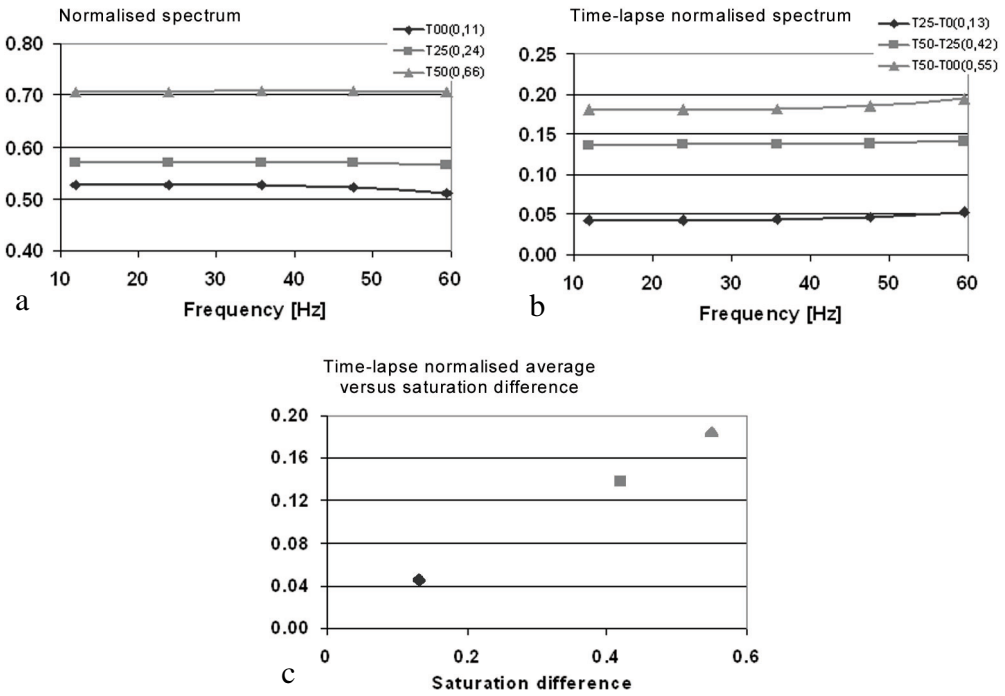


Figure 6.10 a) Normalised spectrum at top reservoir for base (T00) and two monitor surveys (T25 and T50) in the frequency range [10,60Hz]. b) Time-lapse normalised spectrum for the time-lapse differences T25-T00, T50-T00, and T50-T25. c) Average over time-lapse normalised spectrum [10-60Hz] versus saturation difference, taken at top reservoir.

The analysis as described above between the (time-lapse) normalised spectrum and the water saturation is performed at the top reservoir. The same analysis can be performed for the entire reservoir interval. Figure 6.11 shows the entire normalised spectra along the reservoir at position inline 65 and crossline 55. It shows the so-called time - amplitude-frequency plot with corresponding saturation for the three surveys T00, T25, and T50. Figure 6.12 shows the time-lapse normalised spectra along the reservoir against saturation difference for time-lapse data sets T00 - T25, T25 - T50, and T00 - T50.

Employing the base and all 12 monitor surveys yields more data points for analysis. Time-lapse differences between all surveys are used, yielding 78 data points. For each, the combination of saturation difference and average over [10,60Hz] of the time-lapse normalised spectrum is analysed. Figure 6.13 shows the relations at difference levels within the reservoir. A relation is clearly

Normalised spectrum and saturation along depth

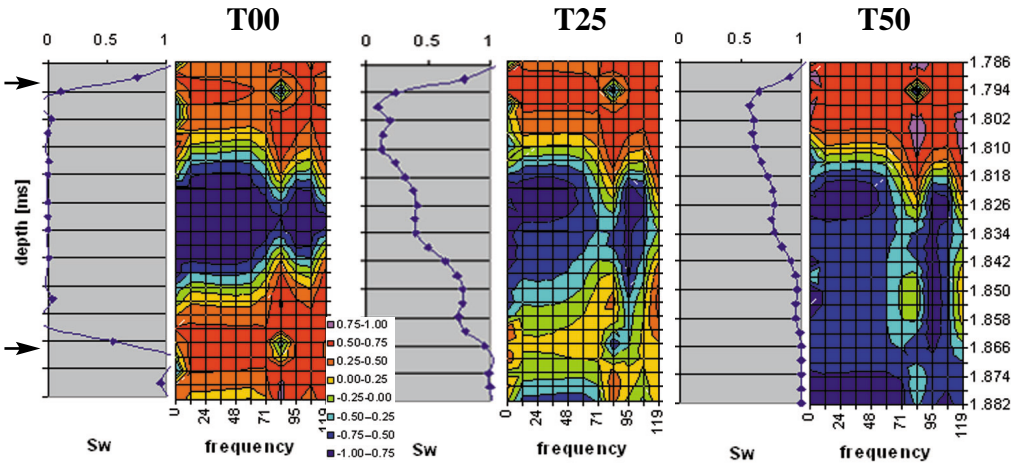


Figure 6.11 Normalised spectrum plots for entire reservoir compared to saturation for surveys T00 (left), T25 (middle), and T50 (right) at position inline 65 crossline 55. The top and bottom of the reservoir are indicated by the arrows. Depth along the reservoir is given in msec.

Time-lapse normalised spectrum and saturation difference along depth

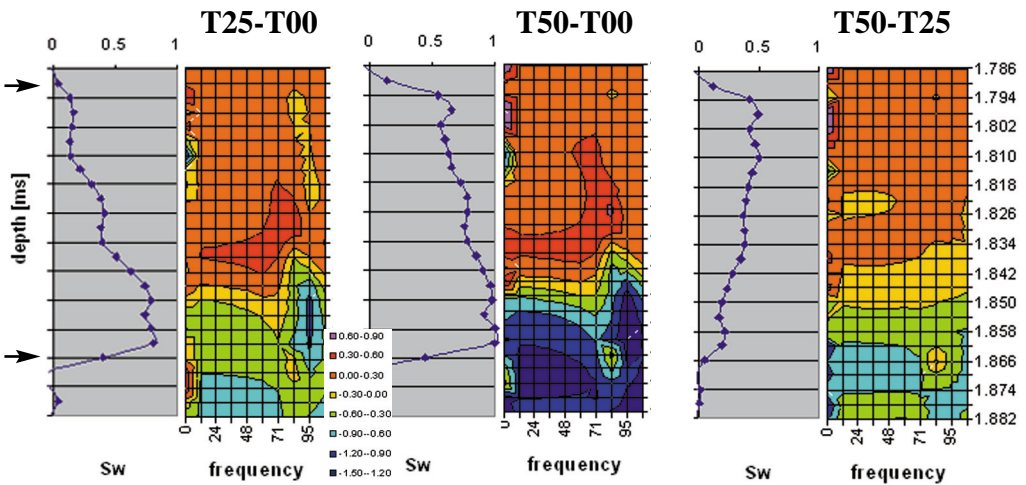


Figure 6.12 Time-lapse normalised spectrum plots compared to saturation difference along the reservoir for surveys T25-T00 (left), T50-T00 (middle), and T50-T25 (right) at position inline 65 crossline 55. The top and bottom of the reservoir are indicated by the arrows. Depth along the reservoir is given in msec.

observed in most of the plots. In some plots, especially halfway within the reservoir (around 36msec), a trend is hard to detect. This is due to the limitation in vertical resolution. All surveys are generated using a 30Hz Ricker wavelet, thus exhibit a central frequency of 30Hz. This yields a resolution of about 20m given a wave velocity of roughly 2400m/s (Table 6.1). The thickness of the layers within the reservoir is 3m, which is far below the resolution of the synthetic seismic. From Figure 6.11, it can be seen that the saturation versus depth is a very smooth curve, which further impedes characterisation of the individual layers.

Time-lapse normalised average versus saturation difference (30Hz)

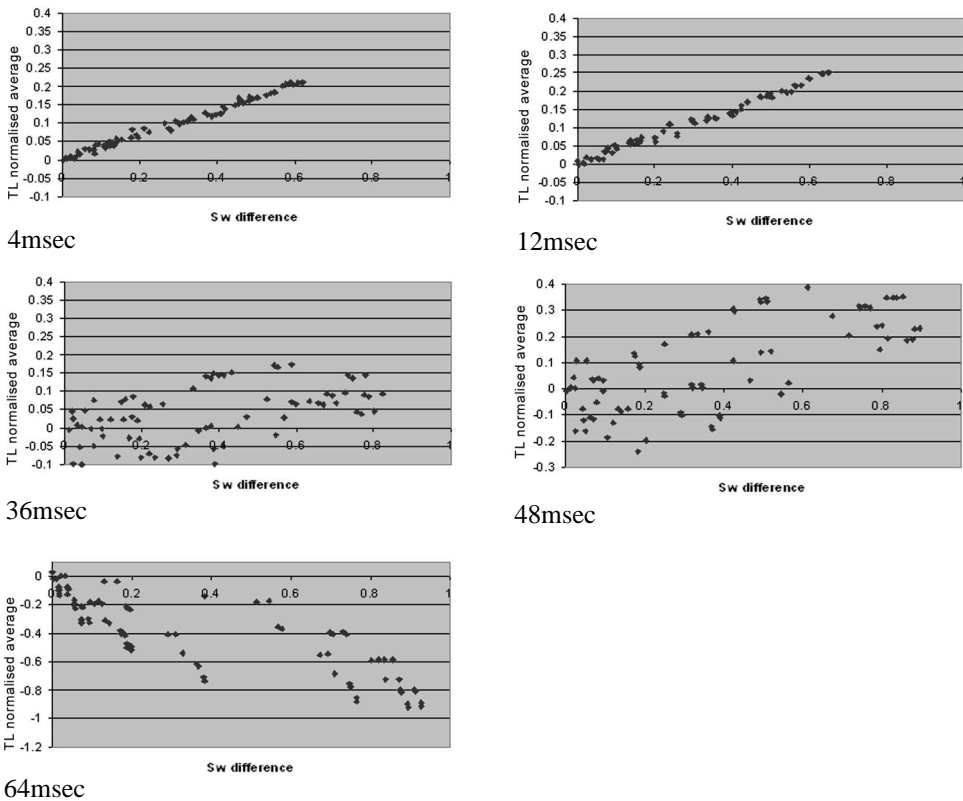


Figure 6.13 The time-lapse normalised average over [10,60Hz] versus saturation difference at different levels within the reservoir. The plots correspond to 4msec, 12msec, 36msec, 48msec, and 64msec below the top reservoir. The time-lapse differences are calculated based on synthetic seismic of 13 surveys (T00 to T60) at position inline 65 crossline 55. The synthetic seismic of all surveys is generated using a 30Hz Ricker wavelet.

6.3.2. Resolution

In the above, it is shown that the resolution can be a limiting factor. This is a known fact when dealing with seismic data. It is important to be aware of the resolution that can be achieved for any interpretation of the seismic. To illustrate the impact of the resolution, the 4D attribute is analysed for synthetic seismic with a central frequency of 90Hz. The resolution of seismic with a 90Hz

Time-lapse normalised average versus saturation difference (90Hz)

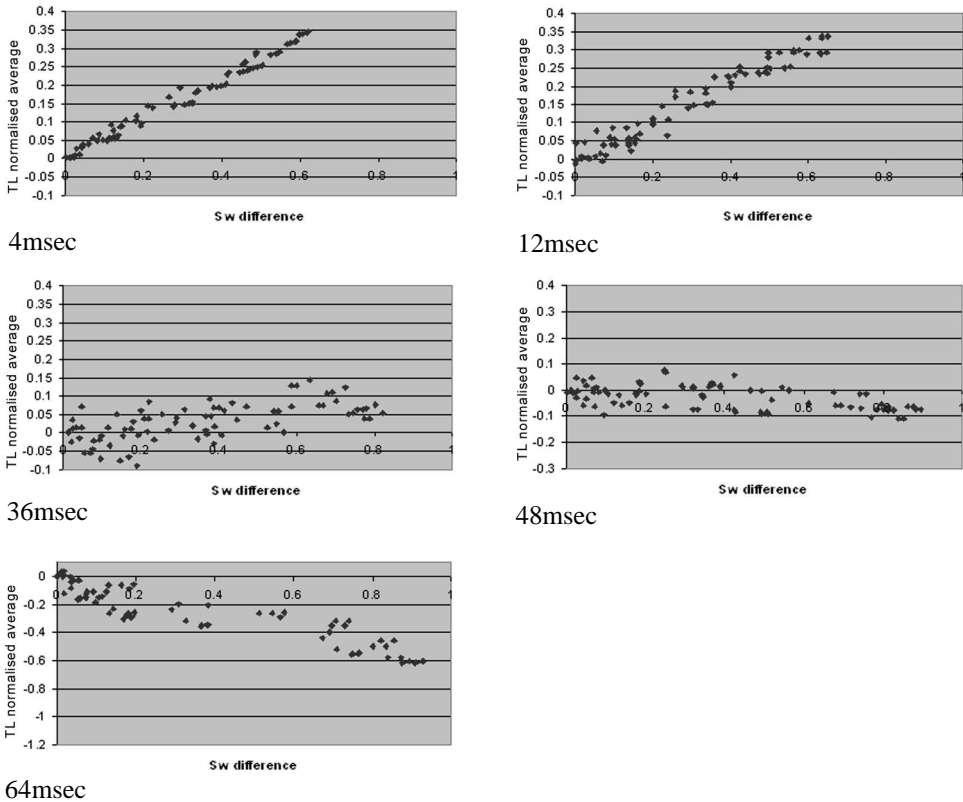


Figure 6.14 The time-lapse normalised average over [10,60Hz] versus saturation difference at different levels within the reservoir. The plots correspond to 4msec, 12msec, 36msec, 48msec, and 64msec below the top reservoir. The time-lapse differences are calculated based on synthetic seismic of 13 surveys (T00 to T60) at position inline 65 crossline 55. The synthetic seismic of all surveys is generated using a 90Hz Ricker wavelet.

central frequency is around 6.5m. Although the layer thickness of 3m is still below the seismic resolution, improved results are expected. Figure 6.14 shows the time-lapse normalised average over [10,60Hz] attribute versus the saturation changes. In comparison with the 30Hz synthetic seismic, the relation has in general improved.

6.3.3. Geological robustness

So far, the analysis has been performed on a single trace location corresponding to inline 65 and crossline 55. To test the robustness for differences in geology, the same analysis is performed for a wider range of trace locations. The 4D attribute is calculated for the entire crossline 55. The results in Figure 6.15 are based on the synthetic seismic of all 13 surveys, T00 to T60. All surveys are generated using a 30Hz Ricker wavelet. The relation between the time-lapse normalised average over [10,60Hz] and the saturation difference is very similar to the relation in Figure 6.13. Some spread in the data points is observed induced by the differences in geological setting.

Time-lapse normalised average versus saturation difference

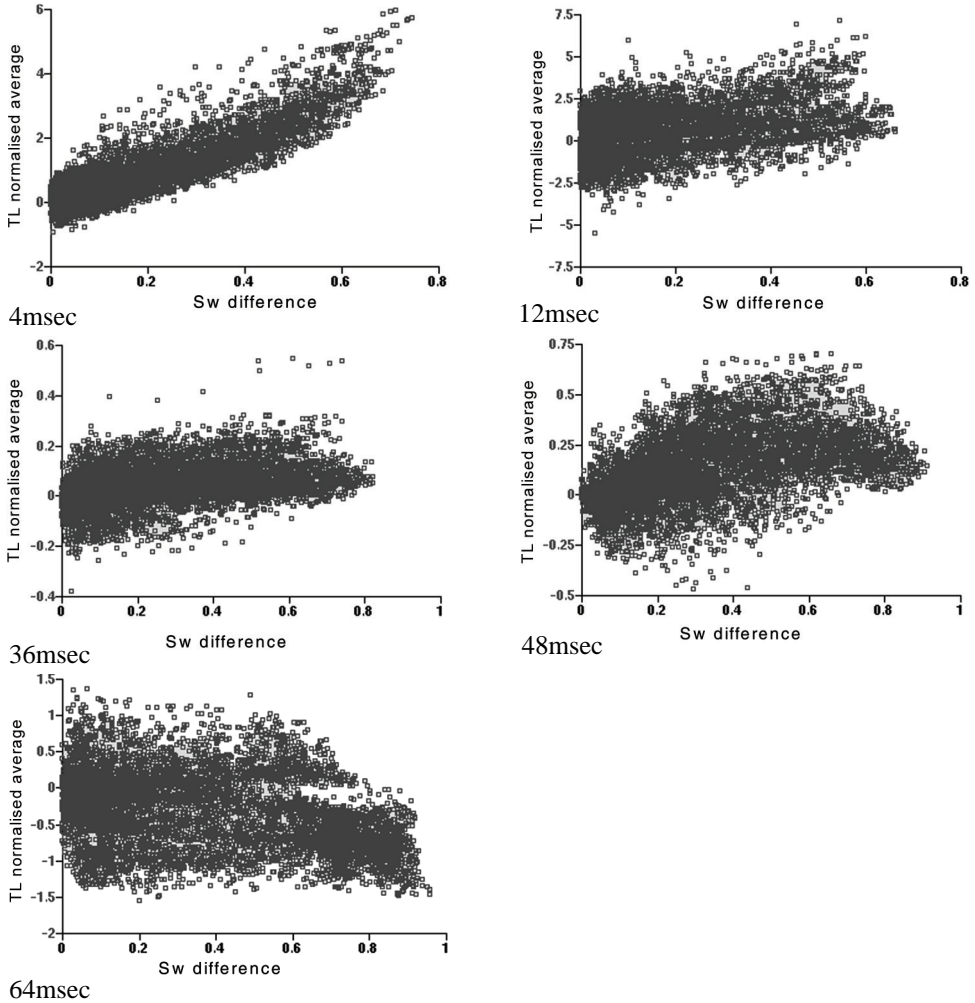


Figure 6.15 The time-lapse normalised average [10,60Hz] versus saturation difference at different levels below top reservoir. The time-lapse differences are calculated based on synthetic seismic of 13 surveys (T00 to T60) for the entire crossline 55. The synthetic seismic has a central frequency of 30Hz.

6.3.4. Repeatability

One-hundred percent repeatability between time-lapse surveys cannot be achieved. Even though care may be taken to reproduce the acquisition set-up of previous surveys, each seismic survey will be acquired differently. Issues beyond human control, e.g. weather and wave behaviour, impact the acquisition. The source wavelet with which the seismic is measured will vary per survey. The difference in wavelet affects the comparison between different time-lapse surveys. In Figure 6.9 the impact of the differently acquired seismic data sets is shown for the amplitude analysis between time-lapse data sets. The amplitude analysis is impeded due to the imprint of the wavelet, which varies per time-lapse data set. In our approach, we correct for the difference in acquisition by normalising the seismic signal yielding a wavelet independent measure.

In the following example, the three surveys T00, T25, and T50 are generated using different wavelets. The wavelets are shown in Figure 6.4. A 30Hz Ricker is used for the base survey T00, a zero-phase 30Hz wavelet is used for monitor survey T25, and a 25Hz wavelet is used for monitor survey T50. The 4D attribute is calculated between the different surveys. For each survey, the amplitude-frequency spectrum at the reservoir level is normalised by amplitude-the frequency spectrum taken from the overburden. Then the time-lapse behaviour of the normalised spectrum is analysed by subtracting the normalised spectra of the different time-lapse surveys. In Figure 6.16, the average over [10,60Hz] from the time-lapse normalised spectrum is plotted against the corresponding saturation difference over time for top reservoir. The relation between the 4D attribute and the saturation difference is similar to Figure 6.10. It teaches us that the proposed 4D attribute is suited to analyse time-lapse data sets. The normalisation allows correcting for the effect of the difference in wavelet, i.e. acquisition.

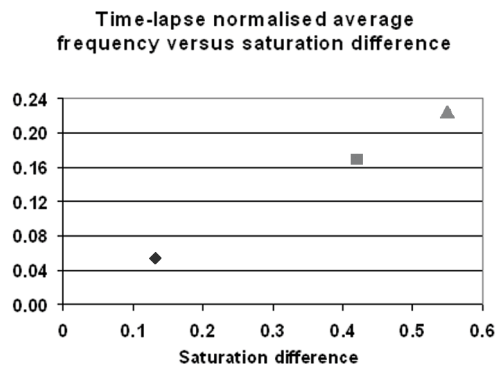


Figure 6.16 The time-lapse normalised spectrum average over [10,60Hz] for T00, T25, and T50. Each surveys is shot with a different wavelet.

6.3.5. Extraction time-gate

The computation of the frequency spectrum is sensitive to the time-gate used. In the above, a time-gate of 24msec is used which corresponds to a time-gate of [-12,12msec] around the point of investigation. The amplitude-frequency spectrum is better defined if a larger time-gate is taken. However a larger time-gate means that one is less specific in time, and vice versa. Figure 6.17 and 6.18

Time-lapse normalised average versus saturation difference (8ms)

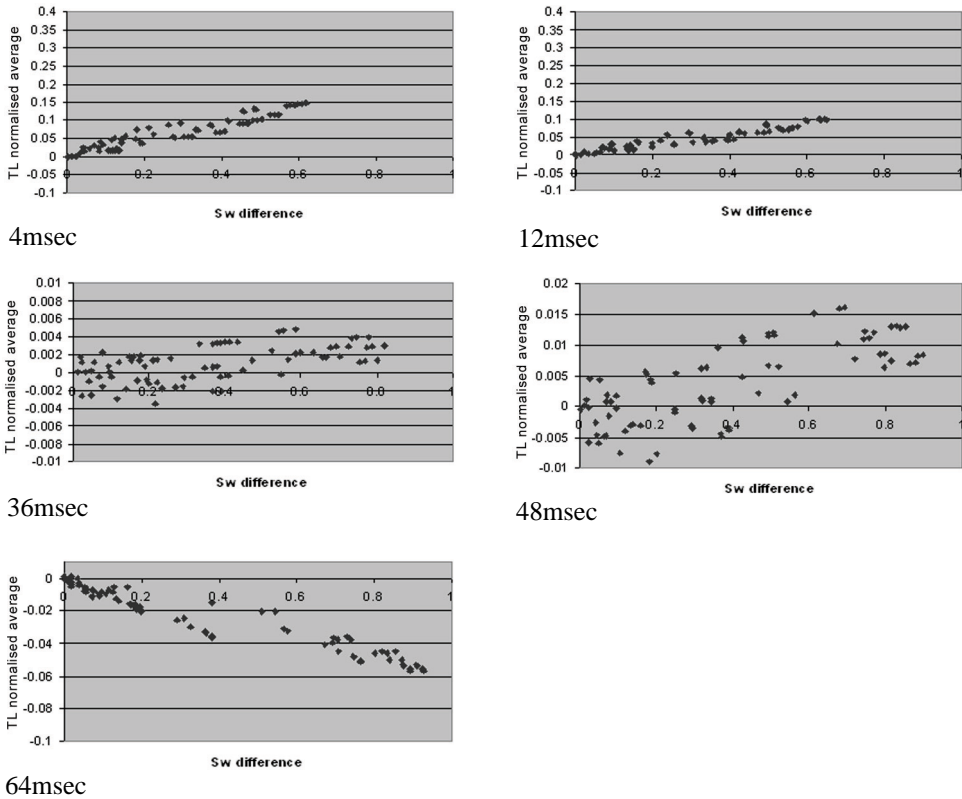


Figure 6.17 The time-lapse normalised average over [10,60Hz] versus saturation difference at different levels within the reservoir. The plots correspond to 4msec, 12msec, 36msec, 48msec, and 64msec below the top reservoir. The time-lapse differences are calculated based on synthetic seismic of 13 surveys (T00 to T60) at position inline 65 crossline 55. The synthetic seismic of all surveys is generated using a 30Hz Ricker wavelet. The time-gate over which the frequency spectrum is calculated is 8ms, i.e. [-4,4msec].

allow analysing the impact of the time-gate used to calculate the amplitude-frequency spectrum. Figure 6.17 is based on an 8msec time-gate. In Figure 6.18 a 48msec time-gate is used to calculate the amplitude-frequency spectrum. Comparison to Figure 6.13 shows that roughly the same behaviour is observed as when using a 24msec time-gate. For the data at 48msec below top reservoir, a difference is observed when using a larger time-gate (Figure 6.18). Due to the large time-gate, the time-lapse normalised average is affected by the bottom of the reservoir for which a negative relation is observed.

Time-lapse normalised average versus saturation difference (48ms)

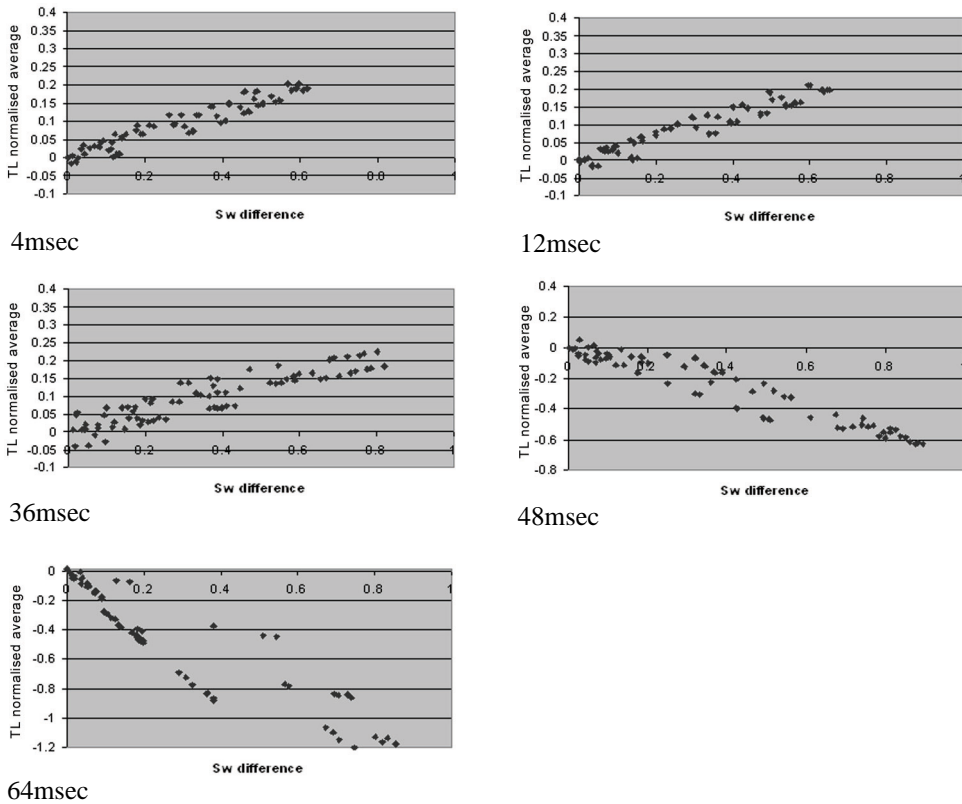


Figure 6.18 The time-lapse normalised average over [10,60Hz] versus saturation difference at different levels within the reservoir. The plots correspond to 4msec, 12msec, 36msec, 48msec, and 64msec below the top reservoir. The time-lapse differences are calculated based on synthetic seismic of 13 surveys (T00 to T60) at position inline 65 crossline 55. The synthetic seismic of all surveys is generated using a Ricker 30Hz wavelet. The time-gate over which the frequency spectrum is calculated is 48ms, i.e. [-24,24msec].

6.4. Discussion

In the above, an ideal picture has been portrayed on the basis of a simple though representative reservoir with perfectly processed seismic. Actual reservoirs are more complex, and the seismic will be contaminated by various types of noise. Future work should test the robustness of the method for noise. In our synthetic reservoir, only the saturation changes over time due to production are considered. In practice, other reservoir parameters change as well, e.g. temperature and pressure. It will be very useful to test the approach for pressure and/or combined pressure-saturation changes. A suitable rock physical model has to be used to model the pressure effect for a saturated rock on the synthetic seismic.

The observed time-lapse seismic difference is influenced by the frequency content of the seismic, as well as the temporal and spatial sampling. In the above (Section 6.3.2) the impact of the frequency content or resolution is analysed. It might also be useful to analyse the effect of the sampling rate, the sampling with time, and space.

To determine the amplitude-frequency spectrum accurately, a large time-gate is needed. This means that the information is less localised in time. When the evaluation is more localised, i.e. by taking a smaller time-gate, the amplitude-frequency spectrum is less well defined. This drawback is associated with the fact that the amplitude-frequency spectrum is obtained using a global transform. Any global transform suffers from the same problem. A local transform of the seismic probably yields better results (van Spaendonck, 2002).

Chapter 7

Integrating time-lapse seismic with reservoir engineering

Time-lapse seismic data is used to monitor the reservoir during hydrocarbon production. Assuming seismic repeatability, it is possible to couple time-lapse seismic changes in the reservoir to saturation and/or pressure changes induced by production. According to Waggoner (2001), the time-lapse seismic signal can be used for reservoir interpretation by any of the following four methods: visual inspection, quantitative interpretation, model screening, and seismic history matching. Another example is described in Section 7.1. In this method, we invert the permeability from time-lapse seismic data. The propagation speed of the saturation front as recorded by the time-lapse seismic allows determining the fluid flow velocity field, which is related to permeability. Furthermore, knowledge about the propagation speed of the fluid front enables forecasting the development of the saturation fronts in time, which is easily translated into water cut profiles at the wells.

The use of time-lapse seismic derived information within history matching requires an unconventional approach. The reservoir engineer often performs history matching manually with only production and well test data available to constrain the reservoir model. For decades, reservoir models have been

matched to production data and abundant experience is present. With the introduction of time-lapse seismic as additional data, history matching enters a different league. A huge amount of data has to be incorporated, whereby its 3D character has to be respected to optimally benefit from the data. There is no experience as to what parameters are to be selected as history matching parameters in order to obtain a fit to both production and time-lapse seismic data. These two types of data are incommensurable and integration requires special attention (Section 3.1).

Automated history matching allows handling some or all of these challenges, especially since computers are becoming very fast and disk space cheap. Moreover, it also answers the call for stochastic or multi-model history matching. Four important issues are to be considered in the (automated) history matching loop: parameterisation, definition of the objective function, choice of optimisation algorithm, and stopping criterion. In all four, it is important to incorporate reservoir engineering skills to avoid obtaining a pure mathematical solution, which may have no physical meaning. Currently, automated history matching is not standard practice in the industry. Its history has seen many failed attempts, as formalising the reservoir engineering skills is not straightforward. Egberts *et al.* (2002) describe the successful application of automated history matching for an actual, albeit simple, reservoir.

The main purpose of a reservoir model is to predict future behaviour of the reservoir and analyse the effect of reservoir management decisions. The forecasts are based on the reservoir model that best fits the observed static and dynamic data. An important issue is the quantification of the uncertainty of the forecast. The uncertainty is related to the measurement error and information content of the data, parameterisation, upscaling, type of reservoir simulation model, and history matching process.

In the following, the work of several MSc students is described or referred to. Their MSc work was under supervision of this Ph.D. project and has contributed to this thesis. Section 7.1 described work by de Haan, Section 7.3 shows results of van Ditzhuijzen, whereas in section 7.4 work by Funatsu is described. The work by van Soest (2001) and Arenas (2000) is not described in detail, but contributed in general to the work described in this chapter.

7.1. Permeability inversion

Permeability is one of the most important reservoir parameters. Accurate permeability maps will result in reliable outcomes of the reservoir simulation and plausible prediction of future oil production. Often, estimation of the permeability turns out to be a difficult task. Since most reservoirs are heterogeneous, well tests do not provide sufficient information on the permeability distribution of the entire reservoir. Several techniques have been developed to relate permeability to other reservoir parameters that are estimated or measured with a higher level of certainty, e.g. porosity. Unfortunately, this relation does not apply in all cases and therefore a more general method of estimating permeability maps is needed. In this section, we propose an alternative method using time-lapse seismic data (de Haan *et al.*, 2001).

Based on the saturation history of the field, the future development of the saturation through the a-priori unknown permeability field can be forecasted. Sequential seismic attribute maps provide information on the position of the saturation fronts in time. These contours give direct information on the flow paths followed during production and enable to predict future water breakthrough at the producing wells. Velocity maps are derived from the successive saturation fronts and are used for the estimation of the underlying permeability field.

7.1.1. Calculation of water cut profiles

For the estimation of the water cut at the wells, the streamline technique (Datta-Gupta, 2000) is used. The streamline technique is a popular technique to model flow through a reservoir. It has proven to be fast. The underlying concept of streamline tracing is decoupling of the flow (pressure) and transport (saturation) calculations by introduction of the time of flight co-ordinate (King *et al.*, 1993). The multi-dimensional conservation equation is converted into a series of one-dimensional equations along the streamlines. Conventional finite difference schemes solve the pressure and saturation equations of the full 3D problem at each time step, whereas the streamline method only solves the expensive pressure equation when there is a need to update the pressure calculation, e.g. when new wells are drilled, or wells are shut in. This makes the streamline method very efficient for fields with gradually changing mobility values. Another advantage is that numerical dispersion can be controlled very well.

Below, the procedure to the water cut estimation is explained. First, the calculation of streamlines between the saturation contours is described, then the displacement from the last contour to the producer is explained and finally the water cut calculation is discussed.

Given the saturation contours derived from time-lapse seismic, the streamlines are traced between the contours (Figure 7.1). At each step, the flow paths are reconstructed and the velocity determined. This enables creating a velocity map of the part of the field with saturation contours. The flow paths are directly related to the underlying permeability field. The principle of streamline tracing demands that each streamtube contains the same flux. Adding the flux of each streamtube leads to the total flux that was injected by the injection well. The placement of the streamlines on the contour is based on the geometry of the streamtube and the underlying velocity field. To determine the position of the streamlines, it is necessary to calculate the velocity at each point perpendicular to the contour. By varying the position on the contour, the size of the streamtube can be varied and the required flux can be obtained. The next streamtube then starts from this point in order to connect the streamtubes without leaving any gaps in between.

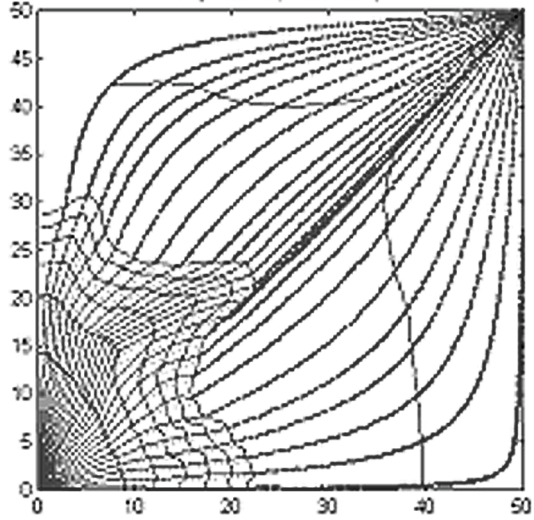


Figure 7.1 Illustration of synthetic model with injector at (0,0) and producer at (50,50), streamline trajectories in grey, and saturation profiles and first time of arrival of water at producer in black.

The tracing from the injection well to the first contour differs from the tracing between two contours due to a different shape of the streamtubes. From the injection well to the first contour all streamtubes have a circle segment shape. Between the contours, the shape changes to a quadrangle. Consequently, the volumetric calculation changes. In the first case, the volume is calculated using the angle of the circle segment and the assumption that the velocity changes inversely proportional to the radius. This leads to a flux per streamtube that is calculated using

$$\Delta Q_i = \int_{\alpha_i}^{\alpha_{i+1}} \frac{R^2(\alpha) - r_w^2}{2\Delta t} d\alpha, \quad 7.1$$

where Q_i refers to the flux through streamtube i , $R(\alpha)$ is the radius taken from the injection well to the first contour at the angle α , r_w is the well radius, t the time that was needed to arrive at the first contour and α is the angle of the circle segment between i and $i+1$. In tracing between contours, the initial velocity at the inlet of the streamtube has to be accounted for. Again, the velocities are calculated using a constant flux through all streamtubes. This velocity is taken from direct paths between the first and the second contour, using the straight distance from point to point and the time between two successive contours. By varying the outlet width, the velocity within the streamtube changes and consequently the time to pass the streamtube changes as well. A wider outlet results in a smaller velocity, since the same flux has to pass a larger area. The time to reach the outlet of the streamtube has to match the time between the recordings of the two contours, i.e. between the two corresponding seismic surveys. Matching of these two travel times yields the connection points of the streamtube at the next contour. The average velocity is dependent on the initial velocity (u_0) at entering the streamtube and the final velocity (u_e) at leaving the tube. The time needed to pass the tube reads

$$t = \int_{x_0}^{x_e} \frac{dx}{\left(\frac{u_e - u_0}{u_e - u_0} \right) (x - x_0) + u_0}, \quad 7.2$$

where x_0 to x_e is the distance perpendicular to the in- and outlet of the streamtube.

The last contour contains the information on saturation obtained from the last time-lapse seismic survey. From this contour, no information on the underlying field is available for the estimation of the flow paths. We use the analytical velocity field to a homogeneous quarter five spot production scenario to predict the position of the streamlines. The position after one time step (Δt) can be written as

$$\bar{x}(t + \Delta t) = \bar{x}(t) + \bar{u}(t)\Delta t + O(\Delta t^2). \quad 7.3$$

By taking a small time step in the direction of the velocity vector, the new position in space for each time step is calculated. The last term can be neglected if the time step is kept small enough. We restrict ourselves to a homogenous permeability field.

Each time a streamline arrives at the producing well, the well produces that amount of water. Adding all arriving streamlines leads to an estimate of the water cut profile of the well. The time of arrival (toa) is calculated as

$$toa = \Delta t_{total} + \sum dt , \quad 7.4$$

in which Δt_{total} is the time needed to reach the last contour and dt the time step of the calculations of the second tracing part. The water cut distribution that is calculated is a relative estimation of the water production. Assuming constant porosity, we use a material balance to scale the time of arrival to pore volumes.

7.1.2. The underlying permeability field

Based on the saturation contours as given by time-lapse seismic, the underlying permeability is estimated. It is estimated at each grid block of a regularly gridded cartesian grid. Via the above described streamline method, the velocity is calculated at the streamline-connection points on the contours. Using inverse distance interpolation, the velocity is estimated at each grid block between injector well and the outer contour. Darcy's Law describes the fluid flow velocity. It applies to horizontal linear flow of an incompressible fluid through porous media and is defined by

$$\vec{u} = -\frac{k}{\eta} \nabla P, \quad 7.5$$

with the velocity, \vec{u} , depending on the permeability, k , viscosity, η , and the pressure gradient, ∇P . Rewriting this equation, yields the permeability as function of the saturation, viscosity and pressure gradient. The fluid flow velocity is derived from the contours as described above, whereas the viscosity is assumed known and constant. The pressure gradient has to be derived. The actual underlying pressure field is unknown, except for the downhole pressures at the injection and production wells. We assume a pressure field based on a homogeneous permeability field, from which the pressure gradient can be determined at each grid block. Given that

$$|\vec{u}| = -\frac{k}{\eta} |\nabla P| , \quad 7.5$$

the permeability at all grid blocks within the outer contour can be calculated using:

$$k = - \frac{\eta \sqrt{(u_x^2 + u_y^2)}}{\sqrt{\left(\frac{\delta p}{\delta x}\right)^2 + \left(\frac{\delta p}{\delta y}\right)^2}} \quad . \quad 7.6$$

The permeability derived from a homogeneous pressure field is not likely to exactly match the real permeability field. Therefore, the procedure is iterated. The streamline simulator is run with the estimated permeability field yielding a pressure field that might be closer to the real pressure field. When necessary, more iterations can be used to optimise the result.

7.1.3. Results

In a number of test cases, we created randomly exponentially correlated heterogeneous permeability fields with different correlation lengths (Bruining *et al.*, 1997). For each case, streamline paths, water cut curves, and permeability inversion plots are compared. The algorithm is verified by comparing the forecasted results with the simulated results. In general, the streamline paths match the original paths very well. Figure 7.2 shows the forecasted and simulated water cut profiles at the production well for four test cases. In general, the calculated profile is much smoother than the original profile. The smoother character is due to the fact that a homogeneous permeability field is assumed beyond the last contour. Differences within the profile have to come from the first tracing part, where a variation in velocity results in a faster streamline. Most curves fit quite well. The starting point of the curve is of particular interest. This point determines the water breakthrough at the well. In general, a good fit is observed. In some cases the first arrival is slightly off; it shows later breakthrough than in reality.

Figure 7.3 shows the results for the permeability inversion for the case with correlation length 0.20. With the presented method, we cannot predict the permeability field outside the last contour. Therefore, only the part within the outer contour is shown and compared to the actual permeability field within that section. Figure 7.3a shows the original permeability field. The permeability inversion is performed with a pressure field derived from a homogeneous permeability field in Figure 7.3c. The inverted permeability field calculated with the real (underlying) pressure field is demonstrated in Figure 7.3b. Figure 7.3d presents the result of using one iteration. The real underlying pressure field provides the best estimate for permeability. In practice, this pressure field is

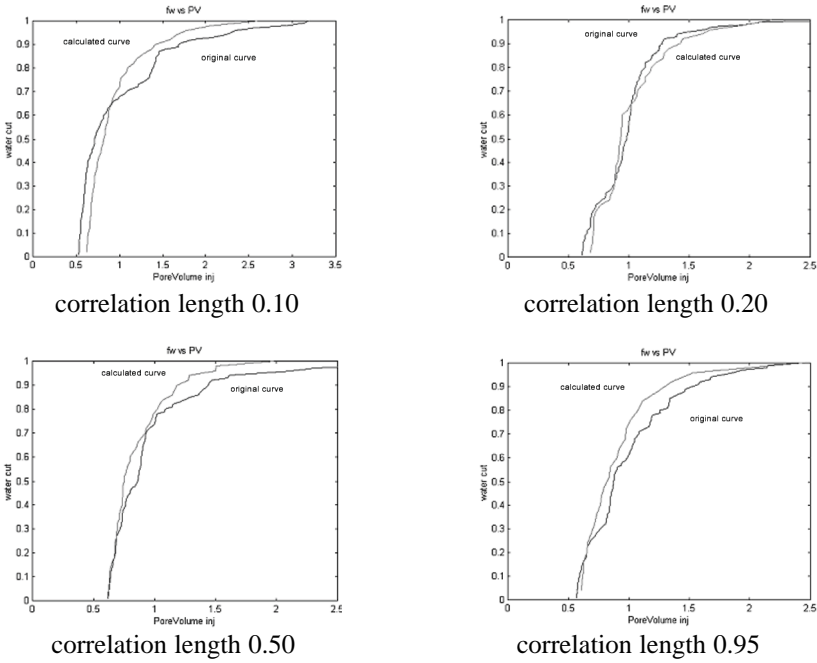


Figure 7.2 Water cut profiles for test cases with different correlation lengths.

unknown and has to be estimated. Important is that one iteration of the pressure field yields an improved estimation of the permeability. The presented method picks up the high and low permeable zones. The general trend of each field is reproduced in the calculated permeability fields. Small zones of high or low permeability are blurred out. In reality, these zones are too small to affect the productivity of the entire field.

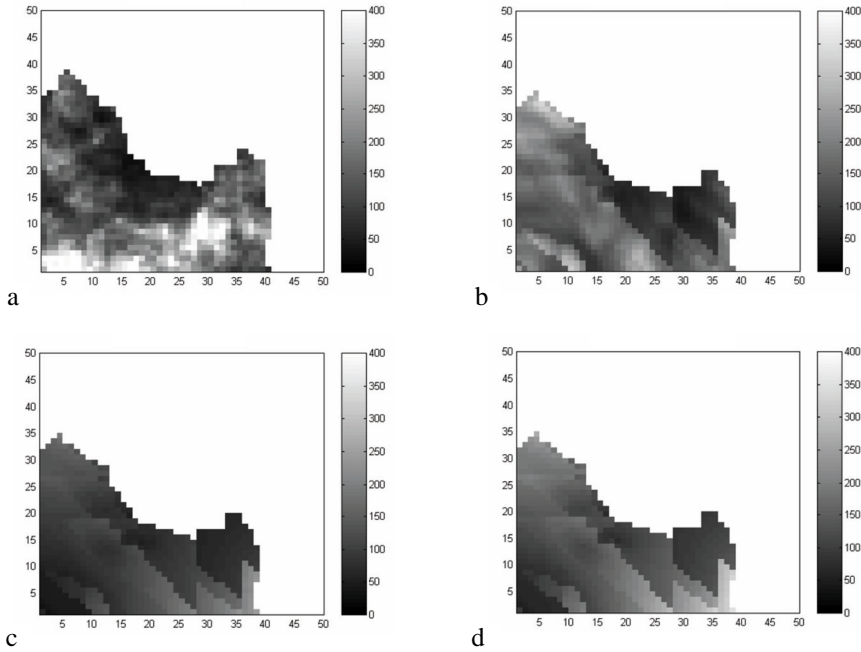


Figure 7.3 Real permeability field (a), inverted permeability field using underlying pressure field (b), inverted permeability field using homogeneous pressure field (c), and inverted permeability field using iterated homogeneous pressure field (d).

7.2. Automated history matching

Two general methods exist for conditioning reservoir models to available data; direct and indirect conditioning. The first assimilates data directly into the subsurface model. In most cases, it is employed to constrain the subsurface model to (point) information obtained from e.g. well logs. Indirect conditioning, on the other hand, adjusts the model based on discrepancies between the forward model results and the observed data. It is regarded as an inverse problem, where reservoir parameters have to be estimated from the production performance. Inversion techniques generally involve perturbing parameters at many locations until the model performance predictions match the observed data within some acceptable tolerance. This process of tuning the reservoir model parameters is commonly referred to as history matching.

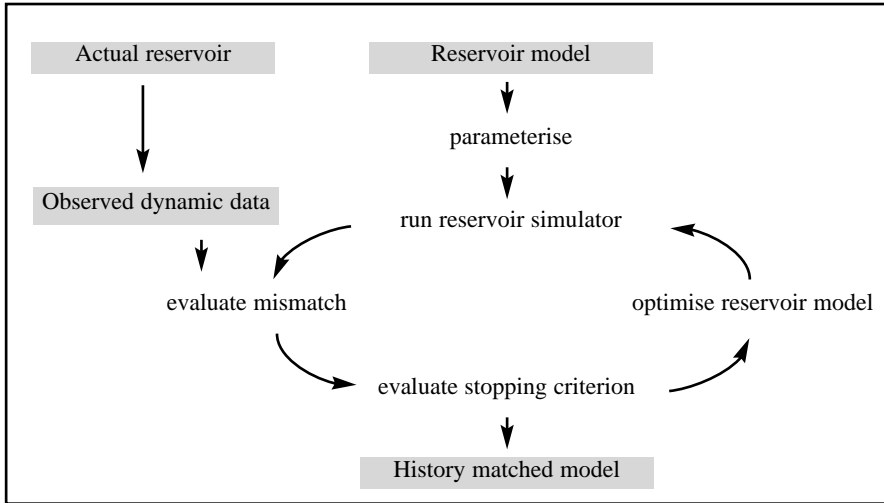


Figure 7.4 Schematic overview of history matching loop.

An automated history matching procedure can be quite advantageous, since a manual approach is labour intensive and may also introduce bias. Moreover, it facilitates the incorporation of the enormous amount of additional data generated by time-lapse seismic. Using automated history matching may reduce the overall cycle time from acquiring time-lapse seismic to its actual use / integration. It also allows simultaneous construction of multiple reservoir models or stochastic history matching. Formalising reservoir engineering skills in tuning the relevant parameters has proven to be difficult. Although (semi-) automated procedures exist, they cannot yet be regarded as standard industry practice.

An automated history matching process comprises the following steps (Figure 7.4). First, the inversion parameters are chosen, in other words the model is parameterised. Second, the misfit or objective function is defined quantifying the disagreement between modelled response and actual measurements. This function allows ranking of the different realisations during the inversion and guides the inversion process. Given the inversion parameters, the question remains how to perturb the parameters. This is determined by an optimisation algorithm. Last but not least, a criterion is chosen to define when the automated history matching process is to be terminated. The stopping criterion depends on the objective of the history matching process.

7.2.1. Objective function

In history matching, the difference between the model and the actual reservoir response can be quantified by defining a so-called objective function. Commonly the objective function is taken to be the sum of the squares of the differences between the model and the actual reservoir response. The objective function is not limited to quantifying differences between dynamic data, i.e. production and time-lapse seismic data. It can also be extended to quantify differences in several other types of data such as: (1) a priori geological knowledge (Bissell *et al.*, 1997, Wences *et al.*, 1998), and (2) the shape, or trend, of a data set (Monico, 1998). The inclusion of geological knowledge and data trends in the objective function is a way of constraining the models produced by history matching. To each of the components in the objective function an arbitrary weighting factor, w , can be assigned expressing the confidence in the data. In addition, if it is known that the conditioning data are dependent on each other, covariance matrices could be included to describe the interdependence. In the following, the objective function is of the form,

$$X_{total}^2 = X_{prod}^2 + X_{seis}^2, \quad 7.7$$

with

$$X_{prod}^2 = \frac{1}{N_{prod}} \sum_t \sum_{well} \sum_a \left[\frac{(A_{t,well,b}^{meas} - A_{t,well,b}^{model})^2}{\sigma_A^2} \right], \quad 7.8$$

and

$$X_{seis}^2 = \frac{1}{N_{seis}} \sum_{seis} \sum_{gb} \left[\frac{(B_{seis,gb}^{meas} - B_{seis,gb}^{model})^2}{\sigma_B^2} \right], \quad 7.9$$

where A and B refer to production (*prod*) and seismic (*seis*) data, respectively. The summation for production data is over the number of time steps (t), the number of wells (*well*), and the types of production data (a), e.g. well water cut or well oil production rate. The seismic data is summed over the number of seismic surveys (*seis*) and the amount of grid blocks (gb). σ is the standard deviation or measurement error of the measured value. N is the number of data points. *Meas* refers to measured data, whereas *model* refers to modelled data. By normalising over the number of data points, the production and seismic term are of equal weight. A different weighting function could be applied. However, quantifying the relative confidence per data type or per well/region is not straight-forward.

7.2.2. Optimisation

In the automated history matching procedure an optimisation algorithm is employed to find the optimal solution. The optimal solution is a combination of parameters that provides the best fit of the observed dynamic data, i.e. exhibits the smallest misfit. The optimisation algorithm tries to find this minimum in the objective function. Optimisation algorithms can be divided into two groups according to the type of objective function and amount of noise they are capable of handling. Global optimisers are capable of handling multi-modal objective functions and are better able to handle noise on the objective function. They generally succeed in reaching the global optimum. However, to do so they require a large number of function calls. Especially within reservoir engineering this is considered a drawback, because a single simulation easily takes a few hours. Efficient sampling of the parameter space may provide a solution. Local optimisers such as a gradient optimiser are fast but tend to find a local optimum. Local optimisers are not very well suited to handle noisy objective functions and tend to get stuck in a local optimum. A gradient optimiser is capable of handling a certain amount of noise as long as large steps can be taken to calculate the gradient. Near the solution the increments to calculate the gradients have to be small and the algorithm is affected by the noise.

The type of optimiser to be used is problem specific. Not only is the type of objective function an issue, also the amount of parameters and runtime of the simulation model affect the choice. In the following, the Levenberg-Marquardt algorithm (Levenberg, 1944, Marquardt, 1963) is employed. Levenberg-Marquardt is a combination of Steepest-descent (Fletcher, 1987) and Gauss-Newton (Fletcher, 1987), both local optimisers. Quite easily, other algorithms can be employed. In part of our work, not discussed here, we employed a genetic algorithm to support stochastic history matching (Van Soest, 2001) or simulated annealing to overcome the limitations of a local optimiser (Funatsu, 2002).

7.3. Geological parameterisation

History matching itself is not an objective. The objective is to create reliable reservoir performance predictions. In this, inversion parameter selection is a crucial step. Parameter selection must be done in close co-operation between

geologists and reservoir engineers with the objective to provide reliable production forecasts. When selecting the model parameters to be used for conditioning the reservoir model to the observations, insensitivity and non-uniqueness must be taken into account. Generally the forecast will be sensitive to the history matching parameters. However, there may be parameters to which the history matching is insensitive but to which the forecast is sensitive.

A reservoir model is described by many parameters. To allow perturbation of the reservoir model during history matching, the number of parameters has to be reduced for two reasons. First, it reduces computer run time to a level that makes history matching feasible. Second, resolving all grid block and model parameters is not possible due to the lack of sufficient data--i.e., the inversion is ill-determined. Parameters that are optimised in most history matching techniques are primarily reservoir properties, e.g., permeability, porosity, aquifer strength, and other flow-related properties. These properties do not directly represent the geometry of the reservoir. Often, in spite of integrated teams, the geologist and other geoscientists are kept out of the history matching process.

The geological structure of the reservoir model is determined early in the life of an oil field. It is sometimes adjusted, but more often kept fixed. However, in structurally complex fields, the geometry of a reservoir is one of the biggest uncertainties and incorrectly identifying structural features, such as fault planes, can have serious consequences--badly placed wells, by-passed hydrocarbon, poor estimates of oil-in-place, and failure to find hydrocarbons trapped in compartments surrounded by no-flow boundaries or with anomalous flow paths due to the presence of faults. Geological parameterisation allows perturbing these geological characteristics and objects as more relevant information becomes available during the life of a field. Relevant information may be obtained from time-lapse seismic data or e.g. water breakthrough at producing wells.

Until recently, only production data were available to condition the reservoir model. Abundant experience is available to history match the reservoir model to the production data. Since the introduction of time-lapse seismic, history matching has entered a new arena. The parameterisation strategy may have to be changed, because different history matching parameters are required to obtain a good fit to the seismic data. Different parameterisation allows honouring the difference (in character) between time-lapse seismic and production information. For example, the time-lapse seismic information is of a 3D nature related to the reservoir behaviour in between the wells, compared

to the 1D production data. Special attention has to be given to the geological information contained within the time-lapse seismic data. For example, information on the sealing capacity of faults may be gained (Lumley *et al.*, 1999). Moreover, the monitor seismic survey often yields additional or higher resolution information regarding the geology or structure, because it is acquired with improved technology compared to earlier surveys.

There are several reasons to introduce geological parameterisation. A good example to benefit from geological parameterisation is the Statfjord field. In Statfjord Field, geological, well, and seismic data indicate that slumps are present (Chapter 8). However, the geometry, number, and position of the slumps are unknown. A slump is defined as a set of layers that has been translated and rotated along a listric detachment surface. Section 8.1.3 gives a detailed description of a gravity slide or slump. Each slump is characterised by four parameters: position (x,y), size, and throw. Parameterising the reservoir model geologically allows the above-mentioned parameters to be changed. It provides a means to find the combination of geological parameters that best fits the observed data.

7.3.1. Synthetic reservoir

The 3D synthetic reservoir used in this chapter is modelled after the Statfjord field (Chapter 8). It consists of 1200 blocks divided over three layers of each 400 blocks. Each layer has 20 blocks in both x-direction and 20 blocks in the y-direction. A grid block is 50m long by 50m wide and 30m thick. The reservoir model is thus 90m thick and measures one km in x-direction and y-direction. The reservoir grid is bounded by four faults, which serve as no-flow boundaries. The tectonic dip is ignored. Producing wells are in the west of the field (left side of Figure 7.5) and water injectors are in the east. As in the Statfjord Field, the open side of the listric slumps is pointed in the downdip direction. Relevant reservoir properties are given in Table 7.1. The synthetic reservoir has four slumps, each with a throw of 50m (Table 7.2). Figure 7.5 shows the oil saturation after 15 years of production. At this point, approximately 65% of initial oil in place has been produced. The residual oil saturation is taken as zero and a 100% recovery is theoretically possible. The bottom layers have been largely produced and are now filled with water. Still a considerable amount of oil is left in the top layer. Water injected by injector 1 (lower right corner) does not flow in the upper layer due to the nearby slump. From the area around injector 2 (upper right corner), injected water flows preferentially in and around the slump but not toward injector 1. Oil is trapped in the middle of the reservoir model and below injector 2.

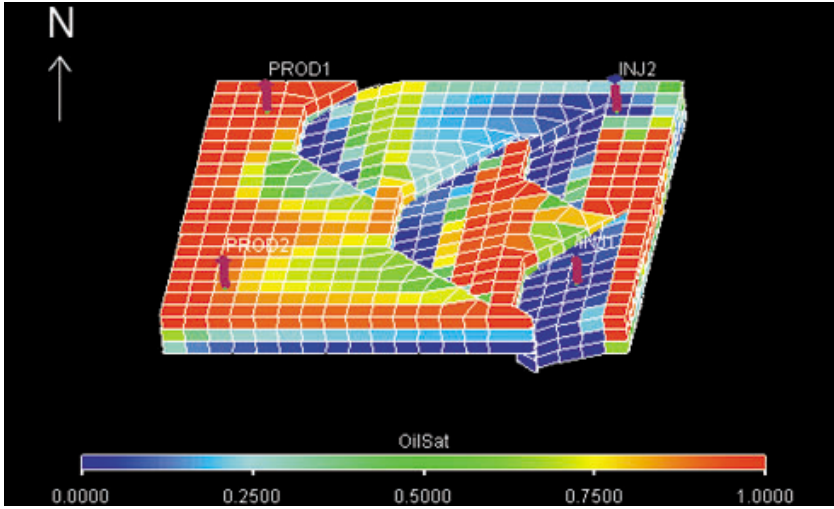


Figure 7.5 Oil saturation after 15 years of production in the synthetic reservoir.

Reservoir properties

Reservoir Depth (m)	1960
Reservoir Thickness (m)	90
Gas Oil Contact (m)	1000
Oil Water Contact (m)	2586
Initial reservoir pressure (barsa)	Approx. 350
Connate water saturation	0
NTG	1 (0.8 in middle layer)
Avg permeability (kx = ky) (mD)	2277
kz/kx	0.001
Type of oil	Oil with dissolved gas
Original Oil in Place (m3)	15.5x10 ⁶

Table 7.1 Reservoir properties.

Parameter	Unit	1	2	3	4
x co-ordinate	-	5	10	15	16
y co-ordinate	-	3	10	6	16
Length	Grid blocks	4	5	3	4
Throw	Meters	50	50	50	50

Table 7.2 Slump parameters.

Production and saturation data are generated using a reservoir simulator (Eclipse, 1999). Saturation directly serves as the time-lapse seismic response. In theory, the saturation values have to be converted to seismic properties using a rock physical model. However, the grid block saturation values are used directly under the assumption that it is possible to invert saturation from time-lapse seismic. Since it concerns a synthetic model, we can make this choice. White noise is added to account for the fact that the inversion is not perfect in reality. Three seismic surveys are shot at intervals of 1, 10, and 15 years after start of production.

7.3.2. Results

The first result comprises a case in which the fault throw of all four slumps is unknown. It is assumed that the positions of the slumps are known. Permeability, porosity, and other reservoir properties in the grid blocks are not considered history matching parameters. The initial values of the throws are guessed as 75, 65, 25, and 25m for slump 1, 2, 3, and 4, respectively. The history matching results are listed in Table 7.3. Comparison with the actual throws shows that the Levenberg-Marquardt optimiser is perfectly capable of reaching the minimum value. It returns nearly correct values for the slump throws. The algorithm converges and the objective function for production and seismic data is very low. The production objective function, X^2_{prod} , which expresses the error between measured and modelled production data, becomes almost zero. The seismic objective function, X^2_{seis} , converges to 1.016. On the seismic measurements (saturation in this case), white noise has been added to account for the fact that the inversion of observed time-lapse seismic yields a saturation estimate with a degree of uncertainty. Due to the white noise, the expected minimum value of X^2_{seis} is 1 rather than 0 (van Ditzhuizen *et al.*, 2001).

*History matching parameter: throw of slump 1, 2, 3, and 4
True values: 50, 50, 50, and 50m*

	Throws	X^2_{total}	X^2_{prod}	X^2_{seis}
Initial	75,65,25,25	28.83	5.88	22.95
Optimised	48,50,51,49	1.018	0.0014	1.016

Table 7.3 Results for history matching the throw of four slumps.

Figure 7.6 shows oil production and water cut behaviour at the two producers for the actual reservoir, the initial guess model, and the history matched model. The initial guess model behaves in a manner similar to the actual reservoir. Based on the production graphs, one can argue that the initial guess model is a representative model and no history matching is required. However, when analysing the oil saturation after 15 years of production (Figure 7.7), it is evident that the initial model does not exhibit the same behaviour as the actual reservoir. Considerable differences are observed--e.g. water encroachment near producer 2 and bypassed oil near injector 2. Thus, considering the initial model as being a representative model, which seemed reasonable when one had access to production data only, would have resulted in an incomplete understanding of the reservoir. After history matching, the distribution of the remaining oil in the optimised model resembles actual reservoir behaviour closely. In this case, the extra information added by using time-lapse seismic is crucial to creation of a representative reservoir model.

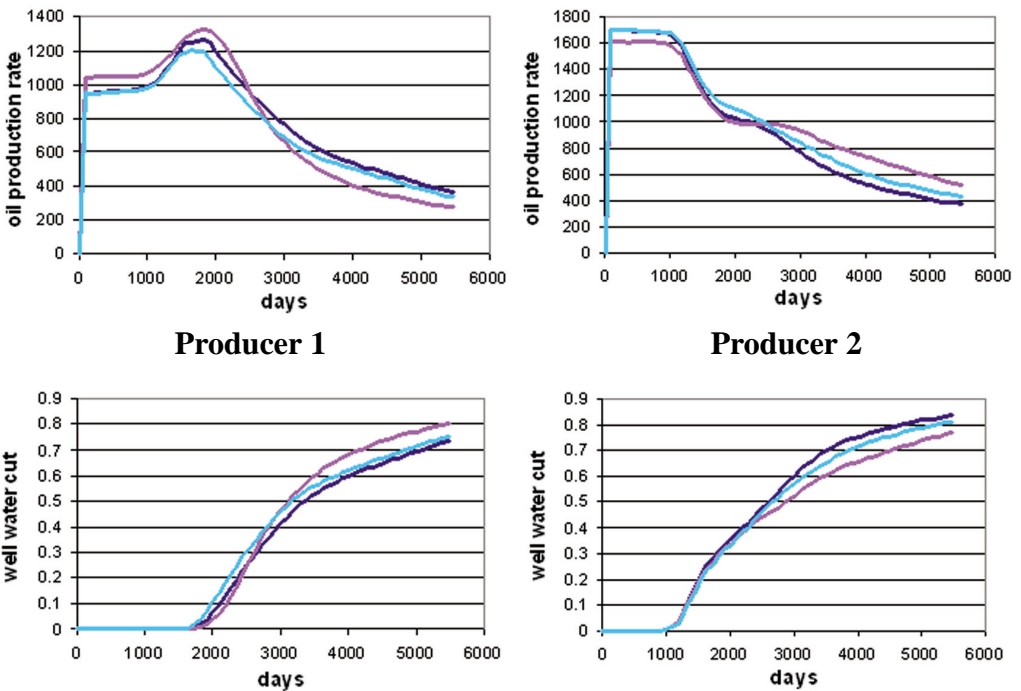


Figure 7.6 Oil production rate (top) and water cut (bottom) for producer 1 (left) and producer 2 (right) for case where slump throws are unknown. Dark blue is actual reservoir, pink is initial model, light blue is history matched model.

The second scenario comprises two unknown y co-ordinates as history matching parameters. The initial guess positions are (5,7) and (10,7). The actual positions of the first two slumps are (5,3) and (10,10). Table 7.4 lists the results of this scenario. Figure 7.8 shows oil saturation after 15 years of production for the reservoir, the initial guess, and the optimised model. A change in y co-ordinate of a few grid blocks for slump 1 and 2 in the initial guess model causes oil to be left behind to the right of the first slump. Also the area around well producer 2 is less invaded by water than in the reservoir itself. The optimised model represents the slump configuration and saturation distribution of the actual reservoir very well.

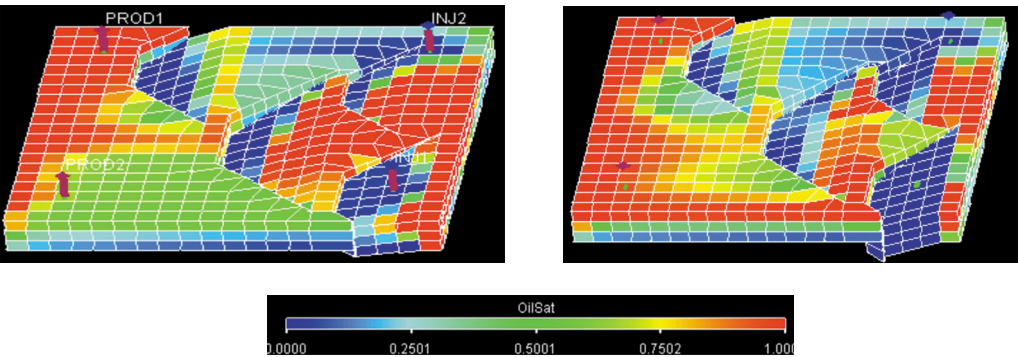


Figure 7.7 Oil saturation after 15 years of production for initial model (left) and optimised model (right) in case slump throws are unknown. Blue is water, red is oil.

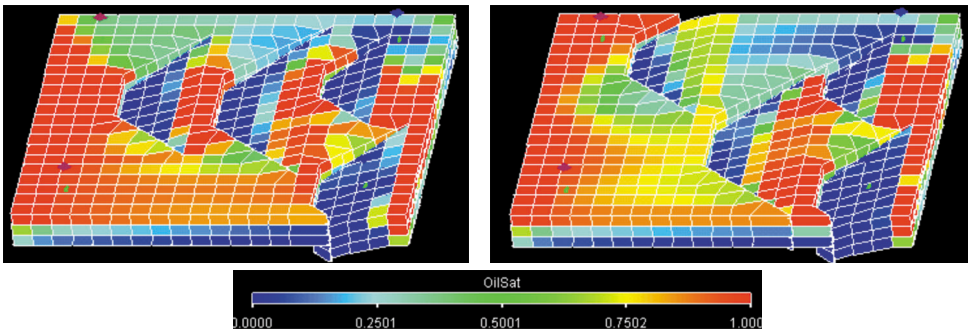


Figure 7.8 Oil saturation after 15 years of production for initial model (left) and optimised model (right) for position history matching. Blue is water, red is oil.

History matching parameter: y co-ordinate of slump 1 and 2
True values: 3, 10

	y co-ord's	X^2_{total}	X^2_{prod}	X^2_{seis}
Initial	7,7	37.2246	6.4994	30.7253
Optimised	3,11	6.6690	0.3279	6.4831

Table 7.4 Results history matching the y co-ordinate of two slumps.

Gradient methods and other local optimisers cannot discriminate between minima that are global solutions and minima that are not, i.e. the so-called local minima. Local optimisers are sensitive to initial values. However, conditioning the objective function with prior information can eliminate non-physical or geologically unrealistic solutions. In this study this included the number of slumps (4). Co-ordinate parameters are constrained by reservoir dimensions, so the x co-ordinate range is 1 to 20 and y co-ordinate range is 1 to 20. The length of the slope is limited to the model size (20 grid blocks) and the throw varies between -100 (an uplifted slump) and +100 m. Another constraint is used during the calculation of gradients. Because the co-ordinates and the slump length are integers, the minimum increase for the calculation of the gradients is 1.0.

Analysis of the objective function.

The contribution of the production and seismic components of the objective function (Equation 7.7) are analysed by plotting them separately (Figure 7.9). The total objective function plotted in Figure 7.10 gives a reasonably accurate minimum. Note that the production objective function has a less defined minimum (Figure 7.9 left) and that the minimum for the seismic objective

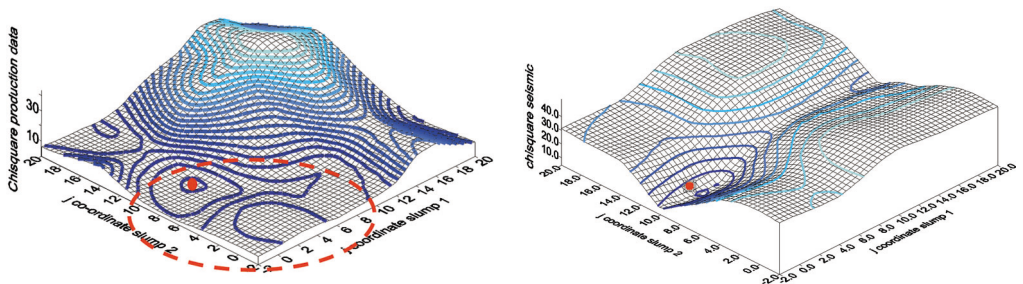


Figure 7.9 The objective function for production (left) and seismic (right) for the y co-ordinate optimisation.

function is much more precise (Figure 7.9 right). This indicates that the seismic information contributes significantly to finding the correct reservoir model. The fact that time-lapse seismic contributes to a more accurate solution has also been observed in several other scenarios not discussed here. The opposite has also been observed, where the production data alone led to a satisfactory history matched model and contribution of the time-lapse data was limited (Arenas, 2000).

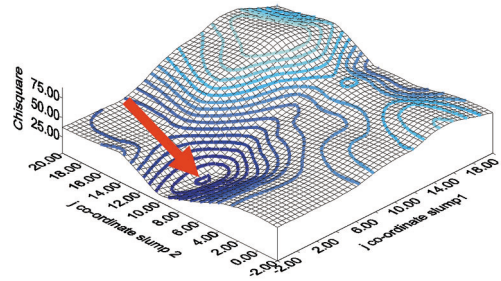


Figure 7.10 The total objective function in case position of two slumps is history matched.

7.4. Production forecast uncertainty

The aim of history matching is to construct a reservoir model to allow forecasting of the production behaviour of the reservoir. A single history matched numerical model is not sufficient to design the field development plan, as it is certain that the forecast has uncertainty. For proper reservoir management, it has to be quantified how much the production forecast is dispersed around the history matched model's forecast. Quite different reservoir models may also respect the available historical data. These models may yield a different production forecast. Using a large number of realisations of the reservoir model, a probability density function can be generated. In this way, the uncertainty of the forecast can be quantified. The drawback of this procedure is the associated cost due to the large number of realisations required. Due to the long computation time per realisation, the procedure is often not feasible within the limits of a project. A more efficient method is required. A series of production uncertainty quantification methods exist that do not require a large number of realisations. For example, linear uncertainty analysis (Kalogerakis, 1994) and perturbation methods are easy and quick to implement, however, at the cost of precision. They consider perturbations around a single “most likely” reservoir model. They do not consider (quite) different models that would also respect the available data. The true uncertainty is thus likely to be underestimated. Geostatistical approaches (Goovaerts, 1997) are based on a number of different though equally probable images of a reservoir. However,

conditioning these models to dynamic data, while honouring their equiprobability, is difficult. Efficiently sampling from the probability density function offers another solution. However, this is a challenging task as explained by Omre (2000). The scenario test method attempts to provide an efficient sampling method (Guerillot and Roggero, 1995). An a posteriori uncertainty model is built by incorporating the a priori geological data and the dynamic production data. This uncertainty model is used to compare the predictive quality of the different simulation models by associating a probability level with each set of parameters. Initial knowledge of the parameters is kept during the history matching procedure, thus the final model (a posteriori model) will be within a reasonable distance from the physical reality (a priori model).

7.4.1. Scenario Test Method

The production scenario test method was first introduced by Guerillot and Roggero (1995). It attempts to reduce the number of simulations that are necessary to identify the uncertainty range by searching for the extreme behaviour models directly. The aim is the same as for the Monte Carlo approach introduced by Oliver *et al.* (1996). However the main difference is the number of numerical simulations required. The scenario test method consists of adding new conditioning data to the production data, based on the production forecast assumptions. The new conditioning data does not consist of actual data, but of future scenarios to which the model is conditioned. Extremes, i.e. worst and best scenario, are searched for these future scenarios or forecast properties, e.g. time of water breakthrough, oil recovery, field total cumulative oil production, or bottomhole pressure of a well at a given future time. The steps of the scenario test method are as follows

1. Construction of an initial geological model, i.e. a priori model.
2. Incorporation of dynamic production data via history matching. The model constrained to the dynamic data is referred to as the a posteriori model.
3. Initial production forecasts by history matched model up to a given future time.
4. Definition of production scenarios by defining future production criterion, e.g. cumulative oil production after 15 years.
5. Simultaneous matching of measured and future constraints. The best scenario is found when both a good history match is obtained and a maximum is found for the future constraint. The worst

scenario corresponds to a good history match and minimum value for the future criterion. A new model is obtained according to the scenarios.

6. Forecasting production behaviour corresponding to the extreme scenarios. For each scenario, a direct simulation gives a new forecast.

To quantify the production forecasting uncertainties, the method searches for extreme scenarios. The optimistic scenario and pessimistic scenario yield the envelope of all possible forecasts from all the simulations. This translates to two optimisation problems at a given confidence level.

The criteria for history matching and production forecasting are expressed in the form of an objective function in order to treat both as an optimisation problem. Given a history matching criterion G_{hmc} , the corresponding probability is $g = const. \times \exp(-G_{hmc})$ assuming that it can be quantified as a Gaussian distribution. The a posteriori probability ratio (ppr) is defined with respect to the maximum (optimum location) probability as follows

$$ppr = \frac{g}{g_{\infty}} = \frac{\exp(-G_{hmc})}{\exp(-G_{\infty})}, \quad 7.10$$

where g_{∞} is the probability of optimised model, G_{∞} is the objective function value of optimised model. Then,

$$G_{hmc} = G_{\infty} - \log(ppr). \quad 7.11$$

For the search of the extreme scenarios, the objective function is expressed as

$$G = G_{geol} + G_{dynamic} + G_{future}, \quad 7.12$$

where G_{geol} represents the history matching criteria to constrain to the a priori information, $G_{dynamic}$ represents the criteria to constrain to the dynamic data such as production rate or bottomhole pressure, and G_{future} represents the production forecasting criterion. They are measured by a least squares criterion and can be calculated as a function of model parameters θ . The term G_{future} is an additional term which is used to obtain the min/max scenarios, defined by

$$G_{future} = \frac{1}{2} w_{future} (o_{future} - \omega_{future})^2, \quad 7.13$$

where w_{future} is a weight coefficient, o_{future} is future constraint based on the production assumptions, and ω_{future} is the forecast of o_{future} by numerical

simulation model. o_{future} is unknown when starting the search for the extreme scenarios and its initial value is set equal to $\omega_{future}(\theta_{\infty})$. The subscript ∞ corresponds to the location of the optimum. During the searching loop it is adjusted to satisfy the constraints. A detailed explanation of the iterative procedure to solve the problem is given in Funatsu (2002).

7.4.2. Synthetic reservoir

The synthetic reservoir is modelled after the Statfjord field and described in detail in section 7.3.1. The y co-ordinate and the throw of the first slump are assumed unknown. The y co-ordinate of the first slump can be any grid number in the model, whereas the fault throw can take all positive number, but cannot exceed 95m. The parameter space is thus defined as:

y co-ordinate	: 20 possibilities, [1,20]
Throw	: 91 possibilities, [5, 95m]

The total number of parameter combinations is 1820 (20*91). If all the possible model realisations have the same probability, the probability corresponds to 0.00055 (1/1820).

The production forecast is characterised as the cumulative oil production from producer 1 and 2 after 15 years of production. The water front reaches both producers within 5 years, after which oil production rate decreases rapidly. The available data for history matching are

production data

1. oil production rate of producer 1 (every 3 months)
2. water cut of producer 1 (every 3 months)
3. oil production rate of producer 2 (every 3 months)
4. water cut of producer 2 (every 3 months)

seismic data

1. water saturation of each grid block at 3 months (1st survey)
2. water saturation of each grid block at 5 years (2nd survey)
3. water saturation of each grid block at 11 years (3rd survey)

The grid block saturation values are used directly under the assumption it is possible to invert saturation from time-lapse seismic. Since it concerns a synthetic model, this choice is possible. White noise is added to account for the fact that the inversion is not perfect in reality. The timing of the three seismic surveys is different from the synthetic model as described in Section 7.3.1.

7.4.3. Results

Using the synthetic reservoir, the impact of time-lapse seismic and production data on the production forecast uncertainty is discussed. In the following, the base case represents 11 years of production. Over this period, the data comprises production data at 44 time steps and three seismic surveys. Figure 7.11 shows the results for the base case. The cumulative oil production after 15 years is plotted against its associated probability for the different (1820) realisations. “Production” refers to the realisations in which only production data is used to constrain the models. “Seismic” refers to realisations, in which only time-lapse seismic data is used, whereas “total” refers to both production and seismic data being available to constrain the realisations. The maximum probability for “production” (0.008) is smaller than that of “seismic” (0.04). Moreover, the variance of “production” is larger than that of “seismic”. The information from the seismic data is thus better able to constrain the reservoir model. Using both types of data, the maximum probability reaches 0.06. Combining both types of information yields a smaller uncertainty. Figure 7.12 shows the result of the base case in terms of cumulative probability. It can be noted that “total” has smaller variance than “seismic”, although the difference is not large. In the following results, all realisations are considered and their probability calculated. When dealing with a larger model, it is better to employ the scenario test method to avoid extensive computation time. In Figure 7.11, the result of the scenario test method is illustrated by the yellow dots. These

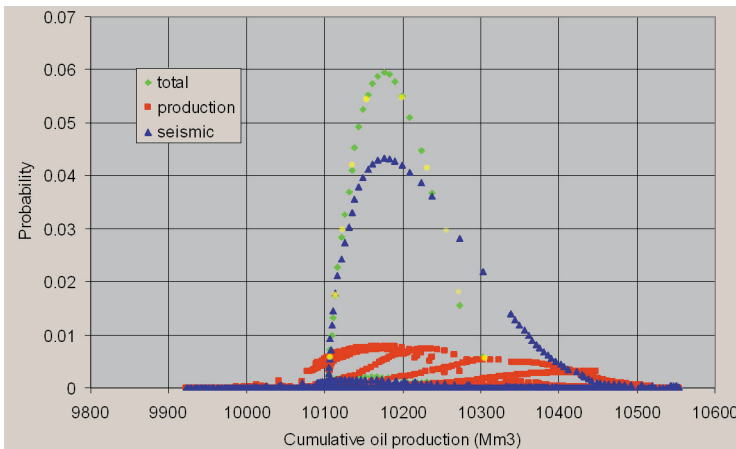


Figure 7.11 Base case probability for all realisations. The yellow points correspond to the extreme scenarios of the scenario test method at probability ratios (ppr) 0.1, 0.3, 0.5, 0.7, and 0.9.

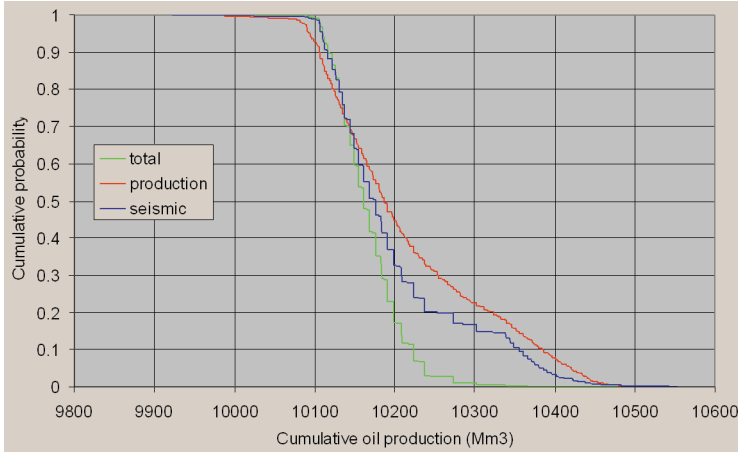


Figure 7.12 Base case cumulative probability curve. Notice that “total” curve is steeper than the other curves.

yellow points represent the extreme scenarios found at different levels of the a posteriori probability ratio (ppr). The scenario test method yields the same envelop as examining all realisations, but requires far less simulations to be run, roughly about 50 to 100 times less.

In the next case, the uncertainty in production forecast is quantified using data up to 3 months after start of production. The constraining data comprises production data of a single time step and the seismic data from the first survey. Figure 7.13 shows that there is hardly any information in the data to reduce the forecasting uncertainty. All model realisations have nearly the same probability

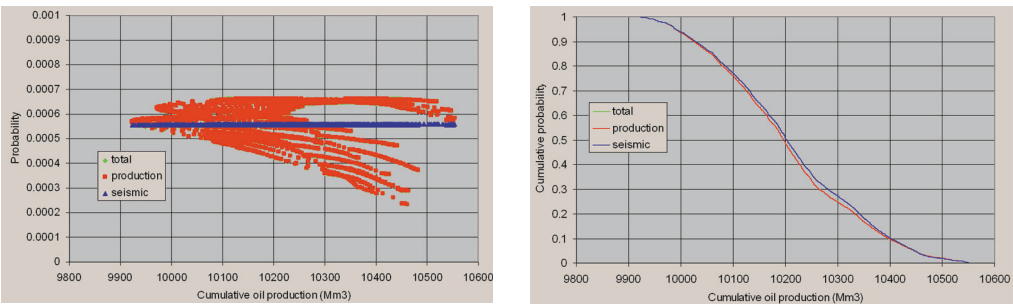


Figure 7.13 Three-months case. Both production and seismic data have little information to constrain the reservoir model. The cumulative probability curve almost displays a Gaussian distribution.

yielding a cumulative probability curve that behaves like a normal distribution. Probabilities of “seismic” are almost constant, but those of “production” have some variation. Comparing the cumulative probability figures, the variance is much larger than the base case. In this case “seismic” has almost no information about cumulative oil production. This is explained by the fact that water saturation in each grid block has not changed due to production except in the vicinity of the injectors.

In the third case, the production forecast uncertainty is quantified after 5 years of production. Production data of 20 time steps and seismic data of two surveys are available. Figure 7.14 shows that the result are similar to the base case. However, the maximum probability is smaller. Note that the vertical axis scale in Figure 7.14 (left) is different from Figure 7.11. The maximum probability is larger than the three-months case. There is some probability that the cumulative oil production is greater than 10400Mm^3 . From the cumulative probability curve it can be seen that the probability is more than 10%. The calculated standard deviation of “total” is 114.8Mm^3 , which is smaller than that of the three-months case (134.2Mm^3). The production data between 3 months and 5 years and the second seismic survey data yield information by which the more probable model realisations can be distinguished. There is still a large uncertainty in forecasting cumulative oil production after 15 years of production. Water breakthrough occurs just before 5 years of production and the water cut after 5 years of production is still low.

In the last case, data up to 15 years of production is used. Compared to the base case, additional production data measured between 11 and 15 years after production is used. A large reduction in uncertainty is not expected, since the wells produce over 90% of water in the entire period. Figure 7.15 confirms that the production data does not contribute additional information.

The tables 7.5 and 7.6 below are presented for record. Some of the numbers are already mentioned in the previous paragraphs. The computation of standard deviation in Table 7.5 is not based on all data points (realisations). The realisations are sorted by their probability in decreasing order before accepting a realisation for standard deviation calculation until the cumulative probability becomes greater than 50%.

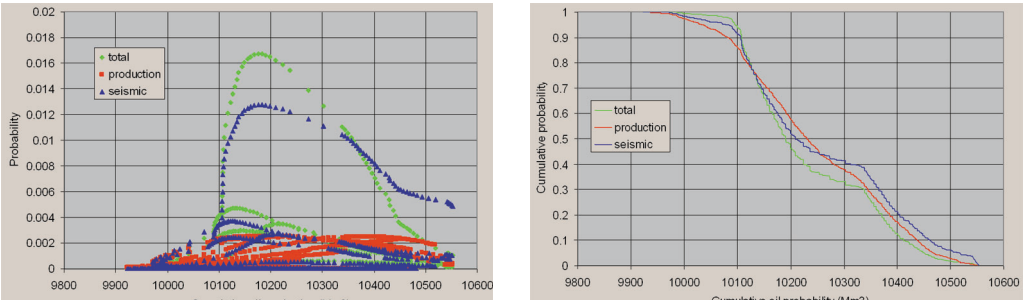


Figure 7.14 The case in which 5 years of production behaviour is available. The maximum probability reaches 0.067.

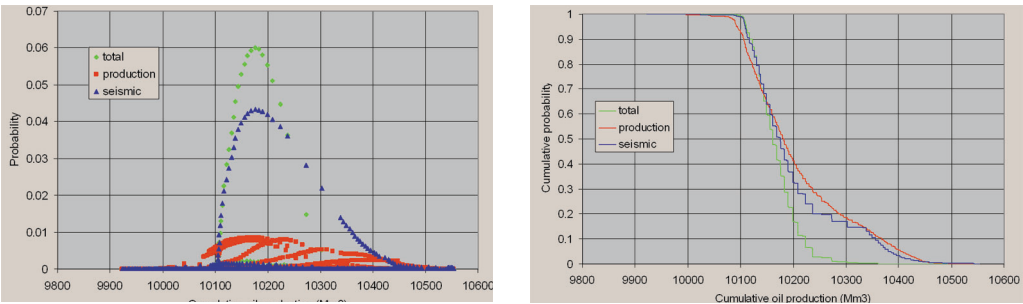


Figure 7.15 Fifteen year case. Additional production data slightly reduces the uncertainty.

case	injected water (fraction of pore volume)	total st dev (Mm ³)	production st dev (Mm ³)	seismic st dev (Mm ³)
3 months	0.016	134.25	134.25	117.85
5 years	0.318	114.78	125.22	134.47
11 years (base)	0.699	19.20	46.78	29.91
15 years	0.954	19.20	40.64	29.91

Table 7.5 Standard deviation of the cases with different amounts of constraining data.

case	injected water (fraction of pore volume)	“total” Mx prob	“production” Mx prob	“seismic” Mx prob
3 months	0.016	0.0007	0.0007	0.0006
5 years	0.318	0.0167	0.0025	0.0128
base (11 years)	0.699	0.0595	0.0078	0.0433
15 years	0.954	0.0601	0.0086	0.0433

Table 7.6 Maximum probability of the cases for different amounts of constraining data.

In general, if the information in the available data to constrain the reservoir model is limited, the uncertainty of its future prediction is larger. Adding more information to the optimisation of the reservoir model leads to a more reliable model. Based on the reduction of the uncertainty, the information content of the production and time-lapse seismic data can be quantified.

The uncertainty in the production forecast for this synthetic model is about 2 to 4%. This is small compared to the uncertainty observed for actual field data. Nevertheless, the model very well illustrates the principles of the uncertainty quantification. For this thesis, it was preferred to use the same synthetic model as in previous sections, rather than design a synthetic model, which displays a more realistic level of uncertainty in the production forecast.

7.5. Seismic data

When using the time-lapse seismic, a range of aspects needs to be considered. Seismic data is incommensurable to the other available static and dynamic data. The seismic data is measured over a large volume, but has a low accuracy and resolution. The vertical resolution of seismic is in the order of 30m. With time-lapse seismic, smaller layers can sometimes be detected. This resolution is very coarse compared to well log and core data (cm scale) and large compared to the grid block size in reservoir simulation models (10m). The areal resolution of seismic is about 25m, which is smaller than the gridblock size used for simulation models (100m). Moreover, the inversion from time-lapse seismic to reservoir properties, e.g. saturation, is not straight-forward, as described in

Chapter 5. In the synthetic examples, the inversion error is arbitrarily chosen to be 5%. In future work, the uncertainty needs to be quantified properly to better represent a realistic scenario. Arenas *et al.* (2001) clearly illustrate the impact of the saturation inversion error on the history matching results for a simple 2D model.

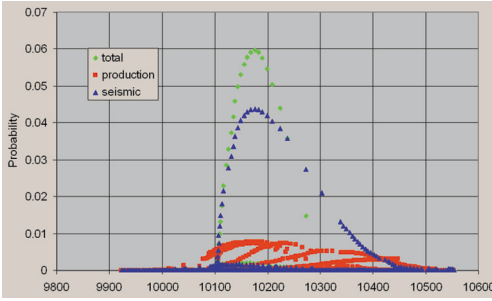
7.5.1. Noise level

When the inversion from time-lapse seismic to water saturation is of low quality, the water saturation data has a low certainty. As a result, the information contained in the time-lapse seismic (or saturation) is lower, which will be reflected in the variance and a posteriori probability function. In the above, the inverted water saturation data is generated by adding 5% white noise on top of the numerical simulation output of the true model. By changing the amount of noise, the sensitivity after the inversion accuracy can be analysed. In the following, the noise level is 0%, 30%, 50%, 100%, or random. The noise is defined as an absolute value within \pm e.g. 30% of the saturation range [0,1]. The noise is added to the saturation value. In case saturation with added noise exceeds the physical limits, i.e. is less than 0 or higher than 1, the saturation is clipped to the physical limit.

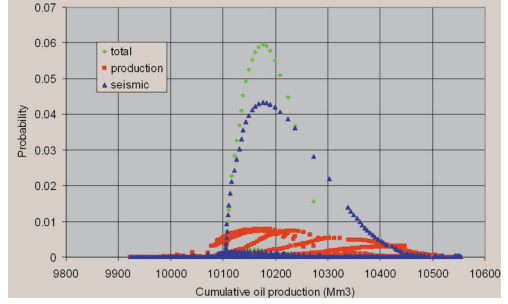
Figure 7.16 is drawn for comparison with Figure 7.11. Not surprisingly, 0% or 5% noise level yield similar results. The 30% noise level figure is slightly different than the base case. The maximum probability is smaller and the variance higher. The variance for 50% noise level is again higher. But even if the 50% noise has been added, the change in maximum probability is small. It yields the maximum probability at the same cumulative oil production, but with a smaller probability. Increasing the noise level to 100% yields a larger variance and smaller maximum probability. The saturation data still contains information. This can be explained by the fact that the noise field does not entirely destroy the trend in the original saturation data. As expected, the random saturation field yields a maximum probability at an incorrect cumulative oil production.

To realistically model the effect of the quality of saturation inversion from time-lapse seismic, the noise should be modelled in a more sophisticated manner. For example, the noise will be correlated laterally and vertically. The noise is also related to the reservoir properties and geology. This is outside the scope of this thesis.

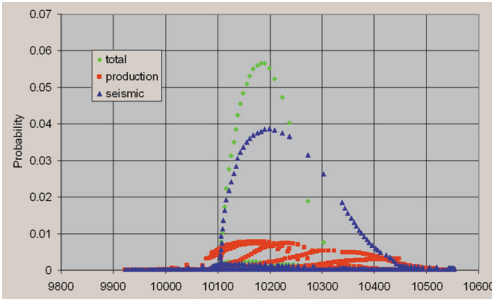
Chapter 7



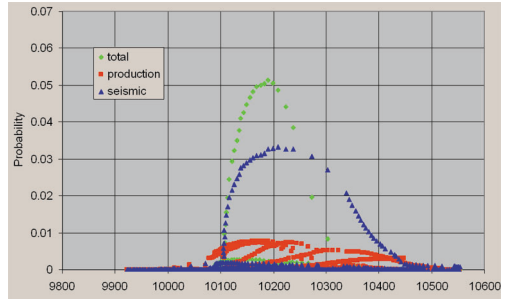
0% noise level



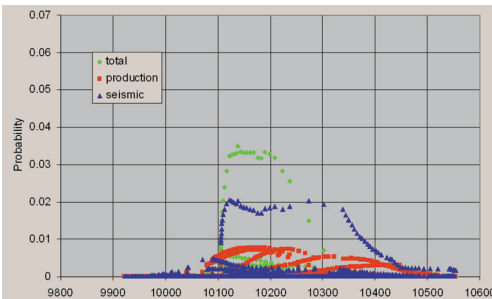
5% noise level (base case)



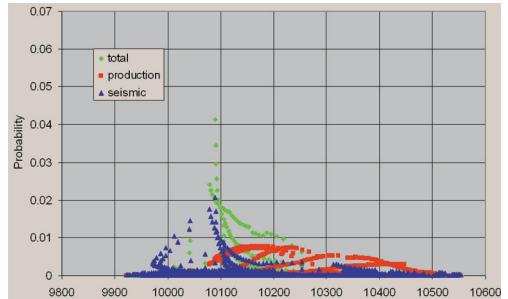
30% noise level



50% noise level



100% noise level



random noise level

Figure 7.16 Sensitivity analysis after the noise level on the water saturation. Noise level x means that observed water saturation has a measurement error of x (absolute value).

7.6. Considerations

Automated history matching in combination with faster computers and cheaper data storage will move reservoir simulation into the stochastic arena. Stochastic reservoir simulation provides multiple equiprobable realisations of the reservoir model that honour both static and dynamic data. The different levels of uncertainty of each piece of data can be taken into account. The stochastic geological modelling can be integrated with the reservoir simulation model as van Soest (2001) showed. Another benefit of stochastic history matching is that it facilitates quantification of the production forecast uncertainty. The probability density function can be better characterised given the large amount of realisations.

History matching of stochastic models requires a suitable optimiser capable of handling the noisy character of the objective function. The optimiser has to be capable of locating the different equiprobable solutions. Simulated annealing or genetic algorithms, both global optimisers, meet the requirements. The stopping criterion is of crucial importance for stochastic history matching. It has to be capable of testing whether the data space is sufficiently sampled. Insufficient sampling of the data space yields incorrect solutions (van Soest, 2001)

The objective function used in this thesis is the often-used sum-of-squares. For some types of data, the shape is more important than the actual values. For such data, an alternative objective function is more appropriate. For example, it is more important to know the point of water breakthrough than predict the entire water cut curve correctly. Different weights can be associated with the different terms, i.e. sorts of data in the objective function. The weight allows expressing the confidence in the data and the desired contribution to the objective function. The latter steers the optimisation process and is based on reservoir engineering judgement. Quantifying the weight to express the confidence in the data is not straight-forward.

When does a model fit the observed data, or in other words, when is it possible to stop the automated history matching process? The definition of an appropriate stopping criterion is complex and problem specific. The objective may be to find the single best-fitting model, or to characterise the probability density function. For the former, the stopping criterion ensures that the proper model is found given the data available. To achieve the latter, the parameters

space has to be sampled sufficiently. Definition of the stopping criteria is related to the amount, quality, and type of constraining data, and type of optimiser.

In the work for this thesis, several stopping criteria are used. In general, it seems unavoidable to optimise “too far” before being able to define an appropriate stopping criteria for the given problem and objective. For example, one can choose to stop optimisation when the modelled data is within a certain range of the observed data, e.g. within 1% of the bottom hole pressure or within 1000 barrels of total production after a year of production. If this criterion is set too loose or too tight, the model might not be optimally history matched or no convergence is reached. Alternatively, the objective function can be used as a threshold. Below a certain objective function value, or when the objective function is not improved over x consecutive runs, models are said to be history matched. However, this does not guarantee that the observed data is matched closely, or that any model satisfies the criterion.

Chapter 8

Statfjord case study

The Statfjord Field is a mature oilfield located in the Norwegian sector of the North Sea near the U.K.-Norwegian boundary (Figure 8.1). Discovered in 1974, it is the largest single oilfield in the North Sea (Lavik, 1997). Statfjord is operated by Statoil from three platforms. The estimated recoverable reserves exceed 4 billion barrels (650 million m³). The main reservoir potential is contained in the Brent, Dunlin, and Statfjord formations, with excellent reservoir properties.

The Statfjord field covers an area of approximately 28 x 9km and is orientated NE-SW along the crest of a northwesterly tilted, major fault block in the northern part of the Viking Graben (Figure 8.2). The field is located on the footwall of one of the major faults created during the development of the Viking Graben in late Jurassic time (Hesthammer *et al.*, 1999). Even though the structure is located next to a major fault with kilometre-scale displacement, most of the structure has undergone little deformation. This part of the field is referred to as the Main field (Figure 8.3). It consists of a major fault block tilted in a westnorthwest direction. The other part is heavily deformed and comprises many reservoir compartments bounded by listric faults. It is referred to as the East flank. The total length affected by gravity collapse is more than 25km and the width of the affected area varies from 2 to 4km. The slumped sections can

be hundreds of meters thick. Gravity slide structures like these are common in oil and gas fields in the North Sea and in fields within similar rift systems. It is a challenge to build a suitable reservoir model for these structurally complex reservoirs. The economic incentive is considerable as a substantial amount of oil is stored in it.



Figure 8.1 Location of Statfjord offshore Norway in the North Sea.

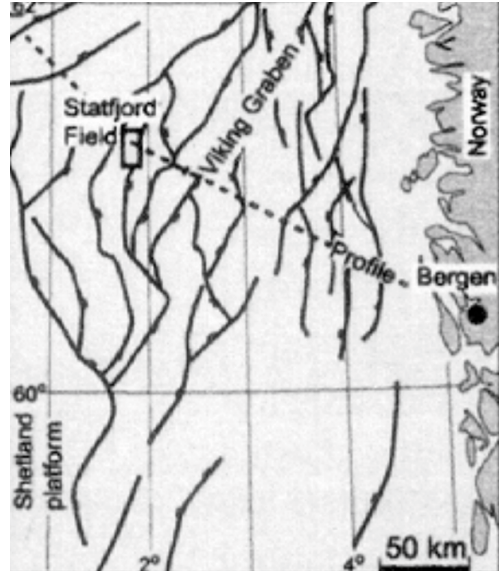


Figure 8.2 Top view of Viking Graben and Statfjord Field after Hesthammer and Fossen (1998).

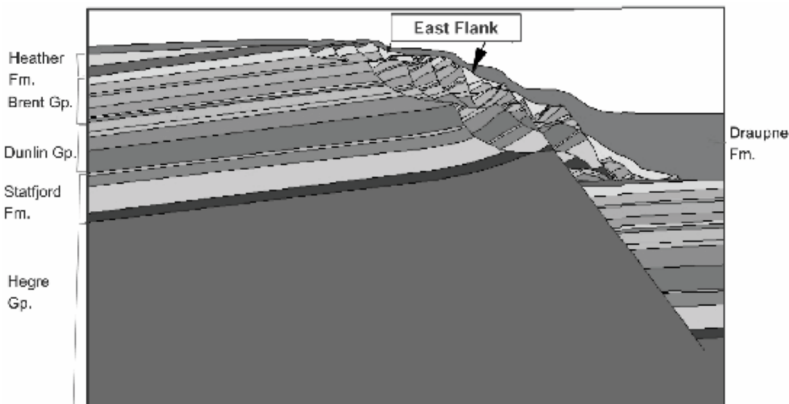


Figure 8.3 A generalised cross section of the Statfjord field. The East flank comprises many reservoir compartments bounded by listric faults (courtesy of Statoil).

In this thesis, the Statfjord field serves two purposes. First, it allows analysing the challenges, which the industry is facing with respect to time-lapse seismic interpretation. Second, it allows testing and comparing new methods for visual inspection, saturation inversion, and rock physical modelling.

8.1. Geology

8.1.1. Stratigraphy

The oldest sequence penetrated by Statfjord wells is the Hegre group (Hesthammer *et al.*, 1999). The thickness of this group is not known, since the base has not been reached in the Viking Graben area. Table 8.1 shows relevant formations in the Statfjord field with their thicknesses and sedimentation. The Statfjord, Dunlin, and Brent groups are subdivided in several members. The Heather formation contains several unconformities. A hiatus separates the Draupne formation from overlying Cretaceous sediments.

Age Layer Thickness Members Sedimentation

Age	Layer	Thickness	Members	Sedimentation	
Cre	Viking	?	Draupne	Organically rich shales	
		?	Heather	Silty shales	
	J u r a	Brent	180-250m	Tarbert	Shallow marine sands.
				Ness	Sandy channel deposits, shale and coal
				Etive	Coarser grained sandstone
				Rannoch	Delta-front sandstones
				Broom	Storm deposits, small distal bar build-ups
	s i c	Dunlin	230-260m	Drake	Shallow marine shales, siltstones
				Cook	Shallow marine silt-sandstones
				Burton	Shallow marine shales
Amundson					
	Statfjord	150-300m	Nansen Eiriksson Raude	Interlayered sandstones, siltstones, shales	
Tri	Hegre	> 180m		Interbedded intervals of sandstone, claystone, shales	

Table 8.1 The formations present in the Statfjord Field after Hesthammer and Fossen (1998). Cre corresponds to Cretaceous and Tri to Triassic.

8.1.2. Tectonic evolution

The area in which the Statfjord field is located underwent at least two major rift phases (Hesthammer and Fossen, 1998). During the first rift phase, in Permo-Triassic time, the Viking Graben was established. The second major rift phase started in Late Jurassic time immediately following the deposition of the Brent group. Uplift of the Graben centre resulted in large, first order faults with kilometre-scale displacement. One of these faults defines the eastern boundary of the Statfjord Field. Because of movement along this fault the Statfjord Field started tilting westward. Rotational block sliding occurred during the deposition of the Heather formation as a result of gravity failure. After the Heather and Draupne formations were deposited, minor tectonic activity took place along northeast-southwest trending faults in Cretaceous time. In the Tertiary, sinistral movement occurred along north-south trending faults.

8.1.3. Gravity collapse structures

In general, gravity collapse structures occur in footwalls of large rotating fault blocks in regions of extensional tectonics. The scale of these structures termed “slumps” here can vary from a few centimetres to several hundreds of kilometres (Hesthammer and Fossen, 1998). The area affected by gravitational failure has a round shape in plan view (spoon-shaped in three dimensions) and

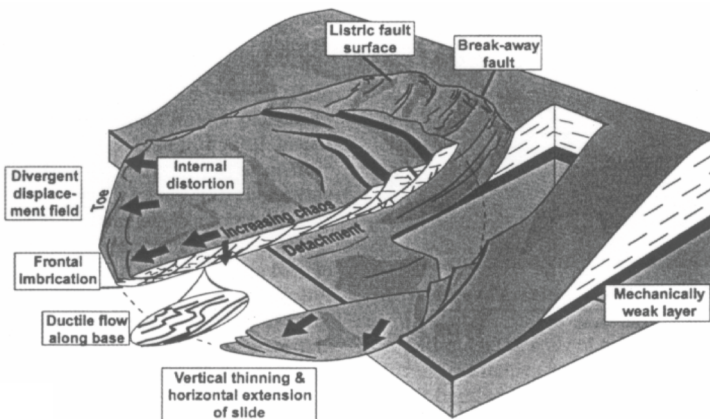


Figure 8.4 General characteristics of a gravity collapse structure after Hesthammer *et al.* (1999).

displays a listric and concave upwards detachment surface in a cross-sectional view. In Figure 8.4 a typical slump is shown. The slumping can be triggered by seismic shocks, over-steepening of slopes, rapid sedimentation, changes in fluid pressures or extensional deformation.

Three stages of slumping have been identified in the Statfjord Field. The first phase involves rocks of the Brent group, the second involves the Dunlin, and the third phase involves the Statfjord formation. Figure 8.5 illustrates the evolution of the slumps according to Hesthammer and Fossen (1998). Rocks that experience only one phase of slumping may have their initial geometries intact, whereas rocks that experience several stages of slumping may exhibit very complex geometries. The internal geometry of the slump blocks in Statfjord is mostly preserved.

On seismic data, slumping in the Brent formation is observed immediately below the strong Base Cretaceous reflection. In general, it is not possible to

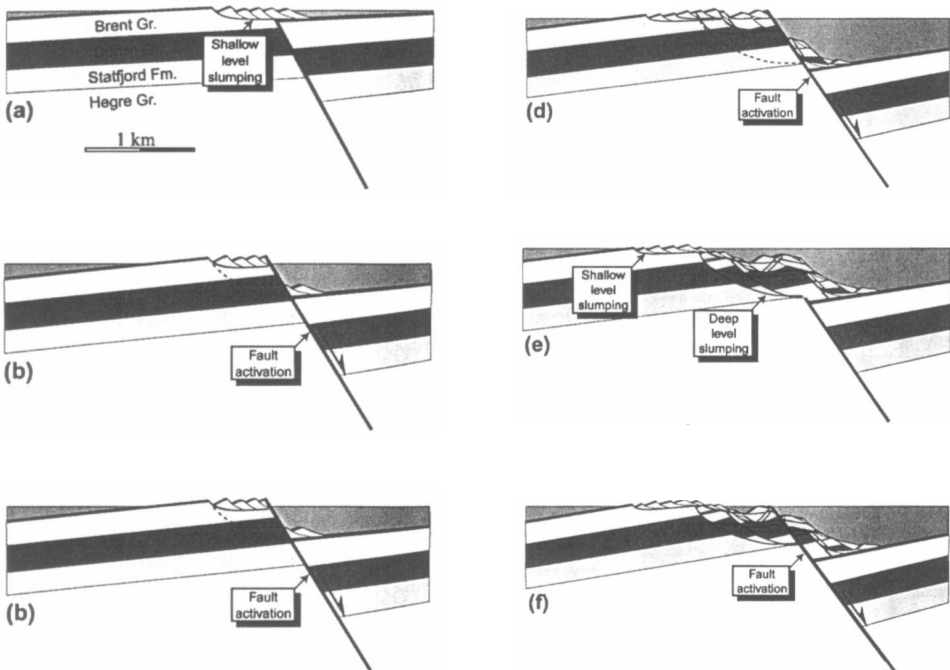


Figure 8.5 Evolution of the slides along the eastern margin of the Statfjord field after Hesthammer et al. (1999).

identify individual slumps in this region. This is mainly due to the very thick Draupne formation that has abnormally low velocities. This results in a strong seismic signal with peg leg multiples. Only in areas where the Draupne formation is thin, the Brent structure becomes visible. The top of the Statfjord formation is commonly marked as a strong seismic reflector. The rotated slump blocks can often be seen on seismic. Together with well data it is sometimes possible to map individual blocks (Figure 8.6). From well data, a total number of 127 faults are identified within the East Flank. The length of the drilled section is 5625m and the estimated length of the cumulative missing section is 4493m. This gives an average missing section for each fault of 35m and a fault spacing of 44m (Hesthammer and Fossen, 1998).

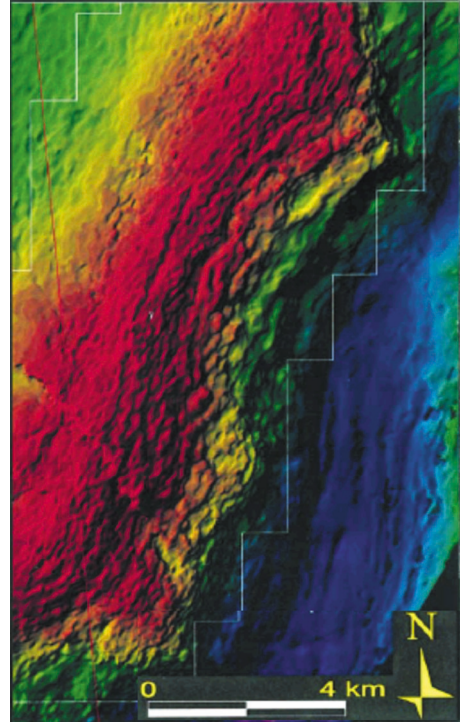


Figure 8.6 Relief map of the Statfjord Formation. Red indicates structural highs and purple structural lows. The map shows the main boundary fault and indicates that slumping took place along all of the East Flank, after Hesthammer *et al.* (1999).

8.2. Reservoir

The two main reservoir units in the Statfjord Field are the Brent formation and the Statfjord formation. These two formations contain reserves in the order of 3 billion barrels, the majority of which is stored in the Brent formation. The Dunlin shales also contain 15m of oil-bearing sandstone, but this reservoir has a limited areal distribution (Hesthammer *et al.*, 1999). The Brent and Statfjord formations have excellent reservoir properties (Kirk, 1980). In the Brent formation, porosity ranges up to 31% and is on average 29%. Permeability goes up to 8 Darcies and is on average 1500 millidarcies. The Statfjord formation has

an average porosity of 22% and the average permeability is 250 millidarcies. Permeabilities up to 12 darcies have been measured.

The field is produced from three platforms. Over 150 exploration and production wells have been drilled, providing an extensive data base on reservoir properties. For development purposes, the Brent group is divided into two major reservoir units: the Upper and Lower Brent. The Upper Brent consists of the Tarbert and Ness formations and the Lower Brent consists of the Etive, Rannoch and Broom formations. Repeat Formation Tester data demonstrate that a laterally persistent shale in the basal Ness formation effectively limits pressure communication between the Lower and Upper Brent reservoirs (Al-Najjar *et al.*, 1999). However, there can be communication between the layers when the faces of the layers are connected through faulting. The two reservoirs have been developed separately using a line drive waterflood pattern. The oil producers are in the east at the crest of the structure and the water injectors, providing pressure maintenance are located downdip in the west. In the Statfjord formation, water injection and WAG (water-alternating-gas) injection have been used. Early in the field life, excess gas has been injected into the Statfjord formation until production in this formation was started.

8.2.1. Time-lapse seismic

To improve recovery, Statoil undertook a large-scale time-lapse seismic monitoring program. One of the objectives of the 4D program is to identify unswept oil pockets and zones with early water influx in the Brent reservoirs. A pre-production survey was done in 1979 and repeat surveys were made in 1991 and 1997 (Al-Najjar *et al.*, 1999, Doyen *et al.*, 2000). All surveys are acquired in the same direction, processed in parallel, and cross-equalised for time-lapse seismic analysis. Gravity failure in the East Flank was not recognised on the first seismic survey, because of the poor seismic resolution and lack of well control. As more wells were drilled, the complex structure of the eastern part of the field became obvious. In 1997, an Ocean Bottom Cable (OBC) survey was carried out to provide better structural imaging of the complex East Flank area with P-wave data (Rogno and Amundsen, 1999). The OBC survey only covers a small part of the main field and the East Flank. Today, more than 85 wells are drilled in the slump area and, with better software, it is possible to map the detachment surfaces separating the slumped rock from the main field.

8.2.2. Reservoir model

A two-phase oil-water reservoir simulation model has been constructed for the Main Field and the East Flank (Figure 8.7). In order to correctly model the non-vertical fault planes and the highly complex structure of the East Flank, the simulation grid is defined using corner point geometry. The grid consists of 47 by 125 grid blocks in East-West and North-South direction respectively. The detailed reservoir zonation is based on sequence stratigraphy. Isochore maps of the individual layers are generated from well correlations. Twenty layers define the Upper Brent while the Lower Brent is defined by 16 layers. Petrophysical models of porosity and permeability are generated using geostatistical techniques and upscaled to the simulation grid. The model has been history matched until the end of first quarter 1996. In order to obtain a good history match, adjustments are made to the geological model and the communication between formations and the aquifer. Water cut has been matched accurately in 95% of the wells (Al-Najjar *et al.*, 1999). The history matched model is the basic input to earth modelling and rock physical modelling.

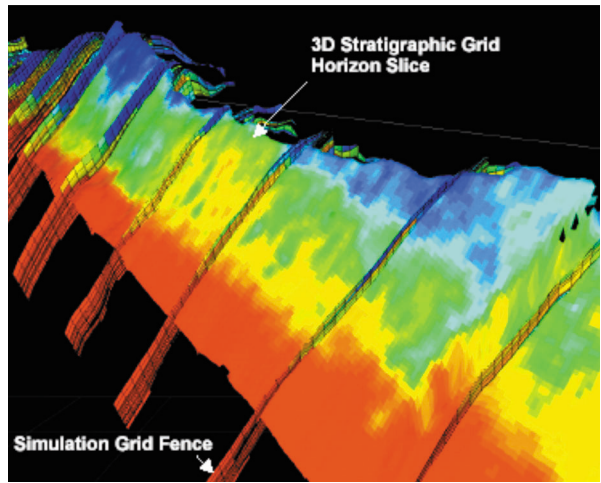


Figure 8.7 Illustration of the reservoir simulator grid color coded with water saturation in 1991.

8.3. Modified Gassmann model

The rock physical model for the Statfjord field is based on the Gassmann equations (Gassmann, 1951)(Section 4.2.1). To fit the observations in the Statfjord field, the Gassmann equations have been modified. For calibration of the model, a suite of wireline logs, core and fluid samples, and in-situ data are used. Fifteen wells with both P-wave and S-wave data are used. The modified rock model represents relations at the well log scale. Prior to be used in seismic

studies, upscaling is required. The upscaling process has to be made using proper averaging techniques, which express the effective properties seen by a seismic wave. In heterogeneous intervals, one has to average the bulk and shear moduli instead of velocities. In homogenous intervals, a simple arithmetical average is preferred (Brevik and Furre, 1998).

Gassmann equations are originally developed assuming a mono-mineralic solid phase. It is not straight-forward to deduce an analytical expression with more than one solid present e.g. sand and clay. Berryman and Milton (1991) derived a modification. However, the modification requires parameters, which are rather difficult to estimate. Alternatively, one of the bounding methods (Section 4.1.1 and 4.1.2.) can be employed to represent a mix of a two-phase solid. However, in general, the bounds are too far apart to be useful. Instead, Brevik and Furre (1998) approach the problem of a two-phase solid empirically. The main challenge is to account for the fact that skeleton or dry frame moduli are strongly dependent on porosity and clay content. The following is proposed

$$k_d = \frac{k_m^{eff}}{1 + \gamma(Vcl)\phi} \quad , \quad 8.1$$

$$\mu_d = \frac{\mu_m^{eff}}{1 + \delta(Vcl)\phi} \quad , \quad 8.2$$

and

where Vcl is the clay content, eff denotes the effective property of the rock, and γ and δ are coefficients which are assumed to be dependent primarily on clay content, but also on cementation, type of saturating fluid, effective stress, and texture (Brevik, 1996). A regression analysis of the data from the Brent reservoir, yields the coefficients γ and δ .

$$\gamma(Vcl) = 12.28 - 1.95 Vcl - 6.44 Vcl^2 \quad 8.3a$$

$$\delta(Vcl) = 18.3 - 20.29 Vcl - 7.15 Vcl^2 \quad 8.3b$$

Another part of the rock model calibration concerns the stress dependency of the dry framework of the rock. In the absence of practical models, the frame's dependency to effective stress is characterised by fitting empirical formulas to laboratory velocity measurements on dry core plugs (Brevik and Furre, 1998). The stress dependency of both P-wave and S-wave in sandstones is typically non-linear. The velocity increases rapidly at low stresses and approaches a finite velocity at high stresses. A typical and often used dependency is

$$V_x = V_x^\infty \left(1 - \frac{C_x}{1 + C_x} e^{-\zeta/D_x} \right) \quad , \quad 8.4$$

where the dependency to stress ζ is characterised by the parameters V_X^∞ , C_X , and D_X . V_X^∞ is the terminal velocity, i.e. at infinite stress. Index X refers to P-wave or S-wave. All three model parameters are expected to depend on porosity, clay content, and fluid type (Vernik, 1997).

Ultrasonic measurements of compressional and shear velocities are made at different stress levels for a total of 37 samples. The samples are taken from different wells and formations, covering a range of porosity, clay content, initial saturation, and grain size distribution. The stress cycles correspond to the reservoir conditions from start of production to present-day. Fitting the observed behaviour yields the following values for the model parameters:

	C_X	D_X	V_X^∞
P-wave	0.39	12.6	1.1
S-wave	0.39	10.4	1.07

The measurements on dry core samples only reveal the stress dependency of the solid part of the rock. The pore pressure dependency of the fluid(s) has to be represented separately by empirical formulas (Batzle and Wang, 1992) or actual laboratory measurements. Brevik and Furre (1998) prefer to measure the velocity on dry rocks because of the dispersion effects at ultrasonic frequencies.

8.3.1. Time-equivalent logs

The well logs are crucial for interpretation of the (time-lapse) seismic data (Section 5.2). Well logs and seismic data are not necessarily, and more often than not, measured at the same time. In the time-span between the log measurement and seismic measurement, the reservoir has undergone changes due to hydrocarbon production. Consistency is required to justify comparison of the well log data to the seismic data or usage of the well logs for interpretation of the seismic. The well log database needs to be adjusted forward and/or backward in time to make the logs time-consistent with the seismic. These modelled well logs are often referred to as time-equivalent logs.

The Statfjord rock physical model is employed to correct the measured logs such that they are representative for the seismic acquisition times (Brevik *et al.*, 1998). The corrections account for the change in effective pressure and saturation between the time of the log measurement and each seismic acquisition time. However, the exact change in the saturation and/or effective pressure is not known. It is only indirectly measured by the (time-lapse)

seismic. The closest is an estimate from the effective pressure and saturation change as predicted by the reservoir simulator for each acquisition time. Not surprisingly, one of the main uncertainties in this time-consistent method is the precision of the reservoir simulator (Brevik *et al.*, 1998).

8.4. Visual inspection of time-lapse seismic

Time-lapse seismic allows for dynamic reservoir characterisation in a true volumetric sense. It is possible to deduct valuable information about changes in the reservoir state. Its value is sometimes limited by the so-called non-repeatability in the time-lapse seismic data. Acquisition introduces non-repeatability, which standard processing does not remove from the time-lapse seismic. Repeatable noise is usually reduced by special cross-equalisation and matching processes, but often remnant repeatable noise is still present in the data. Both types of noise must be reduced as much as possible when analysing time-lapse seismic for time-lapse anomalies. The signals of interest are usually weak and may be completely obscured by the noise.

Conventional visual inspection of time-lapse anomalies is based on the analysis of the time-lapse change of a single attribute on horizon slices or cross sections. Most often, the time-lapse difference in amplitude or impedance at the top of the reservoir is analysed. The anomalies are verified by known production changes in wells (Furre and Brevik, 2000). Often, a high noise level impedes this analysis. Depending on the reservoir at hand, a variety of attributes may exhibit time-lapse behaviour. Of these, each attribute may yield different time-lapse responses. Studying the different attributes in isolation is time-consuming and may also lead to confusing results.

The conventional single attribute time-lapse visual inspection can be improved upon. Below, two different approaches are proposed. The results show that the visual inspection is enhanced considerably. By simultaneously analysing multiple attributes, the information carried by the separate attributes is combined. Moreover, it reduces the non-repeatable noise. The true volumetric character of the seismic information is respected by performing the inspection in three dimensions in terms of bodies rather than on sections or slices.

8.4.1. Multi-attribute match

Single attribute analysis is a quick and simple approach to analyse (time-lapse) 3D seismic data. The time-lapse difference for each attribute is obtained by subtracting the attributes of both data sets. Figure 8.8 shows the time-lapse difference for amplitude. Similar displays can be made for other attributes, of which some attributes are better 4D indicators than others. Each attribute may highlight different time-lapse seismic anomalies. Combining multiple attributes into one single attribute allows studying the information content simultaneously. To that effect, a new 4D attribute is introduced: the Multi-Attribute Match (MAM). It quantifies the time-lapse difference between multiple attributes. It is defined as the distance in hyperspace between the attribute sets of both time-lapse seismic data sets. Mathematically, each multi-attribute set can be regarded as a multi-dimensional vector. The time-lapse difference of an attribute set can then be quantified by calculating the distance between both time-lapse attribute vectors, using the following equation

$$\|L - M\| = \sqrt{\sum_{i=1}^n (l_i - m_i)^2}, \quad 8.5$$

where L is the attribute set extracted from data set 1 and M corresponds to data set 2. N corresponds to the number of attributes in the attribute set. The contribution of each attribute must be scaled to avoid unequal contributions due to differences in absolute value. We choose the scaling to be such that the difference ($l_i - m_i$) of each attribute falls between 0 and 1. The output thus ranges from 0 to n , where 0 indicates that the vectors are equal and n corresponds to the maximum difference.

Figure 8.9 shows an example of the Multi-Attribute Match at the Top Brent. It is calculated using median-dip-filtered amplitude, energy, and time frequency. It can be seen that the time-lapse seismic anomalies stand out clearly with a high Multi-Attribute Match value in yellow-red. The Multi-Attribute Match proves to be a simple and powerful tool to quickly screen time-lapse data sets for time-lapse seismic anomalies. The analysis is based on using multiple attributes simultaneously and does not require subtracting the data sets beforehand. Compared to the single attribute analysis, similar time-lapse seismic anomalies are highlighted, whereas noise is greatly reduced.

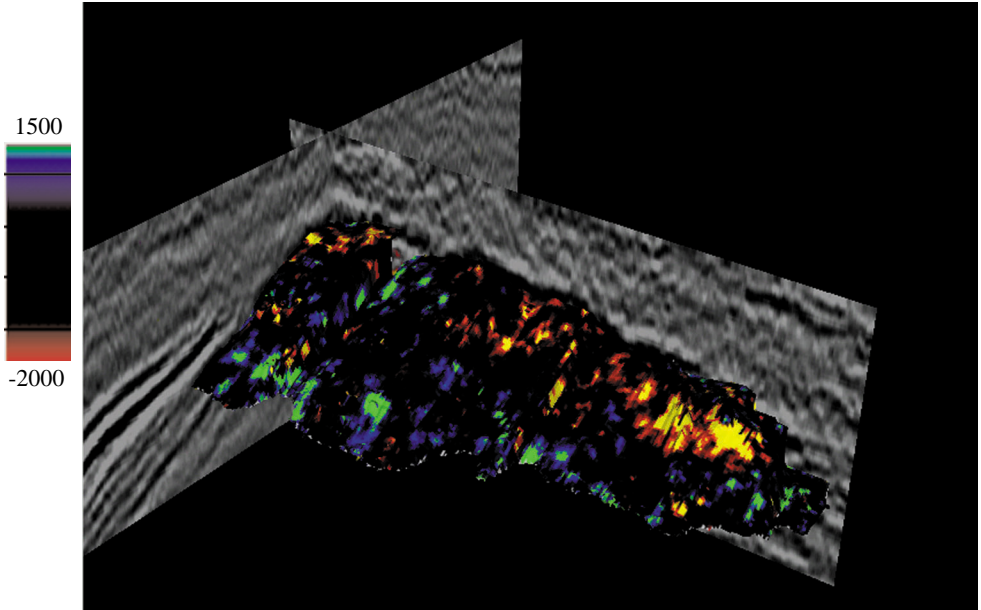


Figure 8.8 Amplitude difference (97-91) at Top Tarbert above initial oil-water contact.

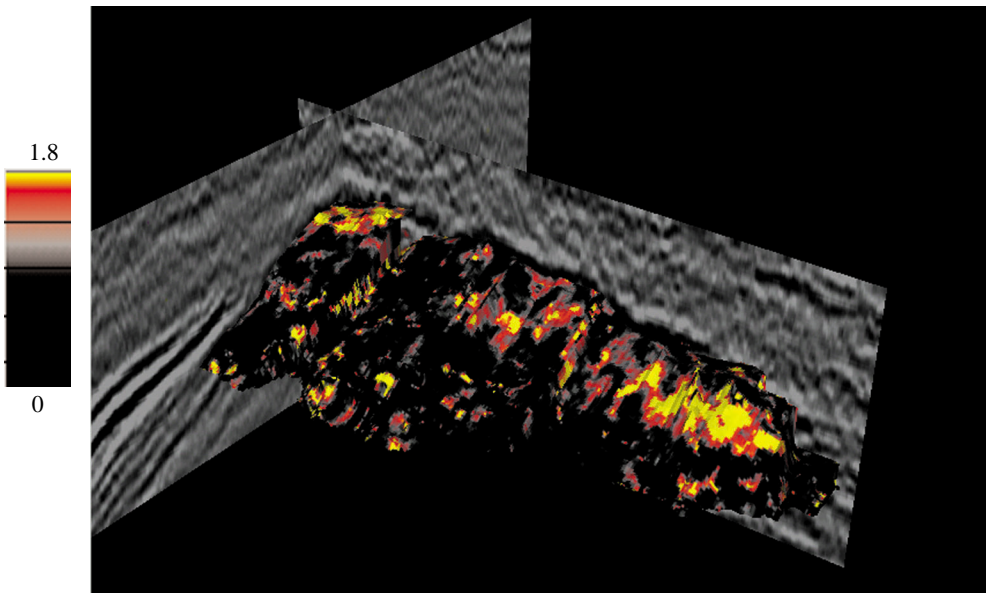


Figure 8.9 Multi-Attribute Match (MAM) at top Tarbert above initial oil-water contact. Time-lapse bodies are highlighted in yellow-red.

8.4.2. Pattern recognition

Both the single attribute difference and Multi-Attribute Match visualise the time-lapse seismic anomalies directly. It is possible to improve the detection of time-lapse anomalies considerably by a supervised pattern recognition approach. The approach is based on careful selection of example locations. “Real” time-lapse anomalies become the sole target of the network. This steering makes the detection procedure extremely powerful. One can imagine training a neural network to find time-lapse anomalies of any character or finding only those anomalies exhibiting a specific character, e.g. an amplitude decrease (Oldenziel *et al.*, 2002). A neural network has the capacity to ignore redundant information. During the learning process, internal weights are assigned to each attribute such that an optimal classification into object and non-object is achieved. In comparison, the Multi-Attribute Match is weighting each attribute equally. Adding attributes with a small 4D effect therefore deteriorates the Multi-Attribute Match while the performance of a supervised neural network is expected to increase with additional attributes, given they are not redundant.

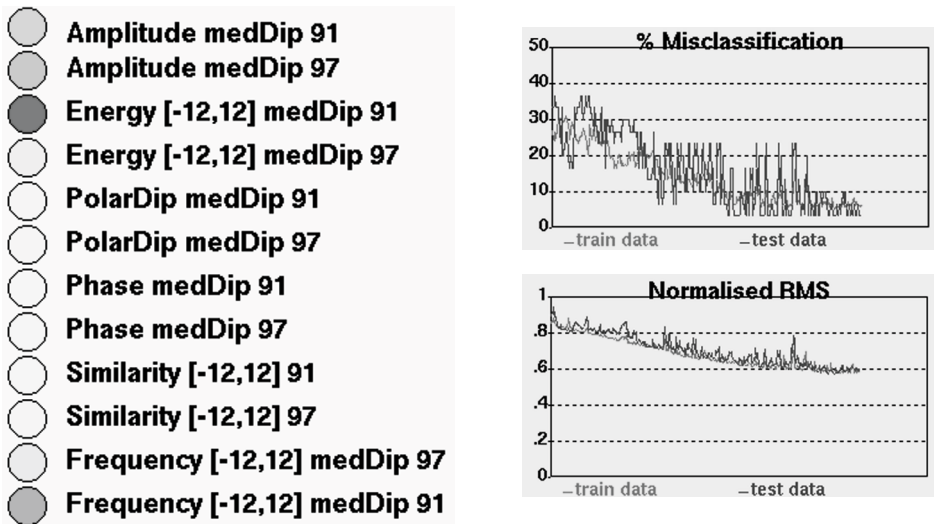


Figure 8.10 Neural network input consist of the same 6 attributes from both time-lapse data sets, 1991 and 1997. The darker the node, the more important is the attribute to distinguish 4D objects from background seismic. The term medDip refers to the median-dip filter that is used when extracting the attributes.

In the supervised approach, a fully connected Multi-Layer-Perceptron (MLP) neural network is employed. The network is trained on a representative set of example locations. The MLP network learns to classify seismic information into 4D anomalies (value 1) and background seismic (value 0) (Meldahl, *et al.*, 1998; Meldahl *et al.*, 2001). In this case the input to the neural network consists of six attributes. The network is fed with the attribute sets of each time-lapse volume; 12 in total (Figure 8.10). This approach has an advantage over feeding the difference of the attribute sets, as we may lose valuable information by subtracting the attributes (sets). The performance of the neural network is monitored during training. The colours in the input layer indicate the relative importance of each node, ranging from light (least important) to dark (most important). Moreover, the misclassification is given for both the 4D anomalies and the non-4D anomalies. As shown in Figure 8.10, a misclassification of less than 10% is achieved.

The trained neural network is applied to the time-lapse seismic data sets. The network has two output nodes with similar but mirrored information. We output only the value of the node representing the 4D anomaly and generate a 4D anomaly probability cube. Values close to 1 represent a high probability of a 4D

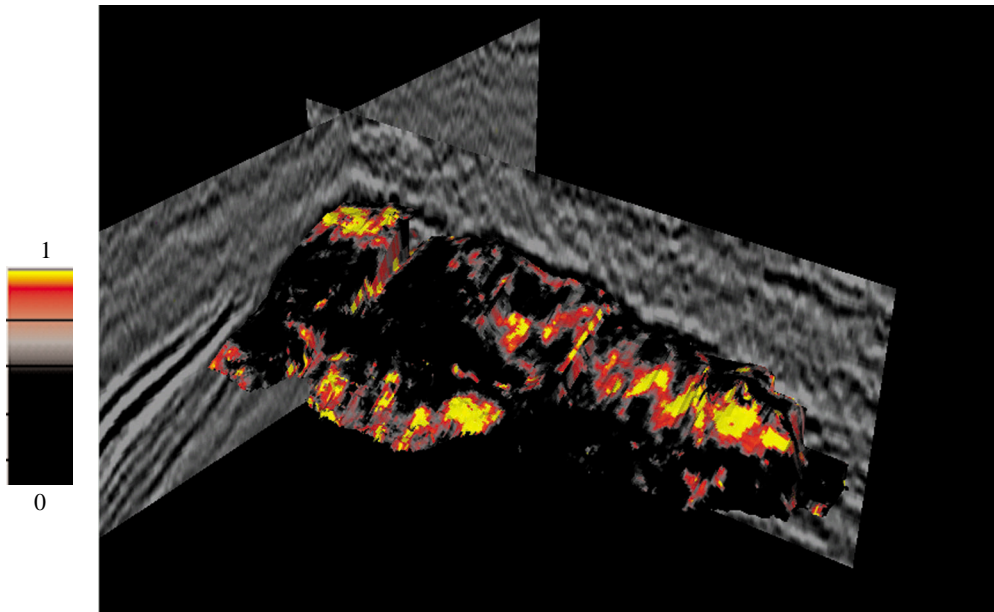


Figure 8.11 4D Object cube at top Tarbert above initial oil-water contact. Red-yellow is highest probability of seismic being a 4D object.

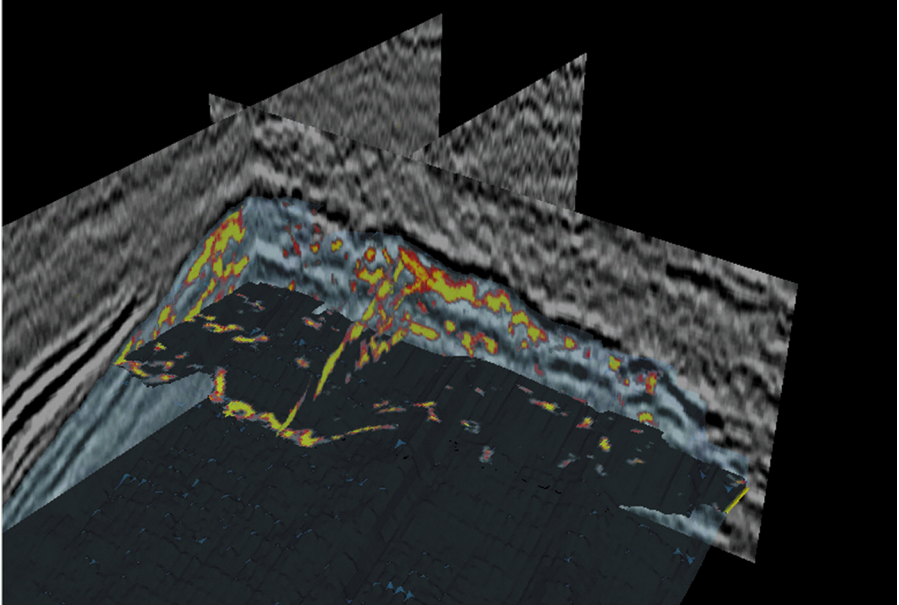


Figure 8.12 A 3D image of the 4D object cube. High probabilities are displayed in red-yellow, low probabilities are made transparent. The '97 seismic is shown in the background. Top Tarbert is displayed in transparent light blue.

anomaly and values close to 0 indicate low probability. Figure 8.11 and 8.12 show the 4D anomaly cube at the top Tarbert and in 3D, respectively. Compared to the Multi-Attribute Match, the detection of 4D anomalies is improved considerably by the supervised approach. First of all, because the user steers the process by careful selection of example locations. Secondly, a neural network has the capacity to ignore redundant information.

8.4.3. Non-repeatable noise

Non-repeatable noise is reduced significantly by using multiple attributes simultaneously compared to the conventional approach (Figure 8.8). Furthermore, the non-repeatable noise is tackled in different ways in the methodology. Firstly robust statistical filters are applied to all attributes upon extraction from the seismic data. The disc- or cylinder-shaped filters follow the local dip and azimuth of the seismic data. The attribute value at the extraction point is then replaced by the median value inside the search range. This filtering decreases the impact of non-repeatable noise, possibly at the expense of losing

a bit of resolution. Non-repeatable noise is also reduced in the second step of the procedure when applying the neural network to detect 4D anomalies. A well-known feature of supervised neural networks is their capability to “see” through noise to capture the general trend in the data (de Groot, 1995). The supervised approach also has the potential to reduce remnant repeatable noise through careful selection of example locations. Example locations can be selected in areas with time-lapse differences that are attributed to repeatable noise. Classifying these example locations as non-4D anomalies gives the network a chance to learn that subtle differences in the attribute sets of repeatable noise and true 4D anomalies may exist .

8.5. Saturation inversion

Monitoring fluid flow is the main driver for many time-lapse surveys. It helps in identifying undrained or by-passed hydrocarbons. A variety of methods aimed at inverting to saturation have been developed. Often these methods are case specific. No general method has been suggested, nor have different methods been cross-validated. On the Statfjord field, two different procedures have been applied. Both approaches and their results are discussed and compared. The objective of these methods is the same, i.e. to invert time-lapse seismic data to saturation. Both estimate saturation at the respective acquisition times 1991 and 1997. The approaches differ in how seismic data is used and in their character. Both rely on time-equivalent logs (Section 8.3.1) although to a different extent.

8.5.1. A non-linear approach

A neural network is employed to non-linearly map the seismic to a saturation estimate for each survey (Oldenziel *et al.*, 2000). Porosity is a desired input for predicting saturation. Variations in time-lapse signals are expected to be larger in porous rocks than in less porous rocks for two reasons. Firstly, the effect of fluid replacement on the seismic response is more pronounced with increasing porosity. Secondly, porosity is in general related to permeability. This implies that porous rocks are more easily drained than less porous rocks resulting in larger changes in saturation. The porosity volume itself is predicted upfront from the time-lapse data set by employing a neural network. In a second step, the saturation is predicted using porosity, acoustic and elastic impedance.

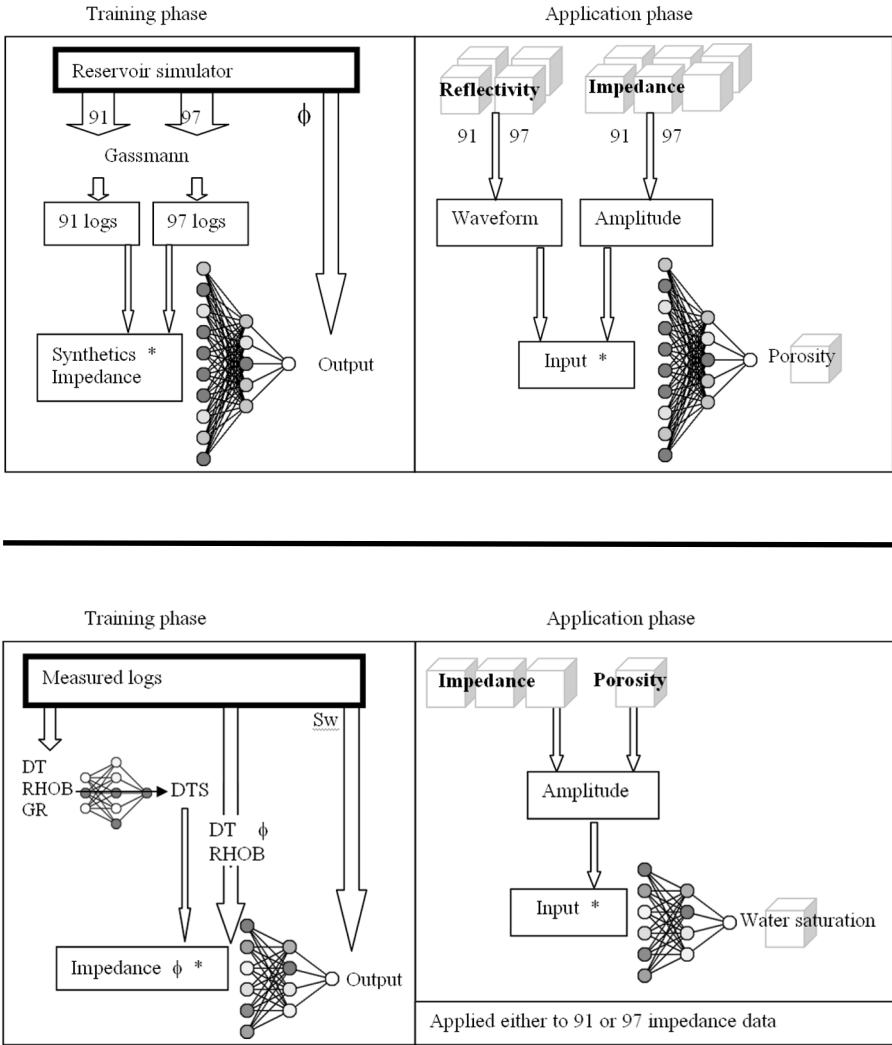


Figure 8.13 Flow diagram for porosity (top) and water saturation prediction (bottom). Impedance means acoustic impedance, and mid and far angle elastic impedance. Reflectivity corresponds to near and far offset stacks.

* Two additional inputs are given to each network; a stratigraphic indicator to distinguish the main area from the East flank and the reference time, i.e. the stratigraphic time relative to top reservoir.

Volume transformation is defined as the process of mapping one or more seismic input volumes to one or more output volumes (de Groot, 1999). In this study, the information from ten seismic volumes is mapped to three output volumes covering the Brent interval. A supervised neural network is employed to non-linear map to input to the output. Figure 8.13 illustrates the process. The input to the neural network is shown schematically. At each sample position the complete waveform rather than some derived attributes is taken from the seismic reflectivity cubes. At the same position the amplitude is extracted from each of the impedance cubes. The network processes this information and predicts the target value(s) for which it was trained. Next, it slides one sample position down the various input cubes, extracts the information it needs and predicts the next value(s).

Fully connected Multi-Layer-Perceptron (MLP) neural networks are used. The networks are trained and tested on examples taken from the well database in a sliding fashion as described above. The target porosity and water saturation traces are constructed from logs. The relevant logs are converted from depth to time using the sonic log and then re-sampled with an anti-alias filter to the seismic sampling rate of 4ms. The input reflectivity waveforms and impedance values are derived from synthetic seismograms rather than from the real data volumes. Synthetic seismic is preferred in the training phase, because this ensures complete alignment between input and output traces over the entire target interval. With real seismic data we are always dealing with mis-picks and log-trace depth-to-time conversion problems resulting in unaligned data that degrades the training set. Synthetic seismograms and log traces are per definition aligned because they are converted from depth to time using the same sonic log. The trained network can thus find the optimal mapping between seismic input and target response. Application of such a “perfect filter” does not remove any mis-picks and stretch / squeeze problems inherent to the seismic data. Before applying the trained network to real seismic data, the input must be scaled to the amplitude range of the synthetic response on which the network has been trained.

Porosity inversion

Although porosity remains constant over time, the seismic response changes as a result of production. To avoid mapping production-induced changes to variations in porosity, we propose to predict porosity from the time-lapse seismic volumes simultaneously. In total we use ten (two times five) seismic volumes (Figure 8.13). As described above, the set to train the neural network

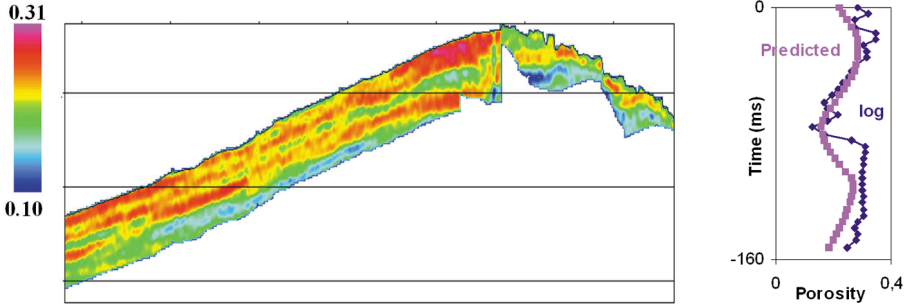


Figure 8.14 East-West profile through the porosity volume and a comparison between predicted and actual porosity at a blind test location.

is constructed from logs and synthetic seismograms. Mid and far angle reflectivity synthetics for 1991 and 1997 are made from time-equivalent sonic and density logs by the convolutional method. Elastic impedance logs are derived from time-equivalent sonic, shear-sonic, and density logs using Shuey's approximation

$$Z_{\alpha} = Z_p \exp([\log(Z_p) - 2\log(Z_s) + \log(5.10^6)] \sin^2(\alpha)), \quad 8.6$$

where α is the average angle of incidence in the target zone, and Z_{α} , Z_p , and Z_s are the elastic impedance, acoustic impedance, and shear impedance, respectively. Two additional inputs are fed to the neural network. The reference time relative to the Top Brent horizon is given to model the vertical porosity trend in the reservoir. The second input is an indicator to reflect the distinctly different structural styles in the field. The main part of the field is a relatively undisturbed block of westerly dipping layers. The East flank is structurally complex and consists of tilted and rotated fault blocks with slumped deposits (Figure 8.3). For each part, a different relation may exist between seismic and porosity. Rather than modelling separate networks for each area, we supply the network with an environmental indicator. The value zero indicates a location within the main area while a value of one is used for the East flank.

Out of the 130 available wells, some 30 are set aside to test the performance of the network. The remainder are used to create a training set. The entire Brent interval covers a time-window of approximately 150msec. With a 4msec-sampling rate this means that the total number of training examples is approximately 3750 vectors ($100 \times 150 / 4$). The actual number is slightly less,

because intervals with missing logs are discarded. The network is capable of finding the desired relationship between seismic and porosity. The trained network is tested at blind test locations by applying it to both the synthetic responses and the real seismic responses. Apart from an overall discrepancy in frequency content between actual - and neural network-predicted porosity, the predictions at these blind test locations are deemed successful (Figure 8.14). The low frequency of the predictions from real data reflects the band-limited frequency content of the seismic and inverted impedance cubes. The latter are made without broadening the frequency bandwidth.

Application of the trained network to the seismic data sets over a window of 150msec hanging from the mapped top reservoir yields the desired porosity volume (Figure 8.14). The results correspond well with the actual knowledge of the Brent group. The Tarbert and Etive formations show the highest porosity, while Lower Ness, Rannoch, and Broom formations show up as lower porosity units.

Saturation inversion

We employ one neural network to predict water saturation at different acquisition times. Applied to the '91 data set, the network predicts '91 water saturation, and applied to the '97 data set, it predicts '97 water saturation (Figure 8.13). This can be explained as follows. Each well has a set of measured and derived logs (sonic, shear sonic, density, porosity, water saturation, mid- and far elastic impedance, and acoustic impedance). Each set represents a consistent combination of neural network inputs and target responses from which examples are extracted every 4msec over the entire target zone. By using all wells to train the neural network, we ensure that the set of measured logs covers the entire range of possible variations. We avoid using the biased time-equivalent logs when we employ the measured logs.

The network for predicting water saturation is trained on most of the 130 available wells. Five wells serve as blind test wells to test the network's performance. The neural network is applied to the same 150msec interval hanging from the top reservoir. Application to the '91 data set yields the desired '91 saturation volume and application to the '97 data results in the '97 saturation cube. Visual comparison of '91 and '97 saturation predictions reveal the overall depletion in the main area of the field. Figure 8.15 shows the southern part of the field. Slices are taken at 12msec below the mapped top reservoir. In the main part of the field the '91 saturation is generally much higher than in '97. At the right, the difference between the '91 and '97 water saturation is shown,

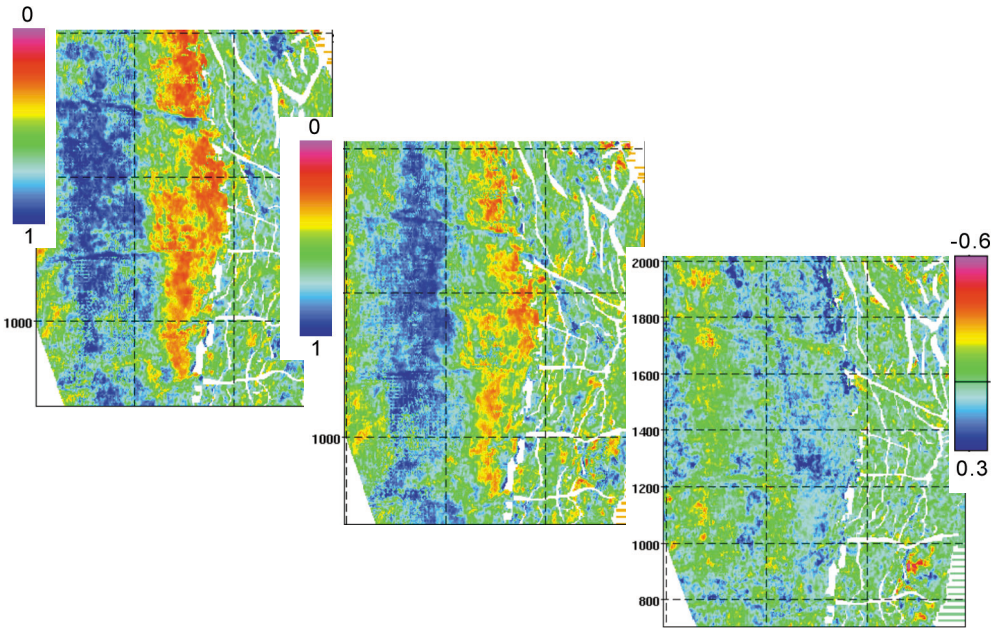


Figure 8.15 Water saturation predicted for '91 (left) and '97 (middle), and their time-lapse difference ('97 - '91) at the right.

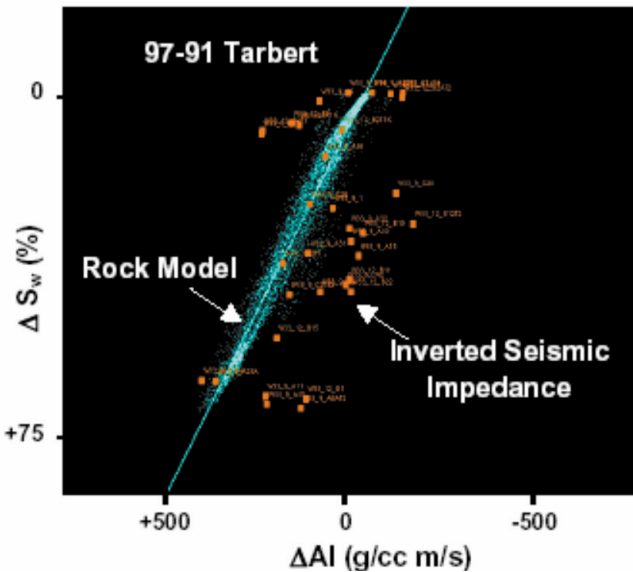


Figure 8.16 Cross plot of time-lapse change in Tarbert average saturation versus average acoustic impedance. Zone average saturations are from flow simulator. Square symbols correspond to zone average seismic impedance extracted at well locations with correlation coefficient equal to 0.6. Small dots and lines correspond to rock physical model predictions. Reasonable agreement is observed between observed and predicted impedance differences, after Doyen et al. (2000).

where the former is subtracted from the latter. An increase in water saturation, i.e. flooding with water, corresponds to a positive value and is indicated in blue. Red or green indicates, respectively, an increase in oil saturation or no change at all. The difference plot reveals the overall level of depletion in the main area. North-south trends are visible, which may indicate permeability trends in the reservoir. The results for the East flank are more difficult to interpret. Some time-lapse differences are observed but in general the variations are small. This may either be a resolution / data quality problem in this complex area, or it indicates that production has not yet had an impact on the seismic response.

8.5.2. A linear approach

Doyen *et al.* (2000) use a linear approach to estimate saturation at the respective acquisition times. In their approach, they determine the linear regression between impedance and saturation time-lapse difference at the wells. First, impedance and impedance difference maps are calculated by vertical averaging over the Tarbert interval. Average impedance differences are then calibrated against simulator-derived saturation changes at the well locations, as shown in Figure 8.16. For validation, the relation between impedance and saturation change is compared to the rock physical model. Next, the collocated co-kriging technique is applied to obtain '91-'79 and '97-'91 saturation difference maps, using average impedance differences to constrain the mapping process. Finally, a '97 Tarbert saturation map is obtained by adding the estimated saturation difference maps to the initial saturation model used as input to the flow simulator. Simulator-derived average saturation differences are used as primary control points in the co-kriging process. Doyen *et al.* (2000) justify this approach based on the fact that the flow model has been history matched to an accuracy of 95% in more than 90% of the wells (Al-Najjar *et al.*, 1999). Figure 8.17 shows the result for the '97 saturation. A comparison is made to the reservoir simulator output.

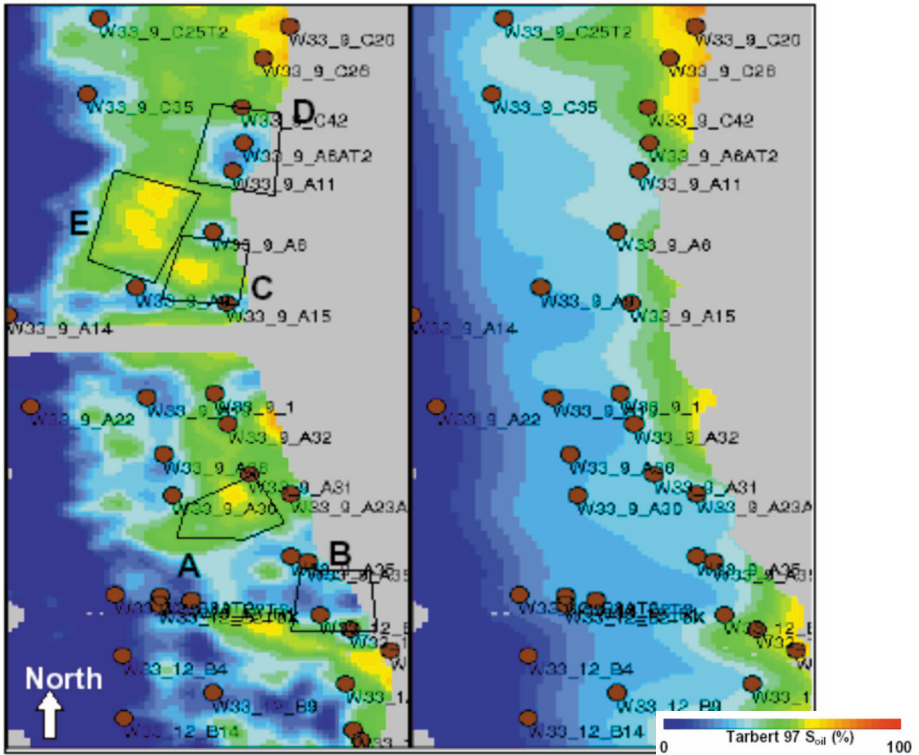


Figure 8.17 Illustration of how the '97 time-lapse seismic derived saturation is used to check the reservoir simulator output (right). Discrepancies are observed within the black shapes, after Doyen et al. (2000).

8.5.3. Discussion

Figure 8.18 shows the 1997 results for both methods at the southern part of the field. Due to the different character of the methods, some manipulations are required to allow comparison. The neural network result is averaged over the Tarbert formation and subsequently averaged laterally to mimic the smooth character obtained using co-kriging in the linear procedure. In general, the two methods yield similar results. Both show the flooding of the west and some undrained pockets in the east. Some discrepancies are observed.

A second comparison is made for wells drilled after 1997. These wells are not considered in both inversion processes and serve as blind test wells. Some production is likely to have occurred between 1997 and logging of the wells.

Well	Logs	Linear		Non-linear	
		value	error	value	error
C30A	0.72	0.746	0.03	0.48	-0.24
A14A	0.41	0.576	0.17	0.64	0.23
C40AT2	0.57	0.626	0.06	0.55	-0.02
C23T2	0.2	0.392	0.19	0.6	0.40
B6B	0.55	0.725	0.18	0.7	0.15
A15B	0.49	0.621	0.13	0.65	0.16
B19AT2	0.836	0.511	-0.33	0.67	-0.17
A42A	0.5	0.791	0.29	0.7	0.2
			0.19		0.22 (st dev)

Table 8.2 Comparison for saturation prediction at wells drilled after '97.

a non-linear way using a neural network. The physical relation itself is not necessarily linear. In the linear approach, the relation between the time-lapse seismic difference and the saturation difference is modelled. The neural network determines the relation between the seismic and the saturation. Often, the relation between the time-lapse seismic and the saturation difference is more obvious.

The time-equivalent logs are used in both procedures, although to a different extent. In the linear procedure, the estimation of the seismic-saturation relation is heavily based on the time-equivalent logs. One can even observe a Catch-22 situation (Section 5.4.3). The reservoir model is used to generate the time-equivalent logs, which in turn are used to translate the time-lapse seismic to a saturation estimate. This saturation estimate is employed to check the validity of the reservoir model. In the neural network approach, the measured logs are used to determine the seismic-saturation relation. Moreover, the porosity is used as an additional factor to the seismic-saturation relation.

For both methods, a saturation estimate is obtained for the '91 and the '97 survey. The linear approach yields a smooth map of the average saturation

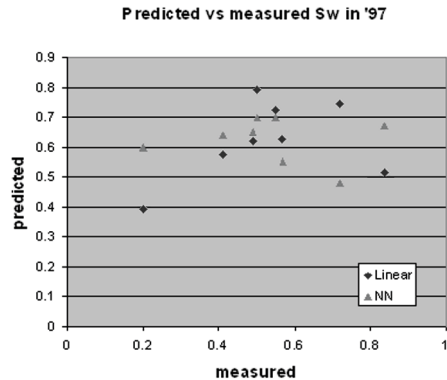


Figure 8.19 Comparison of the '97 saturation values as measured and predicted for 8 blind test wells (Table 8.2).

for the Tarbert formation. At the wells the linear approach corresponds well to the well observations due to the co-kriging in which the reservoir simulator estimate at the well is used. The neural network approach yields an estimate at each seismic trace locations and for each seismic sample, i.e. each 4msec. No lateral correlation is applied.

In general, one has to realise that one method may perform better on a certain data set than another data set. It also depends on the objectives and the available data, which method is preferred.

8.6. Alternative to rock physical modelling

Rock physics is regarded a crucial discipline for time-lapse seismic as described in Chapter 4. It provides the link between the seismic measurement and the reservoir properties, as it describes the behaviour of a (saturated) rock when excited by a seismic wave. Rock physics finds its application in the field of fluid substitution for forward seismic modelling. Additionally, it is applied to translate observed time-lapse changes in terms of reservoir property changes. As one can expect, erroneous models will lead to false interpretation and ultimately to reservoir mismanagement. Ideally, a rock physical model takes into account all aspects related to the rock matrix, the pore-fill, the in-situ conditions, and physical phenomena of wave propagation. However, it is impossible to consider all aspects of the problem in one model given the extraordinary complexity of most rocks. Every theoretical model has its simplifying assumptions. For the Statfjord field, the Gassmann equations (Gassmann, 1951) have been modified to fit the observation on the Statfjord log and core data as described in Section 8.3.

Most rock physical models are described, and their experiments performed, at the core or log scale. These measurements are at a different frequency scale than the seismic measurement. Attenuation and dispersion can have a considerable impact when comparing the rock's behaviour at different frequency scales (Section 4.3.4). Using a rock physical model for time-lapse seismic purposes, thus requires a rock physical model that describes the behaviour at the seismic scale. We propose an alternative data-driven approach, which is described below. The model is data-driven and at the frequency scale of the seismic measurement. This approach is only feasible given the data available and relies heavily on the accuracy of the reservoir model. The reservoir model for the

Statfjord field exhibits a high accuracy of 95% for wells' water cut (Al-Najjar *et al.*, 1999). The main objective is to develop a model free of assumptions about the rock physical mechanisms and empirical relations based on core and well log data (de Roos, 2000). An equally important aim is to describe the decoupled effects of saturation and pressure on acoustic impedance and other seismic properties. The Statfjord field has been in production since 1979 and over 150 wells have been drilled yielding a significant amount of engineering information. The ongoing development and the remarkable amount of seismic, production, geological, and wireline data make Statfjord ideal for studying the effects of production and fluid migration on the seismic character.

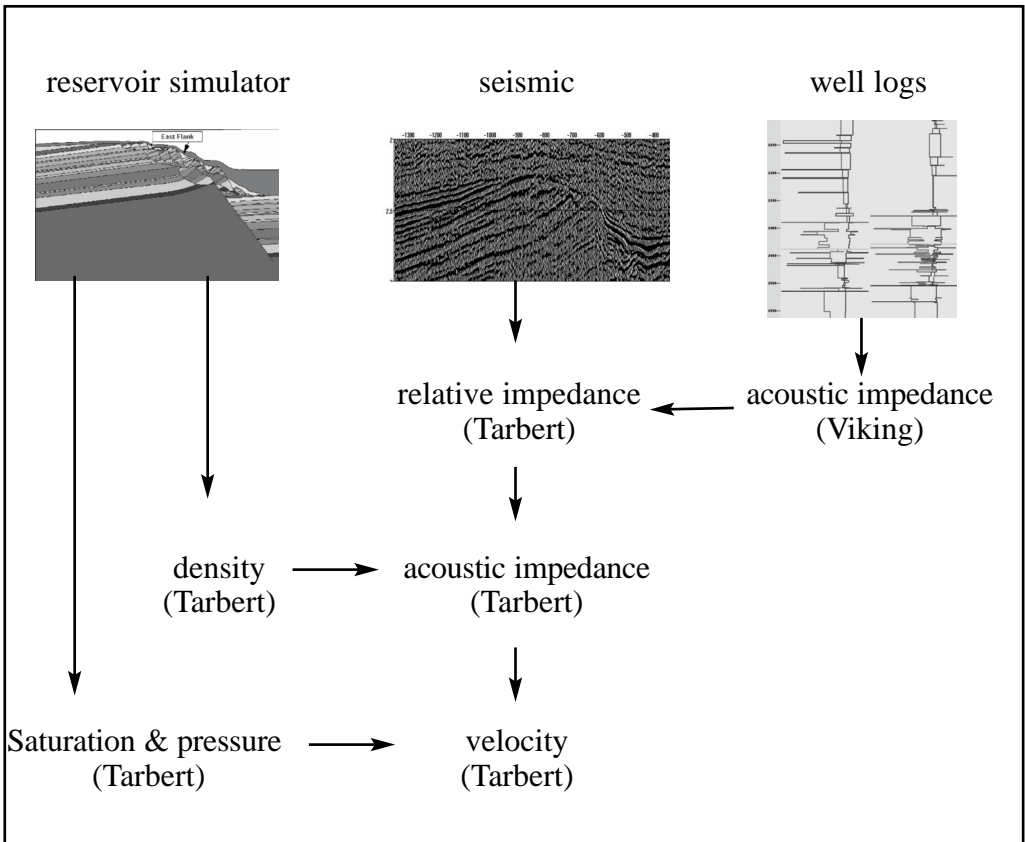


Figure 8.20 Proposed method to invert seismic reflection data to seismic velocity for top reservoir illustrated on Statfjord field.

8.6.1. Procedure

The first assumption is that the reservoir simulation model closely represents the actual reservoir behaviour. In the Main field with its simple geological setting this is a fair assumption, because most of the wells have been closely history matched. Pressure and saturation obtained from the simulator can be expected to be very close to the actual reservoir behaviour. The second assumption is that we can obtain acoustic impedance from the seismic by using non-producing overburden layers as benchmark after constructing the relative impedance volume. Under these assumptions we avoid using time-equivalent log data, which are based on the rock physical model. The procedure is only valid for the top of the Tarbert. Applying the same routine to the underlying reservoir layers probably yields highly inaccurate results due to uncertainties and inaccuracies in the overlying reservoir layers.

In the proposed workflow (Figure 8.20), the seismic signal is deconvolved, yielding a relative impedance volume or the reflection series. The wavelet that is used for deconvolution is extracted from the seismic. Usually the relative impedance is translated to an absolute acoustic impedance volume using the well logs. In our approach, the acoustic impedance from the overlying non-producing Viking shales is used to obtain an absolute impedance value for the top of the reservoir. The Viking shale acoustic impedance value is constant over time and is obtained from the well logs. By Kriging, an estimate of this impedance is obtained to cover the entire reservoir. Using the Zoeppritz equations (Mavko *et al.*, 1998), the acoustic impedance of the Tarbert layer is thus obtained.

The acoustic impedance is the product of velocity and density. Using the density from the reservoir simulator, the P-wave velocity can be estimated from the acoustic impedance. The relation between P-wave velocity and pressure and saturation, as predicted by the reservoir simulator, can now be analysed. A neural network is employed to actually

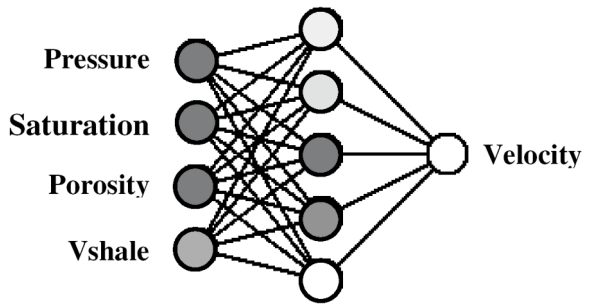


Figure 8.21 Neural network topology to predict velocity using pressure, saturation, porosity, and shale content (*Vshale*) as input.

investigate whether a relation exists (Figure 8.21). Porosity and shale content are used as additional constraints, because both impact the relation between saturation / pressure and velocity.

8.6.2. Results

The results at inline 1773 are analysed and compared to the modified Gassmann model (Section 8.3). Figure 8.22 shows the results for 1991 and 1997 combined with the reservoir properties taken from the reservoir simulator. Both the inverted P-wave velocity and the P-wave velocity as predicted by the neural network are compared to the Gassmann P-wave velocity. A weak correlation between pressure and saturation and any of the three velocities is seen. The lateral changes in inverted P-wave velocity are more pronounced than the Gassmann P-wave velocity. In general, the inverted P-wave velocities as well as the velocities predicted by the neural network are higher than the Gassmann P-wave velocities. The behaviour around point 25 deserves special attention. For the 1991 data, the inverted P-wave velocity shows a sharp decrease. The neural network predicts a smooth velocity development in this region, as does the Gassmann model. This indicates that the inverted velocity may be the result of a local event, perhaps an injector. This local event is not represented in the reservoir properties taken from the reservoir simulator, from which the Gassmann and neural network velocities are calculated. In 1997, the same dip is observed in the inverted velocity, associated with a higher saturation and pressure. In contrast to the 1991 prediction, the neural network picks up the P-wave velocity decrease for the 1997 data. The most likely explanation is the presence of an injector. Near an injector, the water saturation increase yields an increase of the P-wave velocity. On the other hand, the considerable pore pressure increase near the injector results in a velocity decrease, which, being large in value, can override the saturation-induced increase.

Figures 8.23 and 8.24 show the representation for the overall behaviour of P-wave velocity as function of pressure and saturation. Both the modified Gassmann model and the neural network are applied to a range of pressure and saturation values, while porosity and shale content are kept fixed at 0.25 and 0.15, respectively. As mentioned above, the neural network is trained on all the available data points. However, the range of pressure and saturation values is not entirely covered by the data points. The low pressure - high saturation region is not well represented. As a result, the neural network probably extrapolates in this region and the results have to be regarded with caution. In general, we observe the same features for both figures. The P-wave velocity

Statfjord case study

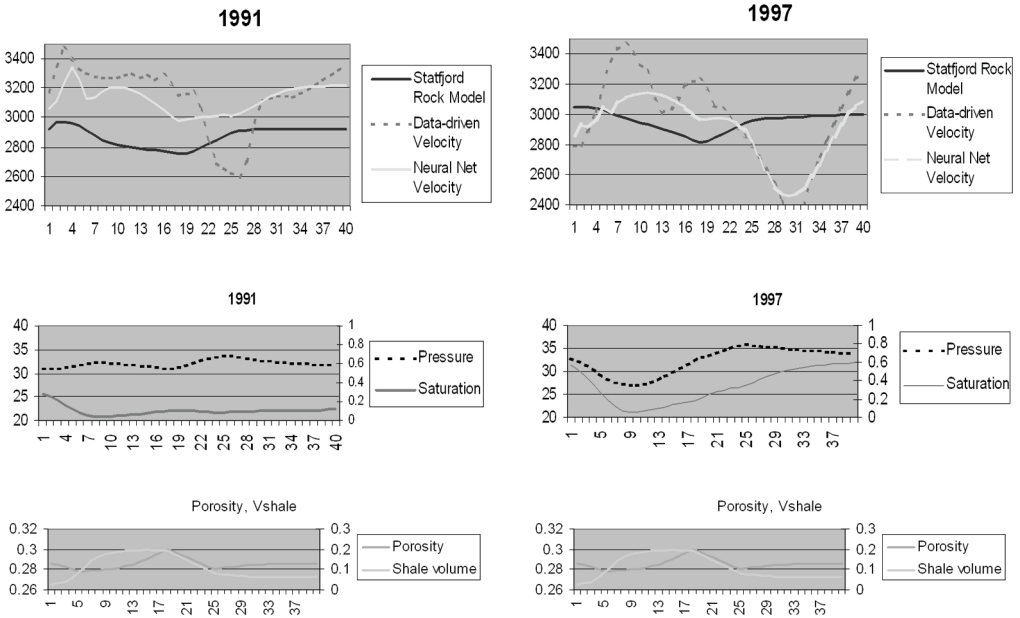


Figure 8.22 Velocity along inline 1773 as calculated by modified Gassmann model, as inverted using data-driven approach, and as predicted by neural network. Neural network prediction and Gassmann velocity are based on reservoir properties pressure, saturation, porosity, and shale content, which are extracted from reservoir simulator.

increases with increasing pressure and water saturation. Note that the vertical axes have different scales.

A strong difference is observed in the high pressure - low saturation region. The neural network predicts higher P-wave velocities. This anomaly may be caused by the 1991 data. The 1991 data only comprises data points in the high pressure-low saturation region, whereas the 1997 data points cover a wider range. To prove this, a new neural network is trained on the 1997 data points. Figure 8.25 shows the result of the 1997 neural network. The P-wave velocity as predicted by the 1997 neural network displays the same behaviour as the Gassmann model in Figure 8.24. Consequently, the earlier observed anomaly is likely to be a distinctive characteristic of the 1991 data. In the high pressure- high saturation region, the result of the Gassmann model differs from both neural network predictions. The Gassmann model predicts an ever increasing P-wave velocity in the higher pressure regime, whereas the neural network predicts a

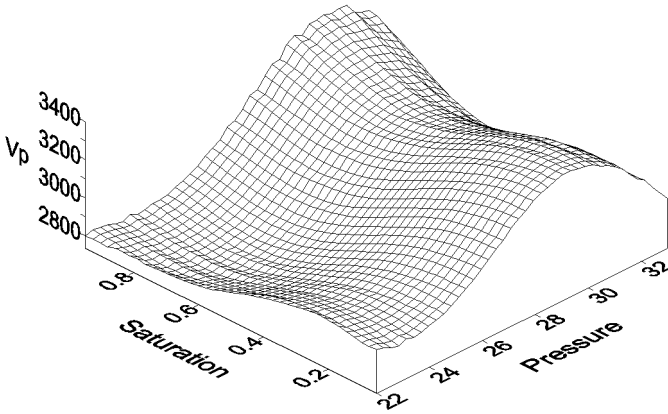


Figure 8.23 Neural network output for P-wave velocity in 1991 as function of pressure and saturation as determined using data-driven approach.

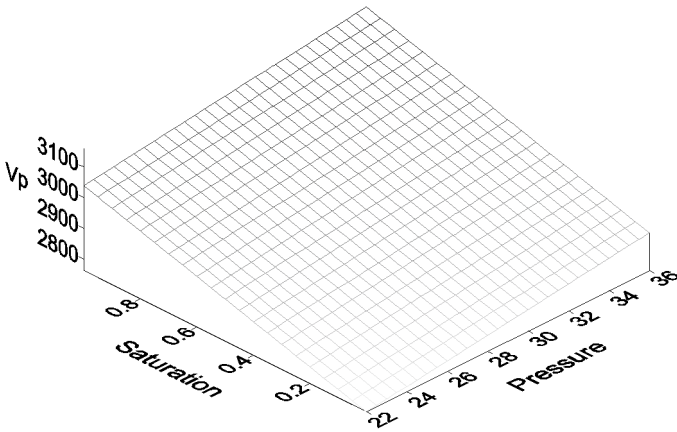


Figure 8.24 P-wave velocity as calculated using the modified Gassmann model as a function of pressure and saturation for fixed porosity (0.25) and V_{shale} (0.15).

decrease in P-wave velocity. This behaviour is also observed in Figure 8.22 near the possible injector with associated pressure build-up. As pointed out by Rogno *et al.* (2000), near an injector it is very likely to observe a velocity decrease. Near an injector, the velocity decrease due to the (pore) pressure increase is larger than the velocity increase due to the water saturation increase.

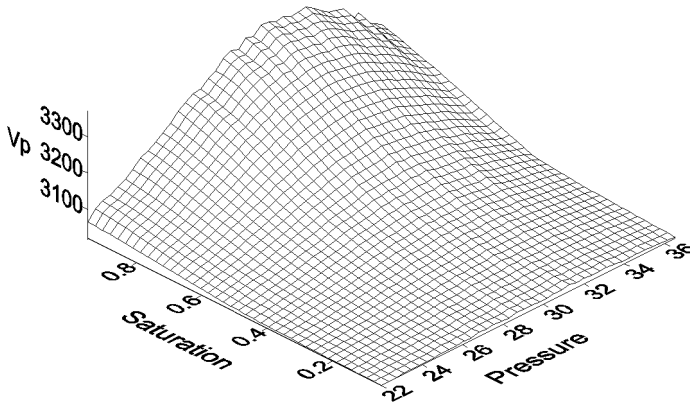


Figure 8.25 Neural network output for velocity in 1997 as function of pressure and saturation as determined using data-driven approach.

Chapter 9

Conclusions and future work

In this thesis, the cycle of time-lapse seismic data analysis within reservoir management is described. Two main challenges are discerned: how to interpret the time-lapse seismic signal in terms of reservoir properties, and how to integrate the time-lapse seismic information within reservoir engineering. State-of-the-art techniques within geophysics, rock physics, and reservoir engineering are analysed to identify problems associated with either of the above-mentioned challenges. For a variety of problems, solutions are sought as described below. Suggestions for future work are discussed in the next section.

9.1. Conclusions

- A 4D attribute is proposed, which allows analysing the time-lapse seismic in a wavelet independent manner. Compared to conventional amplitude analysis, the 4D attribute is not affected by differences in wavelet between seismic surveys. The 4D attribute displays a direct relation with the time-lapse saturation difference as tested on a synthetic data set. The seismic resolution can be an impeding factor.

- An automated history matching loop is developed integrating the time-lapse seismic with production data. The automated procedure is employed in different scenarios to analyse the impact of time-lapse seismic on reservoir management. In general, time-lapse seismic offers valuable information to better constrain the reservoir model. It has the ability to reduce the production forecast uncertainty. In some cases, the time-lapse seismic contributes little information.

- Geological parameterisation of a reservoir model allows honouring the geological information as provided by time-lapse seismic. It is of great benefit for structurally complex reservoirs such as the Statfjord field.

- A Catch-22 can be observed for most time-lapse data sets. The Catch-22 arises when the reservoir model is used to interpret the time-lapse seismic, which in turn is shot with the objective of validating the reservoir model.

- A data-driven method is proposed as an alternative to rock physical modelling to derive the relation between seismic and reservoir properties, pressure and saturation. It derives the rock physical relations at the seismic scale. In the comparison to the modified Gassmann model, similarities and discrepancies are observed. The data-driven method may perform better than theoretical methods such as Gassmann equations, in case the underlying assumptions for these methods are not satisfied.

- A new method is suggested to invert time-lapse seismic to saturation, in which the static and dynamic reservoir parameters are decoupled. A neural network is employed to determine the relation between the seismic properties and saturation, based on the measured logs. The method is tested on the Statfjord field. Compared to an alternative inversion method applied to the Statfjord field, the relation between seismic and saturation is better captured by the neural network approach, but the results at the wells are less precise.

- An innovative visualisation methodology is introduced using attribute sets and neural network-based pattern recognition technology. Compared to the conventional (single attribute) amplitude analysis, visual inspection is improved considerably, non-repeatable noise is reduced, and the 3D character of the time-lapse seismic information is honoured.

9.2. Recommendations

The broadness of the subject and the fact that time-lapse seismic is a rapidly advancing technology means that this thesis can neither be complete, nor that problems and solutions can be covered in great detail. It is limited to some of the main problems. Below, a list of some generic problems follows as well as recommendations for future work.

- Calibration logs are required to interpret the time-lapse seismic signal and avoid a Catch-22 situation. Data cannot be measured once the opportunity has passed, i.e. calibration logs have to be acquired within a reasonable time around the seismic survey. The reasonable time frame is defined such that both seismic and well log measure the same reservoir state. Introduction of the digital oil field and monitor wells is required to allow acquiring time-equivalent (calibration) logs.
- To encourage the acceptance of and allow increased benefit from time-lapse seismic data, its interpretation and subsequent integration has to be performed within a shorter time span.
- To bridge the gap between visualisation and quantification of time-lapse seismic, the pattern recognition methodology can be employed. Time-lapse anomalies of special character, e.g. related to saturation or pressure changes, can be subject of study.
- The definition of the objective function can be improved upon, e.g. by including the relative confidence between different sorts of data, by including the measurement error, and by employing a different format than the sum-of-squares to better honour the character of the data.
- To stimulate acceptance and proof its value for integration of time-lapse seismic, the automated history matching procedure has to be applied to an actual field.
- Interpretation of time-lapse seismic is impeded by non-repeatable noise. Moreover, the inversion to reservoir properties is not straightforward and introduces bias. The impact of both measurement and inversion error on the quality of the reservoir model has to be analysed.

- The proposed 4D attribute is very promising, but is hampered by the resolution of the seismic data. The seismic frequency bandwidth can be boosted or an alternative representation of the seismic can be used, e.g. by using a local transform. Eventually, the 4D attribute has to prove its value on an actual data set.

References

Arenas, E.M., 2000, *Automatic history matching using the pilot point method including 4D seismic*, M.Sc. thesis Delft University of Technology, Faculty of Civil Engineering and Geosciences

Arenas, E.M., van Kruijsdijk C.P.J.W., Oldenziel T., 2001, *Semi-automatic history matching using the pilot point method including time-lapse seismic data*, SPE 71634, SPE 2001 Annual Technical Conference, New Orleans

Aki, K., Richards, P.G., 1980, *Quantitative seismology, Theory and methods, Vol. 1*, W.H.Freeman and co, San Fransisco

Al-Najjar, N., Brevik, I., Psaila, D., Doyen, P.M., 1999, *4D seismic modelling of the staffjord field: initial results*, SPE 56730, SPE 1999 Annual Technical Conference, Houston

Aminzadeh, F., Connolly, D., Heggland, R., Meldahl, P., de Groot, P., 2002, *Geohazard detection and other applications of chimney cubes*, The Leading Edge, Vol. 21, No 7

Barker, J.W., Dupouy Ph., 1999, *An analysis of dynamic pseudo relative*

References

permeability methods, Petroleum Geoscience, Vol. 5, p385-394

Barker, J.W., Cuypers, M., Holden, L., 2001, *Quantifying uncertainty in production forecasts: another look at the PUNQ problem*, SPE Journal, December 2001

Batzle, M., Wang, Z., 1992, *Seismic properties of pore fluids*, Geophysics, Vol. 61, p444-455

Batzle, M., Christiansen, R., Han, D., 1998, *Reservoir recovery processes and geophysics*, The Leading Edge, Vol. 17, No. 10

Batzle, M., Han, D., Castagna, J., 1999, *Fluids and frequency dependent seismic velocity in rocks*, SEG 1999 Annual Technical Conference, Houston

Beasley, C.J., Chambers, R.E., Workman, R.L., Craft, K.L., Meister, L.R., 1997, *Repeatability of 3-D ocean-bottom cable seismic surveys*, The Leading Edge, Vol. 19, No. 9

Bell, D.W., Shirley, D.J., 1980, *Temperature variation of the acoustical properties of laboratory sediments*, Journal of the Acoustical Society of America, Vol. 68, p227-231

Berkhout, A.J., 1987, *Applied seismic wave theory*, Elsevier, Amsterdam

Berryman, J.G., Milton, G.W., 1991, *Exact results for generalized Gassmann's equation in composite media with two constituents*, Geophysics, Vol. 56, p1950-1960

Biot, M.A., 1956, *Theory of propagation of elastic waves in fluid-saturated porous solid I low-frequency range, II higher frequency range*, J. Acoustical Society of America, Vol. 28, No. 2, p168-191

Bissell, R., 1994, *Calculating optimal parameters for history matching*, 4th European Conference on the Mathematics of Oil Recovery

Bissell, R. C., Dubrule, O., Lamy, P., Lepine, O., 1997, *Combining geostatistical modelling with gradient information for history matching: the pilot point method*, SPE 38730, 1997 SPE Annual Technical Conference, San Antonio, Texas

Bos, C.F.M., 2000, *Production forecasting with uncertainty quantification*,

Final report of EC project, NITG-TNO report NITG 99-255-A

Bos, C.F.M., van Kruijsdijk, C.P.J.W., 1995, *How to improve risk management through geosciences*, Proc. New Techn. Applied to Hydrocarbon Production, Delft, p12-35

Brevik, I., 1996, *Inversion and analysis of Gassmann skeleton properties of shaly sandstones using wireline log data from the Norwegian North Sea*, SEG 1996 Annual Technical Conference, paper BG 2.4

Brevik, I., Furre, A-K., 1998, *A rock model for the Brent reservoir at the Statfjord field, Application to seismic 4D analysis*, Internal Statoil report.

Brevik, I., Duffaut, K., Furre, A-K., Rogno, H., 1998, *Statfjord 4D, Establishing time-consistency between acoustic log data and 3D seismic.*, EAGE 1998 annual conference and exhibition, Leipzig, paper 10-16

Bruining J. *et al.*, 1997, *Flexible methods for the generation of random fields with power law semivariograms*, Mathematical Geology, Vol.29, No.6

Caldwell, J., 1999, *Marine multicomponent seismology*, The Leading Edge, Vol. 18, no 11, p1274-1282

Castagna, J., Backus, M. (Editors), 1993, *Offset-dependent-reflectivity – theory and practice of AVO analysis*, SEG's Investigations in geophysics No. 8, ISBN 1-56080-059-3

Castagna, J.P., Batzle, M.L., Eastwood, R.L., 1985, *Relationships between compressional wave and shear wave velocities in clastic silicate rocks*, Geophysics, 51, p571-581

Christie, M.A., 2001, *Flow in porous media – scale up of multiphase flow*, Current opinion in Colloid & Interface Science, Vol. 6, p236-241

Cooper, M., Westwater, P., Thorogood, E., Christiansen, P., Christie, P., 1999, *Foinaven active reservoir management: The benefits from the baseline survey*, SEG 1999 Annual Technical Conference, Houston

Datta-Gupta, A., 2000, *Stream-line simulation: A technology update*, Distinguished Author Series, Journal of Petroleum Tech., Vol. 52, No. 12, SPE 65604

References

- de Groot, P.F.M, 1995, *Seismic reservoir characterisation employing factual and simulated wells*, PhD thesis, Delft University Press
- de Groot, P.F.M., 1999, *Volume transformation by way of neural network mapping*, EAGE 1999 Annual Technical Conference, Helsinki
- de Haan, S.C. , Oldenziel, T., Berentsen, C.W.J., van Kruijsdijk, C.P.J.W., 2001, *Water-cut forecasting and permeability inversion from time-lapse seismic using a stream-line technique*, OTC 13165, OTC 2001 Annual Technical Conference, Houston
- de Roos, M.C., 2000, *Data-driven rock physics modelling in time-lapse seismic reservoir monitoring*, MSc thesis Delft University of Technology, Faculty of Civil Engineering and Geosciences
- Domenico, S.N., 1977, *Elastic Properties of unconsolidated porous sand reservoirs*, 46th Annual international SEG meeting, Houston
- Doyen, P., Psaila, D., Astratti, D., Kvamme, L., Al-Najjar, N., 2000, *Saturation mapping from 4D seismic data in the Statfjord field*, OTC 12100, OTC 2000 Annual Technical Conference, Houston
- Ecker, C., Lumley, D., Tura, A., Kempner, W. and Klonsky, L., 1999, *Estimating separate steam thickness and temperature maps from 4D seismic data: An example from San Joaquin Valley, California*, SEG 1999 Annual Technical Conference, p2032-2034
- Eclipse 100 Reference Manual 99A, Geoquest Schulumberger, 1999.
- Egberts, P.J.P., Brouwer, G.K., Bos, C.F.M., 2002, *History matching and forecasting uncertainty quantification - a reservoir study*, EAGE 2002 Annual conference and exhibition, Florence
- Elliott, S.E., Wiley, B.F., 1975, *Compressional velocities of partially saturated unconsolidated sands*, Geophysics, 40, p949-954
- Fletcher, R. 1987, *Practical methods of optimisation*, Wiley
- Floris, F.J.T., Bush, M.D., Cuypers, M.C., Roggero, F., Syversveen, A-R., 2001, *Methods for quantifying the uncertainty of production forecasts: a comparative*

study, Petroleum Geoscience, Vol. 7, pS87-S96

Funatsu, K., 2002, *Quantification of uncertainty in predicting future performance of hydrocarbon reservoirs*, MSc thesis Delft University of Technology, Faculty of Civil Engineering and Geosciences

Furre, A.K., Brevik, I., 2000, *Integrating core measurements and borehole logs with seismic data in the statfjord 4D project*, Paris 2000 Petrophysics meet Geophysics, paper A-18

Gaiser, J.E., 1999, *Application for vector coordinate system of 3-D converted wave data*, The Leading Edge, Vol. 18, no 11, p1274-1282

Gassmann, F., 1951, *Über die Elastizität poröser Medien*, Vierteljahrsschr. der Naturforsch. Gesellschaft Zurich, 96, p1-21

Goldberg, D.E., 1989, *Genetic algorithms in search, optimization and machine learning*, Addison Wesley, Reading, MA

Goovaerts, P., 1997, *Geostatistics for Natural Resources Evaluation*, Oxford Univ. Press, New York, 483 p.

Gray, D., Goodway, B., Chen, T., 1999, *Bridging the gap: Using AVO to detect changes in fundamental elastic constants*, EAGE 1999 Annual Technical Conference, Helsinki

Gregory, A.R., 1976b, *Fluid saturation effects on dynamic elastic properties of sedimentary rocks*, Geophysics, 41, p895-921

Guerillot, D., Roggero, F., 1995, *Matching the future for the evaluation of extreme reservoir development scenarios*, 8th European Conference on Improved Oil Recovery, Vienna

Han, D., 1986, *Effects of porosity and clay content on acoustic properties of sandstones and unconsolidated sediments*, PhD dissertation, Stanford University

Han, D., Nur, A., Morgan, D., 1986, *Effects of porosity and clay content on wave velocities in sandstones*, Geophysics, 51, p2093-2107

Hashin, Z., Shtrikman, S., 1962, *A variational approach to the theory of elastic*

References

behaviour of multiphase materials, J. Mech. Phys Solids, Vol II, p127-140

Harris, P.E., Henry, B., 1998, *Time-lapse processing: A North Sea case study*, SEG 1998 Annual Technical Conference, New Orleans

Hegstad, B.K., Omre, H., 1997, *Uncertainty assessment in history matching and forecasting*, Geostatistics Wollongong 1996, Baafi & Schofield (eds), Kluwer Academic Publishers, p585-596

Hesthammer, J., Fossen, H., 1998, *Evolution and geometries of gravitational collapse structures with examples from the Statfjord Field, northern North Sea*, Marine and Petroleum Geology, Vol. 16, p259-281

Hesthammer, J., Jordan, C.A., Nielsen, P.E., Ekern, T.E., Gibbons, K.A., 1999, *A tectonostratigraphic framework for the Statfjord field, northern North Sea*, Petroleum Geoscience, Vol. 5, p241-256

Hottman, W.E., Tuttle, C. R., 2001, *Borehole seismic sensors in the instrumented oil field*, The Leading Edge, Vol. 20, No. 6, p630-635.

Huang, X., Meister, L., Workman, R., *Reservoir characterization by integration of time-lapse seismic and production data*, SPE 38695, 1997 SPE Annual Technical Conference, San Antonio, Texas

Huang, X., Jones, T.C., Berni, A., 1999, *Reprocessing of time-lapse seismic data improves seismic history matching*, SEG 1999 Annual Technical Conference, Houston

Johnston, D.H., Toksöz, M.N., Timur, A., 1979, *Attenuation of seismic waves in dry and saturated rocks, II Mechanics*, Geophysics 44, p691-711

Jones, T.D., 1986, *Pore fluid and frequency dependent wave propagation in rocks*, Geophysics, 51, p1939-1953

Jooris, E., 2000, *Plane-wave reflection and transmission coefficients of fluid-saturated elastic media*, MSc thesis Delft University of Technology, Faculty of Civil Engineering and Geosciences

Kalogerakis, N., 1994, *An efficient procedure for the quantification of risk in forecasting reservoir performance*, SPE 27569, 1994 European Petroleum Computer Conference

Kern, H., 1982, *Elastic-wave velocity in crustal and mantle rocks at high temperature: the role of high-low quartz transition and of dehydration reactions*, Phys. Earth Plan. Inter., 29, p12-23

King, M.S., 1965, *Wave velocities in rocks as a function of changes in overburden pressure and pore fluid saturants*, Geophysics, 31, p50-73

King, M.J., Blunt, M.J., Mansfield, M., Christie, M.A., 1993, *Rapid evaluation of the impact of heterogeneity on miscible gas injection*, SPE 26079, 1993 Western Regional Meeting, Anchorage, AK, May 26-28

King P.R., Muggeridge A.H., Price W.G., 1993, *Renormalization calculations of immiscible flow*, Transport in porous media, Vol. 12, p237-260

King, M.J., Datta-Gupta, A., 1998, *Streamline Simulation: A current perspective*, In Situ, No. 2, p91-140

Kirk, R.H., 1980, *Statfjord Field - a North Sea giant, Giant oil and gas fields of the decade: 1968-1978*, AAPG memoir 30, p95-116

Koster, K., Gabriels, P., Hartung, M., Verbeek, J., Deinum, G., Staples, R., 2000, *Timelapse surveys in the North Sea and their business impact*, The Leading Edge, Vol. 19, No. 3, p286-293

Krief, M., Garat, J., Stellingwerf, J., Ventre, J., 1990, *A petrophysical interpretation using the velocities of P and S waves*, The log analyst, 31, November, p355-369

Kurlansky, M., 2002, *Salt: A world history*, ISBN 0802713734

Kvamme, L., Al-Najjar, N., Psaila, D., Astratti, D., Doyen, P., 2000, *Statfjord field saturation mapping from time-lapse seismic data*, NPF, Kristiansand

Landro, M., 1999, *Discrimination between pressure and fluid saturation changes from time lapse seismic data*, SEG 1999 Annual Technical Conference, Houston

Latimer, R.B., Davison, R., van Riel, P., 2000, *An interpreter's guide to understanding and working with seismic-derived acoustic impedance data*, The Leading Edge, Vol. 19, No. 3, p242-256

References

- Lavik, H., 1997, *Statfjord, The largest oilfield in the North Sea*, ISBN 8299429714
- Levenberg, K., 1944, *A method for the solution of certain non-linear problems in least squares*, Quart. J Applied Math., Vol. 2, p164-168
- Lo, T-W, Coyner, K.B., Toksöz, M.N., 1986, *Experimental determination of elastic anisotropy of Berea sandstone, Chicopee shale, and Chelmsford granite*, Geophys., 51, p164-171
- Lumley, D.A., Behrens, R.A., Wang, Z., 1997, *Assessing the technical risk of a 4-D seismic project*, The Leading Edge, Vol. 16, No 9
- Lumley, D.A., Nunns, A.G., Delorme, G., Adeogba, A. A., Bee, Michel F., 1999, *Meren field, Nigeria: A 4D seismic case study*, SEG 1999 Annual Technical Conference, Houston
- MacLeod, M. K., Hanson, R. A., Bell, C. R., McHugo, S., 1999, *The Alba field ocean bottom cable seismic survey: Impact on development*, The Leading Edge, Vol. 18, no 11, p1306-1312
- Marquardt, D.W., 1963, *An algorithm for least squares estimation of non-linear parameters*, J. Soc. Indust. Appl. Math., 11, p. 431
- Mavko, G.M., Nur, A., 1979, *Wave attenuation in partially saturated rocks*, Geophysics, 51, p164-171
- Mavko, G., Mukerji, T., Dvorkin, J., 1998, *The rock physics handbook*, Cambridge University Press, ISBN 0521620686
- McKain, D., Allen, B.L., 2002, *Where it all began*, <http://littlemountain.com/oilandgasmuseum/Pages/whereitallbegan.html>
- Meldahl, P, Heggland, R., de Groot, P., Bril, A., 1998, *Seismic Body Recognition*, Patent Application GB. 9819910.2.
- Meldahl, P., Heggland, R., Bril, A., de Groot, P., 2001, *An iterative method for identifying seismic objects by their texture, orientation and size*, SEG 2001 Annual Technical Conference, San Antonio, Texas

Minkoff, S., Stone, C.M., Arguello, J.G., Bryant, S. , Eaton, J., Peszynska, M., Wheeler, M., 1999, *Coupled geomechanics and flow simulation for time-lapse seismic modelling*, SEG 1999 Annual Technical Conference, Houston, p1667-1670

Monico, C., 1998, *Mathematic comparisons of different history match runs*, 6th European Conference on the Mathematics of Oil Recovery, Peebles, Scotland, Paper B-25

Murphy, W.F., 1984, *Acoustic measures of partial gas saturation in tight sandstones*, J. Geophys. Res., 89

Murphy, W.F., Winkler, K.W., Kleinberg, R.L., 1984, *Frame modulus reduction in sedimentary rocks: The effect of adsorption on grain contacts*, Geoph. Res. Let., Vol. 7, p99-108

Nes, O.-M., Holt, R.M., Fjaer, E., 2000, *The reliability of core data as input to seismic reservoir monitoring studies*, SPE 65180, SPE 2000 European Petroleum conference Paris

Norris, A.N., 1985, A differential scheme for the effective moduli of composites, Mech. of Materials, Vol. 4, p1-6

Nur, A., Simmons, G., 1969a, *Stress-induced velocity anisotropy in rock: an experimental study*, J. of Geoph. Research, Vol. 74, No. 27, p6667-6674

Nur, A., Simmons, G., 1969b, *The effect of saturation on velocity in low porosity rocks*, Earth Planetary Letters, Vol. 7, p183-193

O'Connell, R.J., Budiansky, B., 1977, *Viscoelastic properties of fluid-saturated cracked solids*, J. Geoph. Res., 79, p5412-5426

Odeh, A.S., 1969, *Reservoir simulation – What is it?*, Journal of Petroleum Technology, Nov 1969, p1383-1388

Oldenziel, T., 2002, *Catch-22 in time-lapse seismic; can we proceed?*, In: Fokkema, J.T. and Wapenaar, C.P.A. (Eds.), Integrated 4D Seismics, Journal of Seismic Exploration, 11, p189-195.

Oldenziel, T., de Groot, P.F.M., Kvamme, L.B., 2000, *Neural network based prediction of porosity and water saturation from time-lapse seismic; a case*

References

study on Statfjord, First Break, Vol. 18, No. 2, p65-69

Oldenziel, T., van Ditzhuizen, R., van Kruijsdijk, C.P.J.W., 2002, *Geologic parameterization of reservoir model enhances history-match procedure*, The Leading Edge, Vol. 21, No. 6, p544-551

Oldenziel, T., Meldahl, P., Ligtenberg, H., Stronen, L.K., Digranes, P., 2002, *Multi-attribute analysis of 4D anomalies using pattern recognition technology*, SEG 2002 Annual Technical Conference, Salt Lake City, paper RCT 5.4

Oliver, D., He, N., Reynolds, A.C., 1996, *Conditioning permeability fields to pressure data*, 5th European Conference on the Mathematics of Oil Recovery, Leoben.

Omre, H., 2000, *Stochastic reservoir models conditioned to non-linear production history observations*, paper to appear in Proceedings from Geostats 2000; Cape Town, South Africa ; April 2000

Omre, H., Tjelmeland, H., Qi, Y., Hinderaker, L., 1993, *Assessment of uncertainty in the production characteristics of a sand stone reservoir*; in Reservoir Characterization III, Ed. B. Linville, Penwell Books, Tulsa, Oklahoma, p556-604

Pagano, T.A., Fanchi, J.R., Davis, T.L., 2000, *An integrated flow model: the confluence of geophysics, reservoir engineering, and time*, The Leading Edge, Vol. 19, No. 9, p1020-1023

Pettingill, H.S., 2001, *Giant field discoveries of the 1990s*, The Leading Edge, Vol. 20, No. 7

Pickett, G.R., 1963, *Acoustic character logs and their application in formation evaluation*, J. Petr. Tech., 15, p659-667

Pickup, G.E., Ringrose, P.S., Sharif, A., 2002, *Steady state upscaling: from lamina-scale to full-field model*, Journal of Petroleum Engineering, 5(2), p208-217

Powell, 1971, *A hybrid method for non-linear equations*, in *Numerical methods for non-linear algebraic equations*, P. Rabinowitz ed., Gordon & Breach, p87

Rai, C.S., Hanson, K.E., 1987, *Shear-wave velocity anisotropy in sedimentary*

rocks: A laboratory study, Geophysics, 53, p800-806

RamaRao, B., La Venue, A. M., de Marsily, G., Marietta, M. G., 1995, *Pilot point methodology for automated calibration of an ensemble of conditionally simulated transmissivity fields: theory and computational experiments*, Water Resources Research, Vol. 31, No. 3, p475-493, March 1995

Rasolofosaon, P.N.J., Zinszner, B.E., 2002, *Comparison between permeability anisotropy and elastic anisotropy of reservoir rocks*, Geophysics, Vol. 67, No. 1, p229-240

Rauch, J., 2001, *The new old economy: Oil, computers, and the reinvention of the earth*, The Atlantic, January 2001

Renard, Ph., de Marisly, G., 1997, *Calculating equivalent permeability: a review*, Advances in water Resources, Vol. 20., No. 5/6, p253-278

Reuss, A., 1929, *Berechnung der Fließgrenze von Mischkristallen auf Grund der Plastizitätsbedingung für Einkristalle*, Zeitschrift für Angewandte Mathematik und Mechanik, 9, p49-58

Roggero, F., 1997, *Direct selection of stochastic model realisations constrained to historical data*, SPE 38731, SPE 1997 Annual Technical Conference, Antonio, Texas

Rogno, H., Amundsen, L., 1999, *The Statfjord 3-D, 4-C OBC survey*, The Leading Edge, Vol. 18, No 11, p1301-1305

Rogno, H. *et al.*, 2000, *Integration, quantification and dynamic updating experiences from the Statfjord 4D case*, SEG 2000 Annual Technical Conference, Calgary

Ronen, S., van Waard, R., Keggin, J., 1999, *Repeatability of sea bed multi-component data*, SEG 1999 Annual Technical Conference, Houston

Ross, C.P., Cunnigham, G.B., Weber, D.P., 1996, *Inside the cross-equalisation black box*, The Leading Edge, Vol. 15, No. 11, p1233-1240

Sayers, C., 2002, *Stress-dependent elastic anisotropy of sandstones*, Geophysical Prospecting, Vol. 50, p85-95

References

- Schalkwijk, K.M., Wapenaar, C.P.A., and Verschuur, D.J. 1999, *Application of two-step decomposition to multicomponent ocean-bottom data: theory and case study*, Journal of Seismic Exploration, Vol. 8, p261–278
- Shyeh, J.J., Johnson, D.H., Eastwood, J.E., Khan, M., Stanley, L.R., *Interpretation and modelling of time-lapse seismic data: Lena Field, Gulf of Mexico*, SPE 56731, SPE 1999 Annual Technical Conference, Houston
- Smith, G.C., Gidlow, P.M., 1987, *Weighted stacking for rock property estimation and detection of gas*, Geophysical Prospecting, Vol. 35, p993-1014
- Sprangers, 2002, *Is de aarde op?*, Intermediair, 32, 8 Aug 2002
- Tosaya, C., Nur, A., 1982, *Effects of diagenesis and clays on compressional velocities in rocks*, Geophysical Research Letters, Vol. 9, No. 1, p5-8
- Tura, A., Lumley, D.E., 1999, *Estimating pressure and saturation changes from time-lapse AVO data*, EAGE 1999 Annual Technical Conference, Helsinki
- van Ditzhuijzen, R., Oldenziel, T., van Kruijsdijk, C.P.J.W., 2001, *Geological parameterisation of a reservoir model for history matching incorporating time-lapse seismic based on a case study of the Statfjord field*, SPE 71318, SPE 2001 Annual Conference, New Orleans
- van Soest, C.L., 2001, *Automated stochastic history matching*, MSc thesis Delft University of technology, Faculty of Civil Engineering and Geosciences, TA/PW/01-15
- van Spaendonck, 2002, *Seismic applications of complex wavelet transforms*, PhD thesis, Section of Applied Geophysics, Department of Applied Earth Sciences, Delft University of technology, ISBN 90-9015810-3
- Vauthrin, R., Brid, B., Will, B., Eastwood, J., Johnston, D., 1999, *Improvements in 4D legacy data quality and repeatability through reprocessing, Lena Field*, SEG 1999 Annual Technical Conference, Houston
- Vernik, L., *Predicting porosity from acoustic velocities in siliclastics: A new look*, Geophysics, Vol. 62, p118-128
- Voigt, W., 1928, *Lehrbuch der Kristallphysik*, Teubner, Leipzig

Waggoner, J., 2001, *Integrating time-lapse 3D (4D) seismic data with reservoir simulators*, EAGE 2001 Annual Technical Conference, Amsterdam, paper F-02

Walsh, J.B., 1966, *Seismic wave attenuation in rock due to friction*, J. Geophys. Res., 71, p2591-2599

Wang, Z., 1988, *Wave velocities in hydrocarbons and hydrocarbon saturated rocks - with applications to EOR monitoring*, PhD thesis, Stanford University

Wang, Z., 1997, *Feasibility of time-lapse seismic reservoir monitoring: The physical basis*, The Leading Edge, Vol. 16, No. 9, p1327-1329

Wang Z., 2000a, *The Gassmann equation revisited: comparing laboratory data with Gassmann's predictions*, Seismic and Acoustic Velocities in reservoir Rocks, Volume III Recent Developments, SEG reprint series No. 19, p8-23

Wang Z., 2000b, *Velocity-Density relationships in sedimentary rocks*, Seismic and Acoustic Velocities in reservoir Rocks, Volume III Recent Developments, SEG reprint series No. 19, p258-268

Wang, Z., Nur, A., 1988, *Effect of temperature on wave velocities in sands and sandstones with heavy hydrocarbons*, SPE Reservoir Eng., Vol.3, No.1, p158-164

Wang Z., Nur A., (Editors), 1989, *Seismic and Acoustic Velocities in reservoir Rocks, Volume I Experimental Studies*, SEG reprint series No. 10, ISBN 1-56080-056-9

Wang Z., Nur A., (Editors), 1992, *Seismic and Acoustic Velocities in reservoir Rocks, Volume II Theoretical and Model Studies*, SEG reprint series No. 10, ISBN 0-93183-070-2

Wang, Z., Nur, A. M., Batzle, M.L., 1988a, *Effect of different pore fluids on velocities in rocks*, SEG 1988 Annual Technical Conference, Session:S10.4.

Wang, Z., Nur, A., Batzle, M.L., 1988b, *Acoustic velocities in petroleum oils*, SPE 1988 Annual Technical Conference, p571-563

Weimer, P., Davis, T.L., 1996, *Applications of 3-D Seismic Data to Exploration and Production*, SEG Geophysical Development Series, ISBN 1-89181-050-1

References

- Wences, P. G., Cullick, A.S., Deutsch, C. V., 1998, *An optimization framework for reservoir characterization*, SEG 1998 Annual Technical Conference, New Orleans, RC 1.2
- White, J.E., Martineau-Nicoletis, L., Monash, C., 1983, *Measured anisotropy in Pierre shale*, Geophysical Prospecting, Vol. 31, No. 5, p709-225
- Winkler, K.W., 1986, *Estimates of velocity dispersion between seismic and ultrasonic frequencies*, Geophysics, Vol. 51, p183-189
- Winkler, K.W., Nur, A., 1982, *Effects of pore fluids and frictional sliding on seismic attenuation*, Geophysics, Vol. 47, p1-12
- Xu, S., White, R.E., 1996, *A physical model for shear-wave velocity prediction*, Geophysical prospecting, Vol. 44, p687-717
- Xue, G., Datta-Gupta, A., 1997, *Structure preserving inversion: An efficient approach to conditioning stochastic reservoir models to dynamic data*, SPE 38727, 1997 SPE Annual Technical Conference, San Antonio, Texas
- Yergin, D., 1992, *The Prize: The epic quest for oil, money and power*, ISBN 0671799320
- Yin, H., Han, D., and Nur, A., 1988, *Study of velocities and compaction on sand-clay mixtures*, Stanford Rockphysics Proj., 33, p265-302
- Zhu, X., Altan, S., Li, J., 1999, *Recent advances in multicomponent processing*, The Leading Edge, Vol.18, No. 11, p1283-1288
- Zimmermann, R.W., 1991, *Compressibility of Sandstones*, Elsevier, NY, ISBN 0444883258

List of symbols

Roman

A	production data
AI	acoustic impedance
B	seismic data
bhp	bottom hole pressure
C	coefficient
d	diameter
D	coefficient
E	earth response
f	frequency
g	probability
G	objective function
k	permeability
K	bulk modulus
l	attribute
L	attribute set
m	attribute
M	attribute set
N	number of data points

List of symbols

o	constraint
p	ray parameter
ppr	posteriori probability ratio
P	pressure
Q	flux
r	radius
res	residual
R	radius
RC	reflection coefficient
swat	water saturation
S	saturation
Sw	water saturation
t	time
toa	time of arrival
T	trace
u	fluid flow velocity
v	wave propagation velocity
V	wave propagation velocity
Vcl	Vclay
Vol	volume fraction
w	weight
wopr	well oil production rate
wwct	well water cut
W	wavelet
x	distance
X	objective function
Z	impedance

Greek

α	angle or angle of incidence
β	angle of refraction
γ	coefficient
δ	coefficient
ζ	stress
η	viscosity
θ	model parameters
κ	total permeability
μ	shear modulus
ν	kinematic viscosity

ρ	density
σ	standard deviation
ϕ	porosity
ω	forecast

Subscript

a	production data
A	production data
bhp	bottom hole pressure
B	seismic data
c	characteristic
d	dry
dynamic	dynamic
e	end/outlet
f	fluid
future	future
g	gas
gb	grid block
geol	geological
hc	hydrocarbon
hmc	history matched
HS	Hashin-Shtrikman
i	index
j	index
m	mineral
n	index
o	oil
r	relative
p	pore
prod	production
P	P-wave
PP	incident P-wave, reflected P-wave
PS	incident P-wave, reflected S-wave
R	reuss
s	solid
sat	saturated
seis	seismic
shape	shape
skel	skeleton

List of symbols

swat	water saturation
S	S-wave
SP	incident S-wave, reflected P-wave
SS	incident S-wave, reflected S-wave
t	time step
total	total
V	Voigt
VRH	Voigt-Reuss-Hill
w	water
wcut	water cut
well	well
wopr	well oil production rate
wwct	well water cut
x	position
X	index
y	position
α	phase
ω	optimised
0	origin/inlet
1	index
2	index
3	index
4	index
\pm	upper/lower

Superscript

eff	effective
ref	reference
,	reflection
meas	measured
model	modelled

Summary

Time-lapse 3D seismic is a fairly new technology allowing dynamic reservoir characterisation in a true volumetric sense. By investigating the differences between multiple seismic surveys, valuable information about changes in the reservoir state can be captured. The reservoir state is characterised by effective stress, temperature, and saturation. Currently, the main driver for time-lapse 3D seismic is its potential capability to indirectly measure the saturation. Knowing the reservoir's saturation distribution and its fluid flow behaviour, adds tremendous value to and reduces risk in reservoir management.

The arrival of time-lapse seismic data has forced different disciplines to intensify their working relationship in order to optimally benefit from the information content of the dynamic data. To allow communication and integration between disciplines, modifications to existing methods have to be made within each discipline. The current status of the three main disciplines is described in separate chapters: reservoir management, rock physics, and seismics.

Within **reservoir management**, the objective is to produce each reservoir optimally according to economic, political, technical, and environmental constraints. Reservoir management is a complex task heavily dependent on the

reservoir model. This reservoir model allows analysis of the reservoir behaviour, but more importantly it is used to forecast production behaviour. Building the reservoir model is initiated when the first data on the reservoir is available and continues as long as additional data is gained during production. The reservoir model is continuously updated to match the observed behaviour. At the least, the reservoir model has to correspond with the historical behaviour of the actual reservoir, before one may trust production forecasts and handle accordingly.

Until recently, the reservoir behaviour was only monitored at the wells via production data and well tests. Since the introduction of time-lapse seismic, the reservoir state or its change over time can be indirectly measured over its entire volume. Therefore, time-lapse seismic can serve as an additional constraint for the reservoir model.

Assuming that time-lapse seismic signals can be interpreted in terms of reservoir properties, two challenges remain. To benefit from all the information, including its 3D character, large amounts of data have to be incorporated. Furthermore, the time-lapse seismic information has to be integrated with production and other available data. A complicating factor is that the information provided by time-lapse seismic is indirect and incommensurable with respect to other data.

Rock physics serves two purposes within the time-lapse seismic domain. Rock physical models are utilised to model the effect of a change in the reservoir on the seismic signal. This knowledge is used in the sensitivity analysis to assess the potential of time-lapse seismic before it is actually acquired. After time-lapse seismic is acquired, rock physical models are used to interpret the observed time-lapse seismic signal. Depending on the reservoir and the expected changes a suitable rock physical model is chosen. The objective of any rock physical model is to describe the physical behaviour of the rock when excited by a seismic wave. Due to the complexity of the rock and the impact of the pore fluid, it is impossible to take all aspects into account. Every theoretical model has its simplifying assumptions. For this reason, rock physical models may under- or over- predict the observed time-lapse seismic changes.

The main purpose of 3D **seismic** is to (structurally) image the subsurface. Acquisition and processing techniques have been developed accordingly. With time-lapse seismic, the difference between surveys provides the information regarding the change in the reservoir. Only if the seismic measurements are repeatable, can their difference be related to reservoir changes. To achieve repeatability, acquisition and processing artefacts are to be eliminated by

reproducing the acquisition set-up and re-processing of the seismic surveys followed by cross-equalisation.

The main deliverable and one of the main challenges of time-lapse seismic is to interpret the seismic in terms of reservoir or fluid flow properties. The time-lapse seismic signal is induced by one or more changes in the reservoir state. Each of these production-induced changes can have a different effect on the seismic signal. Decoupling of these effects is crucial and quantification of the reservoir changes presents a major challenge. The properties with the greatest impact on seismic are pore fluid-fill and effective stress. The ultimate objective of time-lapse seismic is to link the seismic directly to the fluid flow. At the moment, no evidence is available that such a direct relation exists.

In this thesis, the use of time-lapse seismic within reservoir engineering is described. The main challenge is expressed as “How to optimally benefit from time-lapse seismic”.

Achieving this will undoubtedly result in a wider acceptance of time-lapse seismic as a standard technique. The challenge is divided in two main categories. The first is to link the seismic measurement directly to fluid-flow properties. The second is to fully integrate the time-lapse seismic data within reservoir engineering.

Link seismic to reservoir properties

The exact relation between time-lapse seismic and reservoir state is rather complex. When a change in the seismic character is observed over time, the reservoir state has changed in the same time period due to production. This basic physical fact holds as long as repeatability of the seismic measurement can be assumed. Using this physical fact, an alternative method is proposed to directly link the observation to its cause. The method yields information about the material (rock and reservoir) parameters at the seismic scale. A 4D attribute is formulated without referring to rock physical modelling, requiring assumptions on the seismic wavelet, or using well data. By normalising in the frequency domain, the 4D attribute accounts for the difference in wavelet between surveys and can be regarded a wavelet-independent measure. The time-lapse change is directly related to the observed saturation difference.

Use of 4D in reservoir engineering

Different examples are given on how to integrate and benefit from time-lapse seismic information. For example, time-lapse seismic yields information on the propagation of the fluid fronts over time. Using the propagation speed, an estimate of the water breakthrough at the producing wells is made. Moreover, it

allows estimating permeability, an important reservoir parameter. Most of the work described comprises integration of the time-lapse seismic information in an automated history matching loop, which is applied to a synthetic model. In each example, time-lapse seismic is used in conjunction with the production data. It is shown that the time-lapse seismic often yields more accurate information than production data. An important issue is the uncertainty associated with the seismic inversion to saturation. Incorrect saturation inversion results yield erroneous reservoir models. Parameterisation is a crucial step in the automated history matching loop. With time-lapse seismic next to production data, different history matching parameters may be introduced, chosen in a sophisticated manner. An example is shown on geological parameterisation, which allows to benefit from the geological information indirectly present in time-lapse seismic data.

Application Statfjord

The use of the Statfjord data set in this thesis is two-fold. It allows recognising challenges the industry is currently facing, as well as testing proposed algorithms. The discussion of the relevant field data is followed by different applications. Visual inspection of time-lapse seismic data is improved by using attribute sets and neural-network-based pattern recognition technology. A comparison is made between two different saturation inversion approaches and their results. Using a data-driven methodology, the relation between the time-lapse seismic and reservoir properties saturation and pressure is derived. The relation is compared to the Statfjord rock physical model.

Delft,

May 6, 2003

Tanja Oldenziel

Samenvatting

Het in tijd herhalen van een 3D seismische meting, ook wel 4D seismiek genoemd, is een nieuwe techniek om het reservoir op een dynamische manier te karakteriseren. Aan de verschillen tussen de metingen kan waardevolle informatie ontleend worden over de opgetreden veranderingen in het reservoir. Deze veranderingen manifesteren zich door verschillen in effectieve druk, temperatuur en saturatie. Het grote belang van het gebruik van in tijd herhaalde seismiek is is gelgen in de mogelijkheid om indirect saturatie te meten. Kennis van de saturatie verdeling en dus van het stromingsgedrag in een reservoir draagt veel bij aan en verkleint de risico's van het beheren van het reservoir.

Door de opkomst van in tijd herhaalde seismiek zijn verschillende disciplines gedwongen om meer samen te werken, zodat optimaal geprofiteerd kan worden van de beschikbare informatie in de dynamische data. Binnen iedere discipline zijn veranderingen van bestaande methodes vereist om de communicatie en integratie tussen de disciplines te bevorderen. De stand van zaken binnen de drie voor dit onderzoek belangrijkste disciplines wordt beschreven in afzonderlijke hoofdstukken: reservoir management, gesteente mechanica en seismiek.

Reservoir management beoogt het naar economische, politieke, technische en milieu maatstaven optimaal produceren van een reservoir. Het is een complexe taak die in belangrijke mate is gebaseerd op analyse met behulp van een reservoir model van het reservoir. Het reservoir model wordt tevens gebruikt om toekomstig productie gedrag van het reservoir te voorspellen. De constructie van een reservoir model begint zodra de eerste data over het reservoir beschikbaar zijn en duurt voort zolang nieuwe metingen verricht worden. Het reservoir model wordt derhalve continu aangepast, opdat het blijvend overeenkomt met de geobserveerde data. Het reservoir model zal op zijn minst moeten voldoen aan het geobserveerde productie gedrag van het reservoir, voordat men de voorspelling van het model kan vertrouwen en er naar kan handelen.

Tot voor kort werd het reservoir gedrag alleen waargenomen aan de hand van de putten met behulp van productie data and put testen. Sinds de introductie van in tijd herhaalde seismiek kan het reservoir gedrag over het gehele reservoir indirect gemeten worden. In tijd herhaalde seismiek is derhalve te beschouwen als extra data waarmee het reservoir model moet overeenkomen.

Aannemende dat het in tijd herhaalde seismisch signaal kan worden geïnterpreteerd in termen van reservoir eigenschappen doen zich een tweetal problemen voor. Ten eerste moeten grote hoeveelheden data verwerkt worden om te kunnen profiteren van de informatie, zoals het 3D karakter van de seismiek. Ten tweede zal de in tijd herhaalde seismische data met de productie en andere data geïntegreerd moeten worden. Een complicerende factor daarbij is dat de informatie uit de in tijd herhaalde seismiek indirect en moeilijk vergelijkbaar is met de andere data.

Gesteente mechanica heeft verschillende toepassingen binnen in tijd herhaalde seismiek. Enerzijds wordt het gebruikt voor gevoeligheidsanalyse naar de toepasbaarheid van in tijd herhaalde seismiek voordat 4D seismiek daadwerkelijk geschoten wordt. Met behulp van gesteente mechanische modellen wordt het effect van de verwachte verandering(en) in het reservoir op het seismisch signaal gemodelleerd. Anderzijds worden gesteente mechanische modellen ingezet nadat in tijd herhaalde seismiek geschoten is om het in tijd herhaalde seismisch signaal te interpreteren. Afhankelijk van het reservoir en de verwachte verandering(en) in het reservoir wordt een geschikt model gekozen. Gesteente mechanische modellen leveren een fysische beschrijving van het gesteente gedrag op, wanneer een seismische golf zich door het gesteente voortplant. De complexiteit van het gesteente en het samenspel tussen gesteente en de vloeistof in de poriën maken dat niet alle aspecten in ogenschouw kunnen worden genomen. Als oplossing voor dit probleem zijn de van toepassing zijnde

theoretische modellen op verschillende aannames gebaseerd. Het gevolg hiervan is dat gesteente mechanische modellen de geobserveerde in tijd herhaalde seismische verandering mogelijk niet correct voorspellen.

De meest gebruikte toepassing van **3D seismiek** is het structureel in kaart brengen van de ondergrond. De technieken voor het schieten en bewerken van seismiek zijn hierop ontwikkeld. Bij in tijd herhaalde seismiek is het juist het verschil tussen de metingen dat informatie verschaft over de veranderingen in het reservoir. Alleen als de seismische meting herhaald kan worden, kan het verschil tussen de metingen gerelateerd worden aan veranderingen in het reservoir. Herhalingen kunnen worden gerealiseerd door artefacten als gevolg van het schieten en bewerken te elimineren, bijvoorbeeld door te meten met dezelfde opstelling en door beide data sets op een gelijke manier te (her)bewerken.

Interpretatie van de in tijd herhaalde seismiek in termen van reservoir- of stromingseigenschappen levert de belangrijkste informatie op. Hier ligt tevens dé uitdaging. Het in tijd herhaalde seismisch signaal wordt veroorzaakt door een of meerdere veranderingen in het reservoir. Elk van deze door productie veroorzaakte veranderingen kan namelijk een ander effect sorteren op het seismisch signaal. Kwantificeren van de veranderingen en het ontkoppelen van de verschillende effecten is cruciaal en vormt zoals gezegd de uitdaging. Veelal hebben saturatie en effectieve druk het grootste effect op de seismiek. Uiteindelijk is het doel om in tijd herhaalde seismiek direct te relateren aan de vloeistofstroming in het reservoir. Tot op heden is er geen bewijs dat een dergelijk direct verband bestaat.

In dit proefschrift wordt de toepassing van in tijd herhaalde seismiek binnen reservoir technologie beschreven. De belangrijkste hier aan gerelateerde uitdaging kan worden omschreven als “Hoe optimaal te profiteren van in tijd herhaalde seismiek”.

Het bereiken hiervan zal leiden tot een bredere acceptatie van in tijd herhaalde seismiek als standaard techniek. De uitdaging bestaat uit twee onderdelen: ten eerste de uitdaging om de seismische meting direct te relateren aan de vloeistofstroming, ten tweede de uitdaging om de in tijd herhaalde seismische data volledig te integreren binnen reservoir management.

Relatie seismiek en reservoir eigenschappen

De relatie tussen in tijd herhaalde seismiek en de veranderingen in het reservoir is complex. Wanneer een verandering in het seismisch karakter wordt geobserveerd (observatie), dan weten we dat een verandering in het reservoir is

opgetreden in dezelfde periode als gevolg van productie (oorzaak). Dit simpele fysische feit klopt zolang herhaling van de seismische meting kan worden aangenomen. Gebruik makend van dit feit, wordt een alternatieve methode om de observatie direct te relateren aan haar oorzaak voorgesteld. Deze methode geeft inzicht in de gesteente en reservoir eigenschappen op seismische schaal. Een 4D seismisch attribuut wordt geïntroceerd zonder te refereren aan gesteente mechanische modellen, zonder aannames te maken over het seismisch golfpatroon en zonder put data te gebruiken. Met behulp van normalisatie in het frequentie domein wordt gecorrigeerd voor verschillen in seismisch golfpatroon tussen data sets. Het 4D attribuut kan derhalve worden gezien als een meting, die onafhankelijk is van het golfpatroon. De veranderingen in tijd van het 4D seismisch attribuut zijn direct gerelateerd aan de geobserveerde saturatie veranderingen.

Het gebruik van 4D seismiek binnen reservoir technologie

Integreren en benutten van in tijd herhaalde seismische informatie kan op verschillende manieren. Zo levert in tijd herhaalde seismiek informatie op over de voortplantingssnelheid van vloeistoffronten in de loop van de tijd. Gebaseerd op de voortplantingssnelheid kan een schatting van de waterdoorbraak bij de productie putten worden gemaakt. Bovendien staat het toe een van de belangrijkste reservoir eigenschappen, de permeabiliteit, te schatten. Een andere manier is de integratie van in tijd herhaalde seismische informatie binnen een geautomatiseerd proces, waarin het reservoir model geconditioneerd wordt met behulp van de voor handen zijnde data. Bij de verschillende voorbeelden wordt de in tijd herhaalde seismiek gebruikt tezamen met de productie data. Het blijkt dat in tijd herhaalde seismiek veelal nauwkeuriger informatie verschaft dan productie data. De onzekerheid die geassocieerd wordt met de seismische inversie naar saturatie kan van grote invloed zijn. Parameterisatie is een cruciale stap binnen het geautomatiseerde proces. Het beschikken van in tijd herhaalde seismische data naast productie data vraagt om introductie van andere conditionerings parameters. Een voorbeeld wordt beschreven van geologische parameterisatie met als doel beter gebruik te maken van de geologische informatie, die indirect aanwezig is in de in tijd herhaalde seismische data.

Toepassing op Statfjord

Het gebruik van de Statfjord data in dit proefschrift is tweeledig. Het stelt zowel in staat om uitdagingen, waar de industrie mee te maken heeft, te herkennen en als om nieuwe methodes te testen. De beschrijving van de relevante data wordt gevolgd door verschillende toepassingen op de Statfjord data. Visuele inspectie van in tijd herhaalde seismische data wordt aanzienlijk verbeterd door het

tegelijkertijd analyseren van meerder seismische attributen en het gebruik van patroon herkenning technologie. Een vergelijking tussen twee verschillende saturatie inversie methodes en hun resultaten is gemaakt. Met behulp van een data gestuurde methode, is een relatie tussen de in tijd herhaalde seismiek en reservoir eigenschappen afgeleid. Deze relatie is tenslotte vergeleken met het Staffjord gesteente mechanisch model.

Delft, 6 mei 2003

Tanja Oldenziel

Acknowledgements

First, I would like to thank everybody who contributed in one way or another to my PhD thesis. Below, I would like to thank some people in specific.

When graduating from university, I never expected to return so soon to pursue a PhD title. I always envisioned taking a “PhD” sabbatical after about 10 years of working in the oil and gas industry. However, four years ago a fantastic opportunity arose that I could not resist. Within dGB, I could pursue my PhD under very favourable circumstances. Financial support was guaranteed, the subject was mine to choose, and my promoter(s) would be from the faculty of Mining and Petroleum Engineering at Delft University of Technology, where I had just graduated. Moreover, I was allowed to combine my work at dGB with my PhD research.

I am grateful to dGB in general, but my employers Paul de Groot and Bert Brill in particular for allowing me to seize this opportunity and for their continuous support on many fronts during the years. Thanks to my colleagues, who, often without knowing, helped me solving problems and making progress just by listening or by asking the simple “why” questions. Special thanks to my colleague Kristofer Tingdahl for writing some dedicated algorithms.

Acknowledgements

For an industry-oriented PhD research it is important to have access to an actual data set. It allows testing ideas and algorithms, but more importantly recognising problems the industry is currently facing. I would like to thank Statoil for their permission to use the Statfjord data set for my PhD research. In special, I would like to thank Leif Kvamme for introducing me to the Statfjord field, Kenneth Duffaut for his support, and Nazih Najjar for the fruitful discussions.

Working on any project for four years can be de-motivating from time to time. Luckily, I can not confirm this from my personal experience. During the four years, I was fortunate to have several MSc students as co-workers on my PhD project. They all generated exiting and valuable results yielding them excellent grades. In the first few months of their projects I taught them, in the end they taught me by sharing the knowledge they gained and by discussing their results. During the many months of co-operation, fresh ideas were born and many discussions took place, not all regarding time-lapse seismic. It was fun to study together. Many thanks to Maarten de Roos, Eliana Arenas, Suzan de Haan, Els Jooris, Roos van Ditzhuijzen, Camiel van Soest, and Funatsu Kunihiro.

I would like to thank my two promoters, Professor van Kruijsdijk and Professor Fokkema for supervising and supporting me with their never ending enthusiasm. I could continue working on this subject for another decade without running out of ideas or solutions to challenges. I thank them for their flexibility and giving me the freedom to manage my PhD research according to my own ideas and schedule.

Furthermore, I would like to acknowledge my examining committee for their time and valuable feedback on my thesis.

I would like to acknowledge dGB and STW for the financial support during the years of my study.

Thanks to my family for their support in the last few months.

Last but not least, special thanks to my husband Cor for his support and understanding during the countless hours of our spare time, in which I chose to communicate with my computer. He motivated me when progress was slow or frustration with my PhD ran high. Since I accepted the challenge four years ago, his support has been unconditional and faded only slightly over the years. After four years of dedication to my PhD, time has come for a change. The birth of our son Lars marks this change. He has made me rediscover and value other important aspects of my life.

Curriculum Vitae

Tanja Oldenziel-Dijkstra

Heerhugowaard, 23-11-1973

Education

- 1980-1986 Primary school, Heerhugowaard, the Netherlands
- 1986-1992 Secondary school (Gymnasium-B), Alkmaar, the Netherlands
- 1992-1997 MSc Delft University of Technology, Delft, the Netherlands
- Faculty of Mining and Petroleum Engineering,
section reservoir engineering
MSc thesis: "Dynamic pore network modelling"

Employment

- 1997-1998 bp exploration and production, Aberdeen, UK
Reservoir engineer at Clair asset team

- 1998-2002 dGB Earth Sciences, Enschede, the Netherlands
Geoscientist
Employed to perform quantitative seismic reservoir characterisation studies for clients in oil / gas industry.
- 1999-2003 Delft University of Technology, Delft, the Netherlands
Department of Applied Earth Sciences
PhD research
“Time-lapse seismic within reservoir engineering”
- current dGB Rotterdam, Rotterdam, the Netherlands
Managing director
Responsible for seismic interpretation services and software sales to oil / gas industry clients in West-Netherlands.

Publications

- Oldenziel, T., Meldahl, P., Ligtenberg, H., Digranes, P., Strønen, L. K., 2002, *Multi-attribute analysis of 4D anomalies using pattern recognition technology*, SEG 2002 Annual Technical Conference Salt Lake City
- Oldenziel, T., van Ditzhuijzen, R., van Kruijsdijk, C.P.J.W., 2002, *Geological parameterisation of a reservoir model enhances history-match procedure*, The leading Edge, Vol. 21, No. 6, p544-551
- Meldahl, P., Najjar, N., Oldenziel, T., Ligtenberg, H., 2002, *Semi-Automated detection of 4D objects*, EAGE 2002 Annual Technical Conference, Florence
- Berge, T. B., Aminzadeh, F., de Groot, P., Oldenziel, T., 2002, *Seismic inversion successfully predicts reservoir, porosity, and gas content in Ibhubesi Field, Orange Basin, South Africa*, The Leading Edge, Vol. 21, No. 4, p338-349
- Aminzadeh, A., de Groot, P., Berge, T., Oldenziel, T., Ligtenberg, H., 2002, *Determining migration path from seismically derived gas chimneys*, AAPG 2002 Hedberg Conference, Vancouver
- Oldenziel, T., 2002, *Catch-22 in time-lapse seismic; can we proceed?*, In: Fokkema, J.T. and Wapenaar, C.P.A. (Eds.), *Integrated 4D Seismics*, Journal of Seismic Exploration, 11, p189-195

Arenas, E.M., van Kruijsdijk, C.P.J.W., Oldenziel, T. 2001, *Semi-Automatic history matching using the pilot point method including time-lapse seismic data*, SPE 71634, SPE 2001 Annual Technical Conference, New Orleans

van Ditzhuijzen, R. Oldenziel, T., van Kruijsdijk, C.P.J.W., 2001, *Geological parameterisation of a reservoir model for history matching incorporating time-lapse seismic based on a case study of the Statfjord field*, SPE 71318, SPE 2001 Annual Conference, New Orleans

Oldenziel, T., 2001, *Geological parameterisation of a reservoir model enhances (time-lapse) seismic history matching*, Workshop "Best of D&P forum 2001", SEG 2001 Annual Technical Conference, San Antonio, Texas

de Roos, M.C., Oldenziel, T., van Kruijsdijk, C.P.J.W., 2001, *Neural network for time-lapse seismic reservoir monitoring*, Journal of Petroleum Technology, August 2001, synopsis of OTC 13162

Oldenziel, T., 2001, *Geological parameterisation of a reservoir model enhances (time-lapse) seismic history matching*, SEG 2001 Development and Production forum, Taos

Oldenziel, T., 2001, *Catch-22 in time-lapse seismic; can we proceed*, workshop EAGE 2001 Annual Technical Conference, Amsterdam

Arenas, E.M., Oldenziel, T., van Kruijsdijk, C.P.J.W., 2001, *History matching a reservoir model to time-lapse seismic using the pilot point method*, EAGE 2001 Annual Technical Conference, Amsterdam.

de Roos, M.C., Oldenziel, T., van Kruijsdijk, C.P.J.W., 2001, *Neural network as Alternative to Rock Physics modeling in time-lapse seismic reservoir monitoring*, OTC 13162, OTC 2001 Annual Technical Conference, Houston

de Haan, S.C, Oldenziel, T., Berentsen, C.W.J., van Kruijsdijk, C.P.J.W., 2001, *Water-cut forecasting and permeability inversion from time-lapse seismic using a stream-line technique*, OTC 13165, OTC 2001 Annual Technical Conference, Houston

Oldenziel, T., van Kruijsdijk, C., Fokkema, J., 2001, *Time-lapse seismic*, published for Delphi consortium, The imaging and characterisation project, Volume XII, January 2001

de Haan, S., Berentsen, C., Oldenziel T. van Kruijsdijk, C., 2000, *Permeability inversion and watercut forecasting using saturation history from time-lapse seismic and seismic attribute maps*, Paris 2000

Oldenziel, T., de Groot, P.F.M., Duffaut, K., 2000, *The impact of the rock physics model on time-lapse analysis of the Statfjord field*, SEG 2000 Annual Technical Conference, Calgary

Oldenziel, T., de Groot, P.F.M., Kvamme, L.B., 2000, *Prediction of static and dynamic parameters from time-lapse 3-D seismic*, EAGE 2000 Annula Technical Conference, Glasgow

Oldenziel, T., de Groot, P.F.M., Kvamme, L.B., 2000, *Neural network based prediction of porosity and water saturation from time-lapse seismic; a case study on Statfjord*, First Break, Vol. 18, No. 2, (Feb. 2000), p65-69

Stellingen

behorende bij het proefschrift

“Time-lapse seismic within reservoir engineering”

Tanja Dijkstra

6 mei 2003

Stelling 1 “There was only one catch and that was Catch-22, which specified that the reservoir state at the wells was needed to interpret the time-lapse seismic. The reservoir state at the wells could have been measured, but in practice never was, so they used the reservoir model to estimate the reservoir state. To prove that the reservoir model was correct they decided to test against measurements of the reservoir state. These measurements were called time-lapse seismic and to interpret these they used the reservoir state at the well locations from the reservoir model.” (dit proefschrift; Catch-22, Joseph Heller)

Stelling 2 Semi-automatische “history matching” vereenvoudigt het meenemen van de parameter onzekerheden in reservoir simulatie modellen. (dit proefschrift)

Stelling 3 De waarde van in tijd herhaalde seismiek wordt voornamelijk bepaald door haar 3D karakter en veel minder door het kwantitatieve karakter. (dit proefschrift)

Stelling 4 Integratie is cruciaal voor interpretatie van in tijd herhaalde seismiek. Het vloeistofstromingsgedrag, zoals gemodelleerd door de reservoir ingenieur, geeft coherentie aan de 3D informatie in de in tijd herhaalde seismiek.

Stelling 5 Integratie wordt bemoeilijkt doordat dezelfde woorden andere betekenissen hebben binnen verschillende disciplines.

Stelling 6 Na decennia is de discussie nog gaande wie beter 3D seismiek kan interpreteren; de geoloog of de geofysicus. Voor het interpreteren van in tijd herhaalde seismiek strijden de geoloog, geofysicus, reservoir ingenieur, en gesteentemechanicus om de eer. Een multi-disciplinair “geo-reservoir-rock” ingenieur zal met de eer strijken.

Stelling 7 Deadlines zijn de beste bron van inspiratie en stimuleren creativiteit.

Stelling 8 De fysica van een probleem wordt geweld aangedaan, zodra men binnen de verscheidene disciplines verschillende aannames doet ter vereenvoudiging van het probleem.

Stelling 9 Structureel complexe reservoirs kunnen beter gemodelleerd worden met behulp van geologische parameterisatie. (dit proefschrift)

Stelling 10 De bevalling van een proefschrift heeft vele overeenkomsten met de bevalling van een kind. De geboorte van een kind is echter meer waard dan 100 titels.

Stellingen

accompanying the PhD thesis

“Time-lapse seismic within reservoir engineering”

Tanja Dijkstra

May 6, 2003

Stelling 1 “There was only one catch and that was Catch-22, which specified that the reservoir state at the wells was needed to interpret the time-lapse seismic. The reservoir state at the wells could have been measured, but in practice never was, so they used the reservoir model to estimate the reservoir state. To prove that the reservoir model was correct they decided to test against measurements of the reservoir state. These measurements were called time-lapse seismic and to interpret these they used the reservoir state at the well locations from the reservoir model.” (this thesis; Catch-22, Joseph Heller)

Stelling 2 Semi-automated history matching facilitates the incorporation of parameter uncertainties in reservoir simulation models. (this thesis)

Stelling 3 The value of time-lapse seismic originates mainly from its 3D rather than its quantitative character. (this thesis)

Stelling 4 Integration is crucial for time-lapse seismic interpretation. The fluid flow behaviour, as modelled by the reservoir engineer, yields the coherence required to interpret the 3D information in the time-lapse seismic.

Stelling 5 Integration is impeded by the fact that the same words have a different meaning within various disciplines.

Stelling 6 After decades, the argument still exists whether the geologist or the geophysicist is the best 3D seismic interpreter. The geologist, geophysicist, reservoir engineer, and rock physicist are competing for the title of being the best 4D seismic interpreter. However, a multi-disciplinary "geo-reservoir-rock"-engineer will win the battle.

Stelling 7 Deadlines are the best source of inspiration and stimulate creativity.

Stelling 8 The physics of a multi-disciplinary problem is violated when different simplifying assumptions are made within the various disciplines.

Stelling 9 Structurally complex reservoirs are often better modelled by geological parameterisation. (this thesis)

Stelling 10 The delivery of a PhD thesis has a lot in common with the delivery of a child. However, the birth of a child has more value than 100 degrees.